Manoj Badoni

Ajay Thesis Final

ABCD

Document Details

Submission ID

trn:oid:::3618:111677797

Submission Date

Sep 10, 2025, 6:52 PM GMT+5:30

Download Date

Sep 10, 2025, 7:09 PM GMT+5:30

File Name

Ajay Thesis Final.pdf

File Size

12.3 MB

208 Pages

55,494 Words

294,869 Characters

8% Overall Similarity

The combined total of all matches, including overlapping sources, for each database.

Filtered from the Report

Bibliography

Small Matches (less than 10 words)

Exclusions

1 Excluded Source

2 Excluded Matches

Match Groups

283 Not Cited or Quoted 7%
Matches with neither in-text citation nor quotation marks

31 Missing Quotations 1%
Matches that are still very similar to source material

0 Missing Citation 0%
Matches that have quotation marks, but no in-text citation

0 Cited and Quoted 0%
Matches with in-text citation present, but no quotation marks

Top Sources

2% Internet sources

6% Publications

5% Submitted works (Student Papers)

Integrity Flags

0 Integrity Flags for Review

Our system's algorithms look deeply at a document for any inconsistencies that would set it apart from a normal submission. If we notice something strange, we flag it for you to review.

A Flag is not necessarily an indicator of a problem. However, we'd recommend you focus your attention there for further review.

Match Groups

283 Not Cited or Quoted 7%
Matches with neither in-text citation nor quotation marks

31 Missing Quotations 1%
Matches that are still very similar to source material

0 Missing Citation 0%
Matches that have quotation marks, but no in-text citation

0 Cited and Quoted 0%
Matches with in-text citation present, but no quotation marks

Top Sources

2% Internet sources
6% Publications
5% Submitted works (Student Papers)

Top Sources

The sources with the highest number of matches within the submission. Overlapping sources will not be displayed.

1	Student papers	
IIT Delhi on 2019-01-15		<1%
2	Publication	
Anjanee Kumar Mishra, Ankit Kumar Singh, M V Gururaj. "A Fuel-Efficient BLDC M...		<1%
3	Internet	
www.displaysearch-japan.com		<1%
4	Publication	
Utsav Sharma, Bhim Singh. "A Bidirectional Charger for Light Electric Vehicle Usin...		<1%
5	Internet	
vdoc.pub		<1%
6	Internet	
www.coursehero.com		<1%
7	Internet	
dspace.lboro.ac.uk		<1%
8	Student papers	
Thapar University, Patiala on 2021-10-12		<1%
9	Publication	
Utsav Sharma, Bhim Singh. "A Bidirectional Charger for Low Voltage Powered Bat...		<1%
10	Student papers	
Thapar University, Patiala on 2023-02-15		<1%

11 Student papers
IIT Delhi on 2017-04-10 <1%

12 Student papers
IIT Delhi on 2016-01-12 <1%

13 Internet
www.researchgate.net <1%

14 Student papers
IIT Delhi on 2019-05-01 <1%

15 Publication
Samir M. Shariff, Mohammad Saad Alam, Furkan Ahmad, Yasser Rafat, M. Syed Ja... <1%

16 Internet
dn720405.ca.archive.org <1%

17 Publication
Anjanee Kumar Mishra, Taehyung Kim. "An Economical Light Plug-in Electric Vehi... <1%

18 Publication
Jitendra Gupta, Radha Kushwaha, Bhim Singh, Vinod Khadkikar. "Improved Powe... <1%

19 Internet
qspace.qu.edu.qa <1%

20 Student papers
IIT Delhi on 2018-02-07 <1%

21 Publication
Natarajan Balasubramanian Muthu Selvan, Venkatraman Thiyagarajan, Cheng Si... <1%

22 Internet
dokumen.pub <1%

23 Student papers
IIT Delhi on 2018-01-04 <1%

24 Publication
Utsav Sharma, Bhim Singh. "A Bidirectional Onboard Charger with Multistep Con... <1%

25	Publication	Sawsan Sayed, Ahmed Massoud. "Review on State-of-the-Art Unidirectional Non-I... <1%
26	Student papers	IIT Delhi on 2014-07-30 <1%
27	Publication	"Advances in Smart Grid Technology", Springer Science and Business Media LLC, ... <1%
28	Publication	Anjeet Verma, Bhim Singh, Ambrish Chandra, Kamal Al Haddad. "An Implementat... <1%
29	Publication	"Power Converters, Drives and Controls for Sustainable Operations", Wiley, 2023 <1%
30	Internet	drum.lib.umd.edu <1%
31	Publication	Radha Kushwaha, Bhim Singh, Vinod Khadkikar. "An Isolated Bridgeless Cuk-SEPI... <1%
32	Publication	Ankit Kumar Singh, Manoj Badoni, Yogesh N. Tatte. "A Multifunctional Solar PV a... <1%
33	Publication	Bhim Singh, Radha Kushwaha. "A PFC Based EV Battery Charger Using a Bridgeles... <1%
34	Student papers	IIT Delhi on 2018-03-15 <1%
35	Internet	lib.buet.ac.bd:8080 <1%
36	Publication	"Technologies and Applications for Smart Charging of Electric and Plug-in Hybrid ... <1%
37	Student papers	IIT Delhi on 2014-12-27 <1%
38	Internet	scholarbank.nus.edu.sg <1%

39	Student papers	
Thapar University, Patiala on 2022-02-07		<1%
40	Student papers	
Uttar Pradesh Technical University on 2025-03-28		<1%
41	Publication	
"Advances in Electrical Power and Embedded Drive Control", Springer Science an...		<1%
42	Publication	
"Automatic Control and Emerging Technologies", Springer Science and Business ...		<1%
43	Publication	
Lecture Notes in Electrical Engineering, 2015.		<1%
44	Student papers	
Thapar University, Patiala on 2023-02-15		<1%
45	Student papers	
Uttar Pradesh Technical University on 2022-08-10		<1%
46	Student papers	
IIT Delhi on 2018-12-31		<1%
47	Publication	
Sudhanshu Mittal, Alka Singh, Prakash Chittora. "Design and development of Red...		<1%
48	Publication	
Hamed Nazi, Ebrahim Babaei, Sajjad Tohidi, Marco Liserre. "An Isolated SRC-Base...		<1%
49	Student papers	
IIT Delhi on 2018-11-05		<1%
50	Student papers	
IIT Delhi on 2015-04-07		<1%
51	Student papers	
IIT Delhi on 2016-10-11		<1%
52	Publication	
Ankit Kumar Singh, Mukesh Kumar Pathak. "A Multi-Functional Single-Stage Pow...		<1%

53	Internet	
dspace.dtu.ac.in:8080		<1%
54	Student papers	
IIT Delhi on 2013-04-16		<1%
55	Publication	
Jitendra Gupta, Bhim Singh. "Single-Stage Isolated Bridgeless Charger for Light El...		<1%
56	Student papers	
Submitted on 1686287806352		<1%
57	Publication	
Angshuman Sharma, Santanu Sharma. "Review of power electronics in vehicle-to-...		<1%
58	Student papers	
Florida International University on 2019-02-28		<1%
59	Publication	
Gowthamraj Rajendran, Chockalingam Aravind Vaithilingam, Norhisam Misron, K...		<1%
60	Publication	
Rajesh Kumar Lenka, Anup Kumar Panda, Ranjeeta Patel, Josep M. Guerrero. "PV I...		<1%
61	Publication	
Utsav Sharma, Bhim Singh. "An adaptive Lyapunov's quadrature signal generator...		<1%
62	Publication	
Xu-Feng Cheng, Chenyang Liu, Dianlong Wang, Yong Zhang. "State-of-the-Art Rev...		<1%
63	Internet	
ebin.pub		<1%
64	Internet	
www.semanticscholar.org		<1%
65	Publication	
"Recent Advances in Power Electronics and Drives", Springer Science and Busines...		<1%
66	Publication	
Ankit Kumar Singh, Anjanee Kumar Mishra, Krishna Kumar Gupta, Pallavee Bhatn...		<1%

67 Publication

Gomes, Ricardo Vieites Salgado Alves. "Unified Motor Drive and Battery Charger f... <1%

68 Student papers

IIT Delhi on 2015-01-23 <1%

69 Student papers

Macquarie University on 2021-11-14 <1%

70 Student papers

unifei on 2025-07-29 <1%

71 Publication

"Advances in Electrical and Computer Technologies", Springer Science and Busine... <1%

72 Publication

Fawzy A. Osman, Mostafa A.R. Eltokhy, Asmaa Y.M. Hashem, Mohamed Y.M. Hash... <1%

73 Student papers

IIT Delhi on 2013-12-29 <1%

74 Student papers

IIT Delhi on 2018-07-10 <1%

75 Publication

Istiak Ahmed, Md. Ashaduzzaman Niloy, Marjan Al Haque, Showrov Rahman et al.... <1%

76 Publication

Jitendra Gupta, Radha Kushwaha, Bhim Singh. "Improved Power Quality Transfor... <1%

77 Publication

Mike Tooley, Lloyd Dingle. "BTEC National Engineering", Routledge, 2019 <1%

78 Publication

Tanta, Mohamed. "Rail Power Conditioners Based on Modular Multilevel Convert... <1%

79 Internet

spectrum.library.concordia.ca <1%

80 Publication

Masago, Anna Loishorawa. "The Role of Socio-Cultural Drivers of Food Choice and... <1%

81	Publication	Xuewei, Pan, and Akshay Kumar Rathore. "Naturally Clamped Zero-Current Com... <1%
82	Student papers	IIT Delhi on 2017-06-06 <1%
83	Student papers	IIT Delhi on 2013-10-28 <1%
84	Publication	Tusharkanta Samal, Ambarish Panda, Manas Ranjan Kabat, Ali Ismail Awad, Suve... <1%
85	Internet	dl.lib.uom.lk <1%
86	Publication	Biswajit Saha, Aryadip Sen, Bhim Singh, Kumar Mahtani, José A. Sánchez-Fernánd... <1%
87	Publication	Jitendra Gupta, Bhim Singh. "A General Purpose Transformerless Charging Syste... <1%
88	Student papers	Higher Education Commission Pakistan on 2019-12-30 <1%
89	Student papers	VIT University on 2017-04-26 <1%
90	Student papers	Visvesvaraya National Institute of Technology on 2022-04-08 <1%
91	Publication	"Smart Grid Stability and Control", Springer Science and Business Media LLC, 2025 <1%
92	Student papers	Brunel University on 2025-09-03 <1%
93	Student papers	Curtin University of Technology on 2014-11-06 <1%
94	Publication	Hussain, Syed Asim. "Robust Controller Design for Voltage Source Inverters in Mi... <1%

95 Student papers
University of Sydney on 2024-11-01 <1%

96 Internet
m.moam.info <1%

97 Publication
Alzeyadi, Ahmed. "Quantifying Moisture and Chloride Contents in Concrete Using... <1%

98 Publication
Anjanee Kumar Mishra, Bhim Singh. "Grid Integrated SRM Driven Solar Water Pu... <1%

99 Student papers
IIT Delhi on 2018-02-21 <1%

100 Student papers
Indian Institute of Technology (ISM), Dhanbad on 2025-08-28 <1%

101 Publication
Sankar Selvakumar, Mohanty Madhusmita, Chandrasekaran Koodalsamy, Sishaj ... <1%

102 Student papers
University of Leeds on 2020-08-20 <1%

103 Student papers
University of Northumbria at Newcastle on 2023-05-29 <1%

104 Student papers
University of Nottingham on 2025-04-30 <1%

105 Publication
Utsav Sharma, Bhim Singh. "A Bidirectional Electric Vehicle Charger for Wide Out... <1%

106 Student papers
Visvesvaraya National Institute of Technology on 2022-11-27 <1%

107 Publication
Azza Keerthi, C Dhanamjayulu. "A thorough review of energy management and a... <1%

108 Publication
G K Naveen Kumar, Arun Kumar Verma. "A Single-Phase Interleaved Buck-Boost P... <1%

109 Student papers
IIT Delhi on 2015-08-03 <1%

110 Student papers
IIT Delhi on 2016-06-23 <1%

111 Student papers
IIT Delhi on 2017-07-06 <1%

112 Student papers
Jawaharlal Nehru Technological University on 2025-05-29 <1%

113 Publication
Mohammad Faisal Akhtar, Siti Rohani S. Raihan, Nasrudin Abd Rahim, Mohamma... <1%

114 Publication
Mpho J. Lencwe, Thomas O. Olwal, SP Daniel. Chowdhury, Maxwell Sibanyoni. "No... <1%

115 Student papers
National Institute of Technology, Rourkela on 2023-05-09 <1%

116 Publication
Pahlevaninezhad, Majid. "Power converters for electric vehicles.", Queen's Univer... <1%

117 Publication
Rajesh Sethuraman, Mageshvaran Rudhramoorthy. "Performance of Bidirectiona... <1%

118 Student papers
TU Delft on 2024-07-22 <1%

119 Publication
Vahid, Sina. "Multi-Port Power Converters for Hybrid Energy System Applications"... <1%

120 Internet
vbn.aau.dk <1%

121 Publication
"Advances in Energy Technology", Springer Science and Business Media LLC, 2022 <1%

122 Publication
"Electric Vehicles", Springer Science and Business Media LLC, 2021 <1%

123 Publication
"Recent Advances in Electrical and Information Technologies for Sustainable Dev... <1%

124 Publication
"Smart Charging Solutions for Hybrid and Electric Vehicles", Wiley, 2022 <1%

125 Publication
Aijaz Ahmad, Kushal Jagtap, Keerti Rawal. "Distributed Energy Resources and Elec... <1%

126 Publication
Ali Emadi. "Advanced Electric Drive Vehicles", CRC Press, 2019 <1%

127 Publication
Ali Emadi. "Handbook of Automotive Power Electronics and Motor Drives", Taylor ... <1%

128 Publication
Alkawaz, Ali Najm Abdulnabi. "Minimizing Charging Cost of Plug-In Electric Vehicl... <1%

129 Publication
Ande Bala Naga Lingaiah, Narsa Reddy Tummuru. "A PV-Utility Integrated Cascad... <1%

130 Student papers
Anna University on 2024-03-16 <1%

131 Student papers
Anna University on 2024-05-03 <1%

132 Student papers
Anna University on 2024-11-27 <1%

133 Publication
Birudala Venkatesh Reddy, Y V Krishna Reddy, Md. Abdur Razzak, Surender Reddy... <1%

134 Publication
Deepak Mohanraj, Ranjeev Aruldavid, Rajesh Verma, K. Sathiyasekar et al. "A Revi... <1%

135 Publication
Jitendra Gupta, Bhim Singh. "A Bidirectional Home Charging Solution for an Electr... <1%

136 Publication
K Suresh, C. Bharatiraja, N. Chellammal, Mohd Tariq, Ripon K. Chakraborrty, Mich... <1%

137 Publication

Mohammad Reza Mohammadi, Hosein Farzanehfard. "Family of Soft Switching Bi... <1%

138 Publication

Patel, Hetal V.. "Modified Sinusoidal Pulse Width Modulation Technique for Speed... <1%

139 Publication

S. Vijayakumar, N. Sudhakar. "A review on unidirectional converters for on-board ... <1%

140 Publication

Sahana Deb, Sumit Pramanick. "Overview and comparative analysis of single pha... <1%

141 Student papers

Thapar University, Patiala on 2022-02-08 <1%

142 Student papers

University of Hertfordshire on 2022-08-22 <1%

143 Student papers

University of Huddersfield on 2021-05-02 <1%

144 Publication

Vinit Kumar, KangHyun Yi. "Single-Phase, Bidirectional, 7.7 kW Totem Pole On-Bo... <1%

145 Publication

Yun Zhang, Qiangqiang Liu, Jing Li, Mark Sumner. "A Common Ground Switched-... <1%

146 Internet

mro.massey.ac.nz <1%

147 Internet

ro.uow.edu.au <1%

Design and Development of Charging Schemes for Light Electric Vehicles

A Thesis

Submitted for the fulfillment of the requirement for the award of degree of

Doctor of Philosophy

Submitted by:

Ajay Singh
(Regn. No. 902104001)

THAPAR INSTITUTE
OF ENGINEERING & TECHNOLOGY
(Deemed to be University)

Under the supervision of

Dr. Manoj Badoni
Associate Professor

Dr. Anjanee Kumar Mishra
Assistant Professor

Department of Electrical & Instrumentation Engineering
Thapar Institute of Engineering and Technology

Patiala-147004, India
September-2025

Certificate

This is to certify that the work embodied in this thesis entitled **"Design and Development of Charging Schemes for Light Electric Vehicles"** has been carried out by Mr. Ajay Singh under my supervision and guidance in the Department of Electrical and Instrumentation Engineering, Thapar Institute of Engineering and Technology, Patiala. The candidate completed all the conditions required for the fulfilment of the award of the Degree of Philosophy.

I also certified that the work represented in this thesis is original and has not been submitted in part or full for the award of any degree in any other University or Institute.

Dr. Manoj Badoni
Associate Professor
Department of Electrical and Instrumentation Engineering
Thapar Institute of Engineering and Technology, Patiala

Dr. Anjanee Kumar Mishra
Assistant Professor
Electrical Engineering Department
Netaji Subhas University of Technology, New Delhi

Candidate's Declaration

I, hereby declare that the work presented in the thesis entitled **"Design and Development of Charging Schemes for Light Electric Vehicles"**, in fulfilment of the requirement for the award of the Degree of Doctor of Philosophy, Department of Electrical and Instrumentation Engineering, Thapar Institute of Engineering and Technology, Patiala, is an authentic record of my own work carried out under the supervision of Dr. Manoj Badoni (Associate Professor), Department of Electrical and Instrumentation Engineering, Thapar Institute of Engineering and Technology, Patiala, India and Dr. Anjanee Kumar Mishra (Assistant Professor), Electrical Engineering Department, Netaji Subhas University of Technology, New Delhi. The matter embodied in this thesis has not been submitted in part or full to any other University or Institute for the award of any degree in India or Abroad.

Ajay Singh

Dr. Manoj Badoni
(Associate Professor and Supervisor)
Department of Electrical and Instrumentation Engineering
Thapar Institute of Engineering and Technology, Patiala

Dr. Anjanee Kumar Mishra
(Assistant Professor and Supervisor)
Electrical Engineering Department
Netaji Subhas University of Technology, New Delhi

Acknowledgement

I am deeply grateful to God, the Almighty, for his abundant blessings and guidance throughout my research journey. His grace has been a constant source of strength, enabling me to bring this work to completion.

The successful completion of this thesis would not have been possible without the invaluable support and encouragement of many individuals. I am immensely grateful to each one of them, and I find that words themselves cannot fully express my gratitude.

First, I would like to express my sincere gratitude towards my research supervisors **Dr. Manoj Badoni** and **Dr. Anjanee Kumar Mishra,** I owe deep gratitude to them for their generous guidance, insightful feedback, invaluable suggestions, and ongoing support. They have mentored me through every stage, from foundational steps to experimental design. Their unwavering support and encouragement have been a steady source of inspiration. Without their dedication and assistance, the goals of this project would not have been achieved.

I would also like to express my deep gratitude to the **Dean** (Research & Development Cell) **Prof. R.S. Kaler**, and **Prof. Sunil Kumar Singla** (Head of the Department of Electrical and Instrumentation Engineering) and **Prof. Mandeep Singh** (Ph.D. Coordinator), for granting me the opportunity to pursue this doctoral research. I am truly grateful to my doctoral committee members, **Prof. Mayank Kumar Rai, Prof. Mukesh Singh**, and **Prof. Surya Prakash**, for their timely and invaluable guidance. I would like to express my sincere gratitude to **Dr. Manoj Badoni** for graciously allowing me to utilize his lab for my work. I deeply appreciate the opportunity and the resources provided, which have been invaluable in furthering my research. My heartfelt thanks also go to **Mrs. Poonam** and **Mrs. Venus Verma** and **Mr. Arvind Kumar Verma**, office staff member for their continuous cooperation, support, and assistance.

I would like to acknowledge my seniors **Dr. Ravi Teja, Dr. Anekant Jain, Dr. Naginder Singh,** and **Dr. Iqbal Singh Brar**. My lab mates and friends **Normdeep Singh,** and **Dr. Sudhanshu Mittal,** for their support and co-operation. I am grateful for my friends from other lab groups **Amninder Singh,** for their endless motivation, support and selfless help.

Special thanks to my friends **Dr. Saudagar B. Dongare, Dr. Saurabh Gupta**, and **Dr. Priti Rohilla,** for always inspiring, encouraging and supporting me during my challenging time. Without their mental support I might not have been able to reach the finish line.

I am deeply grateful to my parents, my grandfather, **Mr. Thakur Shivcharan Singh**, and my father **Mr. Thakur Paramjit Singh,** who always encourage, support and push me to pursue my dreams. I would also like to acknowledge my deepest gratitude to my beloved grandmother, **Mrs. Leela Devi**, and my beloved mother **Mrs. Renu Bala,** for the countless sacrifices she has made throughout her life. Their

unwavering support and encouragement continually uplift me, filling me with positivity and guiding me toward my goals. Words cannot capture the depth of my appreciation for their persistent love, boundless support, and constant blessings. They are, and always will be, my greatest inspiration. I would also acknowledge my little sister, **Ms. Promita Thakur** for their love, mental support and always motivating me to accomplish my dream. Last but not the least, my relatives who always make me feel more fulfilled and complete myself.

I am highly thankful to Thapar Institute of Engineering and Technology, Patiala for providing the PC, Opal-RT, and other equipment.

Besides this, I am grateful to each person who knowingly and unknowingly supported me in the successful completion of this work.

Ajay Singh

DEDICATED

to

My PARENTS

Abstract

In this research work, the design and implementation of various converter topologies integrated with dual energy sources for charging of light electric vehicles (LEVs) are presented. The topologies are broadly classified as unidirectional and bidirectional DC to DC converters. These converters are additionally classified into non-isolated, isolated, and bridgeless types.

This work presents a novel architecture for an on-board charging (OBC) system that integrates dual energy sources, viz., single-phase AC grid and solar PV. The system employs a Modified Single-Ended Primary-Inductor Converter (SEPIC) converter topology to facilitate Light Electric Vehicle (LEV) charging. A diode bridge rectifier is used to convert AC to DC from the AC mains. An improved CC-CV control technique is developed to ensure robust operation of the converter, maintaining unity power factor (UPF) operation. In the event of a grid outage, an integrated solar photovoltaic (PV) system efficiently charges the LEV battery using a Maximum Power Point Tracking (MPPT) converter, adapting to varying environmental conditions. The Modified SEPIC converter manages LEV charging, emphasizing enhanced efficiency, low conduction losses, reduced component count, and high gain. The designed system offers soft-starting features of the BLDC drive in propulsion mode without using any current and voltage sensors on the motor side. The performance of the system is tested by using the MATLAB simulation and validated by a hardware prototype, the results prove the improved performance of the advanced charging methodology by the proposed converter.

This work also proposes an efficient configuration for a solar-powered on-board charging system utilizing a coupled inductor and switched capacitor bidirectional high-gain DC to DC converter with Grid-to-Vehicle (G2V) and Vehicle-to-Grid (V2G) operations. The bidirectional power flow capability of an on-board charger (OBC) benefits utilities and enhances the functionality of light electric vehicles (LEVs). The design of an OBC consists of an active front-end converter (AFC) for bidirectional power flow and unity power factor (UPF) operations. A proposed coupled inductor bidirectional high-gain SEPIC converter and a switched-capacitor bidirectional high-gain ZETA converter are designed and developed for the DC-DC stage. The AFC restricts the THD of supply current within the limits specified in international standards. In the event of a grid outage, an integrated solar photovoltaic (PV) system efficiently charges the LEV battery using a Maximum Power Point Tracking (MPPT) converter, adapting to varying environmental conditions. In addition, the brushless DC (BLDC) motor is used as a traction motor in this work due to its unique features, such as high density, low cost, simple control, etc. The presented LEV with a charging system is simulated in the MATLAB/Simulink platform, and real-time validation is performed using the OPAL-RT platform. The results obtained through both the simulation and real-time prototype indicate the effectiveness of the developed charging schemes with the coupled inductor and switched capacitor converter.

Moreover, it introduces the design and implementation of a high-efficiency bidirectional isolated integrated DC to DC converter intended for the optimal charging and discharging of Light Electric Vehicle (LEV) batteries, utilizing dual power sources. The proposed system supports both Grid-to-Vehicle (G2V) and Vehicle-to-Grid (V2G) operations, ensuring stable performance even during grid voltage disturbances, including sags, swells, and outages. To enhance the robustness of the controller, an advanced mixed second-order–third-order generalized integrator (IMSTOGI) control algorithm is introduced to facilitate reliable operation of the Active Front-End Converter (AFC) under grid disturbances. During normal grid conditions, the converter ensures unity power factor (UPF) and constant current performance. In the event of a grid outage, an integrated solar photovoltaic (PV) system efficiently charges the LEV battery using a Maximum Power Point Tracking (MPPT) converter, adapting to varying environmental conditions. The functionality and power management strategy of the system are validated through real-time experiments, showcasing its effectiveness, reliability, and potential for seamless integration with the smart grids and renewable energy sources. Both simulation and experimental results from an OPAL-RT prototype support the system's economic and operational advantages, confirming the efficiency of the proposed advanced charging methodology with the isolated integrated converter.

Additionally, this work introduces the design and implementation of a modified bridgeless SEPIC AC to DC converter topology with single-stage operations to facilitate LEV charging. The developed system utilizes two energy sources such as solar PV and single-phase grid. In the event of a grid outage, an integrated solar photovoltaic (PV) system efficiently charges the LEV battery using a Maximum Power Point Tracking (MPPT) converter, adapting to varying environmental conditions. The developed bridgeless converter manages LEV charging, with an emphasis on enhanced efficiency, low conduction losses, reduced component count, and high gain. The designed system offers soft-starting features of the BLDC drive in propulsion mode without using any current and voltage sensors on the motor side. The performance of the system is tested by using the MATLAB simulation and validated by hardware prototype, the results prove the improved performance of the advanced charging methodology by the proposed converter.

This research presents an in-depth exploration of advanced DC-to-DC converter architectures integrated with dual power sources, namely solar photovoltaic (PV) systems and single-phase AC grid supply. The proposed solutions, which include modified SEPIC, bridgeless SEPIC, and high-gain bidirectional converters utilizing coupled inductors and switched capacitors, support both unidirectional and bidirectional power transfer—enabling efficient Grid-to-Vehicle (G2V) and Vehicle-to-Grid (V2G) functionality. Advanced control strategies such as Maximum Power Point Tracking (MPPT), Improved Mixed Second-Third Order Generalized Integrator (IMSTOGI), and Constant Current-Constant Voltage (CC-CV) ensure stable and efficient performance under varying grid and environmental conditions. The integration of smart grid capabilities alongside BLDC motor propulsion demonstrates the system's

flexibility. Simulation studies conducted in MATLAB/Simulink, along with real-time validation using the OPAL-RT platform, confirm the reliability, efficiency, and practicality of the proposed converter designs for Light Electric Vehicle (LEV) charging applications.

Table of Content

List of Figures

List of Tables

List of Abbreviations

EVs	Electric Vehicles
ICE	Internal Combustion Engine
BEV	Battery Electric Vehicles
HEV	Hybrid Electric Vehicles
FECV	Fuel Cell Electric Vehicles
EVSE	Electric Vehicle Supply Equipment
AC	Alternating Current
DC	Direct Current
PV	Photovoltaic
MPPT	Maximum Power Point Tracking
PFC	Power Factor Correction
LEV	Light Electric Vehicle
LEVs	Light Electric Vehicles
HEVs	Heavy Electric Vehicles
V2G	Vehicle to Grid
G2V	Grid to Vehicle
OBCs	On-Board Batter Chargers
SAE	Society of Automotive Engineers
IEEE	Institute of Electrical and Electronics Engineers
IEC	International Electro-technical Commission
NEC	National Electrical Code
NFPA	National Fire Protection Association
JEVS	Japan Electric Vehicle Standards
ISO	International Organization for Standardization
CC	Constant Current
CC-CV	Constant Current-Constant Voltage
DCM	Discontinuous Conduction Mode
CCM	Continuous Conduction Mode
PI	Proportional Integral
PHEV	Plug-in Hybrid Electric vehicle
THD	Total Harmonic Distortion
AFC	Active Front End Converter
SEPIC	Single Ended Primary Inductor Converter
UPF	Unity Power Factor
BHGC	Bidirectional High Gain Converter
SCBZ	Switched Capacitor Bidirectional Zeta
IIC	Integrated Isolated Converter

HFT	High Frequency Transformer
DAB	Dual Active Bridge
IGBT	Insulated Gate Bipolar Transistor
MOSFET	Metal Oxide Semiconductor Field Effect Transistor
BBQB	Bidirectional Buck-Boost Quadratic Buck Converter
BBBC	Bridgeless Boost-Buck Converter
CISEPIC	Coupled Inductor Single Ended Primary Inductor Converter
SISEPIC	Switched Inductor Single Ended Primary Inductor Converter
i-BBDC	Interleaved Buck-Boost DC-to-DC Converter
BHSISC	Bidirectional Hybrid Switched Inductor Switched Capacitor
EMI	Electromagnetic Interference
VSC	Voltage Source Converter
CSC	Current Source Converter
PEC	Power Electronic Converter
RB	Regenerative Braking
PP	Propulsion
IMSTOGI	Improved Second Order Generalized Integrators
OSG	Orthogonal Signal Generator
EVCS	Electric Vehicle Charging System
FG	Fixed Gear
SOC	State of Charge
PWM	Pulse Width Modulation
HPF	High Power Factor
CHIL	Controller Hardware in the Loop
RPM	Revolutions Per Minute

List of Symbols

$\mathbf{V_s}$	Single Phase Grid Voltage
$\mathbf{I_s}$	Grid Current
$\mathbf{V_{o.c}}$	Open Circuit Voltage
$\mathbf{V_{s.c}}$	Short Circuit Voltage
$\mathbf{N_s}$	Number of Series Strings
$\mathbf{N_p}$	Number of Parallel Strings
$\mathbf{V_{mpp}}$	MPP Voltage Rating
$\mathbf{I_{mpp}}$	MPP Current Rating
$\mathbf{L_{pv1}}$	Solar MPPT Converter Input Inductor
$\mathbf{C_{pv}}$	Solar MPPT Converter Capacitor
$\boldsymbol{L_1}$	Input Inductor
$\boldsymbol{L_2}$	Output Inductor
$\boldsymbol{L_f}$	Filter Inductor
$\boldsymbol{C_f}$	Filter Capacitor
$\boldsymbol{v_f}$	Filter Capacitor Voltage
$\boldsymbol{C_{DC}}$	DC Link Capacitor
$\boldsymbol{f_s}$	Switching Frequency
$\boldsymbol{C_1}$	Input Capacitor
$\boldsymbol{C_2}$	Output Capacitor
$\boldsymbol{L_{o1}, L_{o2}}$	Coupled Inductors
$\boldsymbol{C_{o1}, C_{o2}}$	Switched Capacitors
$\boldsymbol{D}$	Duty Ratio
W	Watt
V	Volt
A	Ampere
$\boldsymbol{S_1, S_2, S_3, S_4, S_{pv}, S_5, S_6, S_7}$	Switches
$\boldsymbol{D_1, D_2, D_3, D_4, D_a}$	Diodes
Irr.	Irradiance
$\mathbf{I_{pv}}$	Solar PV Current
$\boldsymbol{V_{pv}}$	Solar PV Voltage
$\boldsymbol{P_{pv}}$	Solar PV Power
ΔP_{pv}	Change in Solar PV Power
ΔV_{pv}	Change in Solar PV Voltage
V_{hv}	DC Link Voltage at BLDC Motor Side

V_g	Grid Voltage
I_g	Grid Current
V_{DC}	DC Link Voltage
V_b	Battery Voltage
I_b	Battery Current
I_a	Stator Current
T_e	Electromagnetic Torque
S	Rotor Speed
P_{closs}	Conduction Losses
P_{swloss}	Switching Losses
P_{sdloss}	Diode Switching Losses
$P_{L_{sloss}}$	Input Inductor Losses
$P_{L_{0loss}}$	Output Inductor Losses
$P_{C_{Iloss}}$	Intermediate Capacitor Losses
η	**Efficiency**

CHAPTER-1

INTRODUCTION

1.1 General

127 Electric Vehicle (EV) has a long history and in 1834, the first EV was developed. The first electric car was built by Professor Stratingh in 1835 [1]. In 1847, Moses Farmer built a two-passenger EV. At that time, due to the lack of availability of rechargeable batteries, there will be a failure of EVs. In 1865, Frenchmen Gaston Plante invented the first rechargeable storage battery and in the year 1881 Camille Faure made improvements in the storage battery [1]. In the 19th century, many companies did one's best to design the first electric vehicles, but due to the growing advancement of the internal combustion engine vehicle and certain limitations in batteries, the failure of electric vehicles was imminent by the 1930s [1].

Road vehicles are the popular means of transportation all over the world. These road vehicles mainly employ the internal combustion engine (ICE) [2]. Because of certain advantages (i.e., easy to refuel and longer range), road vehicles are being boosted day by day. The increasing number of ICE road vehicles will lead to the largest sources of air pollution and greenhouse gas emissions, which can be marked as the major cause of climate change and damage to people's health [2]. Due to inflation in petrol/diesel prices and more concern towards the reduction of fossil fuels, greenhouse effects, and the increasing rate of carbon dioxide emissions, automobile industries and customers have to pay attention to investment in environmentally friendly transportation. These types of vehicles use a battery power pack to run the vehicle, thus are superior for zero-pollution emissions.

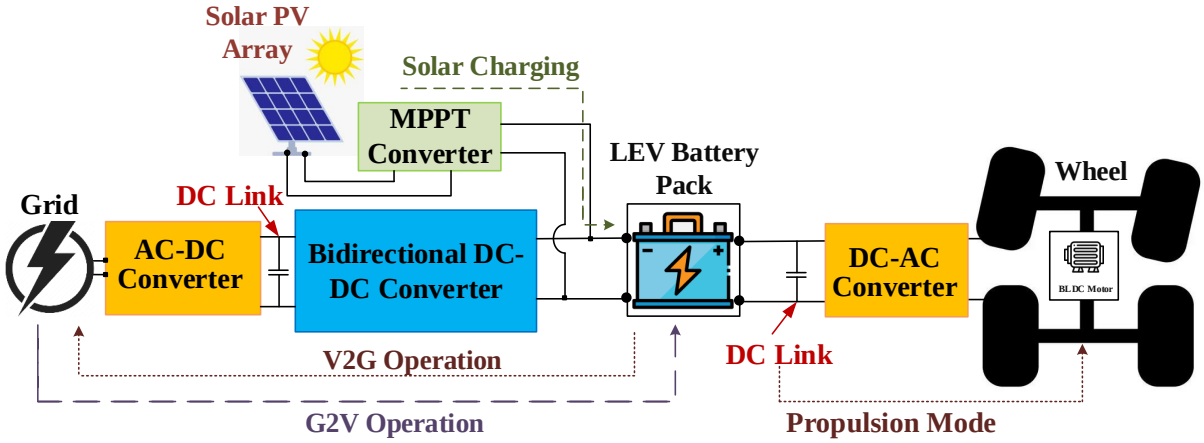

Figure 1.1. Electrical drivetrain of LEVs.

Therefore, electric vehicles (EVs) have gained momentum in both low EVs, i.e., E-scooters, E-bikes, E-carts, E-rickshaws, medium EVs, i.e., E-cars, and heavy EVs, i.e., E-buses, E-trucks

in developing and developed nations [3-4]. The demand for low-voltage powered electric vehicles (EVs) has been increasing in the market over the last few years. Low-voltage powered EVs are considered light electric vehicles (LEVs) [1-2].

But still performance limitations of the LEVs such long charging time, battery degradation, lack of smart charging management, and unregulated multi-unit charging are a matter of concern [3]. Therefore, there is a need to develop a high-performance charging infrastructure to overcome these performance limitations. Moreover, high-performance charging infrastructure required various converter strategies. These strategies must have one-stage charging, two-stage charging, and on/off-board charging. Furthermore, these strategies consist of non-isolated, isolated, bridgeless, and interleaved EV charging strategies. Additionally, the power factor (PFC) correction in compliance with charging standards is a key focus in optimizing the charging process [3]. Basically, the light electric vehicles (LEVs) use more on-board chargers than off-board chargers for vehicle charging. These on-board charging strategies have benefits such as lower initial costs, allowing EVs to charge from any standard electrical outlet or public charging station, space/weight saving portability (i.e., do not have any requirement to carry additional charging devices when traveling), improved charging control, and good safety [4]. The electrical drivetrain of LEVs is shown in Figure 1.1.

Numerous converter strategies include controllers such as improved second-order generalized integrator (IMSTOGI), constant current (CC), and constant current-constant voltage (CC-CV) are used in LEVs system. Furthermore, these controllers utilizes a proportional-integral (PI) controller was discussed in this work. In order to attain a gain (i.e. high gain) in the system, switched inductor converter , switched capacitor converter, isolated integrated converter, and bridgeless converter strategies are employed for both grid-to-vehicle (G2V) and vehicle-to-grid (V2G). Moreover the isolated on-board solar PV array with different converter strategies is used to charge the LEV battery during grid outage. This infrastructure has advantages, like solar-priority charging during grid failure, reducing energy losses, reduces carbon footprint, and can scale with different LEV battery capacities. In addition, brushless DC (BLDC) motor drive system is used to efficiently run the LEV with low electrical and mechanical losses. BLDC motor drive offers advantages, like reduced space requirements, smooth acceleration, low-noise performance, helps in vehicle range per charge, and adaptive driving behavior.

1.2 Types of Electric Vehicles

It is evident that the electric vehicles (EVs) play a major role in minimization of pollution. EVs are considered as the replacement of conventional vehicles which are the main reason for the

carbon radiation in the environmental [4]. EVs are majorly classified as light electric vehicles and heavy electric vehicles as shown in Figure 2. The other types of EVs shown in Table 2 is categorized as battery electric vehicle (BEV), hybrid electric vehicle (HEV), and Fuel cell electric vehicle (FCEV), and carries different salient features [6-8]. These types include various source of energy such as battery, internal combustion engine (ICE), hydrogen fuel cell, ultra capacitor, etc. These energy sources are used by different types of electric vehicles to propel the vehicles.

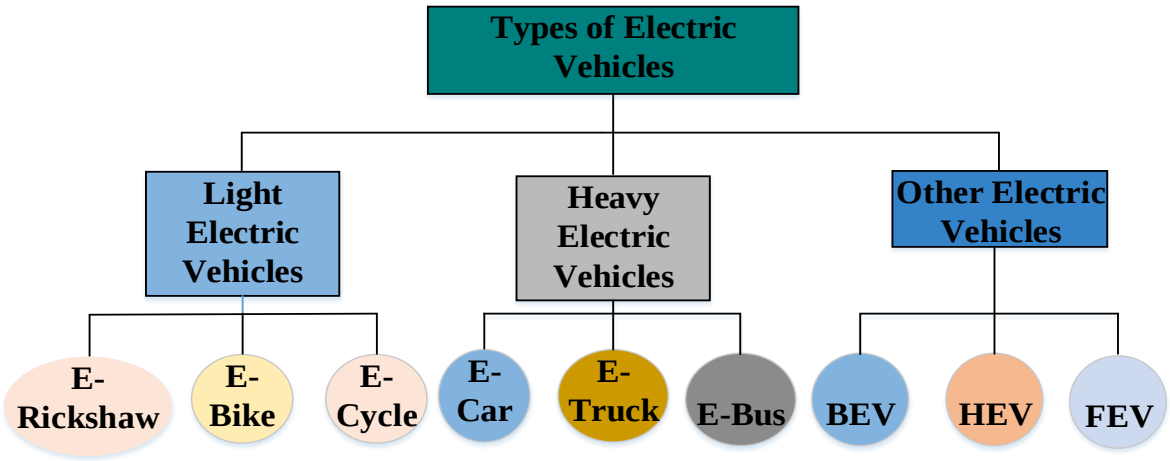

Figure 1.2. Classifications of different types of Electric Vehicle.

1.2.1 Light Electric Vehicles

The light electric vehicles (LEVs) are low voltage or low-speed battery electric vehicles. LEVs consist of electric motor and uses energy storage devices such as battery or fuel cell to propel the road vehicle. LEVs namely E-rickshaw, E-bikes, E-cycle, and skateboards which have a weight of less than 100 Kg [8]. LEVs are powered with batteries having bus voltage ranging from 28 to 168 V. The LEVs are used for short-distance purposes feature with higher power efficiency, smaller size, lesser effective-cost solutions, and are lightweight [9]. Furthermore, the LEVs are sub-divided into low-power LEVs, and high-power LEVs are shown in Table 1.1.

Benefits of LEVs [9]

- They have low operating cost.
- They have zero emission level.
- They can be charged from home power plugs.
- They do not require any specific charging infrastructure.
- They state the use of a low-cost electricity system compared to other expansive gasoline.

Table 1.1. Comparison of low-power and high-power LEVs [9].

Parameters	**Low power LEVs**	**High power LEVs**
Power range	1 to 10 kW	10 to 30 kW
Voltage class	24 to 72 V	48 to 144 V
Distance covered	Short-distance	Short-distance or off-highway EVs
Vehicles categories	E-bike, E-rickshaw, and other E-three wheelers	Light utility vehicles (LUV), E motorbikes, E-forklifts, and golf carts
Speed	< 30 km/h	> 30 km/h
Motor Power	≤ 750 W	> 750 W

Table 1.2. Comparison of LEVs and HEVs [8].

Features	**LEVs**	**HEVs**
Weight	Less than 100 Kg	Higher than 100 Kg
Power range	1 to 30 kW	More than 250 kW
Battery voltage range	24 to 72 V	230 to 900 V
Distance covered	Short-distance	Long-distance

Table 1.3. Other different types of EVs [6,8].

Features	**Battery Electric Vehicles**	**Hybrid Electric Vehicles**	**Fuel Cell Electric Vehicles**
Driving Component	Electric motor	Electric motor and internal combustion engine (ICE)	Electric motor
Energy Source	Battery and ultra-capacitor	Battery, ICE, and ultra-capacitor	Fuel Cell
Dependency on oil	Oil independent	Oil independent	Oil independent
Emission	No	Minor emission	Minor or no emission
Distance range	Short or depend on the battery used	Long	Long
Price	High	Low	High
Problems	Battery high price, distance range, and long charging time	Energy sources management, battery size optimization, and engine size optimization	High fuel price, and non-availability

1.2.2 Heavy Electric Vehicles

The heavy electric vehicles (HEVs) are high voltage or medium or high-speed battery electric vehicles in Table 1.2. The HEVs such as E-cars, E-truck, and E-buses have a weight of more

than 250 Kg with a power range of more than 10 kW, and have a battery voltage class between 230 to 900 V [8]. HEVs are used for long-distance purposes. Furthermore, the other types are classified as battery electric vehicles (BEVs), hybrid electric vehicles (HEVs), and fuel cell electric vehicles (FCEVs) as illustrated in Table 1.3. Here, the BEV involve an electric motor as a driving component and a battery as well as an ultra-capacitor as the source of energy. The BEV show oil independency from conventional fuel and zero emission [6]. BEV covers short distance or range depending on the type of battery being used. The price of BEV is quite high due to high-cost battery use, and consumes more time for charging purposes. The second type of EVs are HEV which uses an electric motor and internal combustion engine (ICE) as driving component and battery, ICE, and ultra-capacitor as a source of energy. HEV show little emission [7]. HEV carry a long-distance range. The price of this is quite low and requires a battery as well as engine size optimization. The third type of EVs is FCEV which use only an electric motor as a driving component and only a fuel cell as the source of energy. FCEV show oil independency and minor emission [6]. FCEV state a long-distance range and high fuel price.

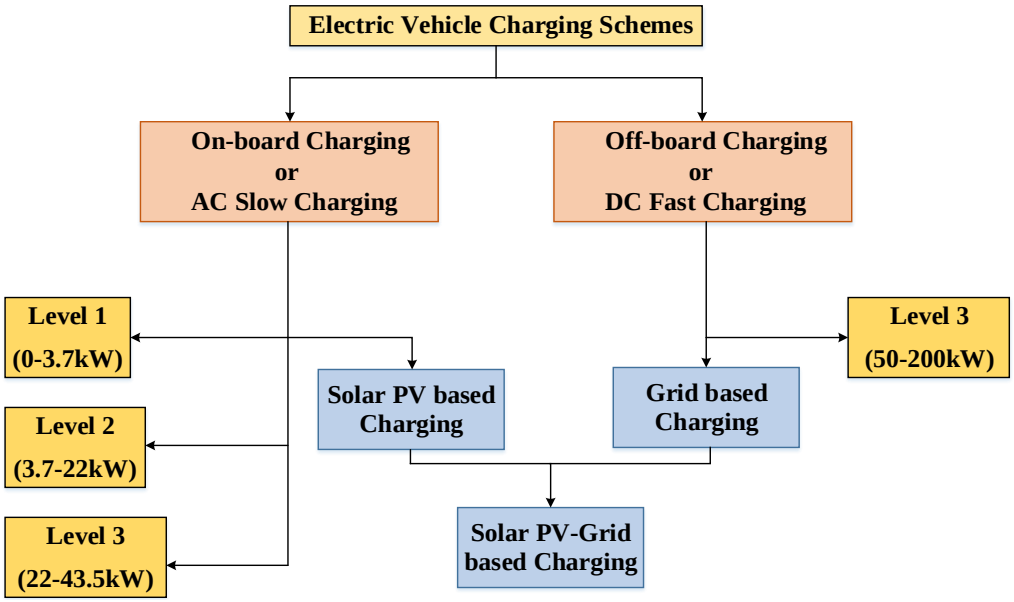

Figure 1.3. Block diagram of charging schemes for an Electric Vehicle.

1.3 Charging Schemes for Electric Vehicles

The classifications of the charging schemes for electric vehicles (EVs) are on-board EV charging scheme, off-board EV charging scheme, only grid EV charging scheme, and solar PV-grid dependent charging scheme [8] as illustrated in Figure 1.3.

1.3.1 On Board Charging Schemes

In the on-board EV charging, converters are set down onboard the road vehicle, and the conversion from AC-to-DC happens on-board within the road vehicle as illustrated in Figure

1.4 [9]. It is named as slow or normal charging, and the onboard EV charging system is classified as Level 1 and Level 2, which is run by AC power [9]. The Level 1 charging practice single phase input voltage 120V RMS with a maximum rated current of 12-20A, and the power which is going to supply is bounded from 1.4 kW to 2 kW [10]. It is suited for home or business usage and does not require any additional infrastructure. The Level 2 charging uses 230V RMS single-phase input voltage with the rated current to 32-80A, and the power which is going to be supplied is bounded from about 8kW to 19.2kW [10]. The charging of EVs with Level 2 is faster than with Level 1 charging of EVs, so most of these makers recommend it as the main charging strategy.

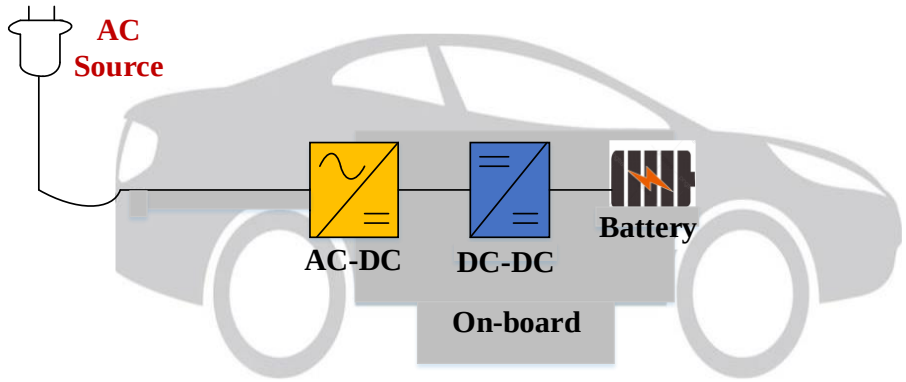

Figure 1.4. Structure diagram of on-board charging scheme for EVs.

1.3.2 Off Board Charging Schemes

In the off-board EV charging, converters are set-down outside the vehicle, and can be positioned in highway road zone and side recharging points of the cities. It is termed as commercial fast charging, consumed less time to recharge the vehicle [10], and a battery management system (BMS) plays the role of is controller to deliver the dc power to the vehicle. The off-board EV charging system is classified as Level 3, which is fed by dc power as illustrated in Figure 1.5 [10,11]. The Level-3 charger is supplied with an input grid voltage grade of 415V RMS, and the fast-charging power rate is 50kW to 200kW [12].

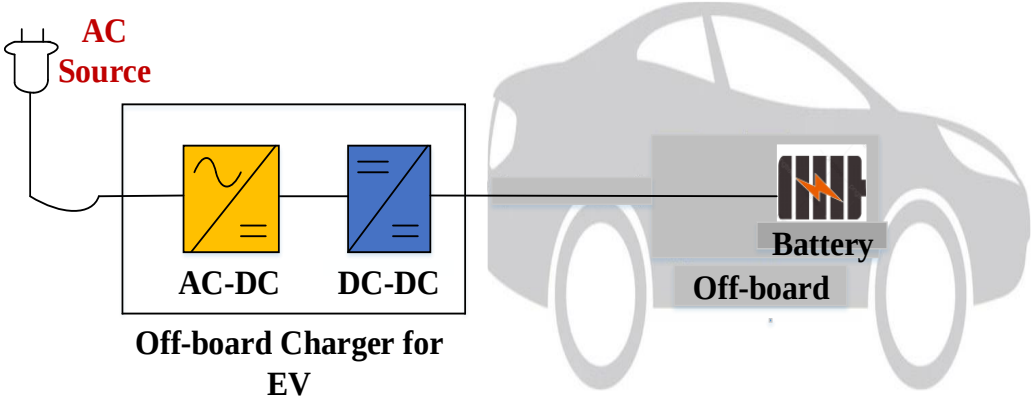

Figure 1.5. Structure diagram of off-board charging scheme for EVs.

Furthermore, the Table 1.4 illustrates the comparison of power level charging for on-board and off-board charging schemes for EVs.

Table 1.4. Comparison of power level charging [12, 13].

Parameters	**Level 1**	**Level 2**	**Level 3**
Voltage range	120 to 230 Vac	240 to 400 Vac	208 to 600 Vac or Vdc
Charger spot	Inside the vehicle or On-board	Inside the vehicle or On-board	Outside the vehicle or Off-board
Phase	Single-phase	Single-phase or three-phase	Three-phase
Utilization	Home and office service	Public and private service	commercial service
Supply system	Outlet	Dedicated charging point	Dedicated charging station
Power range in kW	1.4 at 12 A, and 1.9 at 20 A	4 at 17 A, 8 at 32 A, and 19.2 at 80 A	50 to 200
Charging time in hours	4 to 11, and 11 to 36 respectively	1 to 4, 2 to 6, and 2 to 3 respectively	0.4 to 1, and 0.2 to 0.5 respectively
Vehicles	PHEVs upto 5 to 15 kWh, and EVs upto 16 to 50 kWh	PHEVs upto 5 to 15 kWh, and EVs upto 16 to 50 kWh, and EVs upto 3 to 5 kWh	EVs upto 20 to 50 kWh

1.3.3 Grid-based Charging

In grid charging system, the overall system depends upon single phase grid supply as shown in Figure 1.6. The system charges the LEV battery in one-stage and two-stages, through an attached active front-end AC-DC converter and a DC-DC unidirectional/bidirectional converter. The input grid power containing voltage and current is first perform power factor correction (PFC) and then converted to a stable DC output voltage by using AFC [13-14]. Furthermore, unidirectional/bidirectional with a step-down/step-up strategy is needed to reduce or increase this DC voltage to a regulated DC voltage which is best for light electric vehicle (LEV) battery charging. The LEV battery voltage grades from 48V to 72V. The power electronics system interfaces with different controllers charge the LEV battery in all working states. The grid based charging furthermore categorized as Grid-to-Vehicle (G2V) and Vehicle-to-Grid (V2G) charging [16]. G2V charging is also named as unidirectional charging and will

charge the LEV battery but does not have the functionality to provide power to the grid [16]. Further, V2G charging is also named as bidirectional charging and this charging provides the features of power back to grid.

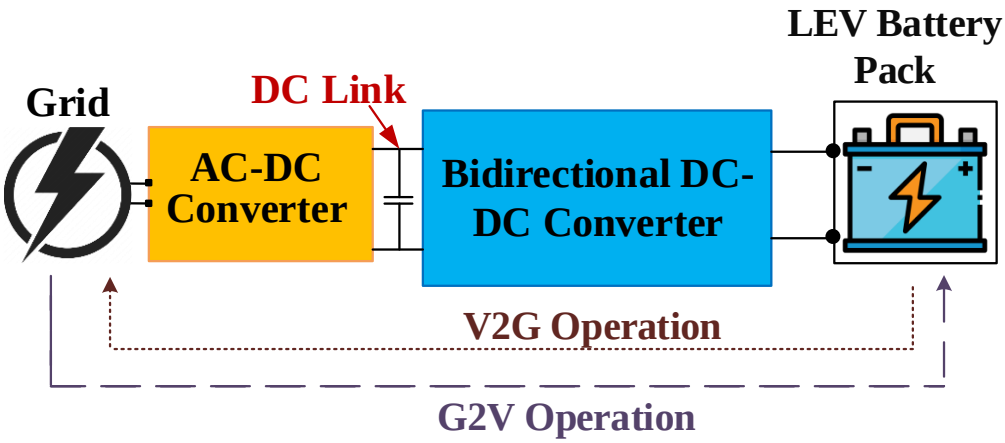

Figure 1.6. Schematic of grid-based LEV charging.

1.3.4 Solar PV-based Charging

In concern with the environmental and fuel economy matter, the best solution is that the EV can be charged daily from a renewable energy source (i.e. Solar PV array) as shown in Figure 1.7. For example, when charging with sourced renewable energy, the user drives the vehicle to work in the morning and overnight. Thus, the vehicle can be charged for the whole sunny day [18]. Solar photovoltaic (SPV) System is looked as an electric vehicle (EV) battery charging resource as well as becoming more affordable strategy and justifying to be more decent strategy than other utilities. In SPV, the solar energy from the sun is converted to electricity by the present PV module circuit. The modules used are made of polycrystalline or monocrystalline strategy. The modules are ordered in series and parallel strings to get PV voltage, current, and power. Further, the MPPT converter is ordered after solar PV array to get the mandatory working voltage and current for the LEV applications.

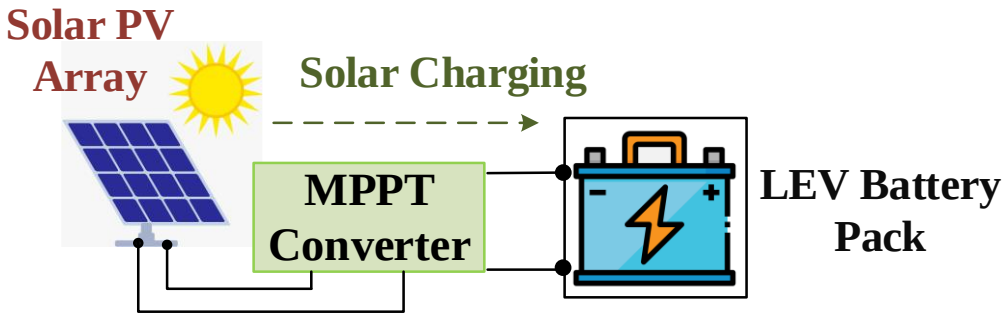

Figure 1.7. Schematic of solar PV based LEV charging.

1.3.5 Solar PV-Grid based Charging

The joint solar photovoltaic (PV) and grid electric vehicle (EV) charging system includes both

the PV panel and grid supply system with feature of continuously EV charging during insufficient solar irradiance by the process of the grid supply [19,20]. The Figure 1.8 show the block diagram of solar PV-grid EV charging system. It has three main components.

MPPT DC-to-DC power converter - It is a DC-to-DC power electronics converter with an in built MPPT strategy which is used to take in the maximal required power from the connected PV array circuit. It is consistently a buck-boost strategy-based converter [20]. The basic operational strategy of MPPT DC-to-DC converter starts as the current and voltage of the PV array circuit are sensed by current and voltage sensors. Then these sensed terms are sent into an MPPT circuit that arranges it and delivers the reference values for the current and the voltage that wanted to be fit by the system.

AC-to-DC Converter - This converter behaves with dual functions such as inversion and rectification. In the case of the AC-to-DC rectification, the AC-to-DC converter is used to arrange the power factor correction between grid voltage and current, and the required regulated DC voltage.

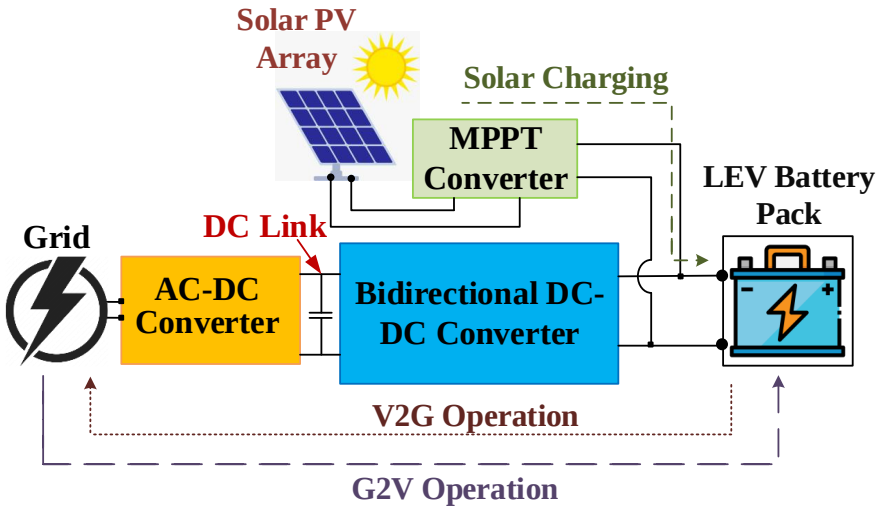

Figure 1.8. Schematic of solar PV-grid based LEV charging.

Bi-directional DC-to-DC Converter - This converter behaves with dual functions such as buck and boost. In the case of the power flow, the DC-to-DC converter is used to arrange the power the LEV battery as well as power back to the grid. In essence, it is noticed that the converter functions as a buck converter at the time of charging and as a boost converter while doing discharging.

1.3.6 Power Management Schemes for Solar PV-Grid Integrated System

It is observed that the solar photovoltaic (PV) tied grid integrated system is powered by a combination of multiple power sources, and required numerous control topologies to handle its operating strategies as shown in Figure 1.9 [25]. This system contains photovoltaic (PV) arrays,

maximum power point tracking (MPPT), bidirectional converters, battery pack, and inverters, which are aimed at controlling the power flow between solar PV arrays, grid, different loads, and EVs battery [26]. In this control process, the controlling units measure the different current and voltage outputs from considered system resources. The measured values are then utilized from the system charging operations. Sometimes, in dark weather conditions, the supply from the solar photovoltaic system is absent. So, the control management algorithm is required to power the corresponding charging system from grid supply [26]. Even in low solar power situations, other power sources are required. Thus, at that time grid system or battery system is used as the primary power source such as grid/battery. Hence, an efficient and least complex power management schemes are needed to take control of several converters used in the photovoltaic (PV)-grid based light electric vehicle (LEV) charging.

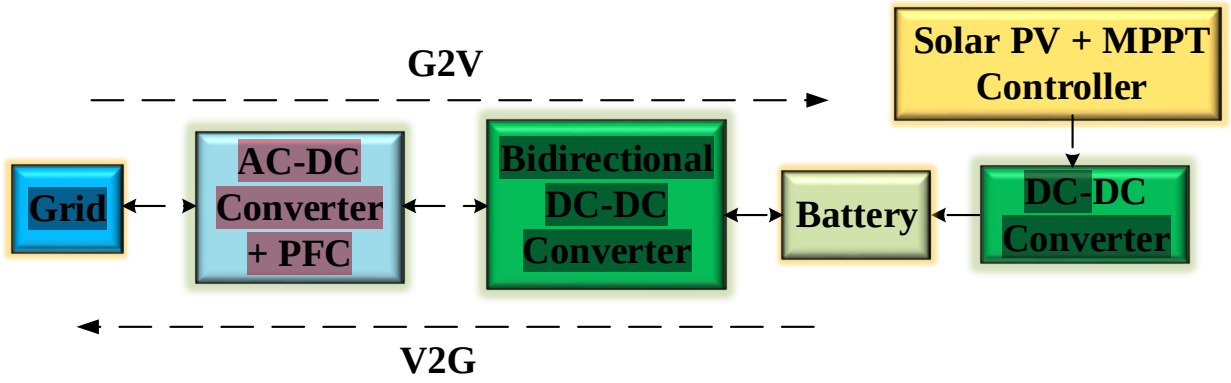

Figure 1.9. Schematic of solar PV-grid power management.

1.3.7 Brushless DC (BLDC) Motor in LEV

The Brushless direct current Motor (BLDC) drive have the good efficiency in all motors available today [28]. It is efficiently observable that advancements in material and design of BLDC motors, with lower price describing the more use of thus motors in many applications [36]. BLDC motor considerately elaborates more benefits, like lengthy working life, higher dynamic response, very good speed versus torque characteristics, greater power speed levels, and operations with low noise. It is noticeable that the BLDC motors are normally constructed with the target of operating in a mode where there is a necessity of frequent stopped with the rotor in an assigned angular position. It is seemed that the effectual efficiency of BLDC motors is normally 80 to 90 ratios, and they can ride at high speeds, as this motor will not use the brushes [36].These features contribute to reliable and energy-efficient performance. With ongoing advancements in motor materials and design innovations, along with reductions in manufacturing costs, BLDC motors are becoming increasingly common in a wide range of applications. One of the most prominent areas of adoption is in light electric vehicles (LEVs),

such as electric scooters, e-bikes, and small electric cars. In these applications, BLDC motors are favored for their high efficiency, low maintenance requirements, and excellent control capabilities. The ability of BLDC motors to deliver precise speed and torque control, even under variable load conditions, makes them ideal for urban transportation systems where frequent starts, stops, and speed variations are required. Additionally, the compact form factor and high torque density of BLDC motors allow for space-saving integration into small vehicle designs. Their silent operation also enhances user comfort, which is especially important in personal mobility devices. As a result, BLDC motors have become the preferred choice in the propulsion systems of many modern LEVs as shown in Figure 1.10 [37].

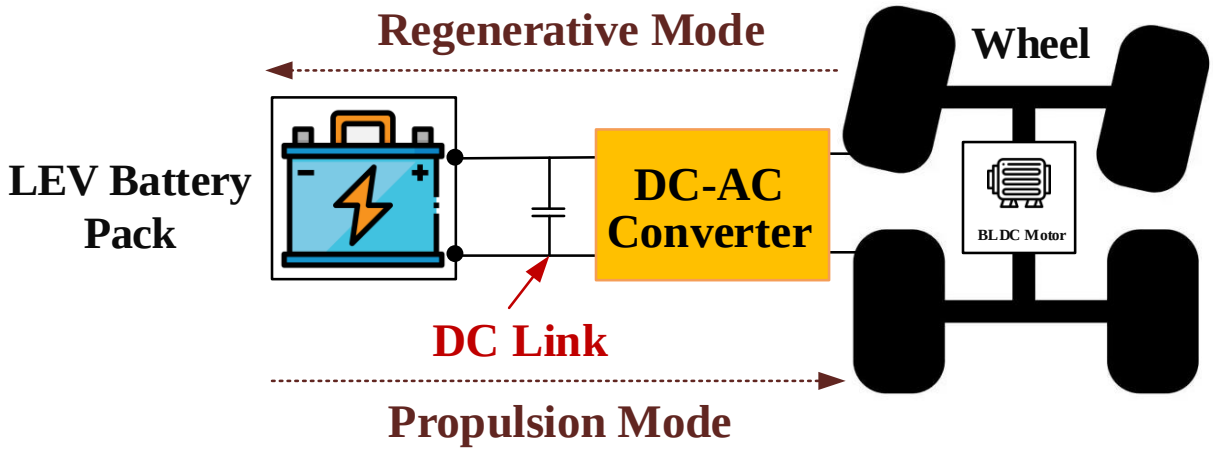

Figure 1.10. Schematic of BLDC in LEV.

Table 1.5. Different charging standards used for EV charging [27].

Purposes	**Standards**
For the electric vehicle quick DC charging	IEEE 2030.1.1
Standards regarding power quality	IEEE 519-2014
Regarding power quality issues	IEC-1000-3-6
For the EVs Charging systems	NEC 625/626
Regarding safety	NFPA 70E
Regarding equipment maintenance	NFPA 70B
For the EVs charging plugs	JEVS C601
Regarding batteries	JEVS D701
Regarding battery system propulsion	SAE J-2929
Solar Integration Standards	IEC 62933
Vehicle-to-Grid / Bi-Directional Charging	ISO 15118

1.4 Electric Vehicle Charging Standards

It is noticeable that a lot of electric vehicles (EVs) charger international standards are well

organized by a experts and universal teams. The purpose of organization is to get the safety problems, to get the reliability as well as to get relief from interoperability problems of EV chargers. The typical ac on-board chargers are mentioned as level-1 (120 V) and level-2 (240 V) chargers as per SAEJ1772 standards [37]. Table 1.5. shows the different charging standards used for EV charging [37].

1.5 Organization of Chapters

This thesis is structured into several chapters to systematically present the work carried out during the research period. Each chapter is designed to build upon the previous one, ensuring a logical flow of information and a comprehensive understanding of the topic. The content is organized to cover the theoretical background, system design, implementation strategies and controls, and the results obtained through simulation or experimentation. A brief overview of each chapter is provided below to guide the reader through the structure of the study.

CHAPTER 1: INTRODUCTION

In this chapter, background along with introduction of EVs, introduction to light electric vehicle charging, different types of EVs, different LEV charging schemes such as grid based LEV charging, solar PV based LEV charging, grid-solar PV based LEV charging, power management schemes for solar PV-grid integrated system, brushless DC motor drive system in LEV, charging codes with standards is presented. This section represents a comprehensive overview of LEVs charging system.

CHAPTER 2: LITERATURE REVIEW

In this chapter, the literature review for works related to proposed methodology is instigated. Review is based on the non-isolated converter, isolated converter, bridgeless converter, grid based LEV charging, and both grid-solar PV based LEV charging which is the combination of single phase grid, on-board solar PV, and light electric vehicle. It analyses the research gap, aim of the research, objectives of research and discuss the organization of the research.

CHAPTER 3: CLASSIFICATIONS AND CONFIGURATIONS OF LIGHT ELECTRIC VEHICLE CHARGING

In this chapter, different classifications of LEV charging systems, highlighting their infrastructure designs, strategies, controls, and power management are as following. These systems are typically categorized into unidirectional converters based LEV charging and bidirectional converters based LEV charging. Each classification supports specific different charging schemes. Additionally, the control strategies involved various pulse generating methods that ensure good efficiency, safety, reliability and growth potential in managing power

distribution across the charging network.

CHAPTER 4: SOLAR POWERED ON-BOARD LEV UTILIZING NON-ISOLATED HIGH GAIN CONVERTER

In this chapter, developed work is on control unidirectional charging from grid to LEV battery through diode bridge rectifier (DBR) and modified DC-to-DC converter as well as on-board solar-based charging during grid outage. Also, it focuses on reducing the number of overall drive train elements and efficiently work on the power management of all operational modes.

CHAPTER 5: SOLAR POWERED ON-BOARD LEV UTILIZING NON-ISOLATED HIGH GAIN CONVERTER WITH G2V AND V2G CAPABILITIES

In this chapter, a solar-powered bidirectional OBC based on the high gain coupled-inductor and switched capacitor converter for a BLDC motor-driven LEV is discussed. The converters strategies has features of both grid-to-vehicle (G2V) and vehicle-to-grid (V2G), as well as charging via solar PV array during grid outage. Furthermore, this section categorized as: solar powered on-board charging system utilizing coupled inductor high gain SPEIC converter with G2V and V2G capabilities and solar powered on-board charging system utilizing high gain switched capacitor ZETA converter with G2V and V2G capabilities.

CHAPTER 6: SOLAR POWERED ON-BOARD LEV UTILIZING ISOLATED HIGH GAIN CONVERTER WITH G2V AND V2G CAPABILITIES

In this chapter, an isolated integrated converter with dual power sources (i.e. single-phase grid and solar PV), employing a BLDC (brushless DC) motor drive.

CHAPTER 7: SOLAR POWERED ON-BOARD LEV UTILIZING BRIDGELESS CONVERTER

In this chapter, a bridgeless converter with dual power sources (i.e. single-phase grid and solar PV), employing a BLDC (brushless DC) motor drive. It employ modified bridgeless SEPIC strategy which perform grid voltage and grid current power factor correction in both LEV battery charging mode.

CHAPTER 8: CONCLUSIONS

In this chapter, the conclusion part of the research and the future scope is presented.

CHAPTER-2

LITERATURE REVIEW

2.1 General

One of the primary areas of research has been the investigation of charging strategies tailored specifically for light electric vehicles (LEVs). Several charging strategies have been proposed and tested, including non-isolated, isolated, and bridgeless power converters, each with unique advantages and challenges. These strategies are evaluated based on their efficiency, cost, size, and ability to handle varying input conditions from sources like solar photovoltaic (PV) arrays or the electrical grid.

The integration of renewable energy sources, such as solar PV systems, into LEV charging infrastructure has added a new dimension to research, aiming to create sustainable and off-grid charging solutions. This integration involves complex power management strategies that coordinate energy flow between the PV system, battery storage, LEV charging circuits, and the grid. Efficient power management not only maximizes the use of clean energy but also ensures stability and reliability during charging, especially under variable solar conditions and fluctuating load demands.

Additionally, the role of motor drives in LEVs, particularly brushless direct current (BLDC) motors, has attracted significant attention. The motor control strategies directly impact the energy consumption and battery life, which in turn affect charging requirements and cycle. Researchers have explored various drive and control schemes that complement advanced charging methods, further enhancing the overall system efficiency.

Factors influencing LEV charging performance are diverse and include battery chemistry and state-of-charge, converter strategy, different charging current levels, and the integration of the renewable power source. These factors must be carefully considered to develop efficient charging protocols that balance charging-discharging operations with battery safety and longevity.

In summary, extensive research in the field of LEV charging has focused on advancing safe, reliable, and fast-charging strategies and integrating renewable energy sources to promote sustainable transportation solutions. By examining a broad range of charging topologies, power management techniques, and motor drive considerations, researchers aim to deliver efficient, reliable, and user-friendly charging systems that can support the growing demand for LEVs

worldwide. This body of work lays the foundation for future innovations in LEV infrastructure and contributes significantly to the transition toward greener urban mobility.

2.2 Literature Survey

Researchers have presented extensive work on the charging of light electric vehicles (LEVs), strategies for the development of LEV charging, and various factors that affect the results. Different LEV charging strategies are studied to represent safe, reliable, and fast-charging characteristics. The various converter topologies proposed by different researchers and the work done by them have been listed below as follows.

2.2.1 Non-Isolated Topology for Light Electric Vehicles

Sayed *et al.* [38] had presented an overview of unidirectional non-isolated power factor correction (PFC) converters for short and long-distance EVs. The authors provide two PFC converters classifications such as the fundamental PFC topologies and the modified PFC topologies and show interest in the EV charging infrastructure with Level 1 and Level 2 with a single-phase unidirectional supply. The authors explained that for the purpose of maintaining the power quality of the ac grid to the charging standards while charging the vehicle from the grid, also said that an on-board power factor correction (PFC) dependent power converter of high-power factor, with low harmonics, and high efficiency at changeable operating conditions is needed with high power density and energy density for improving system losses, its cost, and system size consideration.

Saikumar *et al.* [39] had presented a dual input single-output (DISO) non-isolated DC-to-DC power converter strategy with greater step-up voltage magnitude for grid independent hybrid electric vehicles (GIHEVs). The authors explained that this converter is valued by the well-being of capacity to incorporate diverse sources with different power as well as voltage levels, work in a lesser and little bit or moderate power runs, the unmatchable and high output voltage magnitudes.

Suresh *et al.* [40] had proposed the single-stage four-port buck-boost converter for EV, with lesser parametric counts and a simplified system control strategy that describes the converter as more reliable and lower or cost-effective.

Lin *et al.* [41] presented a study of a simple circuit structure non-isolated bidirectional DC-to-DC strategy-based power converter and said that the given converter can work in a wider voltage-conversion range than the conventional converter, and said that the voltage stresses on the switches are half of the high-voltage side. The authors proposed control topology is easily implemented.

Akar *et al.* [42] had presented a bidirectional strategy-based non-isolated multi-input power converter for EV, which carries the energy storage systems (ESSs) with different electrical operational characteristics. The authors compared the proposed converter strategy with its counterparts concerning various parameters, and the converter has the capability to manage the power of ESSs by permitting active power-sharing.

Abbasi *et al.* [43] had proposed a new family of non-isolated step-up and step-down and step-up switched-capacitor (SC)-based DC-to-DC converters strategy and said that the given strategy-based power converters can present greater voltage gain by having a lower duty cycle in contrast to the other converter strategy.

Banaei *et al.* [44] had presented a transformer-less buck-boost DC-to-DC converter strategy, while utilizing only one switch, which results in decreasing power switch conduction losses and improving efficiency. The authors noticed that the step-up voltage gain of the presented buck-boost converter is higher than that of the classic boost, buck-boost, CUK, ZETA, and SEPIC power electronics converters.

Tofoli *et al.* [45] had presented an overview on non-isolated high-voltage step-up DC-to-DC strategies depending on the power electronics boost converter. In the literature, the authors presented several strategies where the netted output voltage can only be stepped up by increasing the power converter duty cycle.

Varesi *et al.* [46] had outlined an improved non-isolated bidirectional multiple-input DC-to-DC converter that operates as the buck operation, boost operation, and buck-boost operation converting modes for both charging and discharging operations. The authors tested the simulation results to analyze the corresponding results.

Cheng *et al.* [47] had presented an overview of soft switching strategies for non-isolated DC-to-DC power converters and summarized all the new soft switching strategies, their research ideas, and guidance on the discovery and application of soft switching converters.

Mohammadi *et al.* [48] had presented a group of soft-switching bidirectional power converters with an enlarged zero voltage switching range, and all the semiconductor parts are soft-switched over a large variation of power converter operating points. In order to certify the feasibility of the presented converter strategy, the authors tested the 150-W prototype converter for an extensive grade of the power converter operating field.

Sagar Bhaskar *et al.* [49] had explained the overview of various unidirectional multistage DC-to-DC power converter families and conclude that the presented strategies, time and time, attach with switched inductor and many boosting strategies to improve the system administration for various applications.

Anzola *et al.* [50] had explained a partial power converter for an EV fast charging station and said that the proposed power converter only processes a reduced percentage of the power consumed by the load.

2.2.2 Isolated Topology for Light Electric Vehicles

Choi *et al.* [51] had presented an interleaved isolated PFC strategy-dependent power converter module for three-phase EV chargers which is composed of two half-bridge voltage-driven isolated PFC power converters with parallel-input-series-output system formation, which is worked in interleaved discontinuous conduction mode (DCM).

Prasanna *et al.* [52] had presented a bidirectional single-phase single-stage AC-to-DC power converter for EV charging class and explained that a compact and lightweight converter design is needed for onboard chargers. The power converter proposed by the authors has current-driven halfly-bridged power converter with ZCS on the primary side and fully bridged power converter with zero current turn ON at the secondary side. The authors also explained modulation topology to function the power converter in all four quadrants of operation, in order to get all the devices soft switching.

Prasanna *et al.* [53] had presented a zero-current-switching (ZCS) current-fed half bridged isolated dc-to-dc power converter and explained that the defined power converter has several low voltage high current applications such as grid-ended DC-to-DC power conversion for fuel cell and PV inverters, system energy storage, bidirectional power converters for fuel cell vehicles, etc.

Xuewei *et al.* [54] had presented a zero-current commutated soft-switching bidirectional current-fed full-bridge isolated strategy-based DC-to-DC power converter and explained that the switching losses are decreased significantly owing to zero-current switching of the primary system side and zero-voltage switching of secondary-side systems.

Lee *et al.* [55] had presented a DC-to-DC strategy getting greater efficiency of over 97% for EV fast chargers, and summarized various advantages based on this strategy, and explained that this strategy is very feasible for EV fast charger applications.

He *et al.* [56] had presented an overview of 1kW isolated DC-to-DC power converters for electric vehicle charging systems in both directions. The authors discussed the converter topologies, operating principles, and design methodologies, and compared converter performances.

Tang *et al.* [57] had presented an isolated two-output DC-to-DC resonant power converter, which processes the capability of providing electrical power from high voltage traction

batteries to the grid for vehicle-to-grid (V2G) modes of applications and can affiliate low voltage DC loads.

Vaishnav *et al.* [58] had presented a single-stage isolated bidirectional high-frequency link converter for both charging purposes and as well as vehicle-to-grid applications of PHEV that has merits such as less part count, and reduction in size, light-weight, and switching losses. The authors presented steady-state analysis along with simulation results.

Koushki *et al.* [59] had presented an isolated single-stage bidirectional AC-to-DC power converter for an EV battery charger. The authors use only six switches and discussed that low parametric count in the circuit results in lesser cost and volume.

Thasni *et al.* [60] had developed a single-phase isolated converter power factor correction (PFC) based strategy for LEV charging which is done by the duty ratio modulation strategy and by the strategy of interleaving. The authors protect the battery with a constant current or constant voltage mode and power factor correction is nearly about to one with lesser output voltage and ripples.

Nassary *et al.* [61] had presented an overview of the single-phase isolated strategy based on bidirectional AC-to-DC power converter for EV battery charger and the authors focus on bidirectional strategies based on single-stage and two-stage categories and prove that the effectiveness of the bidirectional in the battery charger to increase the grid system power quality.

Nazi *et al.* [62] had presented one phase bridgeless one-stage battery charger by excluding electrolytic capacitors for light electric vehicles. The authors proposed the control method to simultaneously control the output voltage and current as well as to unify the input power factor. The tested results showed that the charger is simple, has a high-power density, high efficiency, and large power factor, and the authors noticed that the defined battery charger is a good perspective to be used in LEVs.

2.2.3 Bridgeless Topology for Light Electric Vehicles

Kushwaha *et al.* [63] designed an enhanced isolated bridgeless converter for EV battery and analyzed it in discontinuous mode. The authors explained that the planned design of the charger provides an advantage of improved productivity by reducing the number of components by integrating Cuk and SEPIC converters in a single-stage converter. The authors said that by lowering the system size and cost of the charger, the output power converter further smoothens the output current at the Cuk converter side for both cycles and appears to be a good solution for cost-effective EV system chargers.

Singh *et al.* [64] had proposed an EV battery for supplying the input current at a unity power factor based on a single-stage bridgeless zeta converter with small harmonics alteration by maximizing the real power consumption in the circuit. The authors explained that the defined power converter efficiency is best suitable for charging the battery and has improved qualities such as thermal utilization of the power switches, less conduction loss, a simple system control strategy, and low ripples in the output. Thus, the proposed converter decreases the charging profile and time of the battery.

Gupta *et al.* [65] had presented a high-power factor AC-to-DC power converter having a universal supply voltage grade that has been examined for charging of LEVs. The authors said that in comparison to the Luo converter a constructive output has been obtained for the present converter and thus offers a minimum volume of magnetic components and low device count. On the supply side, an efficient quality profile is maintained with low harmonic distortions and high-power factor correction (PFC).

Dixit *et al.* [66] had designed a buck-boost strategy-derived power converter that works as a possible front-end power converter for the onboard charger. The made power converter helps in lowering the cost due to the reduced number of sensors and components. For the purpose to get PFC for large input voltage variation, the converter is made to function in DCM. The converter needs high-rated current switches because of DCM operation. The soft turn-on of switches, reduced number of sensors, low control complexity, lower voltage stress, and reduced control complexity of the converter overcome the disadvantage of high-rated switches.

Kushwaha *et al.* [67] had presented the latest bridgeless Cuk charger-based EV battery charger with a high system power factor as well as its efficiency designed and developed. The authors said that the charger incorporates a smaller count of power devices working over one switching cycle, which decreases the extra conduction loss incurred by a diode bridge rectifier of the conventional charger. The designed charger gives a sinusoidal current configuration from the ac supply and the total harmonic distortion in the system supply current is decreased to the foundations specified by IEC 61000-3-2 instructions.

Singh *et al.* [68] had presented an isolated bridgeless SEPIC power converter-based battery charger strategy and explained the merits of low conduction losses with current-dependent conduction through a smaller number of counts over a single switching interval. The input-based current shows a unity power factor operation over the total charging duration. The Test results done by the authors showed adequate power factor correction (PFC) based on charging in a steady-state and under all the lines and loads.

Wang *et al.* [69] had presented an onboard PEV battery charger and explained that an

interleaved boost strategy is given in the first stage for power factor correction (PFC) and to lessen total harmonic distortion (THD).

Musavi *et al.* [70] had presented a bridgeless boost PFC strategy for application in the front-ended ac to dc power converter in PHEV system battery chargers. The authors explained that the experimental results state a power factor greater than 0.99, THD lesser than 5% from half load condition to full load condition, and a peak efficiency of 98.9%. The designed power converter is compliant with the EN 61000-3-2 standard.

Kumar et al. [71] had presented a two-stage battery charger system with an interleaved without bridged PFC strategy-based AC-to-DC power converter for better input current management or shaping compared to conventional strategies. The authors said that the output shows a peak efficiency of 94% with 0.9997 PF and input current THD of 4.76%. The power converter also works for a broad range of input voltage starting from 85 V -135 V. This solution is suitable for LEV battery chargers rating 1 kW-3.3 kW.

Gupta *et al.* [72] had presented a without bridged switched inductor cuk converter (BSIC) strategy-based system charger with only one stage to provide a one-phase one-stage transformer less charging solution for the LEVs. The authors tested and verified the charger operations during line and load regulation.

2.2.4 Solar PV Based Light Electric Vehicles Charging

Kabir *et al.* [73] had presented a photovoltaic (PV) powered station armed with an energy storage system (ESS), which is supposed to be suitable for allocating changeable charging grades to distinct EVs to fulfill their system demands inside their declared deadlines at least possible price.

Verma *et al.* [74] had implemented a solar photovoltaic (PV) array joined grid-connected domestic EV charger system which serves the requirement of an EV, home loads, and the ac grid. The authors explained that the charger is capable of providing unbroken charging and power to home loads and in the non-presence of PV array grid operation mode is used. Also, explained that the charger has synchronization and seamless operating switching control. In this manner, the charger automatically connects and disconnects from the grid not annoying the EV charging system and home supply. The authors also explained the capability of the proposed charger to operate as an active power filter in order to get the unity power factor (UPF) operation and grid current total harmonic distortion (THD) upto 5%.

Shariff *et al.* [75] had implemented a new solar-connected level 2 EV charging station which is managed by a Type 1 vehicle connector. The authors construct the proposed strategy in

MATLAB/Simulink in order to notice the parametric design features. The authors developed the hardware setup and tested the power factor correction (PFC) under the steady-state condition, by referring to the input of 3 kW, 230 Vrms, and 50 Hz system frequency, as well as to obtain a buck power converter output of 48 V DC. Further, the selected case site of 6.4 kW solar PV, located at the Centre of Advanced Research in Electrified Transportation building parking area in Aligarh Muslim University campus is considered by the authors. Also, the circuit of the controller is simulated in PROTEUS software, and a prototype circuit design is been examined in the lab. The authors performed the study on a sharp sunny day on a 10-kWh lithium-ion battery pack at the standard test situation of the PV panel.

Haritha *et al.* [76] had presented an EV battery charging strategy with solar PV array based multipurpose EV charger. The authors managed the operation of the battery charger in such a manner that it carried both the features, either supplied by photovoltaic (PV) power or by a grid. The authors implemented vehicle-to-grid operation for improving the stability of the grid during peak load hours, as well as the vehicle-to-home islanding mode of operation. The authors provide the proportional integral (PI) control system for the regulation of the DC-link voltage from the bidirectional battery converter and it works in buck mode during the charging time of the EV battery and during the discharging time, it works in boost mode. With the use of a voltage source converter (VSC) and the grid current THD which lies within the IEEE 519 standard, the proposed charging system works as an active power filter. Further, the authors tested the various operational modes with the use of MATLAB/Simulink.

Wu *et al.* [77] had presented a non-isolated three-port power converters strategy for the implementation of only a stand-alone renewable source mechanism, which is noticed as a dual-output power converter in reference to the primary source and as a dual-input power converter in reference to the load. The author's examined strategy is tested with given experimental results and verified that the designed strategy can achieve a high system efficiency and is better for applications of stand-alone renewable power systems.

Singh *et al.* [78] had presented a multifunctional power electronic converter (PEC) employing grid joined solar the PV for the system charging strategy of plug-in electric vehicles (PEVs) as well as presented the tested results for all modes. The authors explained that the proposed strategy involves charging, propulsion (PP), and regenerating braking (RB) operating mode of the vehicle, and in-vehicle standstill condition, it is explained by the authors that the system battery can be charged by grid or by both grid and solar PV system. Furthermore, the authors said that the battery can also be charged through regenerating braking operation by employing the kinetic energy of vehicle wheels. The authors said that the in PP and RB modes, the

designed power converter strategy operations work as a both conventional boost power converter and a conventional buck power converter, respectively.

Venkatramanan *et al.* [79] had proposed a simplified linear model of battery fed by a photovoltaic (PV) source for a buck converter. The authors proposed converter strategy includes maximum power point tracking (MPPT) control schemes which are normally used in either dual-operating mode or only standalone PV resource applications. The authors verified the test on a 1 kW hardware prototype and see the accuracy of the considered analytical transfer functions and the working performance of the PV-dependent charger system.

Shukl *et al.* [80] had proposed an electric vehicle charging system (EVCS) that depends on solar PV generation which has the capability of both charging and discharging during base as well as peak load periods. The authors utilized a fractional Lagrange filter for improving the power quality of the distributed network, and the grid currents are noticed in covenant with the IEEE-519 standard. The authors tested the performance validation of the system during various weak grid conditions.

Hassoune *et al.* [81] had presented a smart strategy to load a lithium-ion battery in an electric vehicle charging system (EVCS) through multiple optimization methods. The authors proposed a strategy intended to institute an equilibrium between the three different energy sources including the consideration of the grid. Furthermore, the tested EVCS strategy through various system charging scenarios to feed a battery is explained by the authors.

Lenka *et al.* [82] had presented a convenient system managing strategy for grid-connected photovoltaic (PV) powered multifunctional electric vehicle chargers to charge the EVs as well as to improve grid PQ. The authors verified the capability of the designed system control mechanism in grid PQ improvement under every operating situation as well as including nonideal grid voltage situations. The authors explained that the proposed charger controller has the capability to manage grid voltage and current THD under a set deadline by the IEEE-519 standard.

Hu *et al.* [83] had designed an EV driving system having a union of photovoltaic (PV) panel and switched reluctance motor (SRM) to decrease the cost of the system and to overcome the range of using EVs. They have connected PV panel, SRM, and battery by a tri-port converter, flexible energy flow for these power converters is attained by six working modes. They have also developed a noel-grid charging topology not requiring any external power sources thus increasing solar energy utilization. The designed PV-fed EVs are better technology than the present ICE vehicles providing a reasonable solution to lower the costs and CO_2 emissions of EVs.

Ram *et al.* [84] had presented a detailed study on renewable energy-based electric vehicle (EV) charging techniques categorizing the AC and DC EV charging systems. Of the various charging technique present constant voltage and constant current charging method is appropriate for rapid EV charging. Its high life cycle, safe working operation, small self-discharge grade, and high system energy density of lithium-ion battery make it suitable for EV charging and its great benefits can be obtained only when driven by renewable energy sources thus limiting the CO_2 emission caused due use of earlier transportation vehicles. In this, they also discussed a number of charging topologies like unidirectional, bidirectional, and integrated chargers. Thus, the performance of the electricity grid can be improved by vehicle-to-grid integration.

Singh *et al.* [85] had presented an onboard power integrated power converter that decreases the parametric count for EVs. The authors explained that the proposed strategy can involve a joint solar PV and a grid energy source as input for battery charging. The authors said that during the day, solar PV is used for battery charging, and an overnight grid system is used for battery charging. They removed the sensor requirement by using the strategy for power factor correction (PFC), and the tested results for the 1-kW setup based on the proposed strategy are obtained by the authors.

Acharige *et al.* [86] had presented a solar photovoltaic (PV) dependent electric vehicle (EV) charging strategy that has the capability of charging the battery storage system with the vehicle-to-grid working operation to support the power grid. The authors explained that the PV-based EV charging strategy has a function like either EV battery charging or discharging via a bidirectional DC-to-DC power converter, according to the availability of PV power and grid requirements. In order to get maximal power under changing irradiance and temperature, they have used SEPIC DC-to-DC power converter is controlled with MPPT. From the verified results the authors noticed that the proposed system controllers could take care of the system power flow under various transients and charge or discharge battery currents, under all system verified situations.

Premchand *et al.* [87] had presented a solar photovoltaic (PV) based EV charging circuit design for the grid-to-vehicle and vehicle-to-grid system operations. The authors obtained the solar PV characteristic such as the current-voltage and power voltage while testing the PV array under standard test conditions. They have presented a passive-filter components design strategy, and here they designed solar PV to obtain 200V output voltage which is further stepped to 400V with the use of a boost converter. Furthermore, they filtered the output voltage and then step down on report to battery charging requirements by using a buck power

converter. The authors said that the system PR controller is better for battery charging. They said the SOC is noticed during charging and discharging working modes and the voltage THD or grid current follows IEEE 519 standards.

2.2.5 Power Management Strategies for Solar PV-LEV-Grid Integrated Systems

Badawy *et al.* [88] had proposed a strategy for the management of power flow in electric vehicles (EVs) charging. The proposed model is based on the consideration of a grid-connected solar photovoltaic (PV) battery system. The authors said that the aim of the proposed strategy is to help the penetration of the solar photovoltaic/ battery system into the grid. Also, this proposed strategy is targeted to prop up the increasing requirements of the fast electric vehicle (EV) charging rates. The proposed strategy works on two stages. In the first one, particle swarm optimization (PSO) is used as a prediction layer, in an offline manner. In the second one, dynamic programming (DP) is done as a reactive management layer, in an online manner. Based on simulation results, the authors explained the benefits of adopting the proposed strategy.

Chen *et al.* [89] had designed a strategy for smaller-sized solar-based electric vehicles (EVs). In this design, the authors used a battery, super-capacitor, and solar photovoltaic (PV) panel, with the purpose of getting a highly efficient power system for EVs. The authors' design consists of a power converter and adopts a fuzzy control strategy to cope with the power flow of the system resources.

Biya *et al.* [90] had designed a battery energy storage system and electric vehicle charging stations integrated with solar power. An additional grid support is also used for continuous supply in the charging stations not becoming an extra burden to the grid. For the optimal power management between battery energy storage system (BESS), grid and solar with electric vehicles (EVs) in charging station an effective method of charging station with proportional integral derivative (PID), current control strategy, and maximum power point tracking (MPPT) is designed. The proposed method of charging station is framed and endorsed in MATLAB by considering the dynamic charging needs of EVs.

Ray *et al.* [91] had presented a solar photovoltaic-based smart electric vehicle charging system. The proposed strategy has the capability to allow power to move in bidirectional mode. The authors considered the common direct current (DC) connection voltage, state of charge (SOC) for the electric vehicle battery, and loading condition which determines the corresponding mode of operations of electric vehicle charging.

Rosario *et al.* [92] had presented an integrated structure that describes electric vehicle power

and energy management. The proposed idea provides a base to improve and examine the system in systematic and consistent manner. The method within the power management and energy management shell has been studied with simulations of a designed strategy. The explanation of studied vehicle advanced to validate the concept. The experimental work carried out thus provide a justification for EV power and its energy management.

Gurkaynak *et al.* [93] had proposed and examined the photovoltaic method for plug-in hybrid electric vehicle load to meet the residential requirement. The present system is the grouping of two subsystem that are joined via DC link. The first subsystem comprises of current-controlled boost converter and solar energy harvesting part with PV array and maximum power point tracking system while the second subsystem comprises of a current-controlled bidirectional converter and energy storage system with battery pack. The current controller is chosen as sliding mode controller that is more effective against parametric uncertainties. In order to control the power flow between battery pack and grid a power management algorithm is incorporated according to load profile. A power management algorithm is introduced to control the power flow between grid and battery packs according to load profile.

Swetha *et al.* [94] had designed a sliding technique control method (SMC) for electric vehicle (EV). The supply of EV power for this system is photovoltaic PV source and battery bank. For instantaneous load variations energy management is achieved by proportional integral (PI) and proportional integral discrete (PID) methods that are used for DC-to-DC power converter. During management of power for entire system linear control strategies are less effective as compared to non-linear control strategies. For proper switching action of DC-to-DC converter non-linear control method is used present work. To maximize the power amount for EV SMC is combined with proportional integral (PI) controller and the efficiency of designed controller so examined by MATLAB using escape electric vehicle (EV) model.

K.K *et al.* [95] had designed to fulfil the demand of load designed a system by integrating solar PV with a utility grid. The actual energy generation and its use is monitored by the energy management system (EMS). Using the load data standard solar PV EMS with EV as a storage unit is formed in this paper. To decrease the total cost of variable-priced electricity and extent of energy import linear program-based standardization technique is used. MATLAB with an electric vehicle as a storage unit is used to examine the performance of the designed system.

Hassoune *et al.* [96] had presented for a grid-tied photovoltaic (PV) storage in electric vehicle charging station they have designed a power management strategy to apply it in power control system of charging system. To reduce the cost of consumed energy on electric grid and to reduce stress on existing power the control works depending on integration of renewable

sources. Also, they have proposed a power predictive model that is based on a real time monitoring of supply and power demand achieving the data communication between the charging system and the plugged electric vehicle (EV). To maintain the standard operation mode of a charging process, available energy in the battery storage buffer and sudden power of photovoltaic (PV) arrays a number of parameters are employed in these strategies. To examine the performance of this method simulation results displayed the efficiency of designed control system.

Ali *et al.* [97] had proposed an advance optimal power management ides for multi-source EVs. The depicted idea applies a novel situation perception principle, built on mapping the vehicle operating conditions into a multi-dimensional space designated as grid-space and they are depicted as axes. These variables are named as power demand, speed dynamics and vehicle speed. For every vehicle situation in the grid space power management algorithm control parameter have been optimized offline. Advancement of grid-space is examined on two concept different axes discretization and implementation of variables followed by offline standardization of control parameter and solution to each new grid is provided and real time application of energy saving is analyzed. They have considered six grid space structure for their work and tested them using four driving cycles indicating different operating system.

2.2.6 Light Electric Vehicles with Brushless DC Motor Drives

Xue *et al.* [98] had discussed the six various types of electric motor drives for electric vehicles (EVs) and also presented the need for EVs on an electric motor. To find suitable electric motor drives for EVs application comparative studies on weight, cooling, cost, fault-tolerance, maximum speed, efficiency, reliability, and safety were conducted for induction motor (IM), brushless direct current motor (BLDC), switched reluctance motor (SRM). Showing that switched reluctance motor drives are a good choice for EVs.

Tashakori *et al.* [99] had presented a system to sense faults in a three-phase voltage source inverter (VSI) driving an inner wheel brushless direct current motor (BLDC) motor. To extract the topographies of the line voltages of the BLDC motor discrete Fourier transform is used. To confirm the simulation model of the motor various switch faults is used. In this paper, they have detected switch faults via SED errors and don’t need any exact values of the voltage of the BLDC motor. Hence the designed fault analysis algorithm is appropriate for applications with a change of speed.

Azam *et al.* [100] had increased the voltage capacity of batteries in EVs applications by designing a blocking strategy of direct current (DC) motor drive. A Brushless direct current

(BLDC) motor provides a dynamic performance and robust control by providing a simple torque hysteresis control. The advantages provided by the designed current blocking strategy are highlighted by doing mathematical modeling of the BLDC motor. The designed strategy is beneficial as it can stop the drainage of current from batteries. The presented scheme is confirmed and verified by experimental and simulation results.

Shanmugasundram *et al.* [101] had proposed a fuzzy controller for attaining better performance of servomotor drive. The enactment of this controller is examined under a number of operating conditions like parameter variations, load disturbance, and changes in system speed, etc. This servomotor is used in instrumentation systems, electric vehicles, aerospace, and industrial control application. To achieve the steady and transient state responses present controllers are used with BLDC servomotor. The main trouble related to the earlier proportional integral discrete (PID) controllers is that they do not yield good transient and system steady-state responses. In this paper, they have presented a fuzzy controller and its performance is compared with a conventional PID controller.

Luo *et al.* [102] had proposed a new power supply unit to advance the motion control for a permanent magnet brushless direct current (PM BLDC) motor drive system. To attain higher efficiency, wider speed range, and simple structure compared to conventional motor systems they have designed a novel digital signal processor (DSP) controlled pulse-width modulated (PWM) chopper. Also, they have discussed the complete investigation of the design consideration, implemented control algorithms, and the principle of operation. The presented topology has been proven experimentally.

Alphonse *et al.* [103] had presented a resolution for the coming crisis by proposing a solar-powered brushless direct current (BLDC) motor-driven electric vehicle (EV). The purpose of choosing the suitable components for this exercise is studied and they are simulated to different tests in a real-time environment. This integrated system is consisting of batteries, a boost converter, a solar module, and a BLDC motor thus making it suitable for the development of solar-powered EVs.

Mohanraj *et al.* [104] had presented an overview, control strategy, and applications of brushless direct current (BLDC) motor. The authors also explained that the outer surface rotor-type BLDC motors (i.e., Hub motor) is used mostly for commercial applications. They discussed that the low-speed BLDC motor constitutes high torque ripples and at the high speed of BLDC motor torque ripples are low. Also, they have discussed the comparison of the intelligent controller (i.e. reduces torque ripples more than other controllers) stands preferable amongst the various control strategies used for BLDC motors. At the last, the authors discussed the

challenges to BLDC motors as well as future hopes.

Chu *et al.* [105] had presented a torque control system for brushless direct current (BLDC) motors which is practiced in electrified scooters, with the purpose point of getting nearer system output characteristics to that of a continuously variable transmissions system. The authors said that the fact of BLDC motors is that it needs a higher grade of system operating speeds, field weakening control strategies, and phase advance control. On the basis of theoretical derivation and experimental verification, they said in electric scooter applications for getting torque control, the system control strategy uses only one current sensor in order to calculate the DC bus current.

Lee *et al.* [106] had proposed an advanced brushless direct current (BLDC) motor drive in order to get a lesser cost and high-performance electric propulsion strategy in EVs and HEVs. The authors explained that they have used fewer parts converter strategies and a better PWM system control to obtain the wanted dynamic, static system speed, and torque characteristics. They have used an insulated-gate bipolar transistor (IGBT) based inverter with high-speed digital signal processing (DSP), TI TMS320 F243 to attain the proposed strategy results.

Kivanc *et al.* [107] had presented regenerative braking (RB) a brushless direct current (BLDC) motor. The authors explained that the RB means to drive an electric vehicle (EV). They explained that the small BLDC motor with greater inertial load is useful to simulate the larger energy recovery capacity during EV operations. Also, the main merits of RB in EVs are to get more driving miles by capitalizing the generator working operation of a propulsion motor and motor driver inverter boost working operation.

Hassanin *et al.* [108] had presented a principle of operations for selecting the brushless direct current (BLDC) motors to drive the electric vehicle (EV). The authors illustrated the detailed study of the BLDC motor for the EV as well as about the EV major components sizing. They computed the size of the motor and calculated its acceleration time and acceleration distance. After the simulation is tested, it is notified that a 35 kW BLDC motor is efficient to work the EV in different operation situations.

Jiaqun *et al.* [109] had proposed a new, simple, and cost-effective strategy with regenerative brake with BLDC motor for LEVs. They have used a similar power stage strategy as the traditional BLDC motor controller, only the PWM strategy of the inverter is changed. Here the kinetic energy of the vehicles is getting converted to electrical energy and then gets back to the battery system and a novel regenerative current sensing and control strategy is used for better improvement. At the last, the authors described some work experiments on a BLDC system controller with a new control strategy and noticed that it will efficiently work with EV.

Mishra *et al.* [110] had presented an efficient brushless direct current (BLDC) motor-driven plug-in electric vehicle (PEVs) for a single-phase battery charging strategy. The authors explained that the proposed strategy employs an integrated circuitry-based isolated DC-to-DC power converter for a light PEV that has a BLDC motor as a driving motor to lessen the motor drive parameters cost. They explained that the given strategy has the capacity to work better under all EV working situations such as charging, propulsion, and regenerative operations with double energy sources such as utility grid and solar PV system.

C M *et al.* [111] had proposed a strategy based on a bidirectional DC-to-DC converter fed brushless direct current (BLDC) motor in electric vehicle (EV). The authors explained that in the braking mode of working operation, in spite of wasting kinetic energy, it is efficient to use the operation of a two-way converter, which helps in reducing the addition of extra circuits.

Sincero *et al.* [112] had presented the efficient simulation strategy for brush and brushless direct current motors system for light traction applications. They have presented an analysis that is validated by the simulation of two similar motors, where the motors performance and losses distribution is considered. Hence, brushless motor best suited for light traction applications.

2.3 Research Gap

- There are different types of power converters that can be used for light electric vehicles (LEVs) charging application. Most of the converters are categorized as AC-to-DC, DC-to-AC, and DC-to-DC. Moreover, these power converters are also having different categories as isolated, non-isolated, bridged, and bridgeless power converters. For understanding and utilization of these converters in light electric vehicles (LEVs) applications, a detailed overview is required [41-47, 60-65].
- With the rapid growth of light electric vehicles (LEVs) in the present time, an efficient power converter is required to overcome the power losses and enhance charging efficiency [60-68,72-75,83-87].
- It is possible to recommend that a standard power electronics converter, as well as a bidirectional charger/discharger system, be planned for improved quality of light electric vehicles [38-43,49-51].
- For light electric vehicles (LEVs) applications, power losses are the main factor to protect devices and power converters. By using suitable converters and control strategies, it is possible to improve the harmonic effects, which can help to improve the loss effect [60-63,74-78].

- Different components (i.e., power switches, power diodes, inductors, and capacitors) which are used in power converters require a low current and voltage drop to improve the dv/dt and di/dt stress [35-37, 55-59].
- Most light electric vehicles (LEVs) chargers are adept at taking power from the grid and delivering it to a vehicle, but what if the vehicle could also automatically keep feeding to the load/grid. A vehicle-to-grid (V2G) technology refers to the process of feeding electricity contained in vehicle batteries back to the grid. For designing vehicle-to-grid (V2G) enabled LEV bidirectional power converter is required [38-41, 87-89].
- To design a Maximum Power Point Tracking (MPPT), in order to enhance the power coming from solar PV to a certain precise value [75-77, 82-86].
- The vehicle battery is charged by regenerative recovery power in the brushless direct current (BLDC) motor system drive, so the bidirectional power converter is also required [98-103].
- For a defined case study of solar photovoltaic (PV)-grid-based electric vehicle system, a general power management scheme can be applied by keeping all constraints of system components such as photovoltaic (PV) array, maximum power point tracking (MPPT), sensors, power converter sources, and battery within limits [89-92,95-97].
- The requirement of designing an efficient power management strategy for renewable energy-grid-based electric vehicle (EV) charging [95,96].

2.4 Objectives and Scope of Work

The following section below discussed the research objectives and future work as,

2.4.1 Research Objectives

This section focuses on the design and development of converters and energy management strategies to enhance the performance, efficiency, and sustainability of LEV charging systems. The specific objectives of the study are outlined as follows:

1. **To design various converter topologies for light electric vehicles (LEVs).**
2. **Development of solar photovoltaic (PV) and grid-based charging schemes for light electric vehicles (LEVs).**
3. **Development of different power management strategies for light electric vehicles (LEVs) charging schemes.**

2.4.2 Scope of Work

- The powertrain diagram for LEV charging is presented in Figure 1. It contains various features, such as power factor correction, regulated DC voltage, high gain during both G2V and V2G mode, solar on-board charging with MPPT converter, and brushless DC motor drive during propulsion.
- The brief review on the research on the non-isolated, isolated, and bridgeless power converter topologies for LEV battery charging, solar photovoltaic (PV) based LEV charging as well as power management strategies for solar photovoltaic (PV)-light electric vehicle (LEV)-Grid integrated systems, and LEVs with motor drives is presented in the CHAPTER 2, literature survey.
- After a literature survey, it is identified that most of the work on LEV charging was carried out on solar photovoltaic (PV) based charging and brushless direct current (BLDC) motor-driven aspects.
- There are many conversion strategies that utilize non-isolated, isolated, and bridgeless AC-to-DC strategy, which uses a power converter for light electric vehicle (LEV) charging.
- Non-isolated converters offer advantages in terms of compact size and lower cost, making them attractive for portable or low-power charging units.
- Isolated converters, on the other hand, provide galvanic isolation, enhancing safety and reliability, particularly in high-power or grid-connected systems.
- Bridgeless strategies aim to improve efficiency by minimizing conduction losses and simplifying circuit design, thereby contributing to higher overall system performance.
- The power management schemes for solar-photovoltaic (PV)-grid-battery integrated systems are explained with the purpose of achieving the proposed objective targets. However, keeping various aspects of solar photovoltaic (PV)-grid-fed BLDC motor-driven LEV within the respective scope is identified as work to be done.

2.5 Conclusions

In this chapter, the diverse range of power converter topologies employed in Light Electric Vehicle (LEV) charging applications, including AC-to-DC, DC-to-AC, and DC-to-DC converters, with extended classifications into isolated, non-isolated, bridged, and bridgeless types, are highlighted. These converters play a vital role in improving charging efficiency and reducing power losses, which are critical factors given the rapid growth and increasing demand for LEVs. Research indicates the importance of developing standardized, high-quality power electronics converters and bidirectional charging/discharging systems to enhance LEV

performance. Additionally, losses in strategy emerge as a significant design consideration, necessitating the use of appropriate converter strategies and control techniques to minimize harmonic distortions and improve overall device reliability. The performance of power converters is also influenced by the selection of components such as power switches, diodes, inductors, and capacitors, which must be optimized to reduce electrical stresses and improve durability. Advanced technologies like vehicle-to-grid (V2G) systems have been identified as promising solutions for enabling bidirectional energy flow, allowing LEVs to supply power back to the grid during outages, which requires specialized converter designs. Further, integrating Maximum Power Point Tracking (MPPT) techniques is essential for maximizing the energy harvested from solar photovoltaic (PV) systems, which are increasingly being incorporated into LEV charging infrastructure. The use of bidirectional power converters is also critical in systems employing brushless DC (BLDC) motors, enabling efficient battery charging through regenerative braking.

Eventually, comprehensive power management schemes that account for the constraints of all system components-such as PV arrays, MPPT controllers, sensors, power converters, and batteries-are fundamental for the reliable operation of solar PV-grid-based LEV charging systems. The development of efficient power management strategies tailored for renewable energy and grid-integrated electric vehicle charging remains a key area of ongoing research.

Overall, the surveyed literature underscores the necessity for holistic and optimized designs that integrate converter strategy, power management, renewable energy sources, and motor drives to advance the performance and sustainability of LEV charging systems.

CHAPTER-3

CLASSIFICATIONS AND CONFIGURATIONS OF LIGHT ELECTIC VEHICLE CHARGING

3.1 General

The speeding-up utilization of Light Electric Vehicles (LEVs), such as electric bicycles, scooters, and motorcycles, has resulted in a critical necessity for safe, efficient, and user-friendly charging solutions. As these road vehicles become an integral part of urban transportation, the charging infrastructure must evolve to support a wide range of operational requirements, including fast charging, energy efficiency, and integration with solar PV source. Understanding the classifications and configurations of LEV charging systems is basic to designing safe, reliable and fast charging solutions that satisfy application scenarios.

Charging systems for LEVs can be broadly classified based on several factors, including the type of power conversion involved, the source of energy, and the interaction with the grid or solar PV systems. At the core of these systems lie AC-DC, DC-DC, and DC-AC converters, which perform key functions such as converting AC from the grid to DC suitable for battery charging, or vice versa in cases involving vehicle-to-grid (V2G) operations. The converters are commonly categorized into AC-to-DC, DC-to-DC, and DC-to-AC types, each with distinct functions based on the charging design. Moreover, the classification extends to the various design of the converters, dividing them into isolated, non-isolated, and bridgeless configurations. Isolated converters use galvanic isolation via transformers, offering enhanced safety and noise immunity, which are critical for grid-connected and solar PV applications. Non-isolated converters, on the other hand, provide simpler and more compact designs, often preferred for low-power, portable charging units. Recent converter strategies also include bridgeless converter strategies, which reduce conduction losses by eliminating diode bridges, thereby improving efficiency and reducing heat dissipation in LEV charging systems.

In terms of energy source classification, LEV charging can involve direct grid connection, renewable energy integration-primarily solar photovoltaic (PV) systems. Solar PV-based charging has become highly regarded for its potential to support sustainable grid outage for LEVs, particularly in regions with isolated solar PV. The integration of PV systems introduces additional complexities, such as the need for maximum power point tracking (MPPT) algorithms to maximize energy extraction and power management strategies to balance energy

flow between the PV array, battery, and grid. The G2V and V2G modes of operation also differ in the directionality of power flow. Unidirectional chargers allow power to flow only from the grid to the vehicle battery. In contrast, bidirectional chargers support V2G functionalities, enabling LEVs to supply energy back to the grid during peak demand or power outages, enhancing grid stability and providing additional value to vehicle owners.

Furthermore, the charging and discharging of LEV systems vary based on power levels and charging speeds. Slow and standard charging strategy typically use lower power converters suited for overnight charging, whereas fast and rapid chargers utilize advanced high-power electronics designed to charge the battery more quickly, which is crucial for LEVs charging.

The diversity in LEV charging classifications and configurations underscores the need for adaptable and optimized system designs such as high-gain power electronic converters, appropriate controllers, passive component design, and power management. This chapter explores the different classifications and configurations of LEV charging systems, highlighting their infrastructure designs, strategies, controls, advantages, and challenges to provide a comprehensive foundation for developing next-generation charging solutions that meet the evolving needs of electric mobility.

3.2 Classifications of Light Electric Vehicle Charging

The different classifications of LEV charging systems, highlighting their infrastructure designs, strategies, controls, and power management, are as follows. These systems are typically categorized into unidirectional converters based on LEV charging and bidirectional converters based on LEV charging. Each classification supports specific charging schemes. Additionally, the control strategies involved various pulse-generating methods that ensure good efficiency, safety, reliability, and growth potential in managing power distribution across the charging network.

3.2.1 Unidirectional Converter-based Light Electric Vehicle Charging

The unidirectional converter-based LEV charging system works in the G2V mode, meaning it only allows power flow from the single-phase grid to the vehicle's battery. This type of converter focuses on efficiently transferring power during the charging process without enabling power return to the grid. Unidirectional systems are typically simpler and less costly. These types of strategies are commonly used in straightforward charging setups where power flow is strictly one-way, prioritizing reliability and cost-effectiveness in LEV charging infrastructure. Furthermore, the unidirectional converter-based LEV charging system is

divided into two sub-parts, the non-isolated converter strategy and the bridgeless converter strategy.

3.2.1.1 Non-isolated Converter-based Light Electric Vehicle Charging

Unidirectional non-isolated converter-based LEV charging belongs to a category of power electronic converters used in electric vehicle charging systems where there is no galvanic isolation between the AC-to-DC and DC-to-DC. This means that the passive elements, diodes, and switches are responsible for making a direct electrical path between the grid and the vehicle's battery without the use of a transformer to electrically separate them.

These types of converters are especially recognized for their simple structure, compact design, better efficiency, and higher payback time. This removes the requirement for large and costly transformers, which are especially well-suited for on-board charging systems in LEVs such as electric scooters, e-bikes, e-carts, e-rickshaws, and small electric cars. Typical converter strategies used in unidirectional non-isolated LEV charging include buck, SEPIC (single-ended primary inductor converter), and Cuk configurations. These strategies ensure the voltage is needed to meet battery requirements from the single-phase grid, guaranteeing uninterrupted and safe charging.

As the non-isolated charging strategy continues to evolve, diode bridge rectifier (DBR) integration with high-gain DC-DC unidirectional converter infrastructure with single-stage control is expected to further improve the reliability and charging performance of non-isolated charging systems.

Despite their advantages, unidirectional non-isolated converters have limitations, particularly limited efficiency during light-load conditions, limited voltage gain, high output voltage requirements leading to a high value of the capacitor, and possibly high ripple in charging currents, and an inability to handle bidirectional power flow.

3.2.1.2 Bridgeless Converter-based Light Electric Vehicle Charging

Unidirectional bridgeless converters have become an increasingly popular choice in the design of charging systems for Light Electric Vehicles (LEVs) due to their ability to reduce power losses and improve overall efficiency. Traditional chargers use a diode bridge rectifier, which introduces voltage drops and conduction losses. Unidirectional bridgeless converter strategies remove this diode bridge, enabling more efficient power conversion by allowing current to flow through fewer components.

This is one of the simplest and most common topologies. It replaces the conventional diode

bridge with active switches, allowing for power factor correction and reduced conduction losses. Bridgeless AC-to-DC converters are well-suited for LEV charging applications requiring PFC operations and step-down battery voltage, often found in chargers where the input single-phase AC voltage must be converted to a required DC voltage best-suited for LEV battery.

Unidirectional bridgeless converters are especially recognized for their simple circuit construction, reduced cost, less conduction losses, enabling power factor correction, making it ideal for compact and efficient on-board charging systems, low reverse-recovery losses, improving efficiency, and higher payback time. Since they remove the requirement for diode bridge rectifiers (DBRs), these converters are especially well-suited for on-board charging systems in LEVs such as electric scooters, e-bikes, e-carts, e-rickshaws and small electric cars. Typical bridgeless converter strategies used in unidirectional non-isolated LEV charging include a semi-quadratic high-gain AC-to-DC converter and high step-down gain SEPIC configurations. These strategies ensure the voltage is needed to meet battery requirements from the single-phase grid, guaranteeing uninterrupted and safe charging.

As the bridgeless charging strategy continues to evolve, a bridgeless combination of power electronics switches, passive elements, and single-stage control is expected to further improve the reliability and charging performance of LEV charging systems.

Despite their advantages, bridgeless converters have limitations, particularly reliability issues, zero current switching, complexity in sensing circuit design, and efficiency under varying light-load conditions, and the inability to handle bidirectional power flow.

3.2.2 Bidirectional Converter-based Light Electric Vehicle Charging

The bidirectional converter-based LEV charging system works in the both G2V and V2G mode, meaning it only allows power flow from the single-phase grid to the vehicle's battery or vice versa. This type of converter focuses on efficiently transferring power during the charging-discharging process without enabling power return to the grid. Bidirectional systems are typically do buck and boost operations. These types of strategies are commonly used in charging-discharging step-down and step-up where power flow is two-way, prioritizing safe, reliable, and cost-effective LEV charging-discharging infrastructure. Furthermore, the bidirectional converter-based LEV charging system is divided into two sub-parts: the Non-isolated converter strategy and the isolated converter strategy.

3.2.2.1 Non-isolated Converter-based Light Electric Vehicle Charging

Bidirectional non-isolated converter-based LEV charging belongs to a category of power

electronic converters used in electric vehicle charging systems where there is no galvanic isolation between the AC-to-DC and DC-to-DC. This means that the passive elements, diodes, and switches are responsible for making direct electrical path between the grid and the vehicle's battery or vice versa without the use of a transformer to electrically separate them.

These types of converters are especially recognized for their simple bidirectional structure, compact design, improved efficiency, and higher payback time. Since they remove the requirement for large and costly transformers, these converters are especially well-suited for on-board charging systems in LEVs such as electric scooters, e-bikes, e-carts, e-rickshaws and small electric cars. Typical converter strategies used in bidirectional non-isolated LEV charging include switched inductor, coupled inductor, switched capacitor, buck-boost, modified SEPIC (single-ended primary inductor converter), Zeta and Cuk configurations. These strategies ensure the voltage is needed to meet battery requirements from the single-phase grid or power back to the grid, guaranteeing uninterrupted and safe charging-discharging. As the bidirectional non-isolated charging strategy continues to evolve, active front-end converter (AFC) integration with high-gain DC-to-DC Bidirectional converter infrastructure with two-stage control is expected to further improve the reliability and charging-discharging performance of LEV systems.

Despite their advantages, bidirectional non-isolated converters have limitations, particularly limited efficiency due to losses, operational constraints, larger input and output current ripple, and limited voltage gain.

3.2.2.1 Isolated Converter-based Light Electric Vehicle Charging

Bidirectional Isolated converter-based LEV charging belongs to a category of power electronic converters used in electric vehicle charging systems where there is galvanic isolation between the AC-to-DC and DC-to-DC. This means that the passive elements, diodes, and switches are responsible for making an isolated electrical path between the grid and the vehicle's battery or vice versa, with the use of a transformer, i.e., a high-frequency transformer (HFT), to electrically separate them.

These types of converters are especially recognized for their offering distinct benefits related to efficiency, adherence to regulations, and higher payback time. Since there is a need for reliable and secure charging mechanisms, these converters serve as an efficient choice for integrating on-board charging in LEVs, including e-scooters, e-bikes, e-carts, e-rickshaws, and small-sized electric cars. Typical converter strategies minimize the risk of circuit damage, direct and indirect contact, and improve overall safety in domestic terms. Isolated strategies

used in bidirectional isolated LEV charging include dual active bridge (DAB), bidirectional isolated resonant DC-to-DC converter (CLLC), modified isolated SEPIC (single-ended primary inductor converter), and Cuk configurations. These strategies ensure the voltage is needed to meet battery requirements from the single-phase grid or power back to the grid, through HFT, guaranteeing uninterrupted and safe performance.

Overall, bidirectional isolated converter-based LEV solutions represent a key feature, such as higher charging efficiency, safety, high performance, a design that reduces size, weight, and cost, and facilitates power exchange between the vehicle and the grid or vice versa. By offering these features, a bidirectional isolated converter strategy reinforces its role in shaping the future of electric mobility.

3.3 Configurations of Light Electric Vehicle Charging Schemes

The different configurations of LEV charging schemes highlight their infrastructure designs, strategies, controls, and power management. These configurations are normally categorized into unidirectional converter-based LEV charging and bidirectional converter-based LEV charging. Each configuration supports various converter schemes. Additionally, the converter strategies involved various modes that ensure good efficiency, safety, reliability, and growth potential in managing power distribution across the charging network.

3.3.1 Unidirectional Converter-based Light Electric Vehicle Charging

Unidirectional converter-based charging configurations are growingly favored in LEV charging applications due to their simplicity in circuits, improved efficiency, low cost, and high payback time. These unidirectional systems facilitate a direct electrical path between the grid and the vehicle's battery without the use of a transformer to electrically separate them. The integration of DBR (i.e., AC-to-DC) and a unidirectional DC-to-DC converter ensures regulated voltage and current, which is crucial for battery health. Furthermore, the configuration of the unidirectional converter-based LEV charging system is divided into two sub-parts: Non-isolated converter strategy and bridgeless converter strategy.

3.3.1.1 Non-isolated Converter-based Light Electric Vehicle Charging

Unidirectional non-isolated converter-based LEV charging configuration belongs to a category of power electronic converters used in electric vehicle charging systems where there is no galvanic isolation between the AC-to-DC and DC-to-DC. This means that the configuration uses passive elements, such as diodes and IGBT/MOSFET switches, which are responsible for making a direct electrical path between the grid and the vehicle's battery without the use of a

transformer to electrically separate them. Figure 3.1 shows the configuration of conventional unidirectional a buck-boost rectifier to manage input current with a quadratic buck converter. This configuration utilizes diode bridge rectifier (DBR) with integrated buck-boost quadratic Buck (BBQB) PFC converter for charging applications. Figure 3.2 shows the configuration of conventional unidirectional SEPIC PFC converter for charging applications. This configuration utilizes diode bridge rectifier (DBR) with SEPIC converter. Figure 3.3 shows the configuration of conventional unidirectional SEPIC PFC converter for multiple charging applications. This configuration utilizes diode bridge rectifier (DBR) and SEPIC PFC converter with two resistive loads. In conventional strategies higher passive components count, such as inductors, capacitors, resistors, and switches, of these strategies results in larger power losses, hence providing low efficiency and low charging performance. These strategies have high output voltage and current ripples, which directly affect the life of the LEV battery. It emphasizes the need for new, improved strategies with a lower component count that aim to reduce overall power consumption and enhance charging performance, rather than advising that an increased number of components leads to low efficiency. Figure 3.4 shows the schematic of the developed LEV charging strategy with dual power sources (i.e., single-phase AC grid and solar PV), resulting in equal dependency on both sources. This developed strategy have low passive component count, low input current and voltage ripples, and low stress on switches during charging, which results in high performance, larger efficiency, and high payback time of the

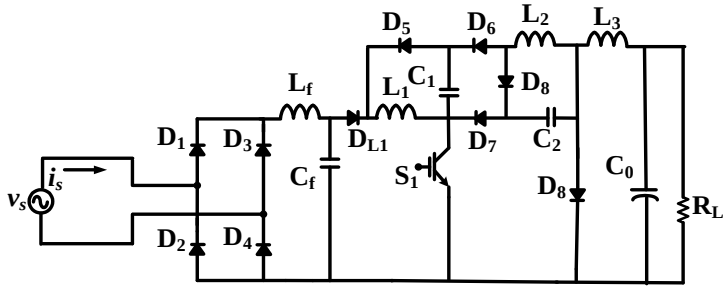

Figure 3.1. Circuit of Conventional BBQB single-PFC Converter.

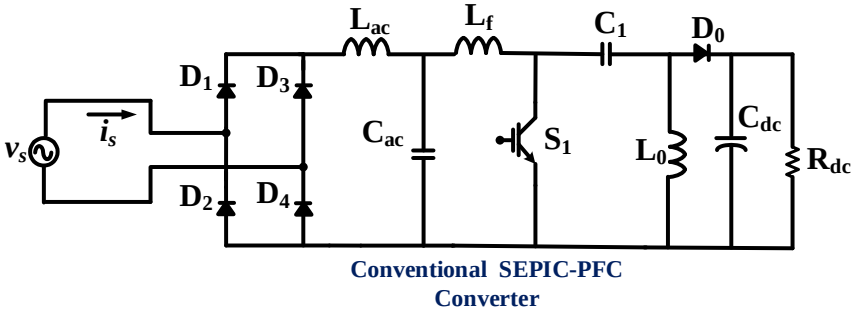

Figure 3.2. Circuit of Conventional SEPIC-PFC Converter.

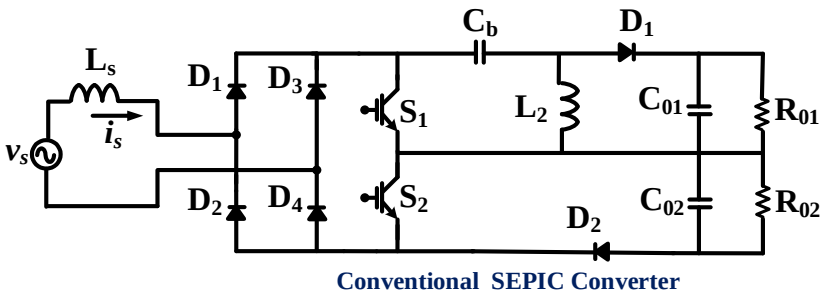

Figure 3.3. Circuit of Conventional SEPIC Converter.

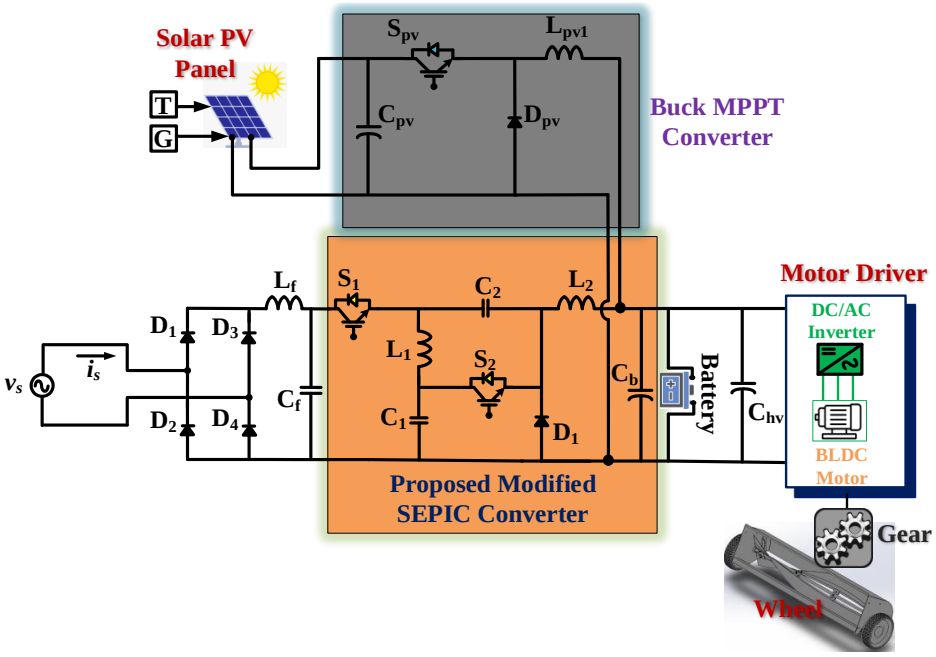

Figure 3.4. Circuit of Proposed Modified SEPIC Converter LEV Charging.

system. The developed system utilizes modified SEPIC converter during grid base charging, and use buck MPPT converter during grid outage to charge the battery through solar PV array. This system also tested with BLDC motor drive. The devolved charging system becomes more compact and lightweight, an essential requirement for LEVs on board charging systems.

3.3.1.2 Bridgeless Converter-based Light Electric Vehicle Charging

Bridgeless converters have become an increasingly popular choice in the design of charging systems for Light Electric Vehicles (LEVs) due to their ability to reduce power losses and improve overall efficiency. Traditional chargers use a diode bridge rectifier, which introduces voltage drops and conduction losses. Bridgeless converter strategies remove this diode-bridge, enabling power factor correction (PFC) and more efficient power conversion by allowing current to flow through fewer components. In contrast, bridgeless LEV chargers rely on a single stage AC-to-DC converter to fulfill both roles with simple control. Figure 3.5 shows the configuration of conventional unidirectional bridgeless boost-buck converter strategies for charging. This configuration emprises higher component count and low efficiency. Figure 3.6

shows the configuration of conventional unidirectional bridgeless SEPIC PFC converter with resistive load. This configuration is utilized to maintain voltage regulation. Figure 3.7 shows the configuration of conventional unidirectional bridgeless Cuk converter for charging application. Figure 3.8 shows the configuration of conventional unidirectional bridgeless coupled inductor SEPIC PFC converter for charging application. In conventional strategies higher passive components count such as inductors, capacitors, resistors, and switches of these strategies results in larger power losses, hence provide low efficiency and low charging performance. These strategies has high output voltage and current ripples which directly affect the life of LEV battery. It emphasizes the need for a new improved bridgeless strategies having lower component count aim to reduce overall power consumption and enhance charging performance, rather than advising that an increased number of count leads to low efficiency.

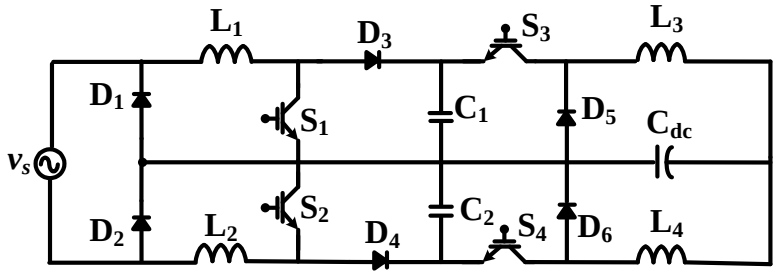

Conventional Bridgeless Boost-Buck Converter

Figure 3.5. Circuit of Conventional Bridgeless Boost-Buck Converter.

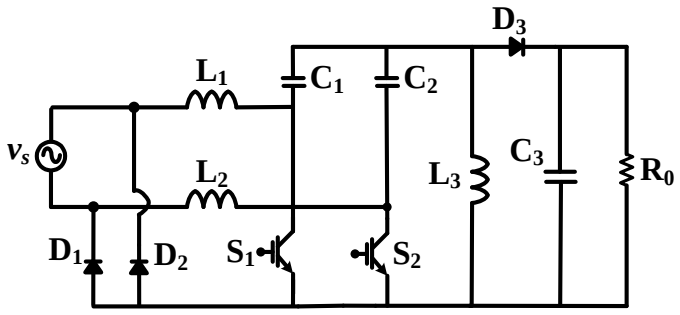

Conventional Bridgeless SEPIC PFC Converter

Figure 3.6. Circuit of Conventional Bridgeless SEPIC PFC Converter.

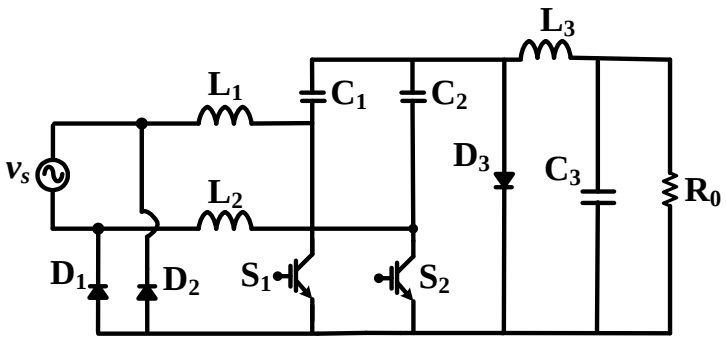

Conventional Bridgeless Cuk PFC Converter

Figure 3.7. Circuit of Conventional Bridgeless Cuk PFC Converter.

Figure 3.9 shows the schematic of developed bridgeless LEV charging strategy with dual power sources (i.e. single-phase AC grid and solar PV), resulting in equal dependency on both sources. This developed strategy have low passive component count, low input current and voltage ripples, and low stress on switches during charging, hence results in high performance, larger efficiency and high payback time of the system. The developed system utilizes bridgeless modified SEPIC converter during grid base charging, and use buck MPPT converter during grid outage to charge the battery through solar PV array. This system also tested with BLDC motor drive. The devolved charging system becomes more compact and lightweight, an essential requirement for LEVs on board charging systems.

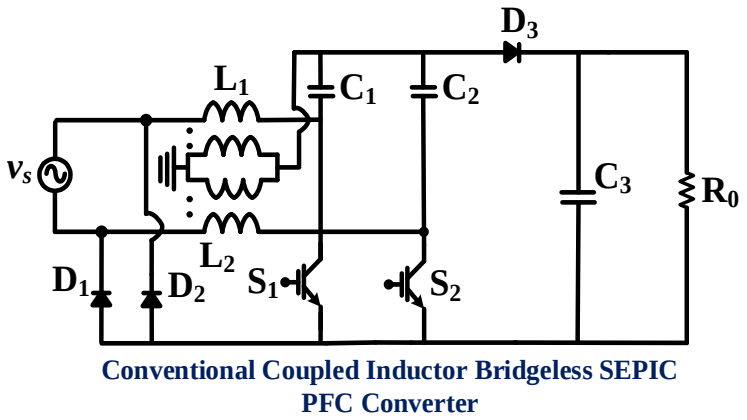

Figure 3.8. Circuit of Conventional Coupled Inductor Bridgeless SEPIC PFC Converter.

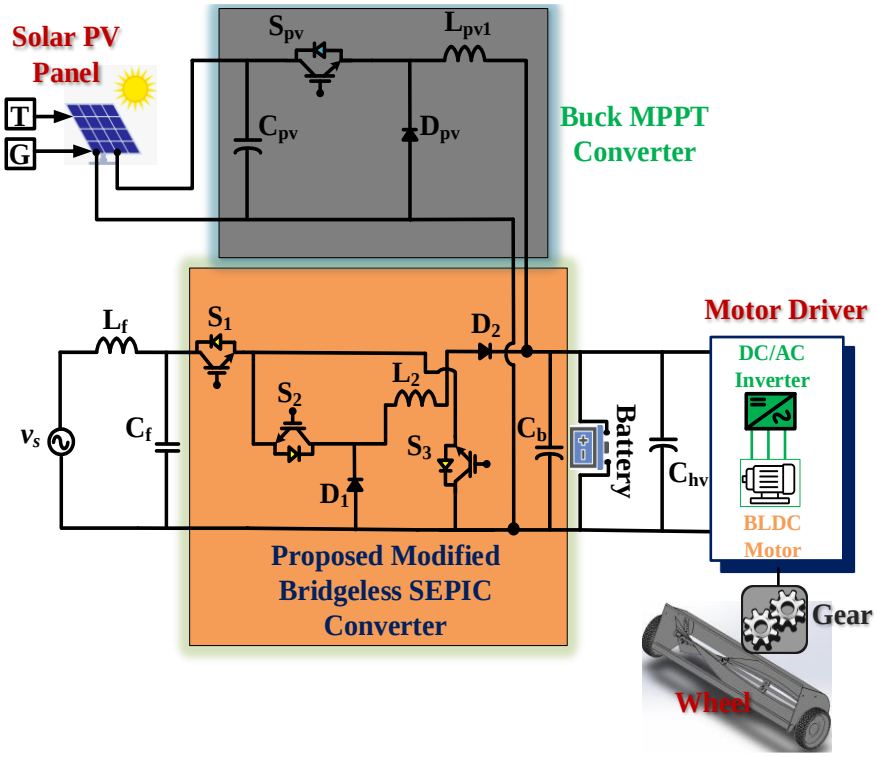

Figure 3.9. Circuit of Proposed Modified Bridgeless SEPIC Converter LEV Charging.

3.3.2 Bidirectional Converter based Light Electric Vehicle Charging

Bidirectional converter based charging configurations are growingly favored in LEV charging applications due to their bidirectional power flow in circuits, improved efficiency, low cost, and high payback time. These bidirectional systems facilitate electrical path between the grid and the vehicle's battery or vice versa. The integration of AFC (i.e.AC-to-DC) and bidirectional DC-to-DC converter ensures regulated voltage and current, which is crucial for charging-discharging. Furthermore, the configuration of bidirectional converter based LEV charging system divided into two sub-parts: Non-isolated converter strategy and isolated converter strategy.

3.3.2.1 Non-isolated Converter based Light Electric Vehicle Charging

Traditional unidirectional strategies use a diode bridge rectifier, which introduces voltage drops and conduction losses. As bidirectional non-isolated charging strategy continues to evolve, active front end converter (AFC) integration with high gain DC-DC Bidirectional converter infrastructure with two stage control are expected to further improve the reliability and charging-discharging performance of LEV systems. These type of bidirectional strategies are commonly used in charging-discharging setdown and setup where power flow is two-way, prioritizing safe, reliability and cost-effectiveness in LEV charging-discharging infrastructure. Figure 3.10 shows the configuration of conventional interleaved bidirectional buck-boost DC-to-DC converter (--BBDC) with charging applications. This configuration successfully achieves the G2V and V2G modes of operation under different load conditions. Due to high component counts i-BBDC have larger power losses and lower efficiency. Figure 3.11 shows the configuration of conventional bidirectional hybrid switched inductor switched capacitor DC-to-DC converter (BHSISC) with charging applications. This configuration has larger stress on switches and larger electromagnetic interference (EMI). Figure 3.12 shows the configuration of conventional switched inductor SEPIC (SISEPIC) DC-to-DC converter for charging application. This configuration has only G2V mode of operation. In conventional strategies higher passive components count such as inductors, capacitors, resistors, and switches of these strategies results in larger power losses, hence provide low efficiency and low charging performance. These strategies has high output voltage and current ripples which directly affect the life of LEV battery. It emphasizes the need for a new improved bridgeless strategies having lower component count aim to reduce overall power consumption and enhance charging performance, rather than advising that an increased number of count leads to low efficiency. Figure 3.13 shows the schematic of developed bidirectional non-isolated LEV

charging strategy with dual power sources (i.e. single phase AC grid and solar PV), resulting in equal dependency on both sources. The developed system in Figure 3.13 utilizes coupled inductor bidirectional high gain converter during grid base charging, and use SEPIC MPPT converter during grid outage to charge the battery through solar PV array. This system also tested with BLDC motor drive. Similarly, the developed system in Figure 3.14 utilizes switched capacitor bidirectional high gain converter during grid base charging, and use Cuk MPPT converter during grid outage to charge the battery through solar PV array. This system also tested with BLDC motor drive. These two devolved charging system becomes more compact and lightweight, an essential requirement for LEVs on board charging systems.

3.3.2.2 Isolated Converter-based Light Electric Vehicle Charging

Bidirectional Isolated converter-based LEV charging belongs to a category of power electronic converters used in electric vehicle charging systems where there is galvanic isolation between the AC-to-DC and DC-to-DC.

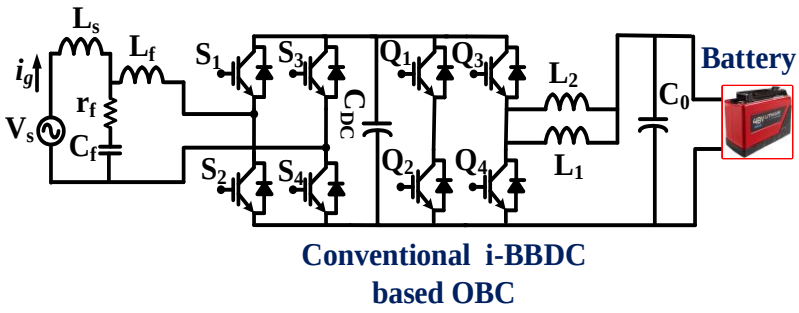

Figure 3.10. Circuit of Conventional i-BBDC Converter.

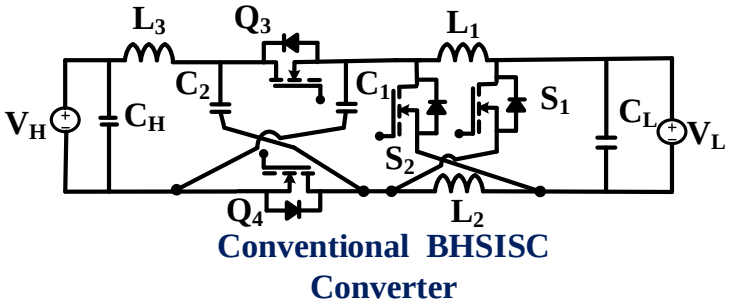

Figure 3.11. Circuit of Conventional BHSISC Converter.

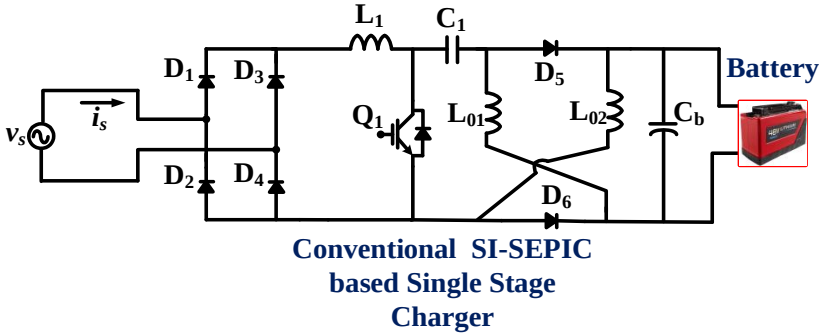

Figure 3.12. Circuit of Conventional SI-SEPIC Converter.

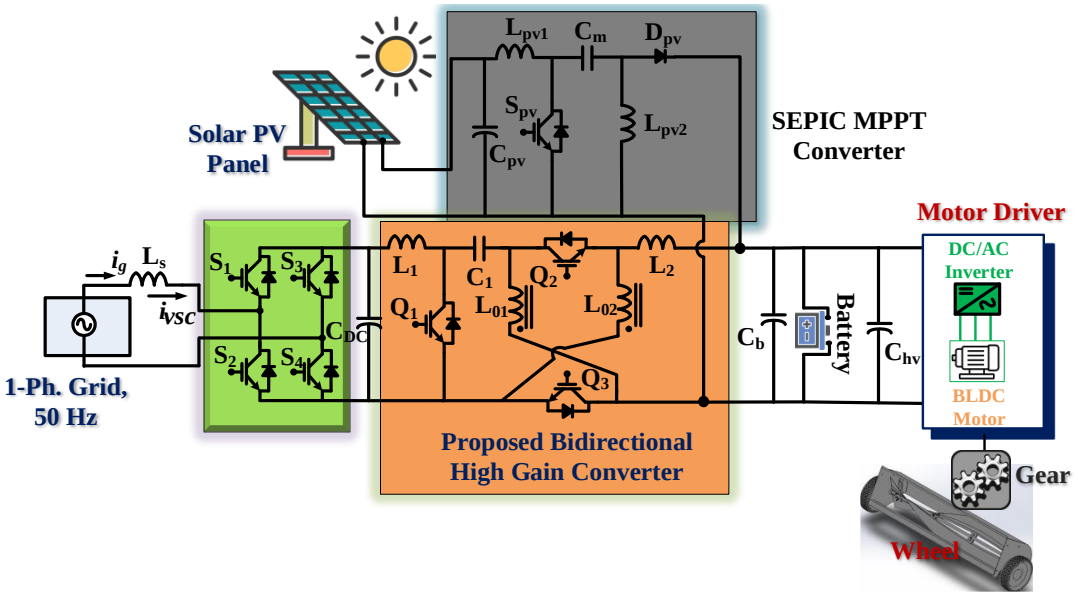

Figure 3.13. Circuit of Proposed Bidirectional High Gain Converter LEV Charging.

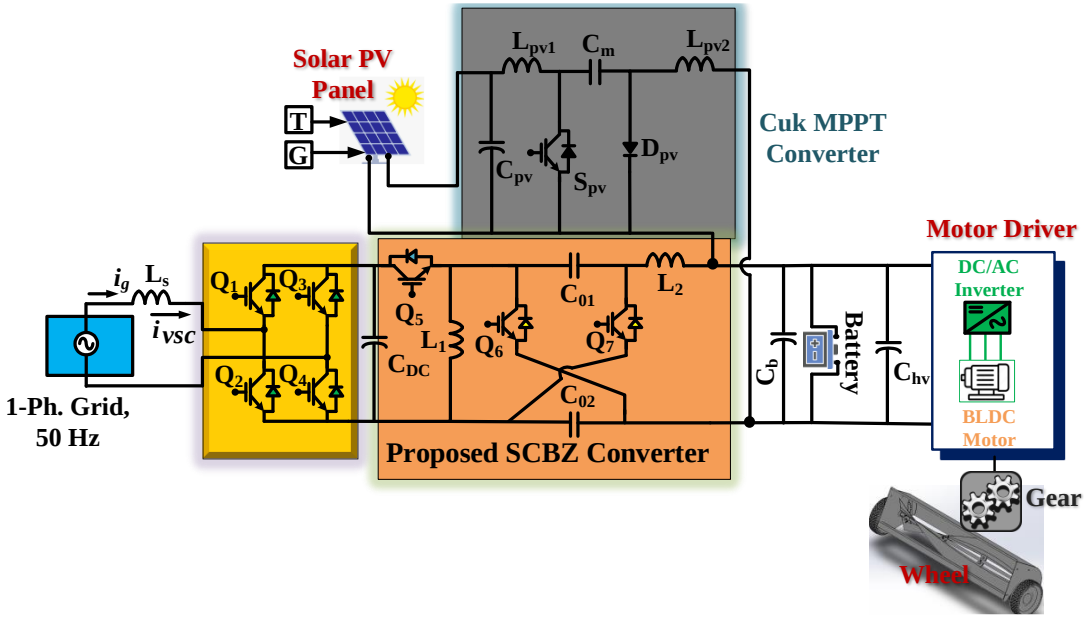

Figure 3.14. Circuit of Proposed Bidirectional High Gain SCBZ Converter LEV Charging.

This means that the passive elements, diodes, and switches are responsible for making an isolated electrical path between the grid and the vehicle's battery or vice versa, with the use of a transformer, i.e., a high-frequency transformer (HFT), to electrically separate them. Figure 3.15 shows the configuration of conventional isolated converter for charging application. This configuration utilizes active front end rectifier (AFC) and bidirectional isolated SEPIC DC-to-DC converter strategy with two high frequency transformers (HFT). Figure 3.16 shows the configuration of conventional isolated ZETA converter for charging application. This configuration has only G2V mode of operation. Figure 3.17 shows the configuration of conventional isolated Cuk converter for charging application. This configuration utilizes AFC but only operates in charging mode. Figure 3.18 shows the configuration of conventional

isolated dual active bridge (DAB) converter for charging application. This configuration features both G2V and V2G modes of operation, but have mismatching in voltage gain. The higher passive components count, such as inductors, capacitors, resistors, transformers, and switches, of these strategies results in larger power losses, hence providing low efficiency and low charging performance. These strategies have high output voltage and current ripples which directly affect the life of the LEV battery.

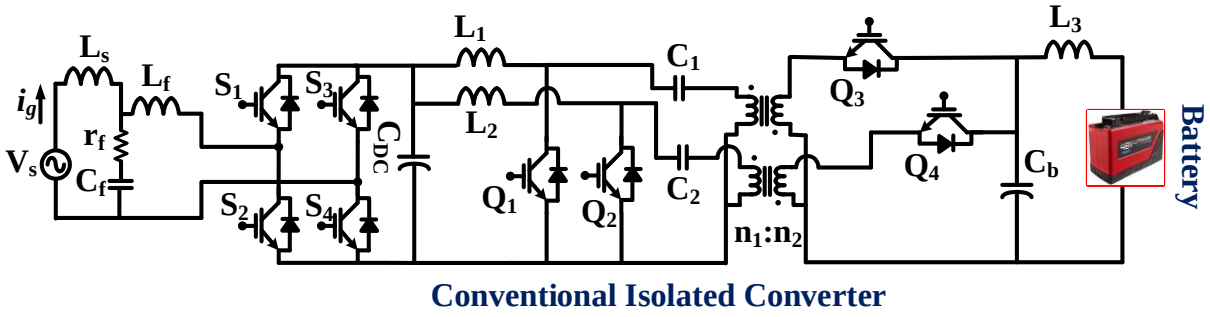

Figure 3.15. Circuit of Conventional Isolated SPEIC Converter.

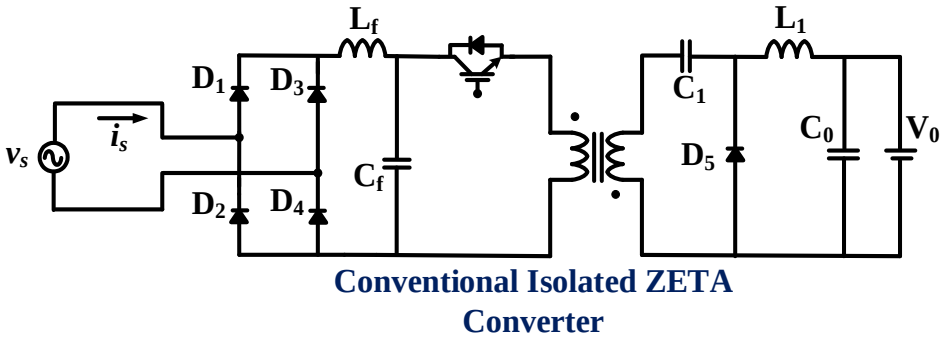

Figure 3.16. Circuit of Conventional Isolated ZETA Converter.

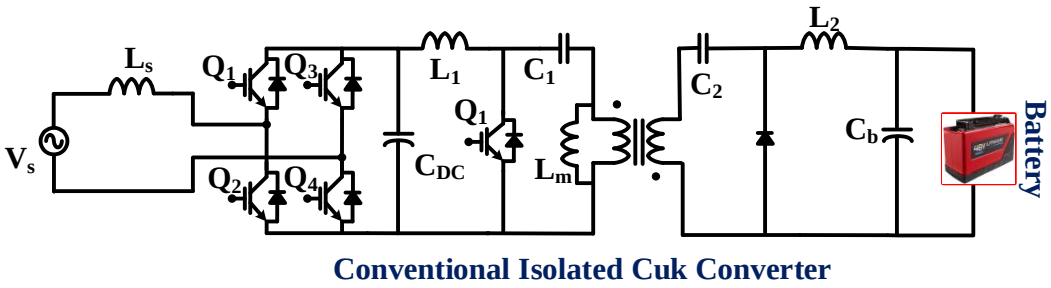

Figure 3.17. Circuit of Conventional Isolated Cuk Converter.

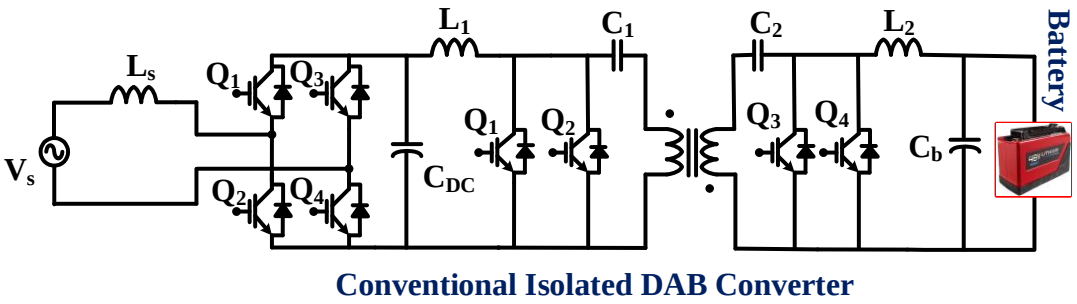

Figure 3.18. Circuit of Conventional Isolated DAB Converter.

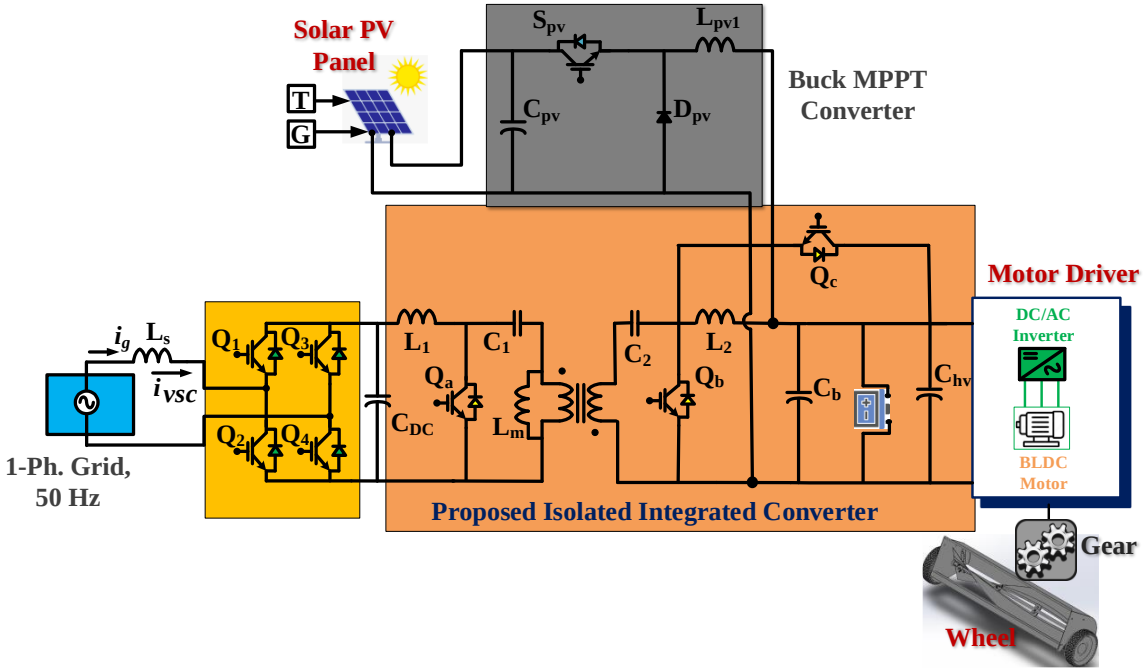

Figure 3.19. Circuit of Proposed Isolated Integrated Converter LEV Charging.

It emphasizes the need for a new improved bridgeless strategies having lower component count aim to reduce overall power consumption and enhance charging performance, rather than advising that an increased number of count leads to low efficiency. Figure 3.19 shows the schematic of developed bidirectional isolated LEV charging strategy with dual power sources (i.e. single phase AC grid and solar PV), resulting in equal dependency on both sources. This developed strategy have low passive component count, low input current and voltage ripples, and low stress on switches during charging, hence results in high performance, larger efficiency and high payback time of the system. The developed system utilizes bidirectional isolated integrated converter during grid base charging, and use buck MPPT converter during grid outage to charge the battery through solar PV array. This system also tested with BLDC motor drive.

3.4 Conclusion

This chapter highlights the classifications and configurations of different converter strategies for LEV charging systems, underlining the value of developed strategies in resolving issues associated with conventional converters. The classifications was composed of both unidirectional and bidirectional configurations, addressing non-isolated, isolated, and bridgeless converter types. Initially, the circuits of various conventional converter strategies is discussed, and comparison indicates that the conventional converters results in bulky designs, larger power losses, hence provide low efficiency and low charging performance. To tackle these limitations, the chapter discussed new developed converter strategies aim not only to

reduce circuit complexity but also to lessen input and output ripples, reduced power losses, minimize switches stress, and improve efficiency. The developed strategies equate to better performance in terms of both power efficiency and system compactness. The reduction in passive components count plays a role to increased reliability and high payback time, making the system more cost-effective and long run of LEV battery. Another key highlight of the developed strategies was the on-board integration with solar PV array through MPPT converters to support the system during grid outage. Lastly, the developed LEV charging systems tested with Brushless DC (BLDC) motor drives, reflecting a well-integrated powertrain solution.

CHAPTER-4

SOLAR POWERED ON-BOARD LEV UTILIZING NON-ISOLATED HIGH GAIN CONVERTER

4.1 General

The need for electric vehicles (EVs) arises from a combination of environmental, economic, and technological factors. As urban pollution and climate change intensify, EVs present a sustainable alternative to traditional internal combustion engine vehicles, significantly reducing greenhouse gas emissions and reliance on fossil fuels. This transition is crucial for achieving cleaner urban environments and addressing the depletion of oil resources. While the push for electric vehicles is strong, some argue that the transition may face challenges such as high initial costs and the need for extensive charging infrastructure. EVs can utilize renewable energy sources, further enhancing their sustainability and reducing dependence on non-renewable energy.

Light electric vehicles (LEVs) represent a significant advancement in sustainable transportation, characterized by their reduced environmental impact and innovative technologies. These vehicles, which include electric bicycles, scooters, and small electric cars, utilize various propulsion systems such as brushless DC motors, which enhance efficiency and performance. LEVs present numerous advantages, but challenges such as infrastructure development and battery technology improvements remain critical for their widespread adoption.

Unidirectional charging strategies for light electric vehicles (LEVs) are designed to allow energy flow from the grid to the vehicle, primarily focusing on efficient and cost-effective charging. These strategies are crucial in managing the load on the grid, especially during peak hours, and in optimizing the charging process to align with low electricity prices. However, these systems often suffer from lower efficiency and higher volume compared to bidirectional systems, which can impact their performance and integration into smart grid environments. Unidirectional converter strategies are essential in various applications, particularly in renewable energy systems and LEVs. These converters facilitate efficient power transfer in a single direction, optimizing performance and reducing complexity. Various unidirectional non-isolated step-down converter strategies have been developed to address the challenges of high step-down voltage conversion. These strategies are essential in applications such as LEVs

charging and renewable energy-based charging systems, where efficient voltage regulation is crucial.

The main focus of the developed work is on control unidirectional charging from the grid to the LEV battery through a diode bridge rectifier (DBR) and a modified DC-to-DC converter, as well as on-board solar-based charging during a grid outage. Also, it focuses on reducing the number of overall drive train elements and efficiently works on the power management of all operational modes in Figure 4.1. The proposed strategy includes the following features and advantages,

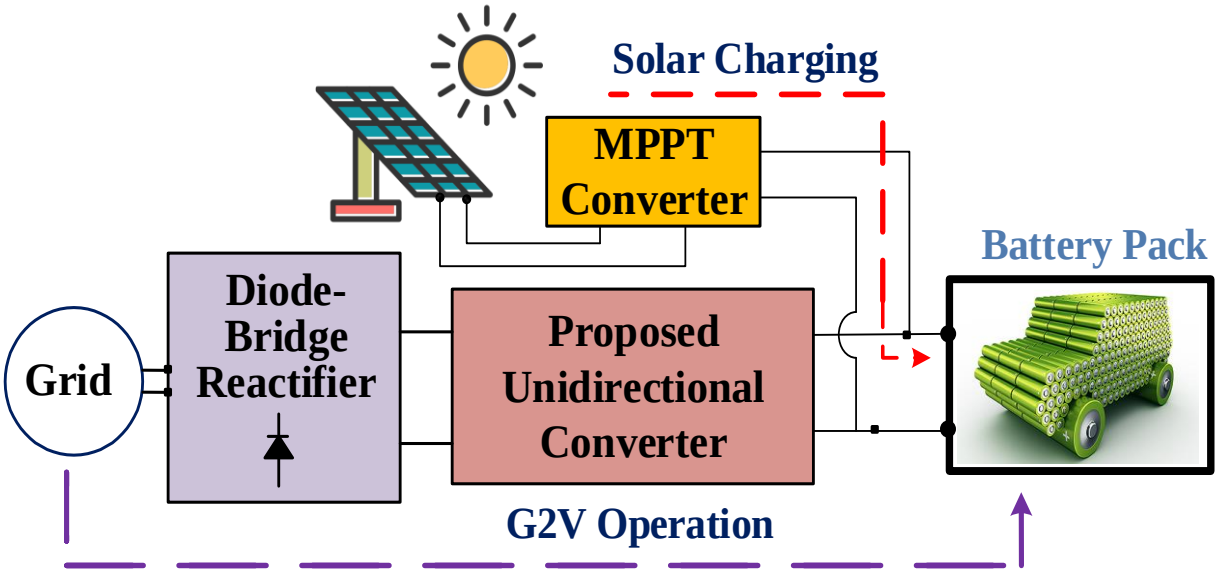

Figure 4.1. Schematic of the on-board grid-integrated solar-powered LEV utilizing a unidirectional converter.

- A unidirectional converter-based charging strategy with on-board solar PV MPPT converter features is designed for LEVs to incorporate G2V and solar-based charging operations.
- The developed system can achieve unity power factor operation, which is essential for reducing harmonic distortion and meeting regulatory standards.
- The developed unidirectional converter has reduced the total number of components to improve efficiency, compact size, and increased reliability.
- The developed unidirectional converter configuration also offers high payback time, lowers stress on semiconductor devices, and passive components.
- The proposed charging strategy manages the battery charging process, as an onboard solar PV-powered array with improved MPPT control algorithms.
- The proposed charging strategy ensures less burden on the grid due to the availability of an alternate source, viz., solar PV.

- The proposed strategy also introduces a brushless DC drive system for the propulsion mode of operation.

4.2 Circuit Configuration of Solar-Powered On-Board Light Electric Vehicle Using Unidirectional Non-Isolated Modified SEPIC Converter

Figure 4.2 shows the schematic of a non-isolated unidirectional modified SEPIC converter with dual power sources (i.e., single-phase grid and solar PV), employing a BLDC (brushless DC) motor drive. It employs a diode bridge reactifier (DBR) and a modified unidirectional SEPIC strategy, which performs power factor correction of the grid voltage and the grid current during charging mode. Moreover, an onboard photovoltaic module possessing a peak power capacity of 800 W utilizes an enhanced drift-free Perturb and Observe (P&O) control methodology to charge the LEV battery through a buck MPPT converter to maximize the efficacy of the solar photovoltaic system. A 750 W, 48V BLDC motor drive is used as a propulsion motor for the electric LEV. The non-isolated unidirectional strategy can meet charging performance with PFC and also use solar power to charge the LEV battery during the grid outage. Furthermore, it will drive the BLDC motor in propulsion mode.

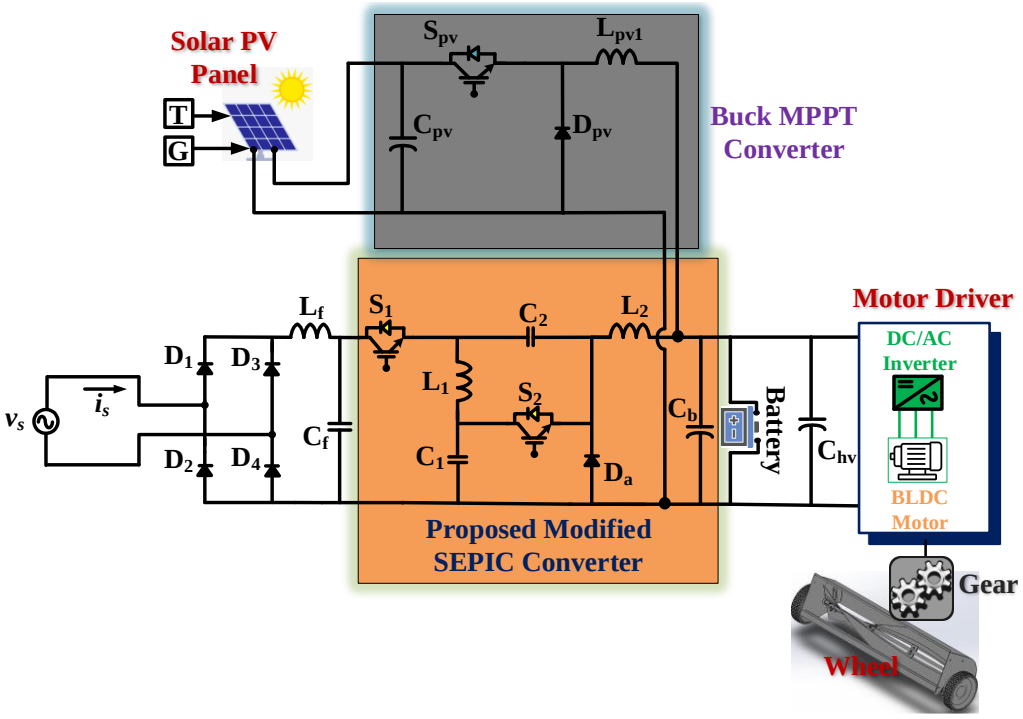

Figure 4.2. Circuit of Proposed Non-isolated Unidirectional Converter LEV Charging.

4.3 Modes of Operation of Solar-Powered On-Board Light Electric Vehicle Using Unidirectional Non-Isolated Modified SEPIC Converter

Mode I (Grid-to-Vehicle) : This mode starts when switches S_1 and S_2 are in active condition.

The inductors L_1 and L_2 store energy in the capacitors C_f, C_1 and C_2 via diode D_1 as shown in Figure 4.3. Hence, the DC-to-DC step-down is done through it, and the waveform in Figure 4.5 represents charging and discharging of passive components.

Mode II (Grid-to-Vehicle) : This mode starts when the switches S_1 and S_2 are in an inactive condition. The inductors L_1 and L_2 discharge their store energy and the capacitor C_1 and C_2 undergoes charging as shown in Figure 4.4. Once, the inductors are completely discharged, the capacitor C_b begins charging the LEV battery. Hence, the charging of the LEV battery is done through a developed converter system. The following equations related to this mode as,

$$V_{L_{1avg.}} = V_f.D + \left(V_f - V_{C_1}\right).(1-D) = 0 \quad (4.1)$$

$$V_{L_{2avg.}} = \left(V_{C_2} - V_{C_1}\right).D + \left(V_{C_2} - V_{C_b}\right).(1-D) = 0 \quad (4.2)$$

$$V_{C_2} = \frac{V_b}{1-D} \quad (4.3)$$

$$V_{C_1} = \frac{V_b.D}{1-D} \quad (4.4)$$

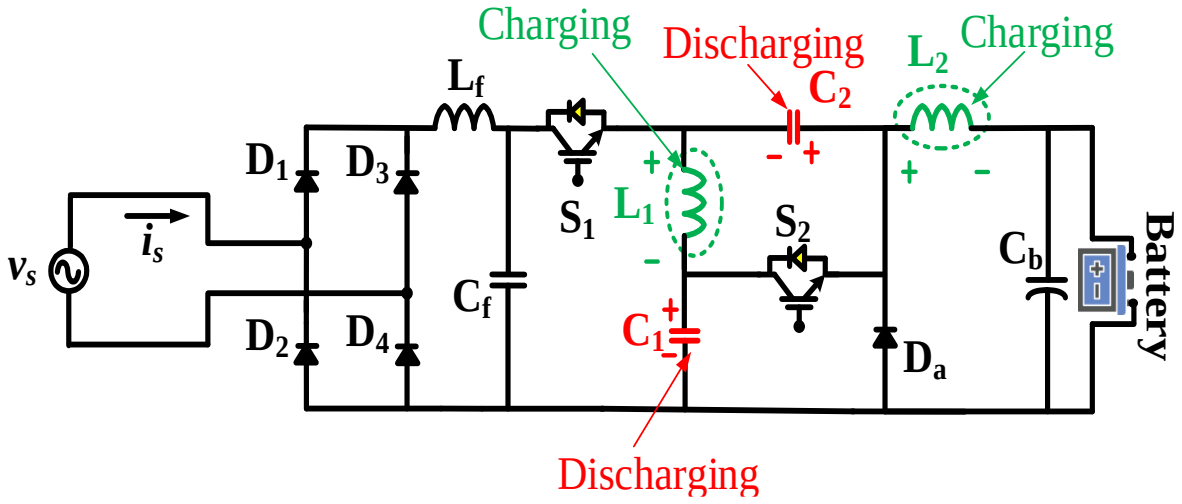

Figure 4.3. Circuit of G2V operational mode during on-state of switches S_1 and S_2.

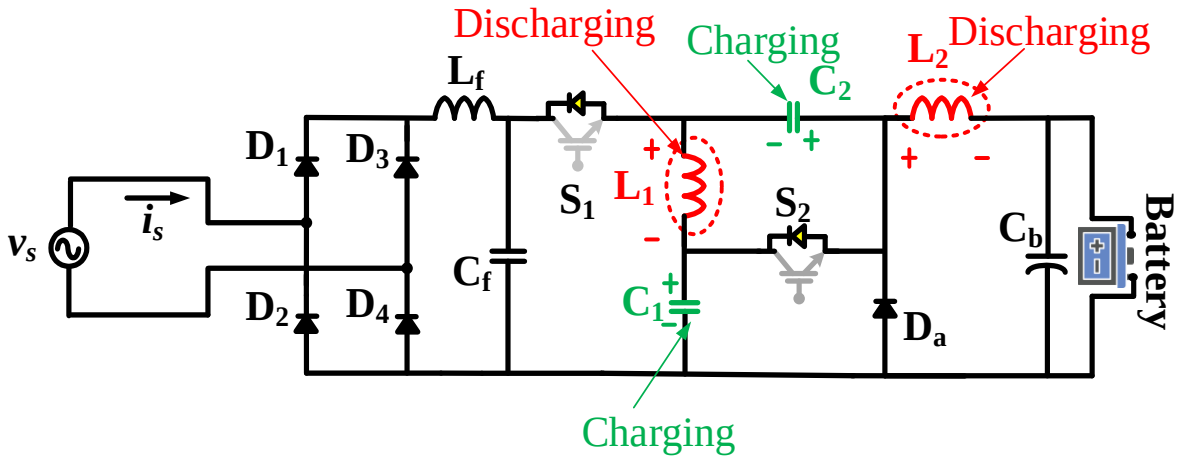

Figure 4.4. Circuit of G2V operational mode during off-state of switches S_1 and S_2.

Mode III (Solar PV based Charging) : In this mode, the solar PV array charged the LEV battery via MPPT buck converter during grid outage. The solar PV array gives power to dc link and the buck converter act as MPPT converter for the on-board solar PV based charging as shown in Figure 4.6.

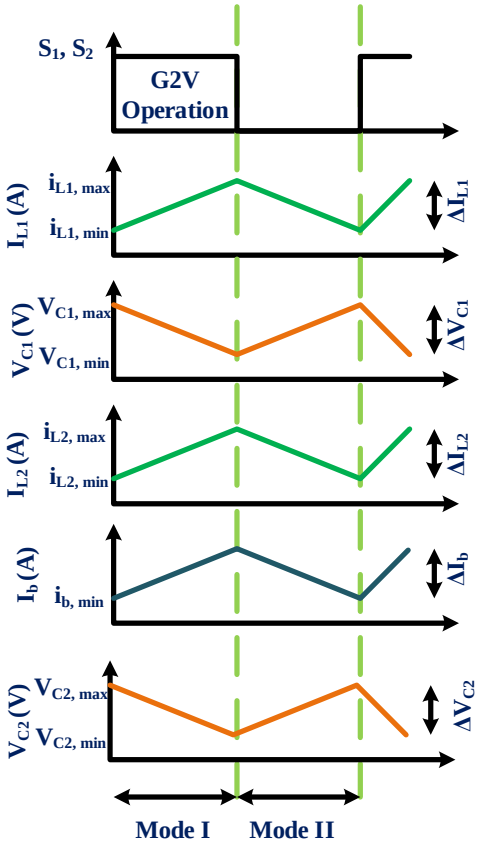

Figure 4.5. Waveform of G2V operational mode during on-off state of switches S_1 and S_2.

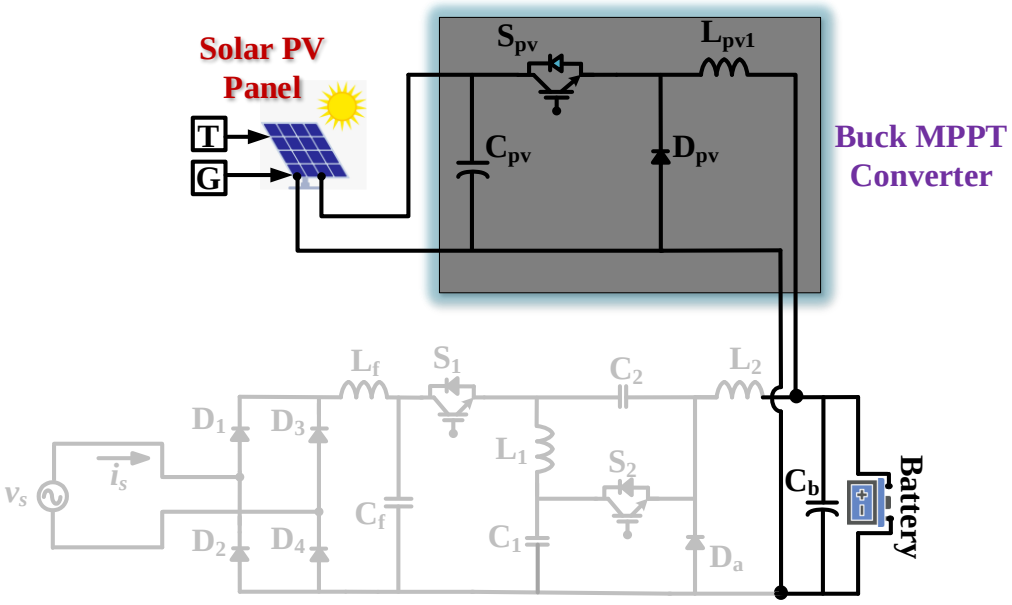

Figure 4.6. Circuit of operational mode solar PV-based charging.

4.4 Designing Solar-Powered On-Board LEV Using Unidirectional Non-Isolated Modified SEPIC Converter

4.4.1 Design of Non-isolated Modified SEPIC Converter

In this developed unidirectional non-isolated converter-based charging system, a single-phase supply *(V_s)* with a nominal voltage of 230V, 50Hz is considered for the circuit design in Table 4.1. The developed charging system is designed for a 48V, 50Ah battery. The design of filter inductors and capacitors is crucial for optimizing performance in LEV charging applications. The focus on optimizing filter components is critical for performance, it is also essential to consider the trade-offs between size, cost, and efficiency. Balancing all the switches, diodes, and passive elements can lead to innovative designs that meet efficient charging demands. The following equations are related to designing of developed unidirectional charging system as,

$$f_{cut} = \frac{1}{2\pi\sqrt{L_f C_f}} \tag{4.5}$$

The inductors L_1 and L_2 can be expressed as a value of the current ripple (Δi_{L_1}-Δi_{L_2}) and the voltage applied to the inductors during the switch $S_1$is active that is equal to v_b, as presented in (4.6) and (4.7).

$$L_1 = \frac{v_b.D}{\Delta i_{L_1}.f_s} \tag{4.6}$$

$$L_2 = \frac{v_b.D}{\Delta i_{L_2}.f_s} \tag{4.7}$$

The C_1 and C_2 capacitors can be expressed as a value of the voltage ripple (Δv_{C_1}-Δv_{C_2}) and by the charge variation, as presented in (4.8) and (4.9).

$$C_1 = \frac{i_{v_f}.D}{\Delta v_{C_1}.f_s} \tag{4.8}$$

$$C_2 = \frac{i_{v_f}.D}{\Delta v_{C_2}.f_s} \tag{4.9}$$

Table 4.1. Design parameter values for the developed unidirectional converter.

Parameter	**Value**
AC input voltage (V_g)	230 V
Line frequency (f)	50 Hz
Nominal Battery voltage (V_b)	48V
Initial SOC	20%
$L_f/C_f/L_1/L_2/C_1/C_2/C_b$	1mH/1µF/4mH/4mH/7.5µF/7.5 µF/1500 µF
Nominal load power	750 W

4.4.2 Design of Solar PV Array with MPPT and Buck Converter

The solar PV array of 800 W (peak power) is designed for LEV battery charging. The value of 53.55 V is selected for the maximum power point (MPP) voltage V_{mpp} of the array. The

other parameters of the PV array are given in Table 4.2. Consequently, the rated current at this condition is stated as,

$$I_{pv} = \frac{P_{pv}}{v_{pv}} \tag{4.10}$$

The number of series-connected modules per string is as,

$$N_s = \frac{v_{pv}}{v_{mp}} \tag{4.11}$$

and the number of parallel-connected strings is as,

$$N_p = \frac{I_{pv}}{I_{mp}} \tag{4.12}$$

Table 4.2. Parameters of solar PV array.

Parameter	**Value**
Peak Power (W)	800 W
Cell per module	36
Voltage at open circuit, $V_{o.c}$ (V)	21 V
Rated current at short circuit condition, $I_{s.c}$ (A)	5 A
Number of series strings, N_s	3
Number of parallel strings, N_p	3
MPP voltage rating, V_{mpp}	53.55 V
MPP current rating, I_{mpp}	12.75 A
L_{pv1}, C_{pv}, C_o	1mH/10µF/1500 µF

4.5 Control of Solar-Powered On-board Charging System Using Unidirectional Non-Isolated Modified SEPIC Converter

This section presents the effective implementation of appropriate controllers for the proposed system, along with the power management strategy for coordinating different sources under various operating modes. The detailed operation of the controller design are explained below,

4.5.1 Control of Unidirectional Non-isolated Modified SEPIC Converter

A single PI controller is commonly used to manage both power factor correction and AC-to-DC voltage regulation, ensuring stable operation during charging. The battery voltage and battery power via the LEV battery, and its output with reference to the battery current. After it, the output of the PI controller is multiplied by the grid voltage template, and the reference output is compared with the grid current, and then the pluses are entered to the switches as shown in Figure 4.7.

4.5.2 MPPT Control of Solar PV Array

Even though the conventional P&O MPPT method is easy to implement and effective, it has

serious deviation problems, particularly when there is variation in irradiance. It further results in additional power losses and tracking time lag. To attempt to solve this deviation problem, it is crucial to take into account the current variation in both cases when there is a positive or negative change in the PV array voltage.

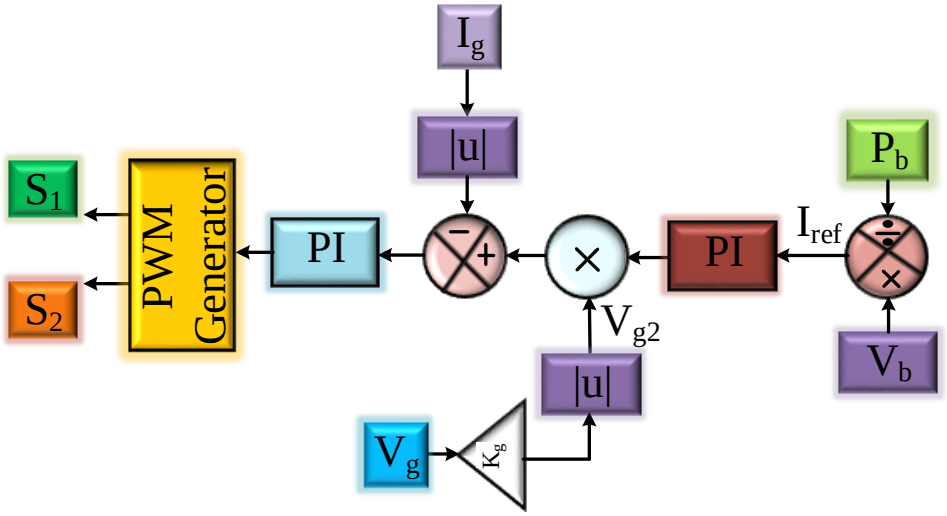

Figure 4.7. Controller of grid-based charging.

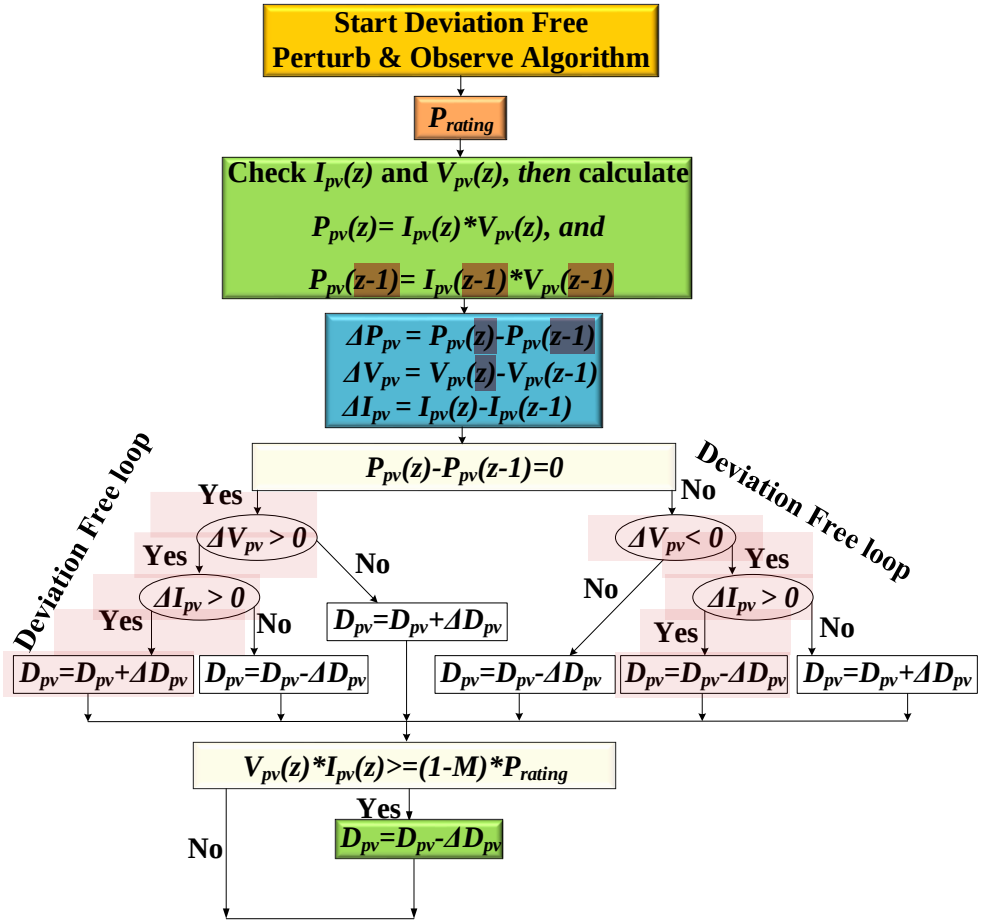

Figure 4.8. Flow chart of the modified P&O MPPT technique.

Thus, by considering the magnitude of alteration in current (ΔI_{PV}) in addition to the change in power (ΔP_{PV}) and in voltage (ΔV_{PV}) in the decision process, the deviation-free MPPT minimizes the deviation difficulty that exists with the conventional P&O technique. This method lowered the MPPT tracking time in the region of 15% to 20% of the total tracking time. Figure 4.8 depicts a flow chart of the proposed deviation-free MPPT controller.

4.5.3 Control of Brushless DC Motor Drive for Propulsion Mode

The primary intent of the controller design for a BLDC motor is to maintain a stable DC-link voltage for smooth operation. Figure 4.9 depicts the block diagram of the BLDC motor, which includes a three-phase voltage source inverter (VSI), position sensor, torque command, current regulator, and commutation logic. Table 4.3 depicts the design parameter of BLDC motor. The high-frequency PWM pulse 'S_{bm}' as shown in Figure 4.10 is generated by propulsion mode control logic developed for the traction motor. As depicted, the input to the voltage control block receives the difference between the desired DC-link voltage, v_{hv}^*, and the assessed DC-link voltage, v_{hv}. Further, the output gives the reference value, which again acts as the battery current discharging value. After that, this coming value is again compared with the sensed i_b* (i.e. battery current), and the output error between the two is input to the current control block. The coming signal is then compared with the high-frequency carrier signal to generate the S_{bm} (i.e. switching pulses).

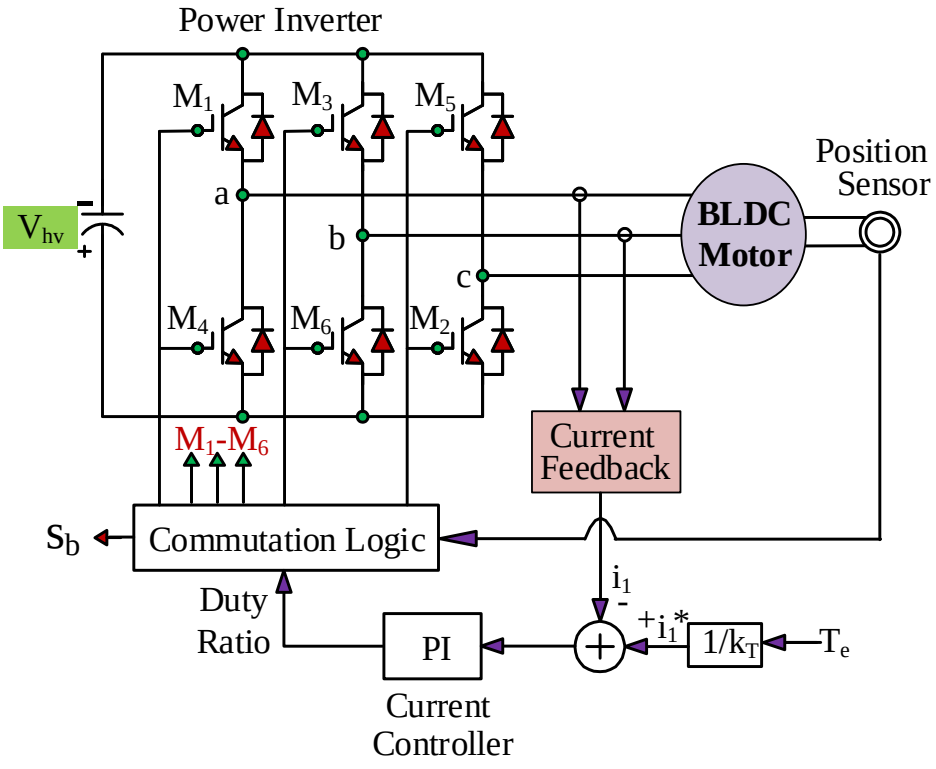

Figure 4.9. Block diagram of BLDC motor.

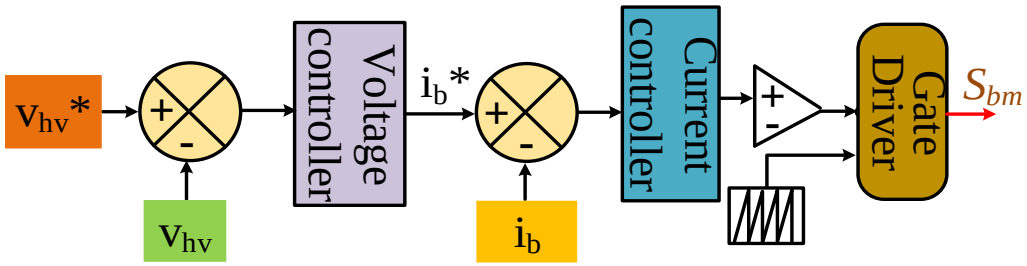

Figure 4.10. Controller of the BLDC motor.

Table 4.3. Design parameter values for BLDC motor.

BLDC Motor Parameter	Value
Rated power (W)	750 W
Rated speed (N-m)	3000 rpm
No. of poles, P	4
Current, I_s	30 A
Torque constant, k_t	0.45 Nm/A
Voltage constant, k_e	68 V/krpm
Phase/phase resistance, R_s	2.58 ohm
Phase/phase resistance, L_s	7.13 mH

4.6 MATLAB Based Modeling and Simulation of Solar Powered On-board Charging System Using Unidirectional Non-Isolated Modified SEPIC Converter

The following models in Figure 4.11(a-b) shows the MATLAB based modeling and simulation of solar powered on-board charging system utilizing unidirectional modified SEPIC converter. Model efficiently works on G2V and V2G modes, and on-board charge the LEV battery via solar PV MPPT converter. This charging strategies also run the BLDC motor drive system.

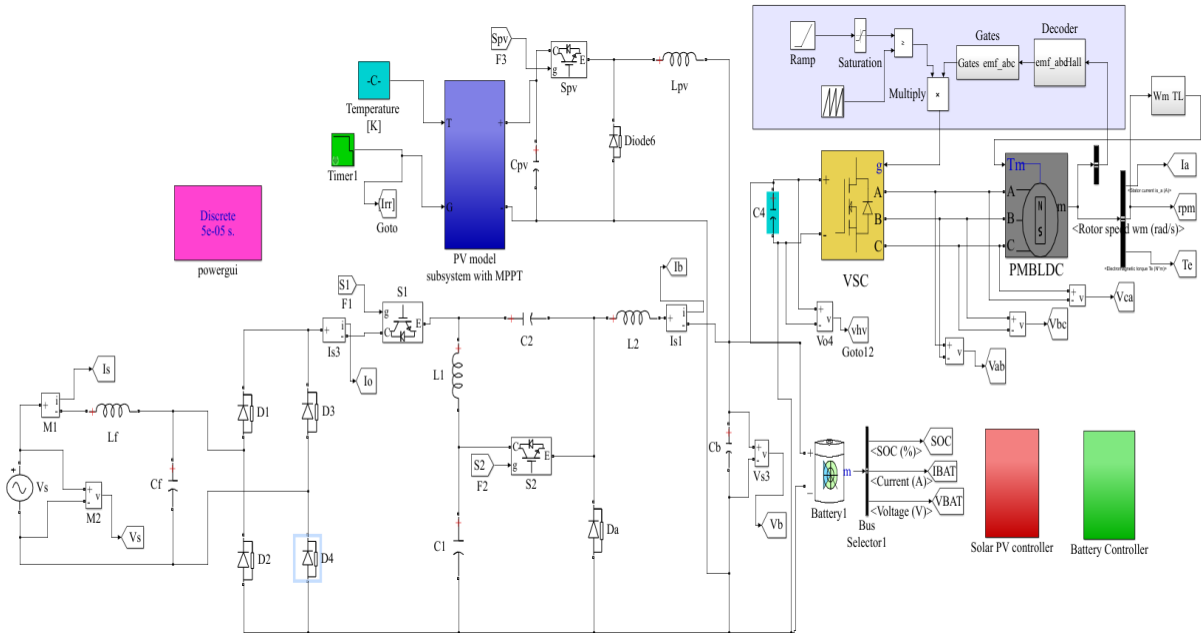

Figure 4.11. MATLAB based modeling and simulation of solar powered on-board charging system utilizing unidirectional non-isolated converter.

4.7 Results and Discussion

In order to ensure the adequate performance of the developed unidirectional non-isolated converter, the whole design and control of the charger are tested using MATLAB/SIMULINK environment and verified experimentally on OPAL-RT. The effectiveness of the developed system is investigated during the steady-state condition to validate the safe and reliable operations. Moreover, during the off condition of grid supply, battery charging through solar PV array is shown through both simulation and real-time study. Also, a comprehensive operational analysis of the BLDC motor is carried out here.

4.7.1 Simulated Performance of Solar-Powered On-Board LEV Utilizing Unidirectional Non-Isolated Modified SEPIC Converter

The developed system is tested using the MATLAB/SIMULINK environment, to ensure optimal charging in both grid power supply and solar-powered conditions, in this section. The effectiveness of the developed charger is demonstrated via simulation results. Also, a simulation operation investigation of the BLDC motor is presented in this section.

4.7.1.1 Grid-Based Charging Performance

Figure 4.12 illustrates the power factor correction (PFC) operation between the grid voltage (V_g) of around 230V, and grid current (I_g) of 13.36A, and grid voltage of 230V. The in-phase operation between both sinusoidal-shaped waveforms demonstrates that the developed system operates in high power factor (HPF). Figure 4.15 illustrates the current across inductor (L_f) which around 14A, and voltage across the capacitor (C_f) which is rectified up to 200V (peak). Figure 4.14 illustrates the waveform of current and voltage across switches, and THD of 3.63 % is observed at grid current of 13.36A in Figure 4.15, indicating that the converter consumes very little reactive power from the grid, which helps reduce the electricity costs for LEV charging. The charging performance of the LEV system, such as battery SOC taken at 20%, battery voltage around 51V, and average battery current of -12A, is observed in Figure 4.16.

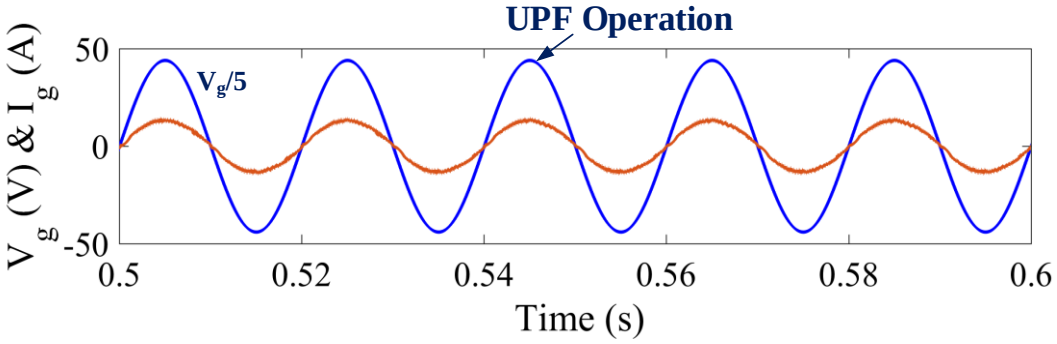

Figure 4.12. Simulated performance of PFC operation between grid voltage $(V_g)$and grid current (I_g).

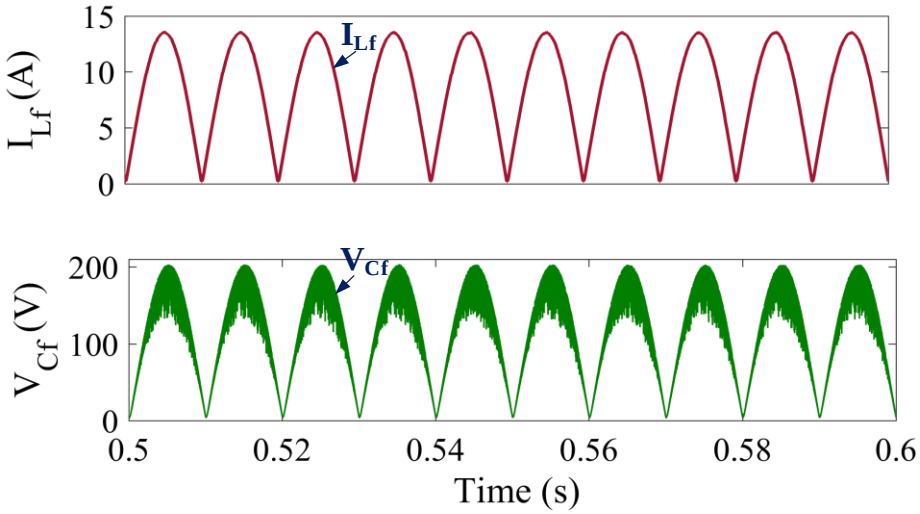

Figure 4.13. Simulated performance of current across inductor (I_{Lf}) and voltage across capacitor (V_{Cf}).

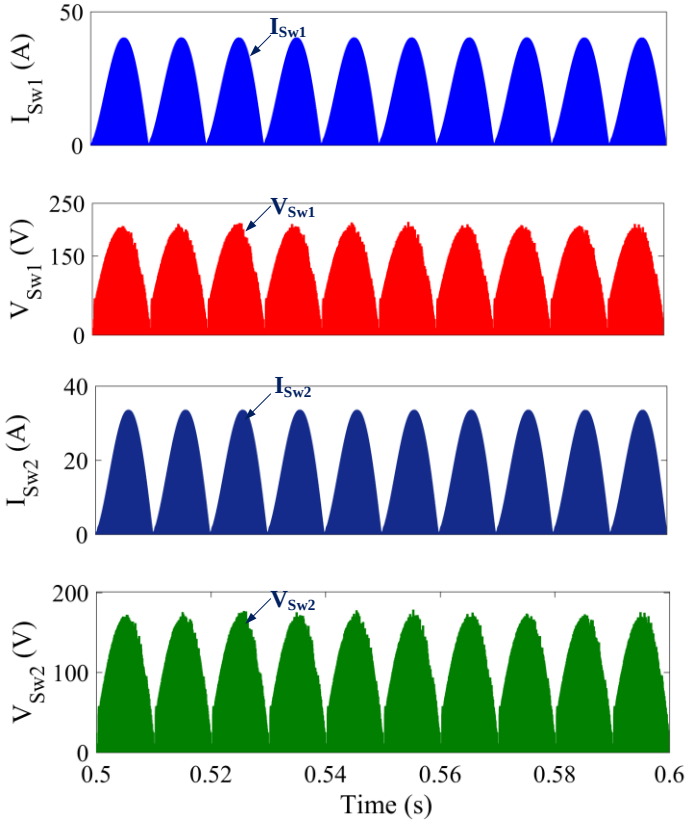

Figure 4.14. Simulated performance of current and voltage across switches $(I_{Sw1}, V_{Sw1}, I_{Sw2}, V_{Sw2})$.

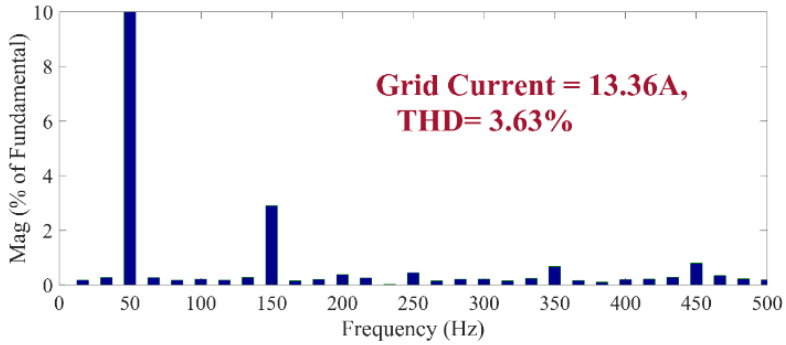

Figure 4.15. Simulated performance of THD of I_g during G2V.

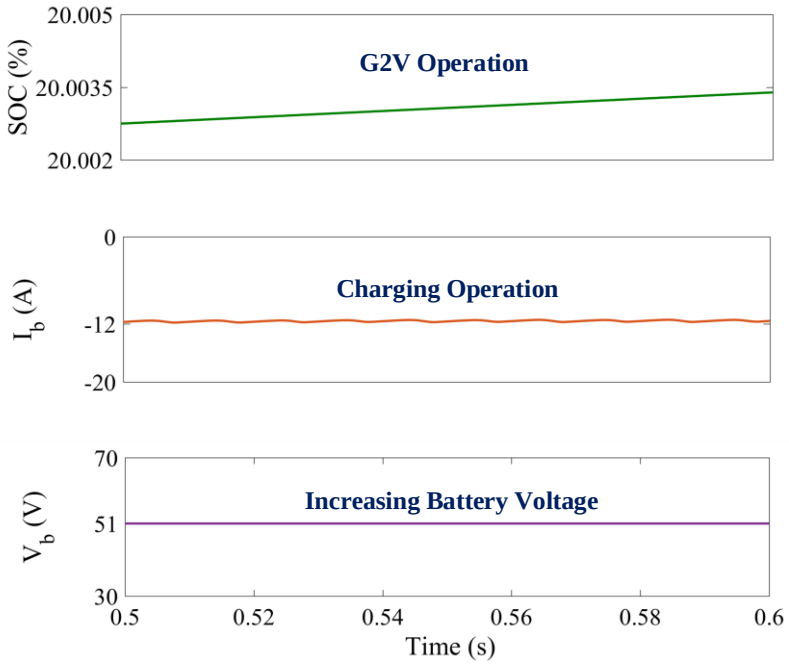

Figure 4.16. Simulated performance of LEV battery charging (SOC, I_b, V_b).

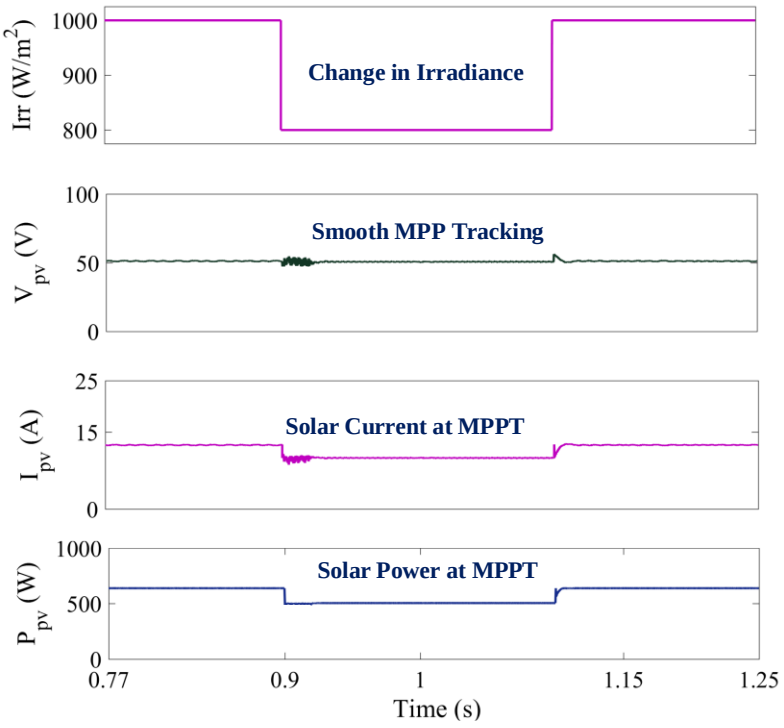

Figure 4.17. Simulated performance of solar PV array $(Irradiance, V_{pv}, I_{pv}, P_{pv})$.

4.7.1.2 Solar PV-Based Charging Performance

The simulated waveforms in Figure 4.17 illustrate the on-board solar PV charging operation during the grid disconnection. The on-board solar PV MPPT converter functions under solar irradiation of (1000, 800, 1000) W/m². At this level of irradiation, the solar PV has maximum power output is 800 W. These are changes in irradiance, PV voltage (V_{pv}) at MPPT, PV current

(I_{pv}) at MPPT, PV power (P_{pv}) at MPPT, and in Figure 4.18, the waveform of battery state of charge (SOC), battery charging current, and increasing battery voltage. It confirms the efficient energy conversion, stable LEV battery charging despite varying solar PV input.

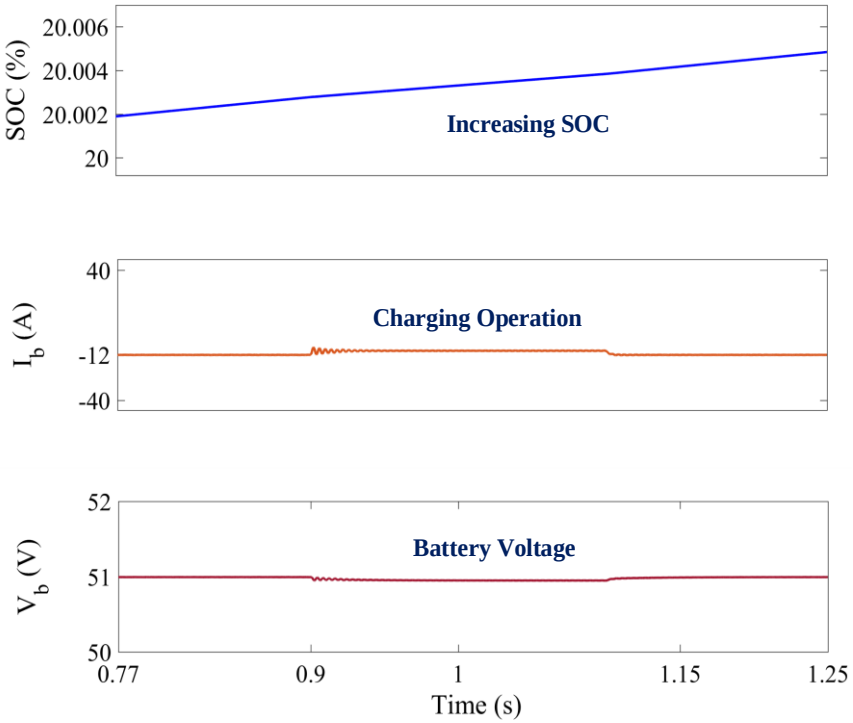

Figure 4.18. Simulated performance of solar PV array-based charging (SOC, I_b, V_b).

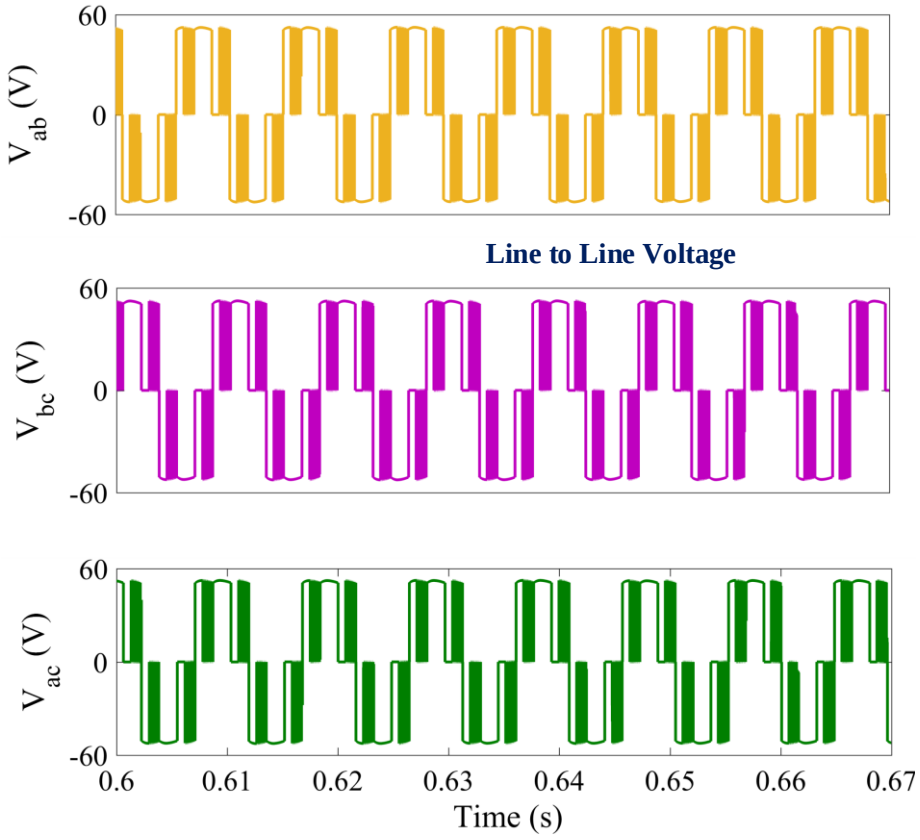

Figure 4.19. Simulated performance of BLDC motor three phase line-line voltages (V_{ab}, V_{bc}, V_{ac}).

4.7.1.3 Brushless DC Motor Performance

The brushless DC motor performance in propulsion mode is illustrated in Figure 4.19, like line-line voltages (V_{ab}, V_{bc}, and V_{ac}) of all three phases indicating consistent voltage levels across the BLDC motor phases, which are around 50V, the stator current (I_a) is around 20 A suggesting efficient current regulation and minimal losses during operation, and motor torque around 2.5 N-m and rotor speed of 2100RPM are shown in Figure 4.20. These waveforms illustrate that the BLDC motor is operating efficiently under the given battery conditions, providing stable propulsion with reliable torque and speed characteristics.

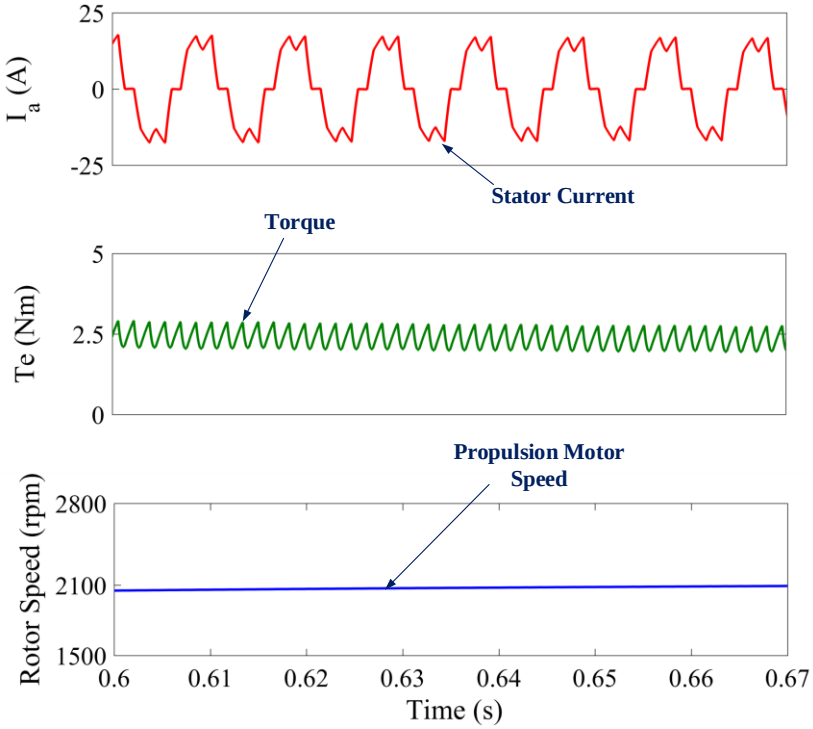

Figure 4.20. Simulated performance of the BLDC motor during propulsion mode $(I_a, Te, Rotor\ Speed)$

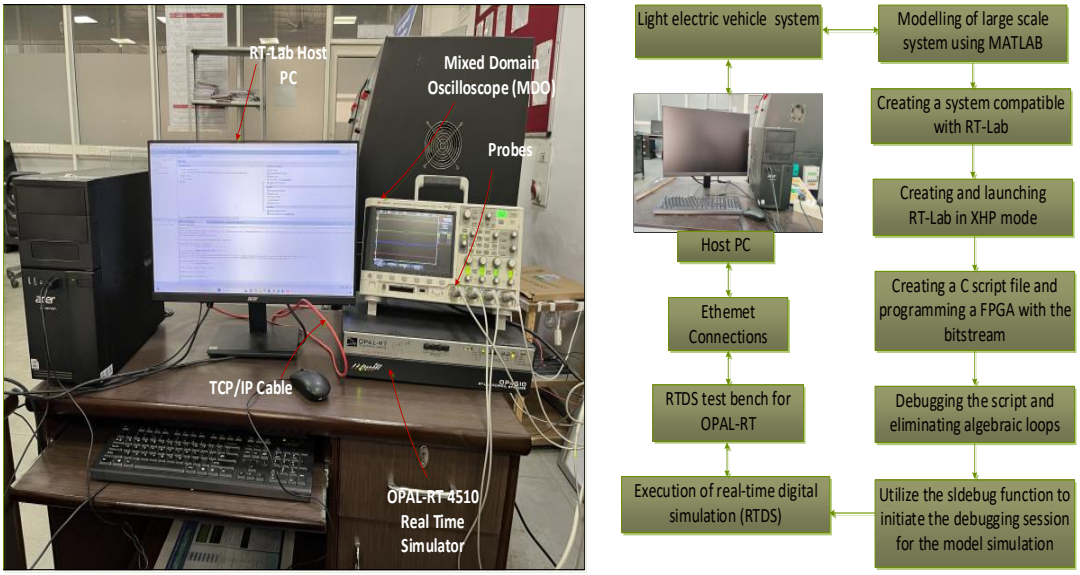

Figure 4.21. Real-time CHIL test setup.

4.7.2 Experimental Performance of Solar-Powered On-Board LEV Utilizing Unidirectional Non-Isolated Modified SEPIC Converter

The developed unidirectional non-isolated converter is validated via an OPAL-RT interface to ensure the optimal charging efficiency in both grid power supply and solar-powered conditions in this section. Also, a hardware operation investigation of the BLDC motor has resulted here. Referring to Figure 4.21, a diagram of the CHIL (controller hardware in the Loop) test with an algorithm is given. Various test results are performed in this setup, and this section studies the same specifications as the simulation study. This section explained the G2V operations, on-board solar PV-based charging, and BLDC motor operation.

4.7.2.1 Grid-Based Charging Performance

Figure 4.22 illustrates the UPF operations between the grid voltage V_g and grid current I_g during G2V mode. The UPF between V_g and I_g indicates that the developed system transfers energy from the grid to the LEV battery with improved distortions in grid current. The LEV battery charging operation parameters, like grid voltage V_g, grid current I_g, battery current I_b, and battery voltage V_b is illustrated in Figure 4.23. These parameters are important for controlling the LEV battery charging process with safe, reliable, and efficient operation.

4.7.2.2 Solar PV-Based Charging Performance

In Figure 4.24, the performance of on-board solar PV-based charging is validated under different environmental conditions. These parameters include the change in irradiance, PV voltage (V_{pv}), and battery current I_b, and battery voltage V_b. This validation confirms the efficient energy conversion, stable LEV battery charging despite varying solar input, and reliability of integrating solar PV technology for on-board charging applications in LEV.

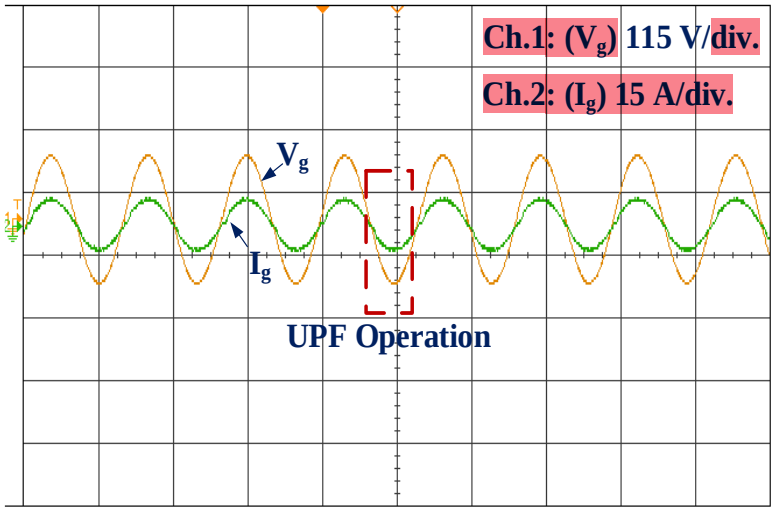

Figure 4.22. Experimental performance of PFC operation between grid voltage (V_g) and grid current (I_g).

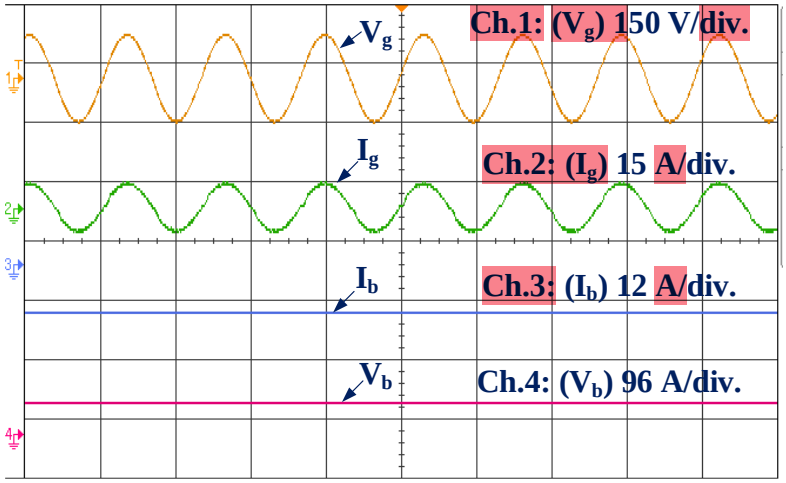

Figure 4.23. Experimental performance of grid-based LEV charging operation (V_g, I_g, I_b, V_b).

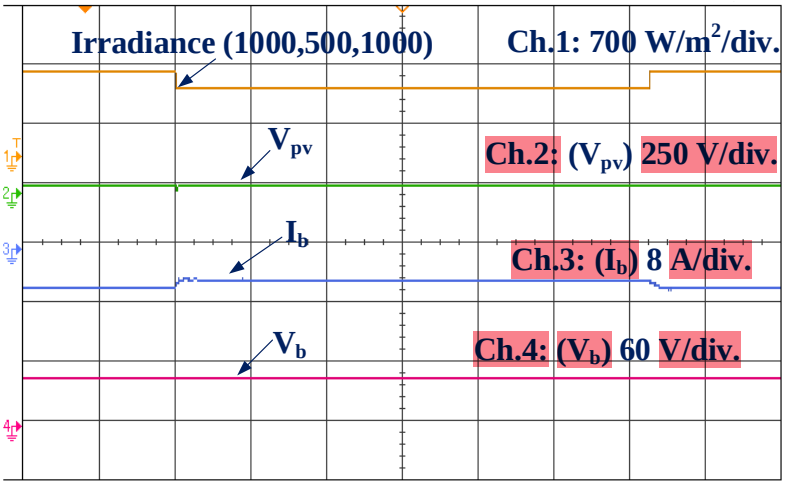

Figure 4.24. Experimental performance of on-board Solar PV array-based LEV charging $(Irradiance, V_{pv}, I_b, V_b)$.

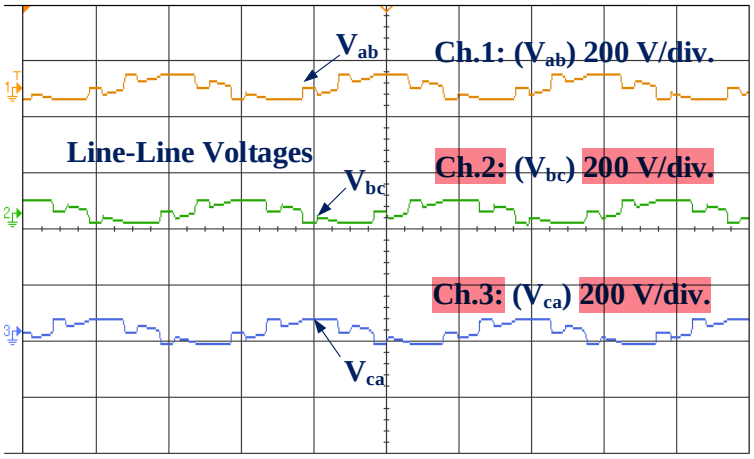

Figure 4.25. Experimental performance of BLDC motor three-phase line-line voltages (V_{ab}, V_{bc}, V_{ca}).

4.7.2.3 Brushless DC Motor Performance

Figure 4.25, brushless DC motor performance in propulsion mode is validated. The line-line

voltages (V_{ab}, V_{bc}, and V_{ac}) of all three phases provide insight into the BLDC motor's voltage supply and switching characteristics, the stator current (I_a), motor torque, and rotor speed in propulsion mode are shown in Figure 4.26. This validation demonstrates the effectiveness of the BLDC motor control strategy in achieving smooth and stable operation.

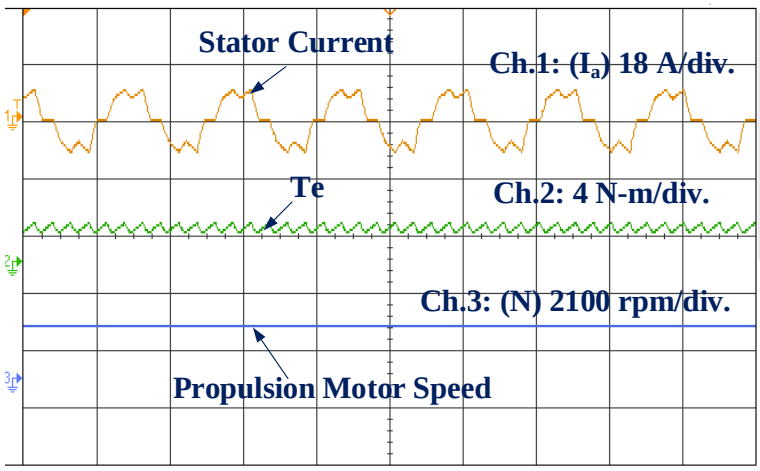

Figure 4.26. Experimental performance of the BLDC motor during propulsion mode $(I_a, Te, Rotor\ speed)$.

4.8 Losses and Efficiency Calculation

The voltage & current stresses handled via various components of the developed unidirectional non-isolated LEV charger are examined to ensure its safe, reliable, and efficient operation. The system performance is verified by performing power loss manipulations. The losses in diodes, capacitors, switches, and inductors are considered as power losses in converters as shown in Figure 4.27. The mathematical formulations (4.13)-(4.20) explain the calculation of power losses and efficiency of the proposed system, given as follows,

Switches $(Q_1 - Q_2)$ conduction losses (P_{closs}):

$$\left(V_{CEO}.I_{Q1avg.} + r_{CE}.I_{Q1rms}^2\right) = \left((1.02 \times 5.21) + (0.0058 \times 10.13^2)\right) \quad (4.13)$$
$$= 5.90W$$

Switches $(Q_1 - Q_2)$ switching losses (P_{swloss}):

$$\left(V_{Q1max}.I_{Q1avg.}(t_r + t_f).f_s\right) = (500 \times 5.21) \times (35 + 75) \times 10^{-9} \times 20000 \quad (4.14)$$
$$= 5.7\ W$$

Diode switching losses for (D_a) switches (P_{sdloss}):

$$0.5 \times \left(V_{rev}.I_{rr(peak).}.(t_{rr}).f_s\right) = 0.5 \times 100 \times 50 \times 10^{-9} \times 20000 \quad (4.15)$$
$$= 0.05\ W$$

Input Inductor Losses $(P_{L_{sloss}})$:

$$I_{L_s}^2 rms \cdot r_{L_s} = 2.56^2 \times (32 \times 10^{-3}) = 0.21\,W \quad (4.16)$$

Output Inductors Losses ($P_{L_{oloss}}$):

$$2 \cdot I_{L_o}^2 rms \cdot r_{L_o} = 2 \times 8^2 \times 20 \times 10^{-3} = 2.56\,W \quad (4.17)$$

Intermediate Capacitor Losses ($P_{C_{Iloss}}$):

$$2 \cdot I_{C_I}^2 rms \cdot ESR_{C_I} = 2 \times 3.1^2 \times 80 \times 10^{-3} = 1.54\,W \quad (4.18)$$

The total power loss of the proposed converter is given in Equation (4.19), and the efficiency of the converter for the output power of 720W is calculated by using Equation (4.20).

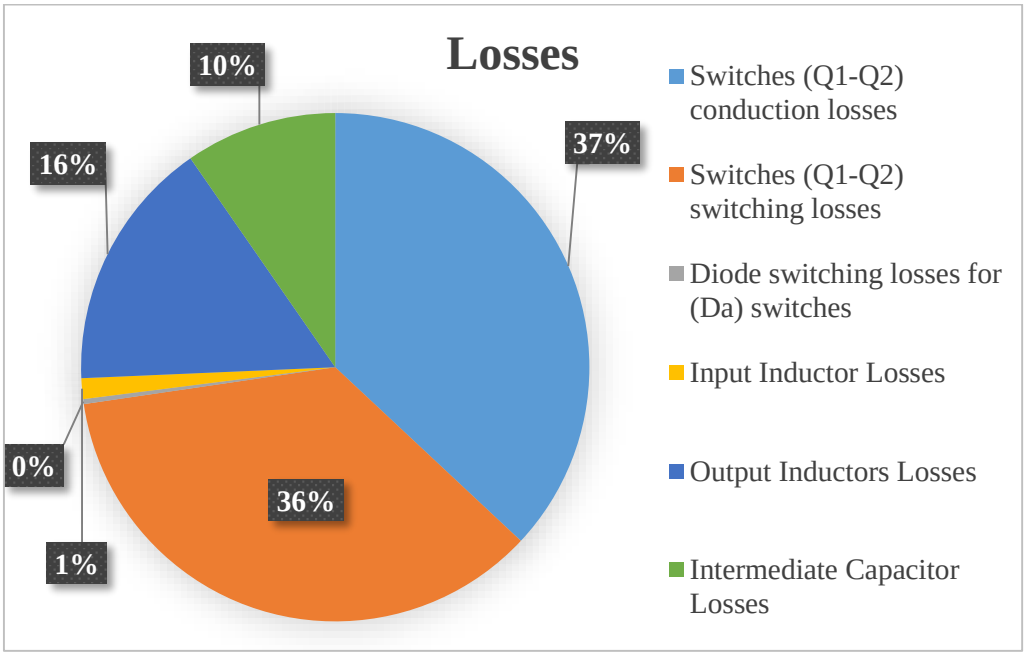

Figure 4.27. Graphical representation of power losses in the developed LEV charging system.

$$P_{loss}^{Total} = P_{closs} + P_{swloss} + P_{sdloss} + P_{L_{sloss}} + P_{L_{oloss}} + P_{C_{Iloss}} \quad (4.19)$$

$$P_{loss}^{Total} = 15.96\,W$$

$$\text{Efficiency } (\eta) = \frac{P_0}{P_0 + P_{loss}^{Total}} \quad (4.20)$$

$\eta = 97.83\ \%$

4.9 Conclusion

The proposed solar-powered on-board charging system utilizing a unidirectional non-isolated converter demonstrates effective charging operation. The single-stage design of a unidirectional non-isolated converter reduces the size of passive components, making them more suitable for compact applications such as on-board LEV chargers. Moreover, the unity power factor operation is also achieved in the charging mode. The developed system efficiently

charges the LEV battery via on-board solar PV with an MPPT converter during a grid outage. The control technique is well-suited for a 48V, 50 Ah LEV battery, as verified through MATLAB simulations and real-time validation using OPAL-RT. Results demonstrate that the modified SEPIC DC-to-DC converter offers stable voltage regulation, reliable LEV battery charging, and smooth drive of BLDC motor in propulsion mode, making it a robust and scalable solution for next-generation LEV charging systems.

CHAPTER-5

SOLAR POWERED ON-BOARD LEV UTILIZING NON-ISOLATED HIGH GAIN CONVERTER WITH G2V AND V2G CAPABILITIES

5.1 General

The worldwide concern of global warming and fossil fuel, the transportation industry necessitated to present an electric vehicle (EVs). In the last few years, the integration of these EVs sales to the transportation sector reached the highest level. However, understanding of sustainable energy, betterment in battery technology, and lowering in cost of EVs, the integration largely depends upon the efficient topologies and control techniques. For a good charging infrastructure, controlled charging technique demands low harmonics injected to the grid, improved power quality and a unity power factor (UPF) operation within guidelines. Furthermore, the main attention is to provide electrical power for the appropriate controlled battery charging speed. Integrating solar, wind or other renewable sources can lower dependency on fossil fuels and decrease greenhouse gas emissions, contributing to a more sustainable transportation setup.

The previous development based on EV charging infrastructure has been overworked. Some performance limitations of the LEVs while charging are a concern for LEV battery chargers. The LEVs are stuck to unidirectional charging only. Therefore, there is a need to develop a high-performance bidirectional charging infrastructure with broad output voltage handling capability. In comparison to single-stage strategies, the two-stage strategies, which offers ripple-free charging to the battery, seem convenient for low-voltage powered EVs. The two-stage strategy comprises two conversion stages, AC-to-DC and DC-to-DC [4]. The AC-to-DC conversion stage regulates the DC side voltage at the desired level while the parallel setting of the AC current waveform is achieved according to the existing power quality standards [5]. In the process of battery charging, the regulated DC voltage from the first stage is modulated to a suitable level in the DC-to-DC conversion stage. Both conversion stages, AC-to-DC and DC-to-AC, are comprised of bidirectional charging infrastructure. The usability of on-board charger (OBC) is boosted by its bidirectional operation. Peak shaving will be achieved in operating mode, i.e., vehicle-to-grid (V2G), when the vehicle is not in operation.

Numerous charging strategies include pulse charging, constant current (CC), and constant current-constant voltage (CC-CV). High-gain bidirectional converters (i.e. DC-to-DC) with two-stage OBC are needed for a LEVs that have low charging power. Normally, the high-gain converter categories such as coupled inductor, and switched capacitor. This chapter presented a two-stage OBC strategy with dual power sources i.e., single phase grid and solar PV in Figure 5.1. In this OBC solutions, front-end AC-to-DC and DC-to-DC conversion is essential. Front-end converters feature a power factor correction (PFC),

improved output voltage regulation, and a decrease in input current harmonics. High gain bidirectional DC-to-DC converters, an essential part of an LEV charger, make it easier to obtain an efficient OBC. Further, integrating solar PV power with the grid is one practical solution for providing a reliable power source for LEVs battery, during grid outage. Moreover, an OBC must be capable to derive a BLDC motor which is regularly adopted in low-power LEVs applications for the reason that it has various gains, such as easiness in control, low power losses, and propulsion operations. By the purpose of getting a gain in the DC-DC topologies, switched capacitor/ inductor arrangements are hired. This chapter proposes a both grid-to-vehicle (G2V) and vehicle-to-grid (V2G) operable charger, considering the previously mentioned scenario.

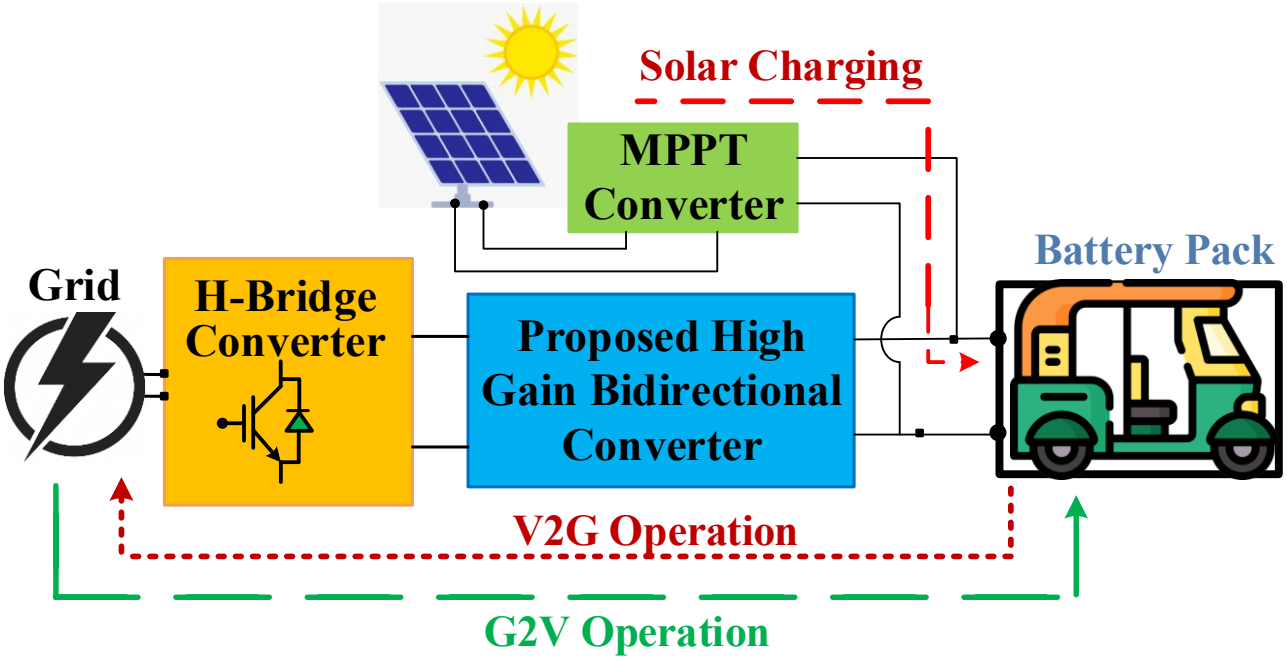

Figure 5.1. Schematic of developed on-board grid-integrated solar-powered LEV utilizing high-gain bidirectional converter.

5.2 Configuration of Solar Powered On-board LEV Utilizing Non-Isolated High Gain Converter with G2V and V2G Capabilities

A solar-powered bidirectional OBC based on the high-gain coupled-inductor and switched-capacitor converter for a BLDC motor-driven LEV is discussed in this section. The converters strategies has features of both grid-to-vehicle (G2V) and vehicle-to-grid (V2G), as well as charging via solar PV array during grid outage. Furthermore, this section is categorized as solar powered on-board charging system utilizing coupled inductor high gain SPEIC converter with G2V and V2G capabilities and solar powered on-board charging system utilizing high gain switched capacitor ZETA converter with G2V and V2G capabilities.

5.2.1 Circuit Configuration of Solar Powered On-board Charging System Utilizing Coupled Inductor High Gain SEPIC Converter with G2V and V2G Capabilities

The schematic of solar-powered bidirectional OBC based on the coupled-inductor high gain converter with grid-to-vehicle (G2V) and vehicle-to-grid (V2G) operations is shown in Figure 5.2. This configuration implements single-phase supply with nominal voltage (V_s) rating of 230V, and line

frequency of 50 Hz. Further, the input inductor (L_s) acts as a filter inductor for the supply current (I_s), and the DC-link capacitor (V_{DC}) with a suitable controller regulates the DC-link voltage after AC-to-DC conversion. The active front-end converter also maintained the unity power factor operation between grid voltage and grid current. The high gain converter employs two switched inductors (L_{01}) and (L_{02}) to increase the gain (i.e. high gain) of SEPIC, which increases the durability of the power electronics switches. The inductor (L_2) is used to reduce the ripples from the charging current.

An isolated solar photovoltaic (PV) array with a SEPIC converter is also being used in the system configuration. The purpose of the PV array is to support batteries during the non-availability of grid power supply and to feed auxiliary loads. The 48V, 50Ah lithium-ion batteries are being used in light electric vehicles. Moreover, the DC-to-AC inverter in the motor derive is used to operate the BLDC motor.

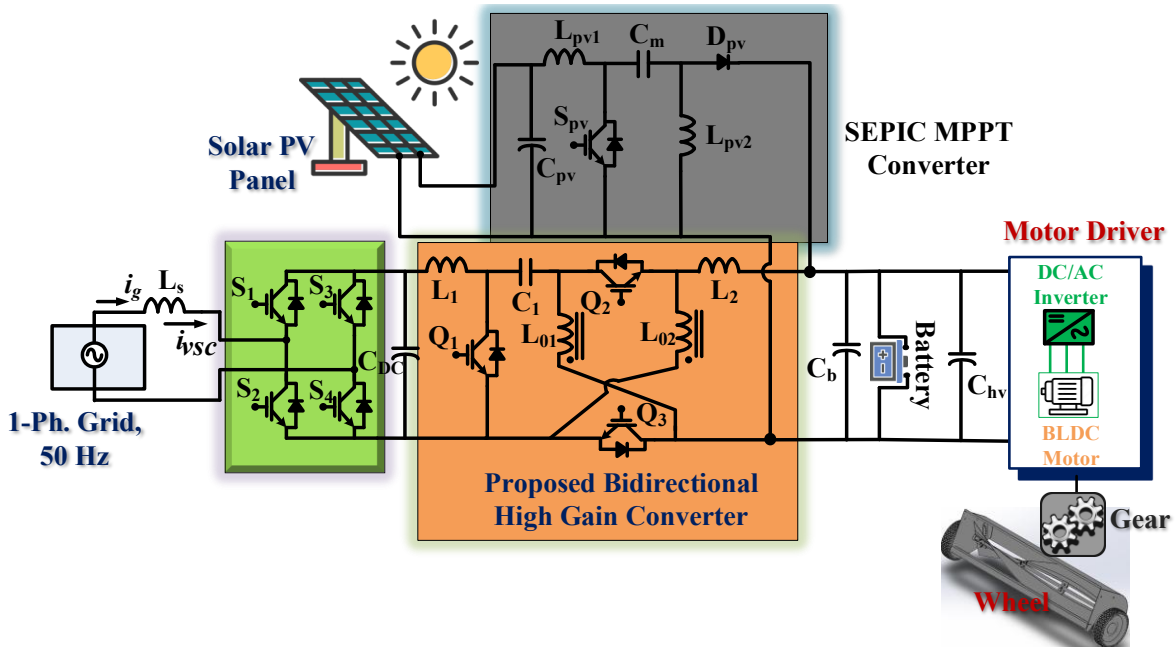

Figure 5.2. Schematic of proposed bidirectional high-gain converter LEV charging.

5.2.2 Configuration of Solar-Powered on-board Charging System utilizing High-Gain Switched Capacitor ZETA Converter with G2V and V2G Capabilities

The diagrammatic representation of the grid and solar-powered LEV charging strategy with switched capacitor bidirectional ZETA (SCBZ) is referred in Figure 5.3. At the initial stage, this scheme consists of an AFC input supply (V_s) of 230V, 50 Hz. This stage includes an input inductor (L_s), which filters for the grid current. Further, the capacitor (V_{DC}) with an adequate value is used to set the voltage in the AC-DC conversion. The AFC also continued to maintain the UPF operation between grid voltage and grid current during G2V and V2G. Furthermore, at the back-end stage the SCBZ converter includes two switched capacitors (C_{01} and C_{02}) to increase the gain of ZETA, which raises the stability of the converter. The battery side inductor (L_2) is exercised to mitigate the fluctuations from the incoming current (i.e. the current that pay a role for the battery charging). The system schematic also consists of an on-board MPPT-based solar array coupled with a Cuk converter. This on-board PV serves to assist the LEV, such

as e-rickshaw batteries, during a grid outage. At the end side DC-to-AC inverter is active to operate BLDC motor in propulsion mode.

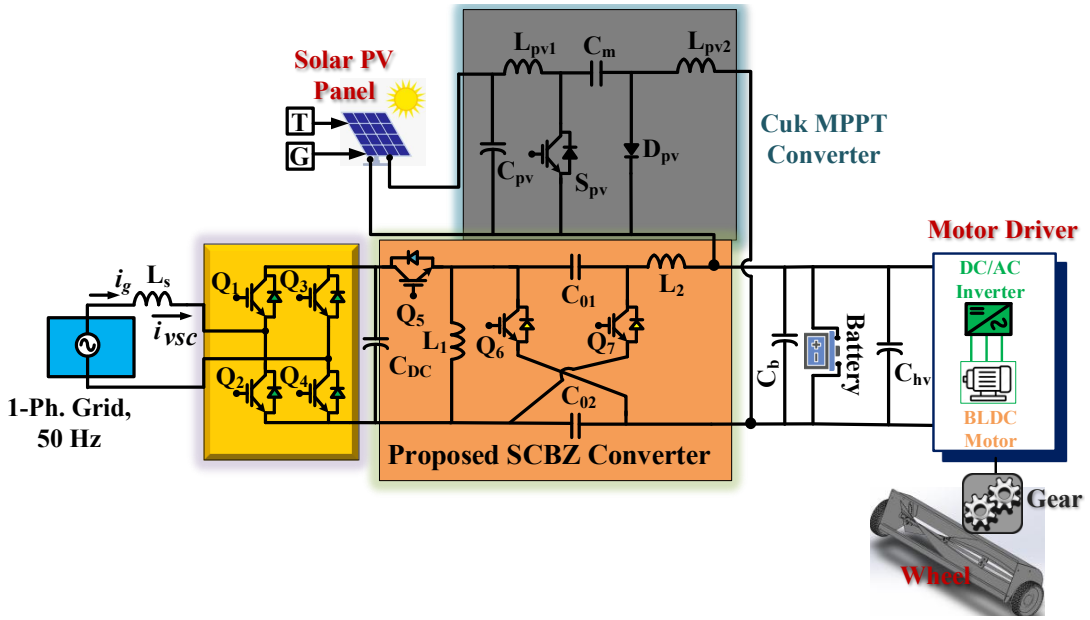

Figure 5.3. Schematic of proposed bidirectional high-gain SCBZ converter LEV charging.

5.3 Modes of Operation of Solar Powered On-board LEV Utilizing Non-isolated High-Gain Converter with G2V and V2G Capabilities

13 The developed bidirectional high-gain converters perform both in grid-to-vehicle (G2V) and vehicle-to-grid (V2G) modes of operation as well as solar PV MPPT converters-based LEV charging as below.

5.3.1 Modes of Operation of Solar Powered On-board Charging System Utilizing Coupled Inductor High Gain SEPIC Converter with G2V and V2G Capabilities

13 The developed bidirectional high-gain converter performs both in grid-to-vehicle (G2V) and vehicle-to-

119 grid (V2G) modes of operation, as illustrated in Figure 5.4(a-b).

Figure 5.4(a) illustrates the G2V operation. Modes of operation of the proposed converter during the G2V operation are discussed as follows,

37 *Mode I*: As depicted in Figure 5.4(a), this mode of operation starts with turning the Q_1 switch 'ON'. Switch Q_1 allows charging the inductor L_1 as stated by (5.1), while the discharging of capacitor C_1 begins in this mode. Moreover, the resultant waveforms are depicted in Figure 5.6(a). In this mode, switches Q_2 and Q_3 remain 'OFF'. Furthermore, the inductor current of L_{o1}, L_{o2}, and L_2 is increasing.

$$v_{L1} = v_{DC} \tag{5.1}$$

$$L_1 \frac{di_{L1}}{dt} = v_{DC} \tag{5.2}$$

4 where, v_{DC} is the DC link voltage and V_{L1} is the voltage across the input inductor.

$$v_{C1} = v_{L2} + v_{Lo2} + v_b + v_{Lo1} \tag{5.3}$$

4 where, v_{C1} is the intermediate capacitor voltage, which is the total addition of the output inductor voltages (v_{Lo1}, v_{Lo2}, and v_{L2}) and battery voltage (v_b) as stated by (5.3).

Mode II: As depicted in Figure 5.4(b), this mode of operation starts with turning the Q_1 switch 'OFF'.

Antiparallel diodes across the switches are in operation. Input inductor L_1 distribute its stored energy. Decrease in the input inductor I_{L1} as well as the increase in the capacitor C_1 voltage is depicted in Figure 5.6(a). Moreover, the inductor current of L_{o1}, L_{o2}, and L_2 is decreasing.

$$v_{DC} = v_{L1} + v_{C1} + v_b \quad (5.4)$$

$$v_{Lo1} = -v_b \quad (5.5)$$

$$v_{Lo2} = -v_b \quad (5.6)$$

$$v_{L2} = -v_b \quad (5.7)$$

The voltage gain of the developed system is calculated using (5.1) and (5.4) as,

$$M = \frac{v_b}{v_{DC}} = \frac{D}{2(1-D)} \quad (5.8)$$

Mode I: As depicted in Figure 5.5(a), the switches Q_2 and Q_3 turn 'ON' and switch Q_1 remain 'OFF' in this mode of operation. The power flows from the battery to the grid. The inductors L_{o1}, L_{o2}, and L_2 store the energy and current through these inductors start increasing as the waveform depicted in Figure 5.6(b). This mode ends when Q_2 and Q_3 switches are turned 'OFF'. The following equations concerned to this mode are depicted as,

$$v_{L01} = v_b \quad (5.9)$$

$$v_{L02} = v_b \quad (5.10)$$

$$v_{L2} = v_b \quad (5.11)$$

$$v_{C1} - v_{L1} + v_b = v_{DC} \quad (5.12)$$

Mode II: As depicted in Figure 5.5(b), this mode starts by turning both the Q_2 and Q_3 "OFF" switches. The antiparallel diode across the switch Q_1 is in operation during this mode. The inductors L_{o1}, L_{o2}, and L_2 deliver stored energy.

$$v_{L1} = -v_{DC} \quad (5.13)$$

$$v_{L2} - v_{L02} + v_{L01} = v_{C1} - v_{C0} \quad (5.14)$$

Increase in capacitor C_1 voltage is depicted in Figure 5.6(b). Inductor L_1 delivers its energy and the current I_{L1} decreases.

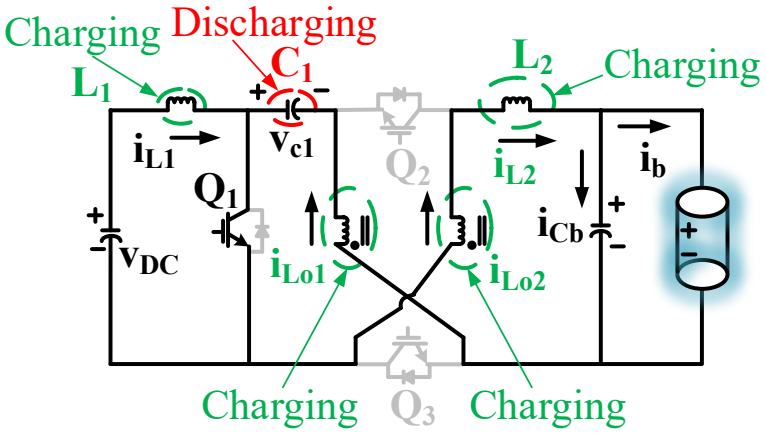

(a)

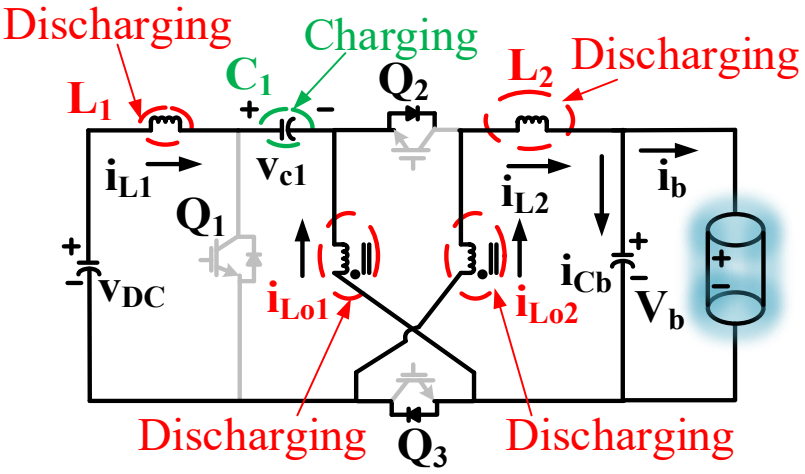

(b)

Figure 5.4. Operation during grid to vehicle mode (Charging).

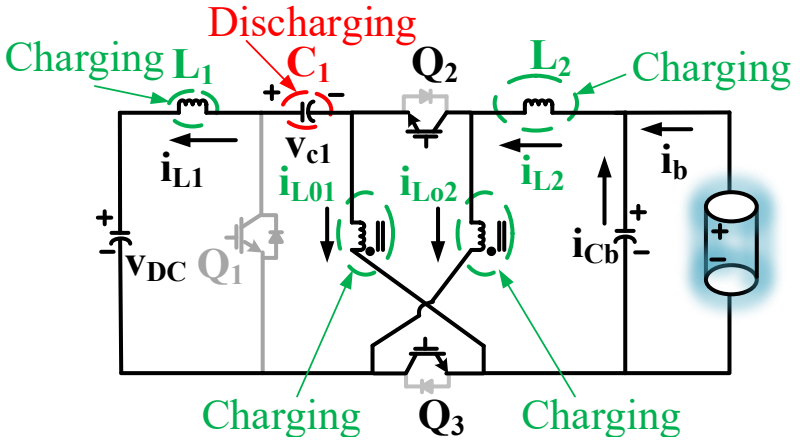

(a)

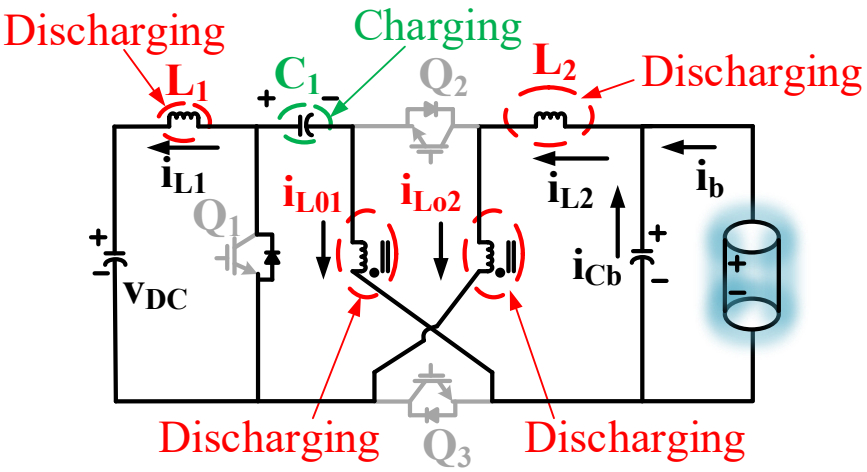

(b)

Figure 5.5. Operation during vehicle to grid mode (Discharging).

This mode ends when Q_2 and Q_3 switches turn 'ON'. Voltage gain of the proposed bidirectional high gain converter is calculated as,

$$M' = \frac{v_{DC}}{v_b} = \frac{2D'}{(1-D')} \tag{5.15}$$

Here, D' is the duty ratio of switches Q_2 and Q_3 using (5.8) and (5.15),

$$D' = 1 - D \tag{5.16}$$

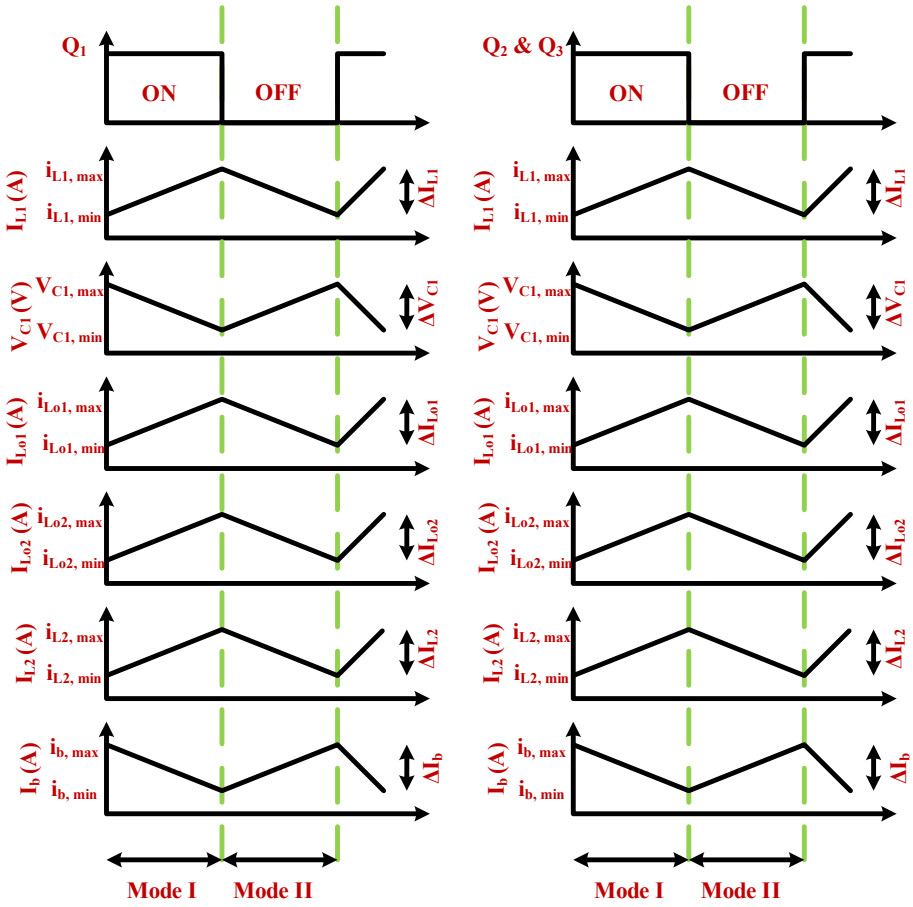

Figure 5.6. Switching cycle electrical waveforms, (a) grid to vehicle mode (Charging), and (b) vehicle to grid mode (Discharging).

Mode III : Figure 5.7 depicts the solar PV-based battery charging operation through the proposed BHGC. The buck-boost capability of the SEPIC converter and its other unique features offer flexibility in selecting solar PV panel ratings. This mode starts when grid power is absent or in ideal condition. The switch S_{PV} is turned 'ON' using high-frequency pulses generated by the MPPT controller.

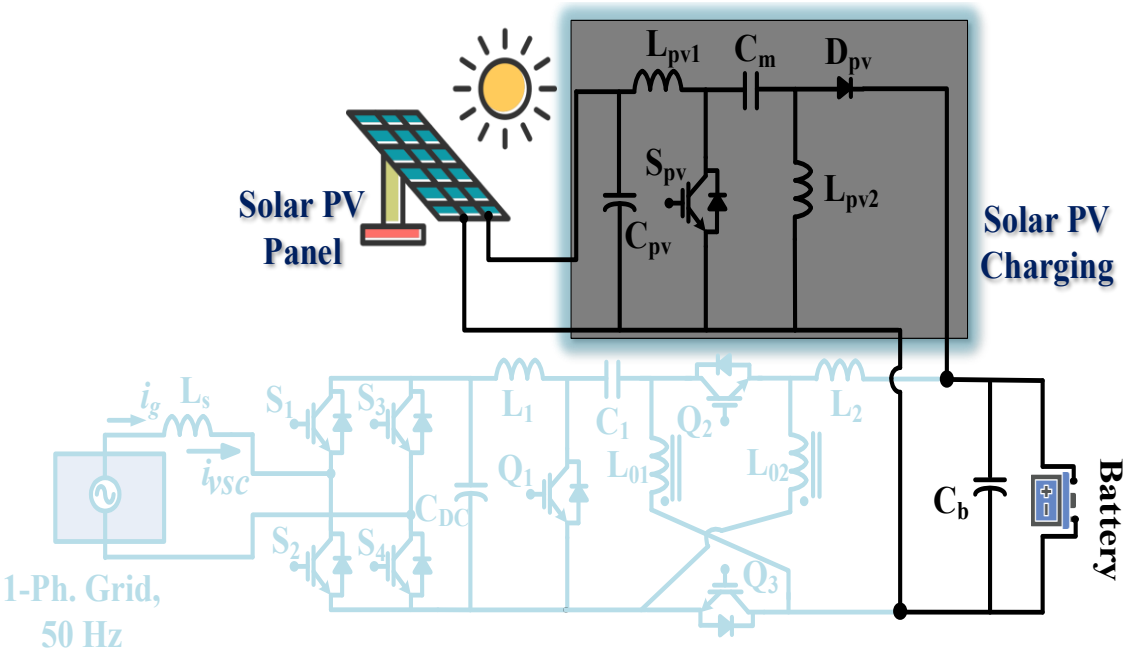

Figure 5.7. Solar PV charging mode when the grid is absent or in ideal condition.

5.3.2 Modes of Operation of Solar Powered On-board Charging System Utilizing Switched Capacitor High Gain ZETA Converter with G2V and V2G Capabilities

The proposed SCBZ converter enables its operation under two modes i.e. G2V and V2G modes. Notably, during G2V, the switch (Q_5) is active, whereas the switches (Q_6 and Q_7) are active in V2G mode operation. Further, each mode with switching waveforms is discussed. Moreover, the solar PV based on-board charging is also elaborated. The BLDC motor operation in propulsion mode is also given in the study.

97 Referring to Figure 5.8(a-b) and Figure 5.9(a-b), the operation of the proposed SCBZ in both G2V and V2G modes relies on the switching states of the active IGBT devices at the back end (Q_5-Q_7).

Mode I : During G2V mode, the semiconductor device Q_5 is turned ON, while others remain OFF. Inductors L_1 and L_2 are in energy storage mode, and the current rises as it takes energy from dc link voltage through Q_5 referred in Figure 5.8(a). During this phase, the capacitors C_{01} and C_{02} works in discharging mode, with diodes D_6 and D_7 remaining in the OFF state. The next equations related to this mode are derived as,

$$v_{L1} = v_{DC} \tag{5.17}$$

$$i_{L1} = \frac{i_b.D_{G2V}}{(2-D_{G2V})} \tag{5.18}$$

$$T_{G2V} = \frac{v_b}{v_{DC}} = \frac{D_{G2V}}{(2-D_{G2V})} \tag{5.19}$$

$$i_{L2} = i_b \tag{5.20}$$

$$v_{C01} = v_{C01} = \frac{v_b}{D_{G2V}} \tag{5.21}$$

Where DC-link voltage is v_{DC} and voltage belongs to the input inductor and output inductor is v_{L1}/v_{L2}, v_{C01} and v_{C02} are voltages belonging to SCBZ converter capacitors, and T_{G2V} is voltage transfer ratio as given by (5.17)-(5.21).

Mode II : In this mode, the gate drive Q_5 is set low, results in synchronous rectification mode state of diodes (D_6 and D_7), as refereed in Figure 3(b). The inductor L_1 and L_2 follow a decaying curve whereas the capacitor voltages v_{C01} and v_{C02}, start following an increasing curve. Thus, these G2V modes of operation ensure the high step-down between v_{DC} and v_b.

The waveforms belonging to SCBZ converter in G2V mode are drawn in Figure 5.10(a).

Mode 1: During V2G mode, the semiconductor devices Q_6-Q_7 is turned ON, and power transfer is realized through Q_6 and Q_7 as referred in Figure 5.9(a). The inductors L_1 and L_2 start storing energy and operate in charging mode but polarity is reversed and the capacitors C_{01} and C_{02} operate in discharging mode as the diodes (D_5) remain in OFF state. Next equations (5.22)-(5.25) concerned to this mode are derived as,

$$i_{L2} = i_b \tag{5.22}$$

$$i_{L1} = \frac{\{i_b.(1-D_{V2G})\}}{(1+D_{V2G})} = i_{DC} \tag{5.23}$$

$$T_{G2V} = \frac{v_{DC}}{v_b} = \frac{(1+D_{V2G})}{(1-D_{V2G})} \quad (5.24)$$

$$v_{C01} = v_{C01} = \frac{v_b}{(1-D_{V2G})} \quad (5.25)$$

Mode II : In this mode, the gate drive of Q_6-Q_7 is set low, results in to ON state of diodes (D_5), as referred in Fig. 5.9(b). The performing pattern of passive components is same as the G2V performance, only polarity of voltage and current reverses which shows the discharging operation. Thus, these V2G modes of operations ensure the high step up between v_b and v_{DC}.The waveforms belonging to SCBZ converter in V2G mode are draw in Fig. 5.10(b).

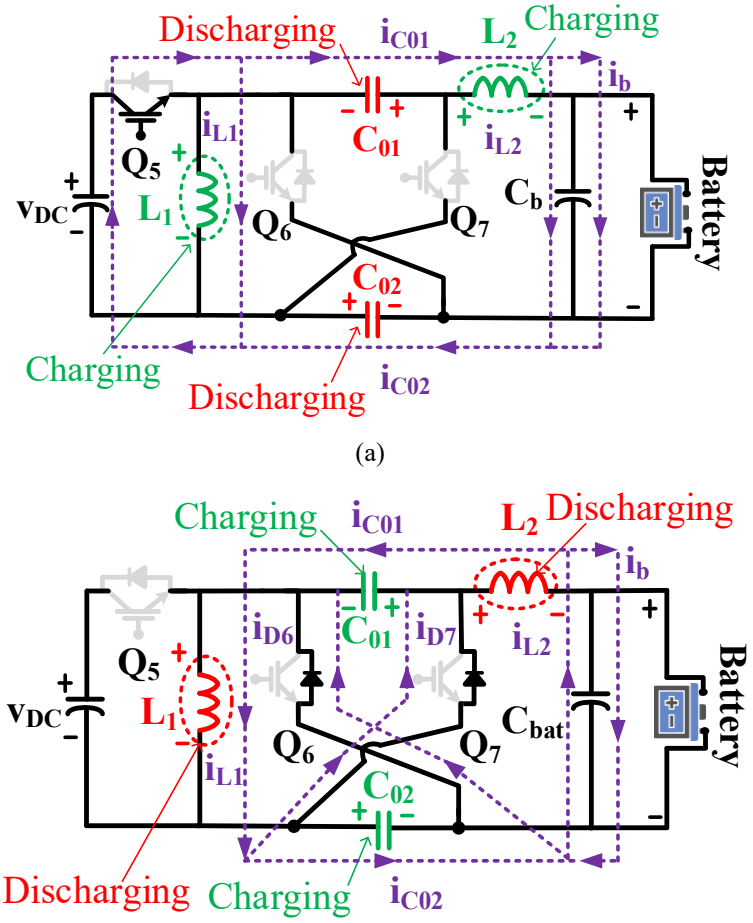

Figure 5.8. Operation during grid to vehicle mode (Charging).

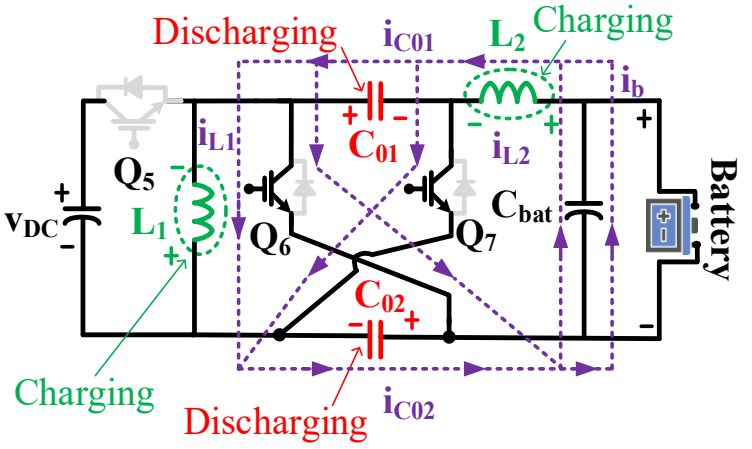

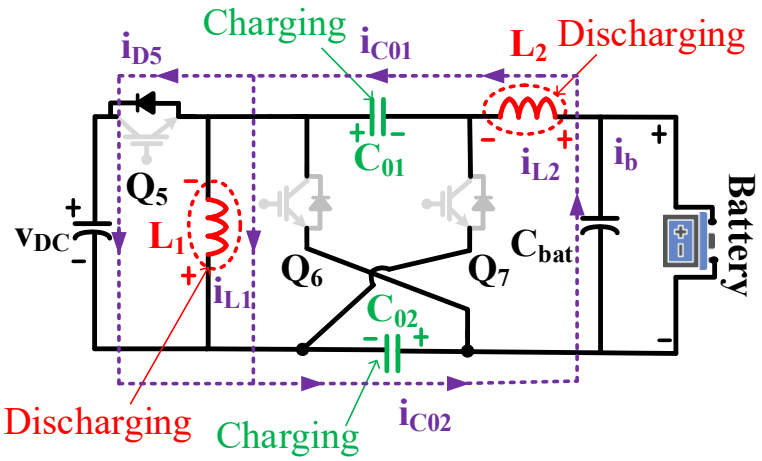

(b)

Figure 5.9. Operation during vehicle to grid mode (Discharging).

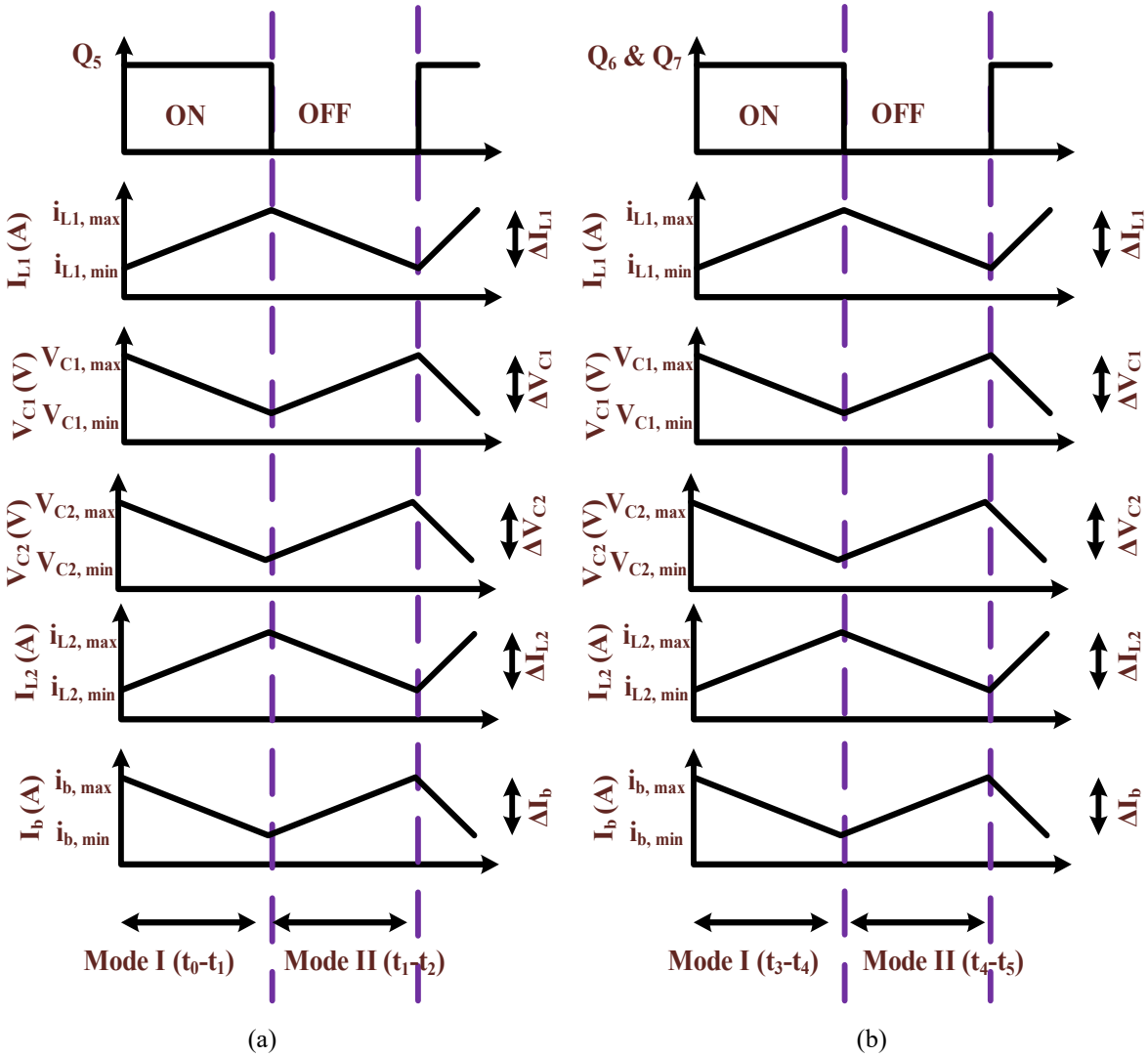

(a) (b)

Figure 5.10. Electrical waveforms of the switching cycle for the SCBZ, (a) G2V mode (Charging), and (b) V2G mode (Discharging).

Mode III - Referring to Figure 5.11, the on-board solar PV with a modified MPPT controller is utilized for the e-rickshaw battery charging operation via the proposed SCBZ converter. The Cuk converter with a modified MPPT controller provides flexibility when selecting solar PV array ratings. This on-board mode comes into play when there is grid outage. The IGBT S_{PV} in Cuk converter is operated using PWM pulses produced by the modified MPPT controller.

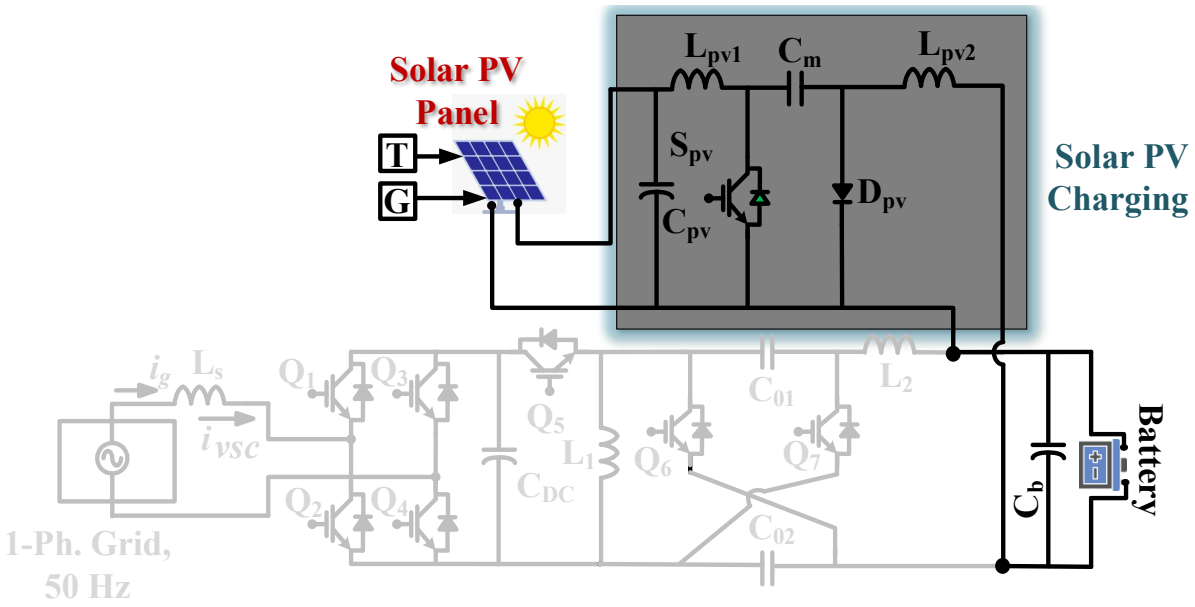

Figure 5.11. On-board solar PV charging mode during grid outage.

5.4 Designing of Solar Powered On-board LEV Utilizing Non-Isolated High Gain Converter with G2V and V2G Capabilities

In this developed bidirectional high gain converters-based charging systems, includes designing of active front end converter (AFC), bidirectional DC-to-DC converters, and on-board solar PV with MPPT converters as follows,

5.4.1 Design of Solar Powered On-board Charging System Utilizing Coupled Inductor High Gain SEPIC Converter with G2V and V2G Capabilities

In this developed charging system, a single-phase supply (V_s) with a nominal voltage of 230V, 50Hz is considered for the circuit design. The proposed system is designed for a 48V, 50Ah battery. Different parameter selections for the proposed system are computed as follows,

5.4.1.1 Design of Active Front End Converter

In the design of AFC, the design and selection of line L_s inductor and DC link capacitor C_{DC} are primarily done. The selection of these components is significant for the AC-DC operation. The value of the inductor connected in a line is calculated according to the voltage drop in the line due to the inductive reactance. This voltage drop is usually taken to be 3% of the line voltage. Similarly, the value of capacitance to be connected in the DC link is governed by the maximum tolerable voltage and the maximum ripple current at the converter's switching frequency and operating temperature. The expressions for calculating the values of inductance are given as under,

$$X_L = \frac{0.03 \times v_{phase}}{\sqrt{3} \times I_{phase}} \tag{5.26}$$

$$I_{peak} = I_{phase} \times \sqrt{2} \times 2 \tag{5.27}$$

$$2\pi f L = \frac{0.03 \times v_{phase}}{P} \tag{5.28}$$

where V_{phase} is the input phase voltage, I_{phase} is the phase current, I_{peak} is the peak current flowing in the inductor through the line, L is the inductance, f_s is the frequency of the AC supply, and P is the power rating of the converter. Along the same lines, the useful relation for the calculation of the value of capacitance is given as follows,

$$C_{\min} = \frac{0.2 \times I_{peak}}{\Delta v_{p-p} \times f_s} \tag{5.29}$$

$$I_{ripple} = \frac{0.46 \times I_{peak}}{\eta} \tag{5.30}$$

$$D = \frac{2v_b}{2v_b + v_{DC}} = \frac{2 \times 48}{2 \times 48 + 400} = 0.80 \tag{5.31}$$

$$L_s = \frac{Dv_{DC}}{f_{sw} \Delta i_{Ls}} = 2.03\ mH \tag{5.32}$$

$$C_{DC} = \frac{I_{DC}}{2\omega \Delta v_{DC}} = 1244.01\ \mu F \tag{5.33}$$

where C_{min} is the minimum capacitance value for sustaining the voltage ripple, I_{peak} is the peak current flowing through the line, I_{ripple} is the ripple current to be sustained by the capacitor, ΔV_{p-p} is the peak-to-peak dc voltage ripple, f_s is the switching frequency of the IGBTs, D is duty ratio, and η is the compensating factor to be found out from the datasheet of the capacitor, which depends on the value of switching frequency and operating temperature. For simulation purposes, the parameters input phase voltage and switching frequency are taken as 230 V_{rms}, and 20 kHz, respectively.

5.4.1.2 Design of Coupled Inductor Bidirectional High Gain Converter

The duty ratio of the bidirectional high gain converter (BHGC) is considered when designing the passive components in the converter. Keeping the constant current/constant voltage charging of a 48V, 50Ah battery in context, the following equations are estimated in Table 5.1.

$$D = \frac{2v_b}{2v_b + v_{DC}} \tag{5.34}$$

$$= \frac{2 \times 48}{2 \times 48 + 400} = 0.1$$

$$L_1 = \frac{Dv_{DC}}{f_{sw} \Delta i_{L1}} \tag{5.35}$$

$$= \frac{0.21 \times 400 \times 400}{20000 \times 0.3 \times 10} = 5.6mH$$

$$C_1 = \frac{2(1-D)P}{v_{DC} f_{sw} \Delta v_{c1}} \tag{5.36}$$

$$= \frac{2(1 - .21)1000}{400 \times 20000 \times 0.05 \times (400 + 48)} = 8.81\mu F$$

$$L_{01} = L_{02} = \frac{(1-D)v_b}{f_{sw} \Delta i_{L0}} \tag{5.37}$$

$$= \frac{(1 - 0.21)48}{20000 \times 0.3 \times 10} = 2.5mH$$

For the simulation and hardware experimentation value of 'C_{DC}' is taken as 1500 µF, 'L_1' is considered as 5.5mH, 'L_{01}', 'L_{02}' is selected as 3mH.

Table 5.1. Design parameter values for BHGC.

Parameter	Value
AC input voltage (V_g)	230 V_{rms}
Reference DC-link voltage (V_{DC})	400 V
Line frequency (f)	50 Hz
Nominal Battery voltage (V_b)	48V
Initial SOC	20%
$L_s/L_{o1}/L_{o2}/L_2$	4mH/3mH/3mH/3mH
C_{dc}/C_o	1500 µF/500 µF
Nominal load power	1 kW

5.4.1.3 Design and Selection of Solar PV Array with MPPT and SEPIC Converter

The solar PV array of 800 W (peak power) is designed for LEV battery charging. The value of 53.55 V is selected for the maximum power point (MPP) voltage V_{mpp} of the array. The other parameters of the PV array are given in Table 5.3. Consequently, the rated current at this condition is stated as,

$$I_{pv} = \frac{P_{pv}}{v_{pv}} = \frac{900}{53.55} = 16.8A \quad (5.38)$$

The number of series-connected modules per string is as,

$$N_s = \frac{v_{pv}}{v_{mp}} = 3 \quad (5.39)$$

and the number of parallel-connected strings is as,

$$N_p = \frac{I_{pv}}{I_{mp}} = 3 \quad (5.40)$$

Table 5.3. Parameters of solar PV array with MPPT and SEPIC Converter.

Parameter	Value
Peak Power (W)	800 W
Cell per module	36
Voltage at open circuit, $V_{o.c}$ (V)	21.3 V
Rated current at short circuit condition, $I_{s.c}$ (A)	6.6 A
Number of series strings, N_s	3
Number of parallel strings, N_p	3
MPP voltage rating, V_{mpp}	13.55 V
MPP current rating, I_{mpp}	16.83 V
L_{pv1}/L_{pv2}	3mH/4mH
C_{pv}/C_o	10 µF/500 µF

5.4.2 Design of Solar-Powered On-board Charging System Utilizing Switched Capacitor High Gain ZETA Converter with G2V and V2G Capabilities

In this developed charging system, a single-phase supply (V_s) with a nominal voltage of 230V, 50Hz is considered for the circuit design. The proposed system is designed for a 48V, 50Ah battery. Different parameter selections for the proposed system are computed as follows,

5.4.2.1 Design of Active Front End Converter

In the design of AFC, the design and selection of line L_s inductor and DC link capacitor C_{DC} are primarily done. Design of AFC is same as the in section 5.4.1.1 and given in Table 5.2.

5.4.2.2 Design of High-Gain Switched-Capacitor ZETA Converter

The proposed SCBZ passive and active components are designed and selected for rated power of 720 W (P_{max}). Here, the grid and battery voltage range is selected as 230 V and V_{bat} (48 V) to ensure effective charging/discharging. In AFC, v_{dc} is set higher (400 V). Besides, inductors (L_1/L_2) and capacitors (C_{01}/C_{02}) are designed under CCM operation. A small filter capacitor (C_0) is placed at the battery end to filter out switching frequency ripples of i_{L1} and to ensure ripple-free battery current in G2V & V2G operations. Keeping the constant current/constant voltage (CC/CV) charging of a 48V, 50Ah battery in context, the following equations are estimated as (10)-(16),

$$L_1 = \frac{\left(v_{dc}-\frac{v_{bat}}{D}\right)D}{f_{sw}\Delta i_{L1}} = \frac{\left(\frac{2v_{bat}}{1-D}-v_{dc}\right)D}{f_{sw}\Delta i_{L1}} = \frac{(v_{dc}-v_{bat}).v_{dc}}{f_{sw}.\alpha.i_{bat}.(v_{dc}+v_{bat})} = 2.75\ mH \quad (5.41)$$

$$L_2 = \frac{v_{bat}(1-D)}{f_{sw}\Delta i_{L2}} = \frac{v_{bat}D}{f_{sw}\Delta i_{L2}} = \frac{(v_{dc}-v_{bat}).v_{bat}}{f_{sw}.\beta.i_{bat}.(v_{dc}+v_{bat})} = 2.75\ mH \quad (5.42)$$

Switched capacitors are designed to operate in CCM with optimum voltage ripples to limit switching devices voltage stress within a defined range. C_{01}/C_{02} is designed as,

$$C_{01} = C_{02} = \frac{i_{L1}(1-D)}{f_{sw}\Delta i_C} = \frac{i_{L1}D}{f_{sw}\Delta i_C} = \frac{2.v_{bat}(v_{dc}-v_{bat}).i_{bat}}{f_{sw}.k.v_{dc}.(v_{dc}+v_{bat})2} = 3.51\ \mu F \quad (5.43)$$

$$C_0 = \frac{i_0}{4\pi f_{sw}\Delta v_0} = 375.34\ \mu F \quad (5.44)$$

The selected value for L_s,$C_{dc,}$ L_1, L_2, C_{01} , C_{02} and C_0 is shown in Table I.

Table. 5.2 Design parameter values for SCBZ

Circuit Parameter	Used Value
AC input voltage (V_g)	230 V_{rms}
Reference DC-link voltage (V_{DC})	400 V
Line frequency (f)	50 Hz
Nominal Battery voltage (V_b)	48 V
Initial SOC	20 %
$L_s/L_1/C_{o1}/C_{o2}/L_2$	2.5mH/3mH/4µF/4µF/3mH
C_{dc}/C_o	1300µF/500µF
Nominal load power	720W

5.4.2.3 Design and Selection of Solar PV Array

The solar PV array of 800 W (peak power) is designed for LEV battery charging. The value of 53.55 V is selected for the maximum power point (MPP) voltage V_{mpp} of the array. The other parameters of the PV array are given in Table 5.4. Consequently, the rated current at this condition is stated as,

$$I_{pv} = \frac{P_{pv}}{v_{pv}} = \frac{900}{53.55} = 16.8A \quad (5.45)$$

The number of series-connected modules per string is as,

$$N_s = \frac{v_{pv}}{v_{mp}} = 3 \tag{5.46}$$

and the number of parallel-connected strings is as,

$$N_p = \frac{I_{pv}}{I_{mp}} = 3 \tag{5.47}$$

Table 5.4. Parameters of solar PV array with MPPT and Cuk Converter

Parameter	**Value**
Peak Power (W)	800 W
Cell per module	36
Voltage at open circuit, $V_{o.c}$ (V)	21.3 V
Rated current at short circuit condition, $I_{s.c}$ (A)	6.6 A
Number of series strings, N_s	3
Number of parallel strings, N_p	3
MPP voltage rating, V_{mpp}	13.55 V
MPP current rating, I_{mpp}	16.83 V
L_{pv1}/L_{pv2}	3mH/4mH
C_{pv}/C_o	10 µF/500 µF

5.5 Control of Solar Powered On-board LEV Utilizing Non-Isolated High Gain Converter with G2V and V2G Capabilities

Achieving regulated operation of the converters in the proposed LEV charger requires the development of a suitable controller. The controllers are developed for different converters such as active front-end converter (AFC), high-gain bidirectional DC-DC converter, and the BLDC motor derived to control the operation within the relevant standards. The primary aim of the controller is to achieve PFC using an active front-end converter, to control the charging of the battery using CC and CV modes, achieving MPPT and BLDC motor speed control as per the necessary conditions. The detailed explanations of the controller design are given below;

5.5.1 Control of Solar Powered On-board Charging System Using Coupled Inductor High Gain SEPIC Converter with G2V and V2G Capabilities

The controllers are developed for coupled inductor bidirectional high gain converter such as active front-end converter (AFC), high-gain bidirectional DC-DC converter, and the BLDC motor derived to control the operation are given below,

5.5.1.1 Control of Active Front Converter (AFC)

During the AFC operation, the controller regulates the grid current's power quality within the IEEE standard limits. Moreover, its principal goal is to map the control unit to the regulated voltage of the DC-link at a defined value throughout the operation. The unity power factor functioning at a low line current distortion is observed by the PI controller. Figure 5.12 depicts the controller for AFC, in which the DC

link voltage V_{DC} is sensed with reference V_{DC*}, then fed to the voltage controller.

$$v_{err,DC}(n) = v_{ref}(n) - v_{DC}(n) \tag{5.48}$$

The 'v_e' is compared with 'v_s', which gives i_s*, and further, it will feed to the current controller. Thereafter, the PWM pulse is sent to the respective switches (S_1, S_2, S_3, S_4).

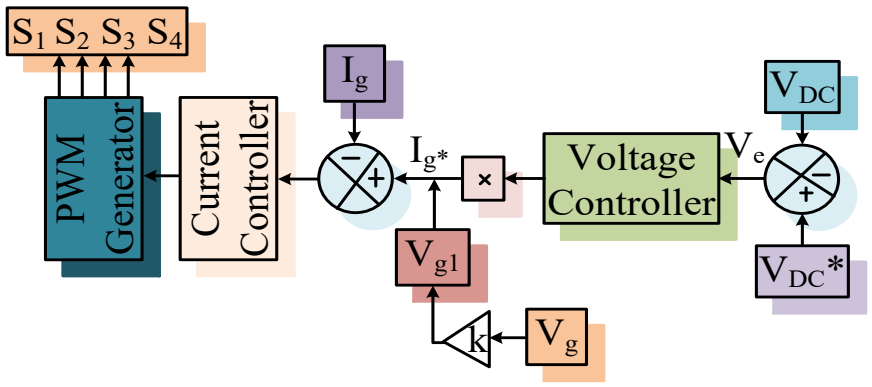

Figure 5.12. Block diagram of controller for AFC.

$$i_r(n) = i_r(n-1) + \{K_{p1} \times [v_{error,DC}(n) - v_{error,DC}(n-1)]\} + [K_{I1} \times v_{error,DC}(n)] \tag{5.49}$$

$$i_{g,r}(n) = i_r(n)\sin\omega t \tag{5.50}$$

5.5.1.2 Control of Bidirectional DC-to-DC Converter

Notably, during bidirectional operation (i.e. G2V and V2G), the proposed bidirectional DC-to-DC liable to maintain the battery current as per the requisite limit. A constant "κ" is given to the controller of the proposed DC-to-DC converter, which regulates the direction of power flow. A positive constant "κ" represents the active power drawn from the grid during charging (G2V operation). In contrast, a negative constant "κ" indicates the reverse process (V2G operation), where power is fed back to the grid during discharging (V2G operation). The control unit of the design system, firstly, measures the battery voltage (v_b) and the battery current (i_b). The measured 'v_b'

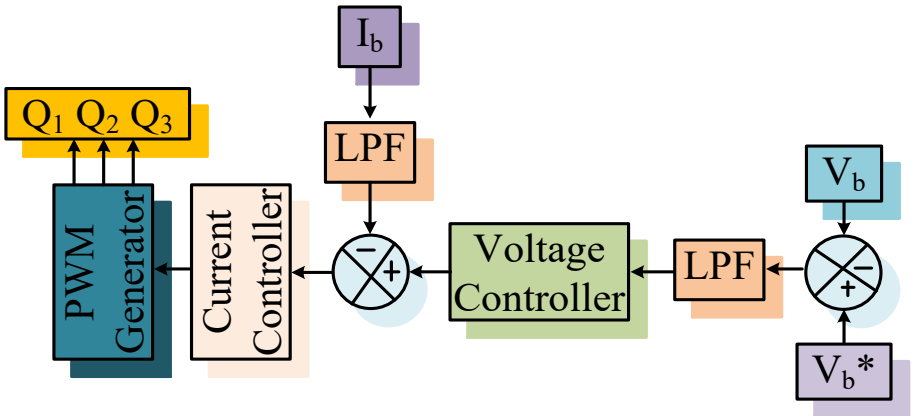

Figure 5.13. Block diagram of the controller for bidirectional DC-to-DC Converter.

The output error is addressed by a voltage control block. The coming output of the voltage is minus from the reference voltage 'v_b*' (i.e., the maximum allowable battery voltage). Control block is restricted to

the rated battery current 'i_b' value, as depicted in Figure 5.13. Moreover, the I_b is minus from the estimated reference current 'i_b*'. Then, the PWM pulses are given to switch Q_1, Q_2, and Q_3. The CC-CV charging/discharging method has been employed in this work to confirm the satisfactory operation.

$$v_{Err,b}(n) = v_{ref}(n) - v_b(t_n - 1) \quad (5.51)$$

$$I_{Err,b}(n) = I_{ref}(n) - I_b(t_n - 1) \quad (5.52)$$

5.5.2 Control of Solar Powered On-board Charging System Using Coupled Inductor High- Gain SEPIC Converter with G2V and V2G Capabilities

The controllers are developed for switched capacitor bidirectional high gain converters such as active front-end converter (AFC), high-gain bidirectional DC-DC converter, and the BLDC motor derived to control the operation are given below,

5.5.2.1 Control of Active Front Converter (AFC)

Concerned with Figures 5.14(a-b), the IMSTOGI filter rejects all harmonic components, resulting in a pure sinusoidal component. Furthermore, its principal goal is to obtain the defined DC-link voltage in the regulated unit. Further, some low-line THD is controlled by the proportional-integral (PI) controller. Concerned to Figure 5.14(a-b), the next equations (5.53)-(5.62) present a controller for AFC, which is inspired by the structure of an IMSTOGI-OSG method.

$$V_e(z) = V^*_{DC}(z) - V_{DC}(z) \quad (5.53)$$

$$I_{sp}(z) = I_{sp}(z-1) + k_{pc} * \{V_e(z) - V_e(z-1)\} + k_{ic} * V_e(z) \quad (5.54)$$

$$I_{sq} = (2 * Q_{ref})/ V_t \quad (5.55)$$

$$V_{time} = \sqrt{v_q^2 + v_p^2},\ u_p = v_p / V_{time},\ and\ u_q = v_q / V_{time} \quad (5.56)$$

$$i_{sp}(time) = I_{sq} * u_q,\ i_{sp}(time) = I_{sp} * u_p \quad (5.57)$$

$$i_s^*(time) = i_{sp}(time) + i_{sp}(time) \quad (5.58)$$

$$I_{er}(k) = I_{bat}^*(k) - I_{bat}(k) \quad (5.59)$$

$$d_c(n) = d_c(k-1) + g_{pc} * \{I_{er}(k) - I_{er}(k-1)\} + g_{ic} * I_{er}(k) \quad (5.60)$$

$$V_{er}(k) = V_{bat}^*(k) - V_{bat}(k) \quad (5.61)$$

$$d_v(k) = d_v(k-1) + q_{pc} * \{V_{er}(k) - V_{er}(k-1)\} + q_{ic} * V_{er}(k) \quad (5.62)$$

5.5.2.2 Control of Bidirectional DC-to-DC Converter

Notably, during bidirectional operation (i.e., G2V and V2G), the bidirectional DC-to-DC converter liable to maintain the battery current as per the requisite limit. A constant "κ" is given to the controller of the proposed bidirectional DC-to-DC converter, which regulates the direction of power flow. A positive constant "κ" represents the active power drawn from the grid during charging (G2V operation), whereas a negative constant "κ" indicates the reverse process, where power is fed back to the grid during discharging (V2G operation). The control unit of the design SBCZ, firstly measures the battery voltage

(v_b) and the battery current (i_b). The measured 'v_b' is minus from the reference voltage 'v_b*' (i.e., the maximum allowable battery voltage). The output error is addressed by a voltage control block. The coming output of the voltage control block is restricted to the rated battery current 'i_b' value, as depicted in Figure 5.15. Moreover, the I_b is minus from the estimated reference current 'i_b*'. Then, the PWM pulses are given to switch Q_5, Q_6, and Q_7. For the reason that the CC-CV charging/discharging method has been employed in this work to confirm the satisfactory operation.

$$v_{Err,b}(n) = v_{ref}(n) - v_b(t_n - 1) \tag{5.63}$$

$$I_{Err,b}(n) = I_{ref}(n) - I_b(t_n - 1) \tag{5.64}$$

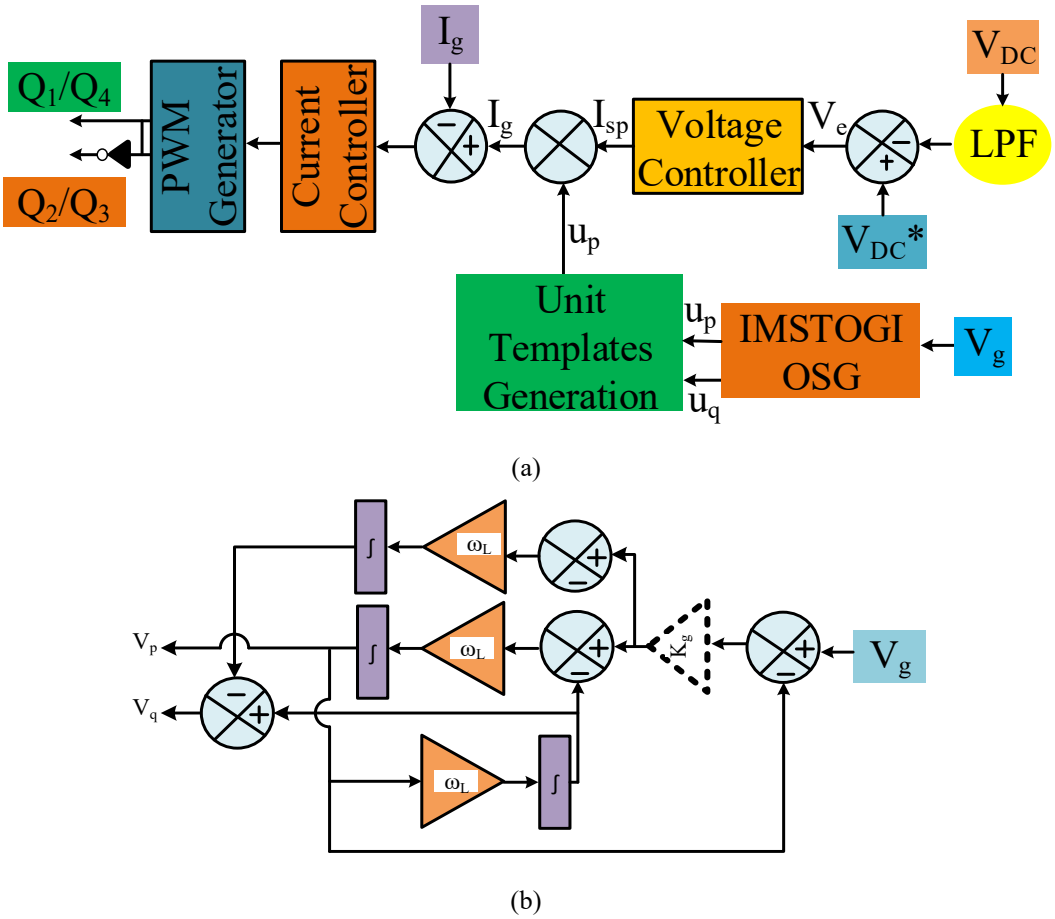

Figure 5.14. Block diagram of controller. (a) Grid side AFC, (b) IMSTOGI based OSG method.

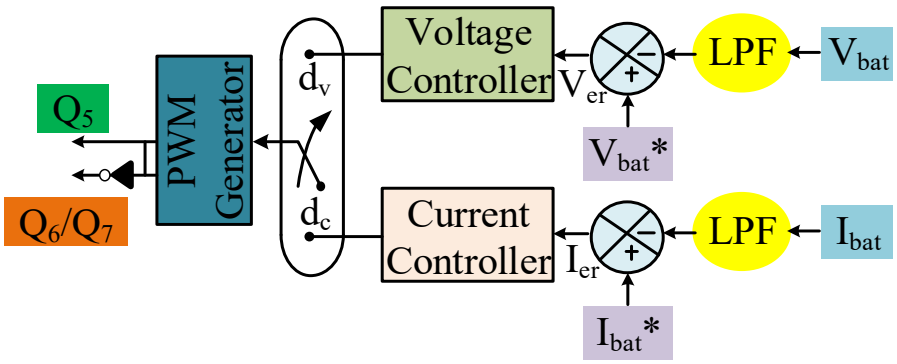

Figure 5.15. Block diagram of controller for the proposed SCBZ converter.

5.5.3 MPPT Control of Solar PV Array

Even though the conventional P&O MPPT method is easy to implement and effective, it has serious deviation problems, particularly when there is variation in irradiance. It further results in additional power losses and tracking time lag. To attempt to solve this deviation problem, it is crucial to take into account the current variation in both cases when there is a positive or negative change in the PV array voltage. Thus, by considering the magnitude of alteration in current (ΔI_{PV}) in addition to change in power (ΔP_{PV}) and change in voltage (ΔV_{PV}) in the decision process, the deviation-free MPPT to minimize the deviation difficulty that exists with the conventional P&O technique.

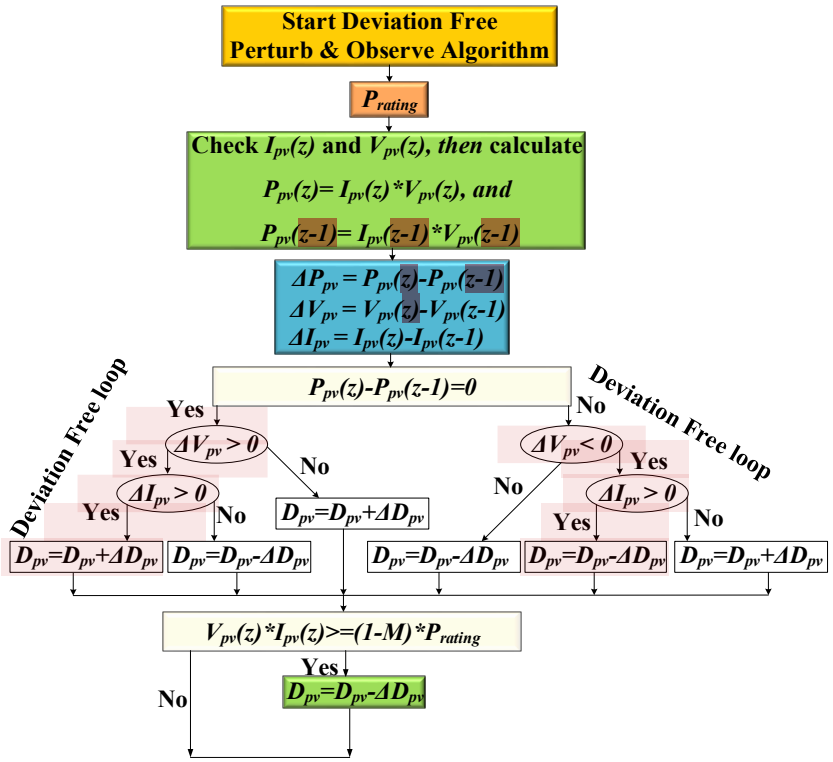

(a)

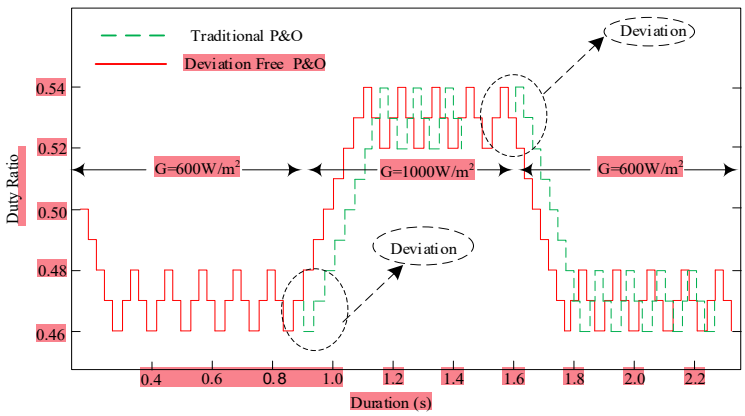

(b)

Figure 5.16. MPPT Technique (a) flow chart of the utilized modified P&O MPPT technique (b) Variation of duty cycle with conventional and deviation-free modified P&O technique.

This method lowered the MPPT tracking time in the region of 15% to 20% of the total tracking time. Figure 5.16(a) depicts a flow chart of the proposed deviation-free MPPT controller. Figure 5.16(b) depicted the pursuing waveforms with the traditional P&O method and the proposed deviation-less improved P&O MPPT method. Both methods appear to follow the relevant operating point with

proficiency. However, the recommended method is free from deviation problems during insolation change. In contrast, the conventional P&O method experiences a deviation issue during changes in insolation.

5.5.4. Control of Brushless DC Motor Drive for Propulsion Mode

The primary intent of the controller design for a BLDC motor is to maintain a stable DC-link voltage for smooth operation. Figure 5.17(a) depicts the block diagram of the BLDC motor, which includes a three-phase voltage source inverter (VSI), position sensor, torque command, current regulator, and commutation logic. The high-frequency PWM pulse 'S_b' is, as shown in Fig. 5.17(b) is generated by propulsion mode control logic developed for the traction motor.

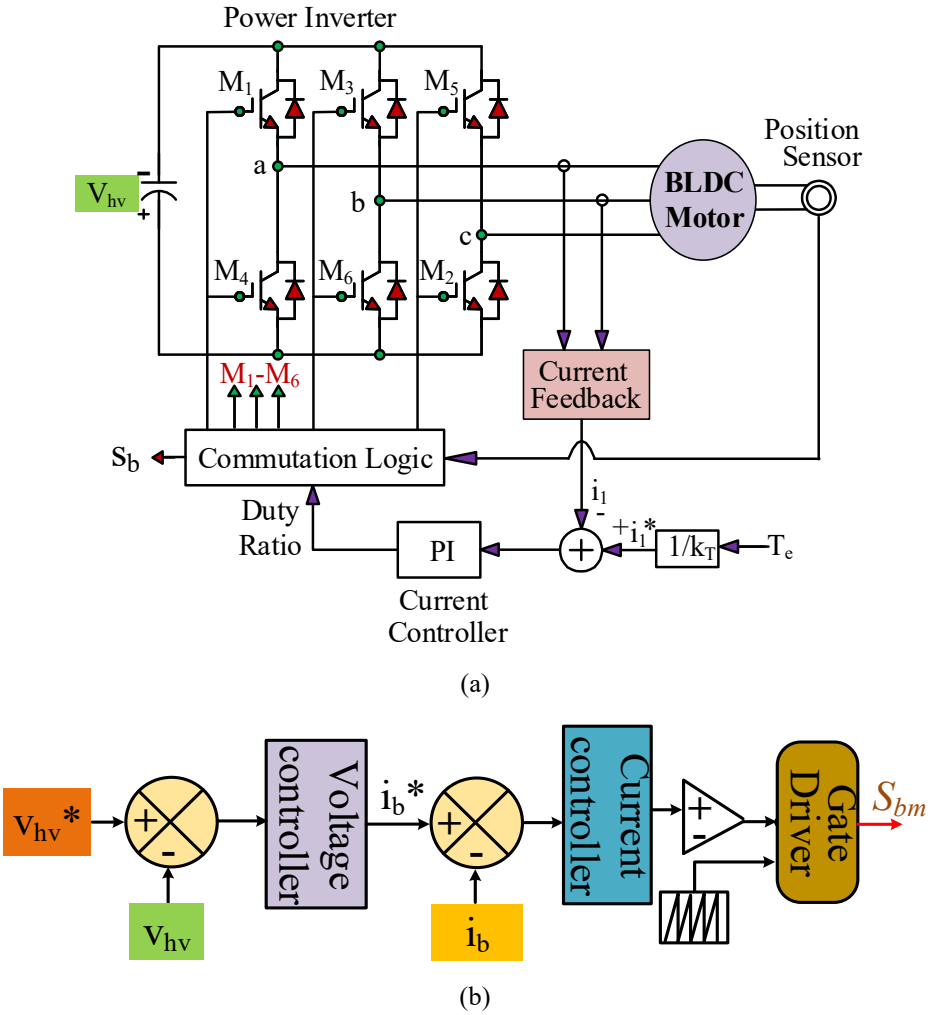

Figure 5.17. Block diagram (a) BLDC motor, (b) Controller.

As depicted in Figure 5.17(b) the input to the voltage control block receives the difference between the desired DC-link voltage, v_{hv}^*, and the assessed DC-link voltage, v_{hv}. Further, the output gives the reference value, which again acts as the battery current discharging value. After that, this coming value is again compared with the sensed i_b* (i.e. battery current), and the output error between the two is input to the current control block. The coming signal is then compared with the high-frequency carrier signal to generate the S_b (i.e. switching pulses).

5.6 MATLAB-Based Modeling and Simulation of Solar-Powered On-board Charging System

Using Coupled Inductor High-Gain SEPIC Converter with G2V and V2G Capabilities

The following models in Figure 5.18 show the MATLAB-based modeling and simulation of solar-powered on-board charging system utilizing coupled inductor high-gain converter. This system integrates an active front end Converter (AFC) for AC-to-DC conversion, a high-gain bidirectional DC-to-DC converter featuring a coupled inductor strategy too effectively for charging and discharging of LEV battery. Then solar PV with MPPT SEPIC converter for charging of battery during grid outage. The simulation demonstrates the G2V and V2G performance of the system under various operating conditions, highlighting its reliability for sustainable and efficient LEV charging. This charging strategy also run the BLDC motor drive system.

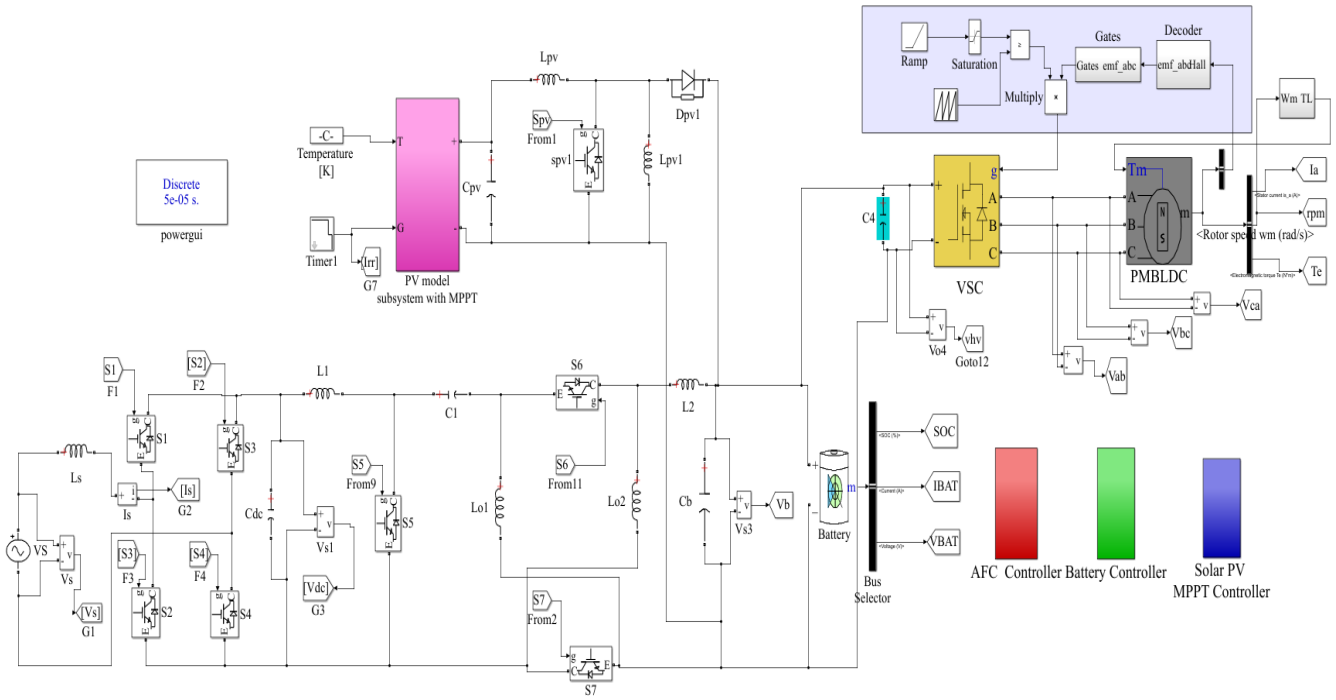

Figure 5.18. MATLAB based modeling and simulation of solar powered on-board charging system utilizing coupled inductor high gain converter.

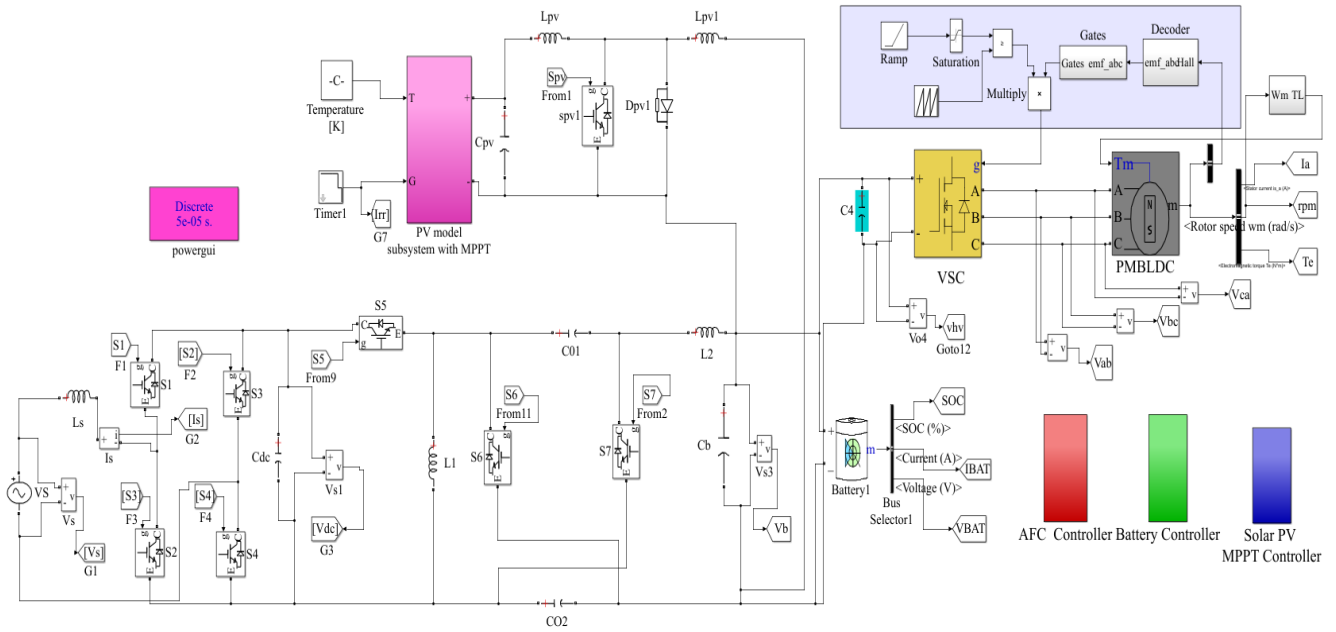

Figure 5.19. MATLAB based modeling and simulation of polar powered on-board charging system utilizing switched

capacitor high gain converter.

5.7. MATLAB-Based Modeling and Simulation of Solar-Powered On-board Charging System Using Switched Capacitor High-Gain ZETA Converter with G2V and V2G Capabilities

The following models in Figure 5.19 shows the MATLAB-based modeling and simulation of solar-powered on-board charging system utilizing a switched capacitor high-gain converter. This system integrates an active front end Converter (AFC) for AC-to-DC conversion, a high-gain bidirectional DC-to-DC converter featuring a switched capacitor strategy too effectively for charging and discharging of LEV battery. Then solar PV with MPPT Cuk converter for charging of battery during grid outage. The simulation demonstrates the G2V and V2G performance of the system under various operating conditions, highlighting its reliability for sustainable and efficient LEV charging. This charging strategy also run the BLDC motor drive system.

5.8 Results and Discussion

In order to ensure the adequate performance of the developed bidirectional high-gain converter, the whole design and control of the charger are tested using MATLAB/SIMULINK environment and verified experimentally on OPAL-RT. The effectiveness of the developed system is investigated during steady-state conditions to validate safe and reliable operations. Moreover, during the off condition of grid supply, battery charging through solar PV array is shown through both simulation and real-time study. Also, a comprehensive operational analysis of the BLDC motor is carried out here.

5.8.1 Simulated Performance of Solar-Powered On-board LEV Using Coupled Inductor High-Gain Converter

The developed system is tested using the MATLAB/SIMULINK environment, to ensure the optimal charging in both grid power supply and solar-powered conditions in this section. The effectiveness of the developed charger is demonstrated via simulation results. Also, a simulation operation investigation of the BLDC motor is presented in this section. The operational performance of the developed system includes G2V (charging) and V2G (discharging) modes of operation, as depicted in Figures 5.20-5.30. The parameters such as, grid voltage (V_g) and grid current (I_g), power factor correction (PFC), distortion factor, state of charge (SOC), battery current (I_b), and battery voltage (V_b) are discussed by using the simulation results.

5.8.1.1 Grid-Based Charging Performance

Figure 5.20 shows the grid voltage (V_g) which is around 325V, grid current (I_g) of 5A represents the amount of current being drawn to charge the battery, and the regulated DC link voltage (V_{DC}) response of 400V in the grid to vehicle charging mode. Moreover, Figure 5.21 shows the grid voltage (V_g) of around 325V, grid current (I_g) of 3A, and DC link voltage (V_{DC}) response remains constant at 400V in vehicle-to-grid discharging mode. The grid current (I_g) of 3A is characteristic of discharging situations,

where the battery provides power to the grid instead of receiving it. Figure 5.22 shows the grid voltage and grid current, which are in phase because of the power factor correction control strategy of the AC-to-DC converter in charging mode. This means the converter's control strategy aligns the current with the voltage, decreasing reactive power and improving the system's efficiency. Figure 5.23 shows the grid voltage (V_g) and grid current (I_g), which are out of phase, i.e., UPF operation is also maintained in discharging mode. The UPF operation is essential for maximizing the grid efficiency and ensuring that the discharging process doesn't introduce significant losses or inefficiencies.

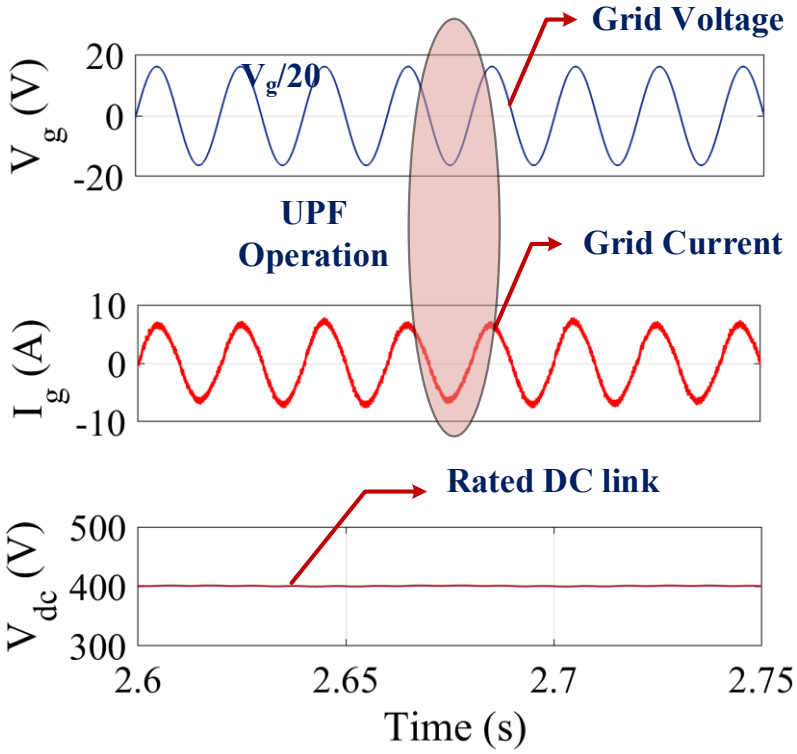

Figure 5.20. Simulated performance of developed system during G2V (V_g, I_g, V_{DC}).

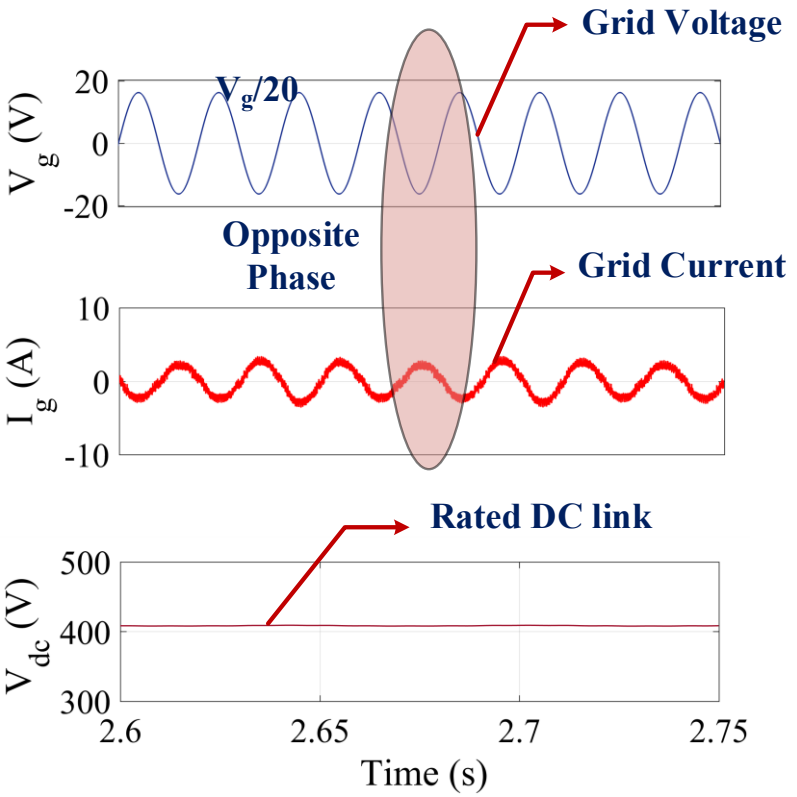

Figure 5.21. Simulated performance of developed system during V2G (V_g, I_g, V_{DC}).

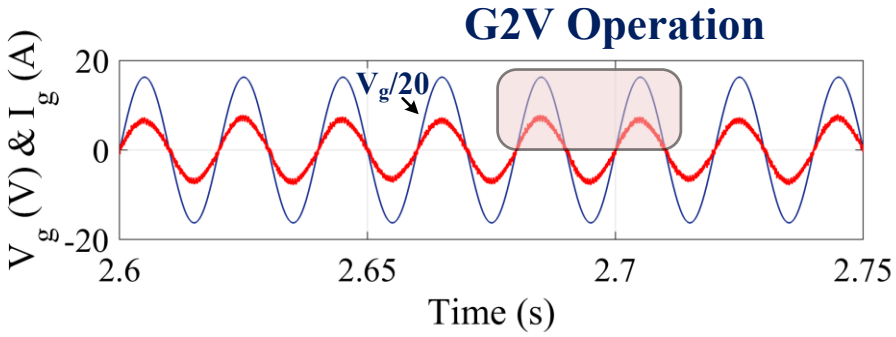

Figure 5.22. Simulated Performance of UPF operation during G2V (V_g, I_g).

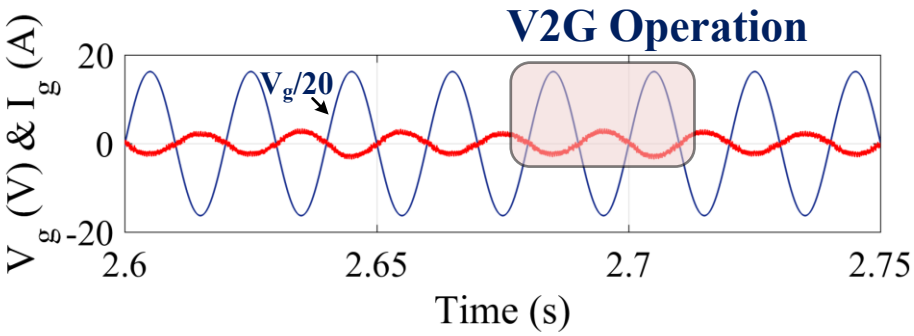

Figure 5.23. Simulated performance of UPF operation during V2G (V_g, I_g).

Figure 5.24 shows the battery SOC taken at 20%, battery voltage around 51.7V, and battery current of -15A, during charging mode. The negative value of the battery current indicates that the battery is receiving current from the grid. Figure 5.25 shows the battery SOC which is taken at 85%, battery voltage of around 51.7V, and battery current of 15A during discharging mode. The positive value of the battery current indicates that the battery is discharging and supplying power to the grid. Figure 5.26 shows the grid current's total harmonic distortion (THD) which is around 3.98 % in charging mode. Thus, the developed system follows the power quality standard as per international standards viz. IEEE519.

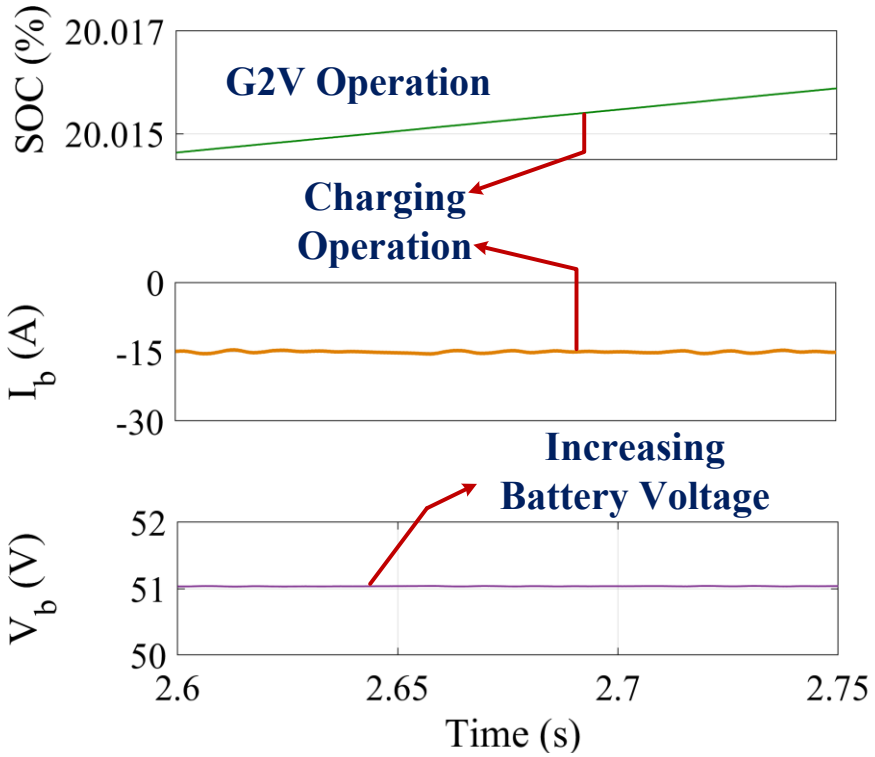

Figure 5.24. Simulated performance of battery charging operation (SOC, I_b, V_b).

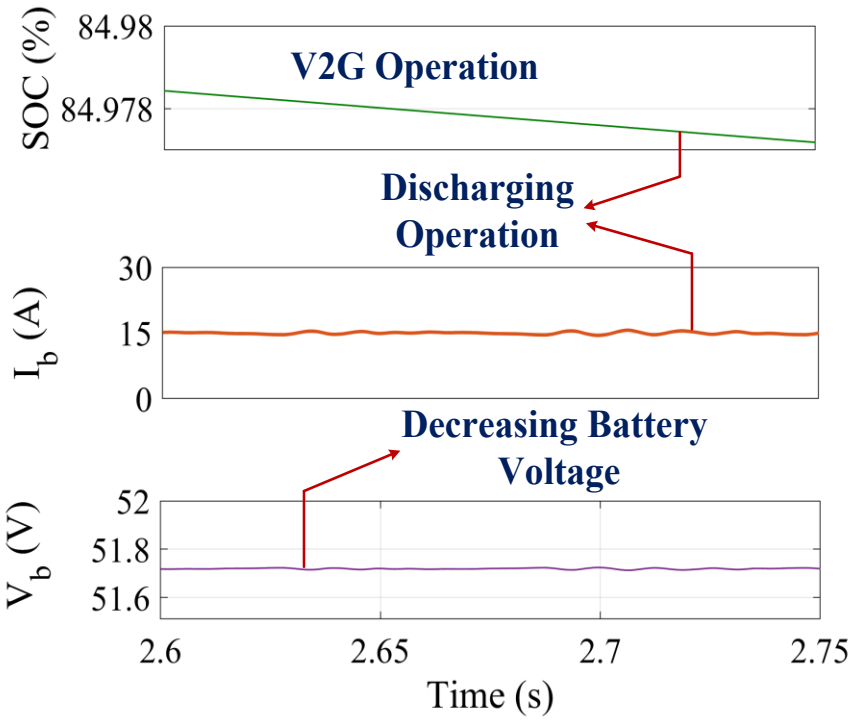

Figure 5.25. Simulated performance of battery discharging operation (SOC, I_b, V_b).

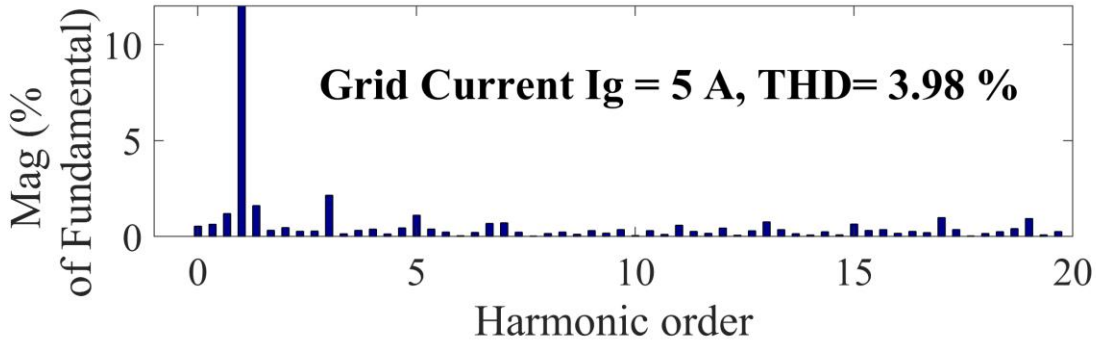

Figure 5.26. Simulated performance of THD of I_g during G2V.

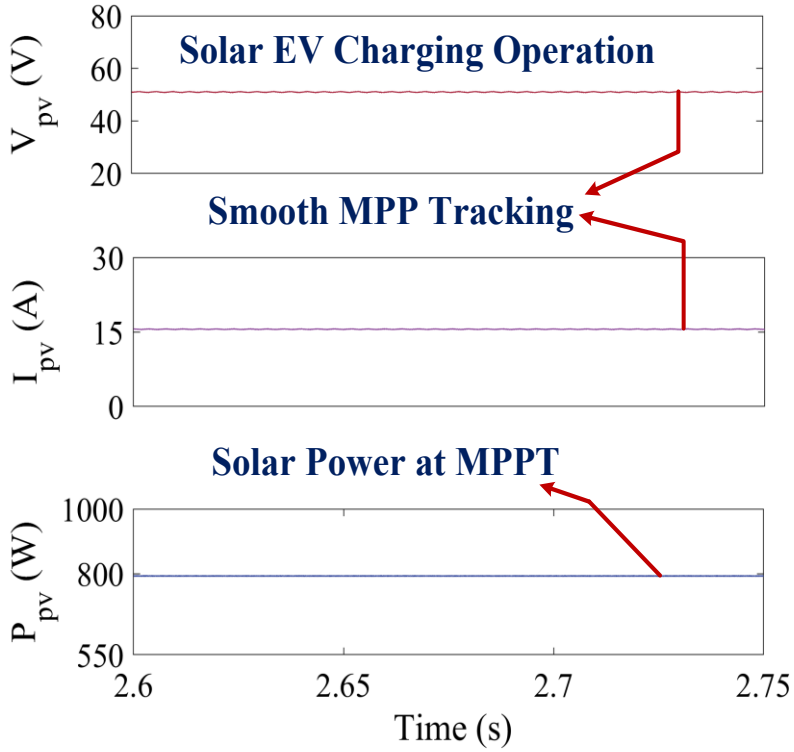

Figure 5.27. Simulated performance of solar PV array (V_{pv}, I_{pv}, P_{pv}).

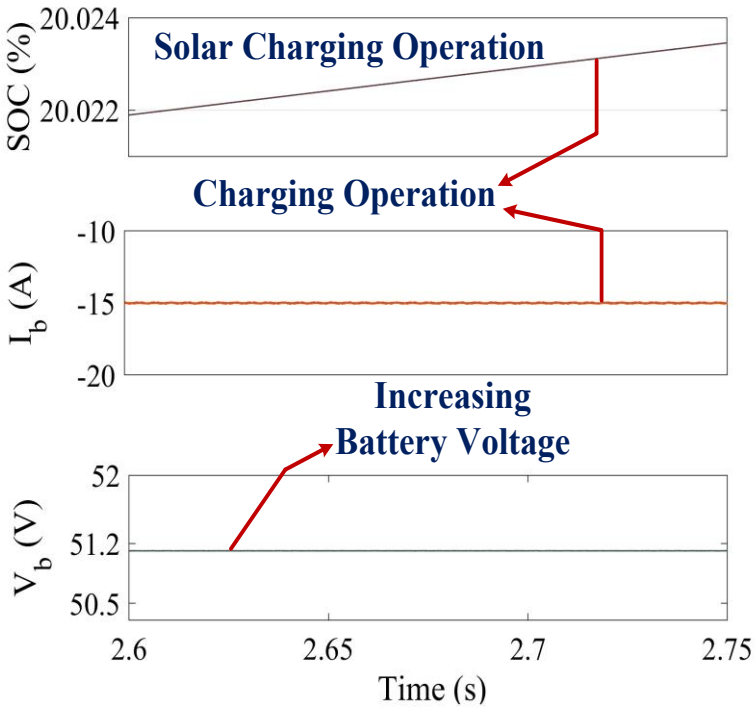

Figure 5.28. Simulated performance of solar PV array-based charging (SOC, I_b, V_b).

5.8.1.2 Solar PV-Based Charging Performance

The operational performance and effectiveness of the presented solar PV array with MPP are evaluated for different irradiance conditions. In this, various parameters of solar PV array like irradiance, PV power (P_{pv}), PV current (I_{pv}), PV voltage (V_{pv}) and battery state of charge (SOC), battery current, and battery voltage are discussed with waveforms as depicted in Figure 5.27 and Figure 5.28. Figure 5.27 shows the assumed irradiance of 1000W/m^2 which directly affects the amount of power generated by the PV array, PV voltage of 54V, PV current around 15A, and PV power output which is around 800W. This PV voltage results from the solar panel internal characteristics and the operating conditions set by the MPPT algorithm. Figure 5.28 shows the state of charge (SOC%) of the battery during the change in irradiance, battery current around -15A, and battery voltage around 51.7V. The negative value of the battery current indicates that the battery is receiving current from the solar PV.

5.6.1.3 Brushless DC Motor Performance

The effectiveness and operational performance of the presented BLDC motor, along with its control in the DC-to-AC inverter, are simulated and experimentally implemented. The battery's state of charge (SOC) indicates it is almost fully charged. The discharging battery current could be related to the load being driven by the BLDC motor. Moreover, waveforms of line-line voltages (V_{ab}, V_{bc}, and V_{ac}) of all three phases, which are around 50V is depicted in Figure 5.29, the stator current (I_a) is around 20 A is shown in Figure 5.30, and rotor speed is around 2100 RPM. The line-line voltages are typical operating voltages for the inverter-controlled three-phase system in this setup. The line-to-line voltages of all three phases show the operation conclusiveness. The recorded stator current indicates the current supplied to the motor's stator. In the case of BLDC motors, the stator current directly the torque generated. Thus, the

waveform confirms that the motor operates within safe ranges and that there are no overcurrent possibilities that could damage the system.

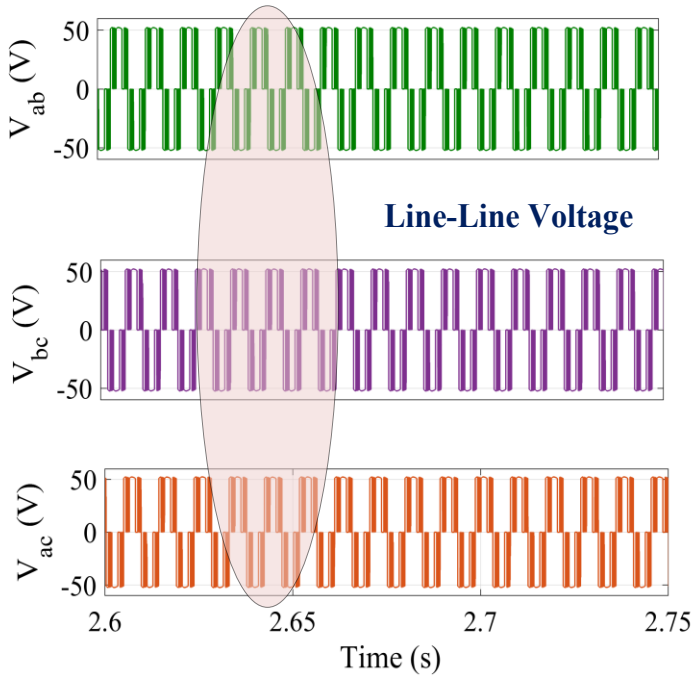

Figure 5.29. Simulated performance of line-line phase voltages (V_{ab}, I_{bc}, V_{ac}).

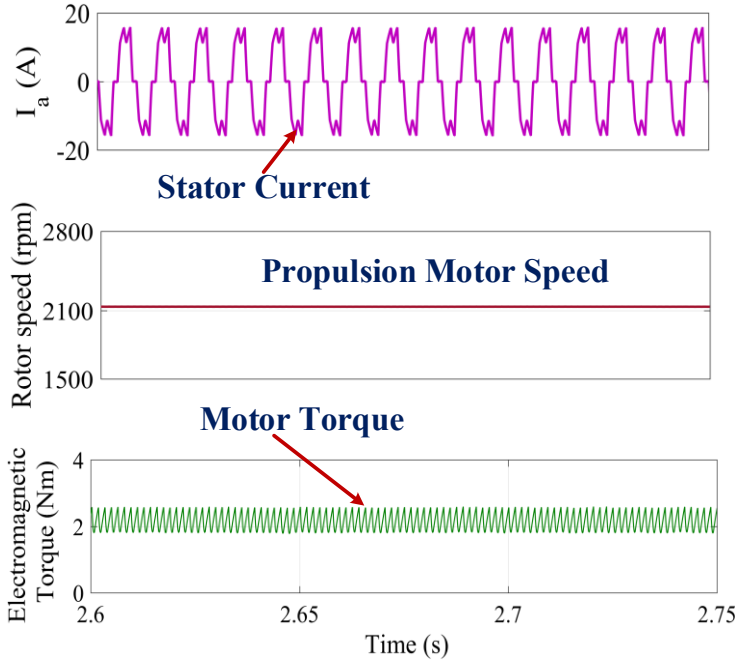

Figure 5.30. Simulated performance of BLDC motor in propulsion mode ($I_a, Rotor\ Speed, T_e$).

5.8.2 Simulated Performance of Solar-Powered On-board LEV Using Switched Capacitor High-Gain Converter

The developed system is tested using the MATLAB/SIMULINK environment, to ensure the optimal/good charging in both grid power supply and solar-powered conditions in this section. The effectiveness/efficiency of the developed charger is demonstrated via simulation results. Also, a simulation operation investigation of the BLDC motor is also resulted in this section. The operational performance of the developed system includes G2V (charging) and V2G (discharging) modes of

operation, as depicted in Figure 5.31-5.39. The parameters like, grid voltage (V_g) and grid current (I_g), power factor correction (PFC), distortion factor, state of charge (SOC), battery current (I_b), and battery voltage (V_b) are discussed by using the simulation results.

5.8.2.1 Grid-Based Charging Performance

The proposed SCBZ undergoes two modes of operation during grid availability that comprise G2V (battery charging) and V2G (battery discharging), as referred in Figure 5.31-64. The resulting parameters belongs to the proposed system, such as grid voltage (V_g) and grid current (I_g), in-phase and out of phase, THD, DC link voltage (V_{DC}), active power, reactive power, at the battery side SOC (in %), its charging/discharging current (I_b), and its increasing/decreasing voltage (V_b), are explained via the results. Referring to Figure 5.31 the results of grid voltage, that is 325V, its current of 6.277A with low THD, active power *P (80W),* and reactive power *Q* (0VAR) during battery charging mode (grid to vehicle). Next, referring to Figure 5.32 the grid voltage (V_g) now 325V, (I_g) current at grid side of 3A, active power *P (-3W),* and reactive power *Q* (0 VAR) during battery discharging mode (vehicle to grid). The results in Figure 5.33 refer to the resulting waveforms of the regulated DC-link voltage response (400V-350V), state of charge (20 %), -15A battery current (I_b), and 51.7V battery voltage (V_b) during battery charging mode (grid to vehicle). The results in Figure 5.34 refer to the resulting waveforms of the regulated DC-link voltage response (400V-350V), state of charge (20 %), 15A battery current (I_b), and 50.5V battery voltage (V_b) during battery discharging mode (vehicle to grid).

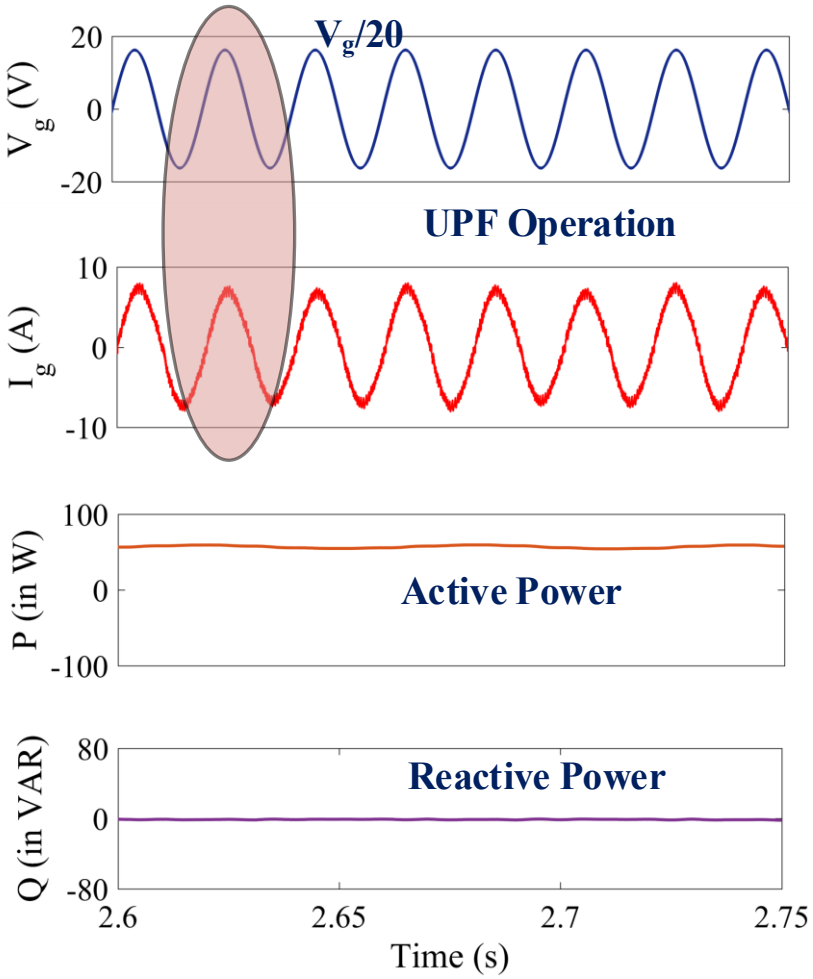

Figure 5.31. Simulated performance of developed system during G2V(V_g, I_g, P, Q).

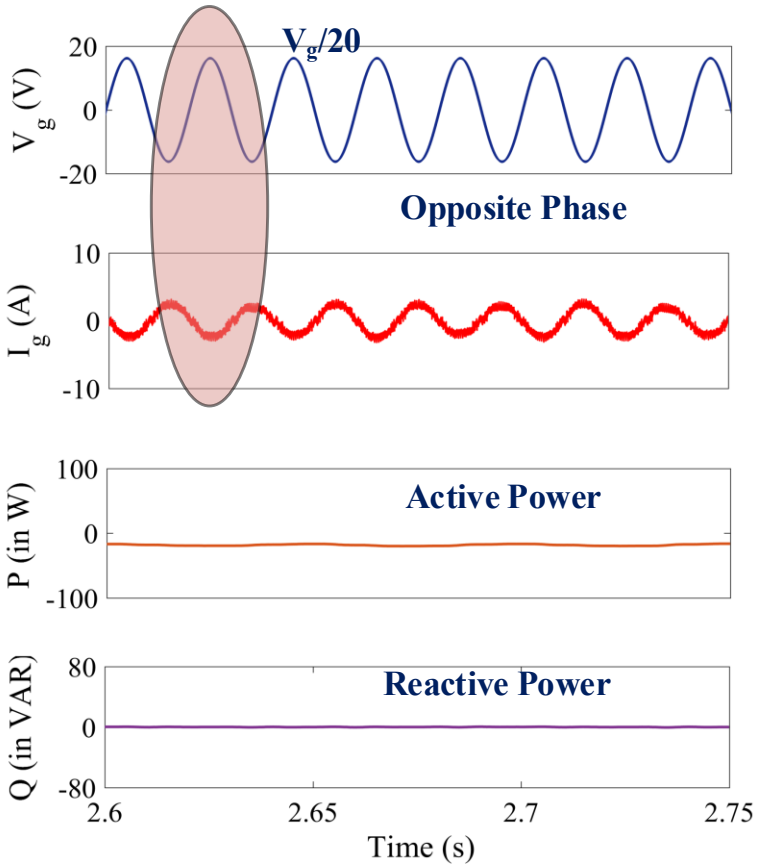

Figure 5.32. Simulated performance of developed system during V2G (V_g, I_g, P, Q).

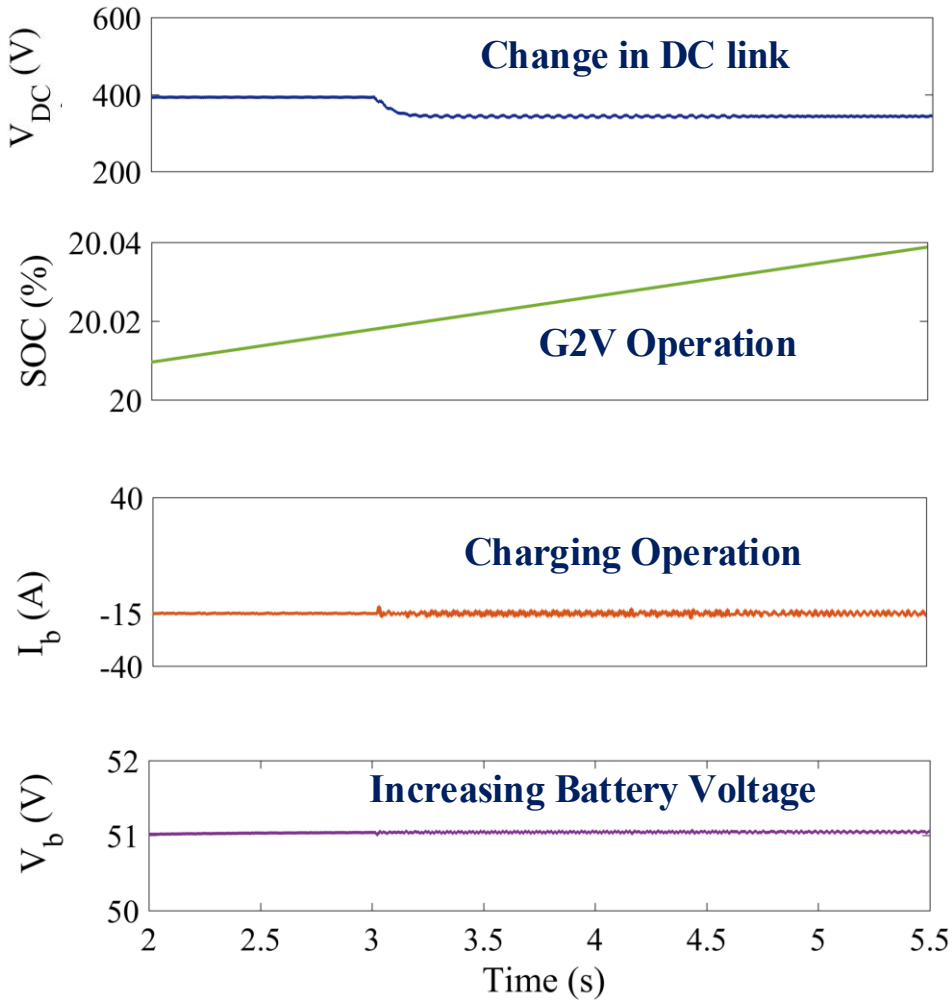

Figure 5.33. Simulated performance of battery charging (V_{DC}, SOC, I_b, V_b).

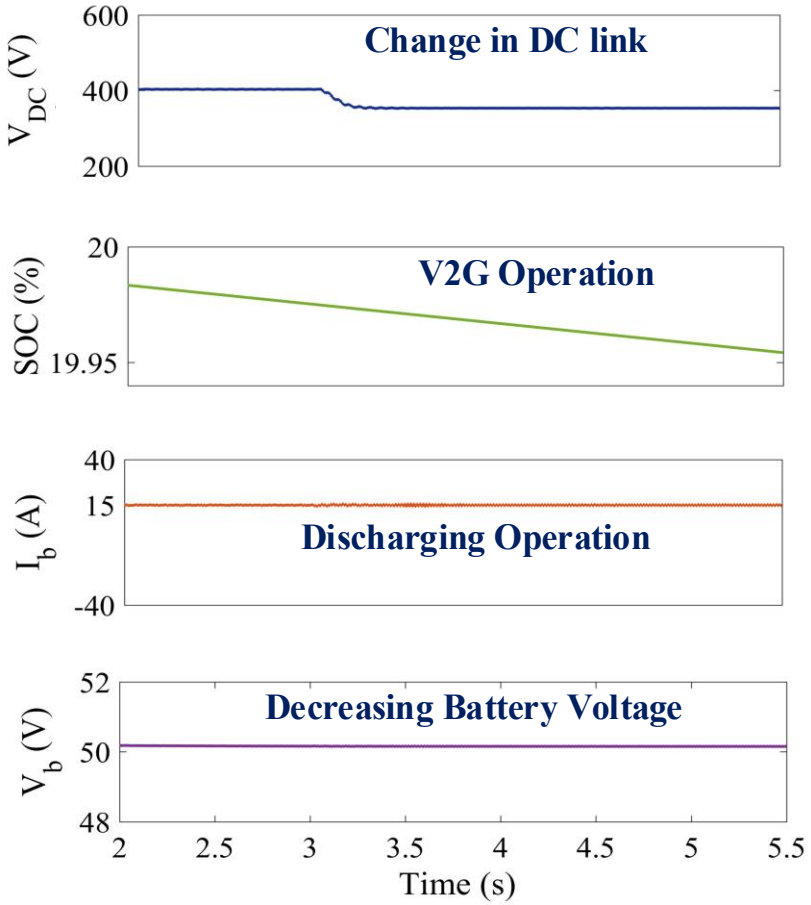

Figure 5.34. Simulated performance of battery discharging (V_{DC}, SOC, I_b, V_b).

The results in Figure 5.35 refer to the THD's resulting waveforms, which is 3.98 % during G2V. The proposed system operates with no reactive power, which is an essential aspect of the system. Since the converter operates at the unity power factor (UPF), the reactive power is effectively zero. This is significant because it highlights that the system operations does not impose any additional reactive power burden on the system, ensuring efficient energy transfer without generating or consuming reactive power.

5.8.2.2 Solar PV Based Charging Performance

The resulting investigation of the on-board array with MPP are referred in Figure 5.36 and Figure 5.37, with different irradiance conditions. The resulting parameters of this on-board system like change in irradiance, its voltage (V_{pv}), its power (P_{pv}), its current (I_{pv}), and battery SOC (in %), its charging current (I_b), and increasing voltage (V_b).

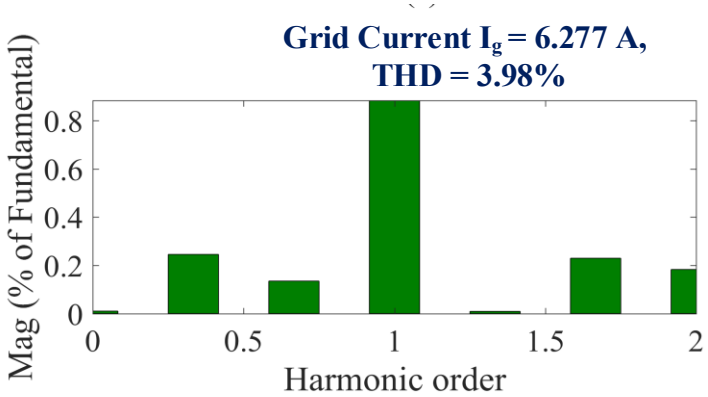

Figure 5.35. Simulated performance of THD of I_g during G2V.

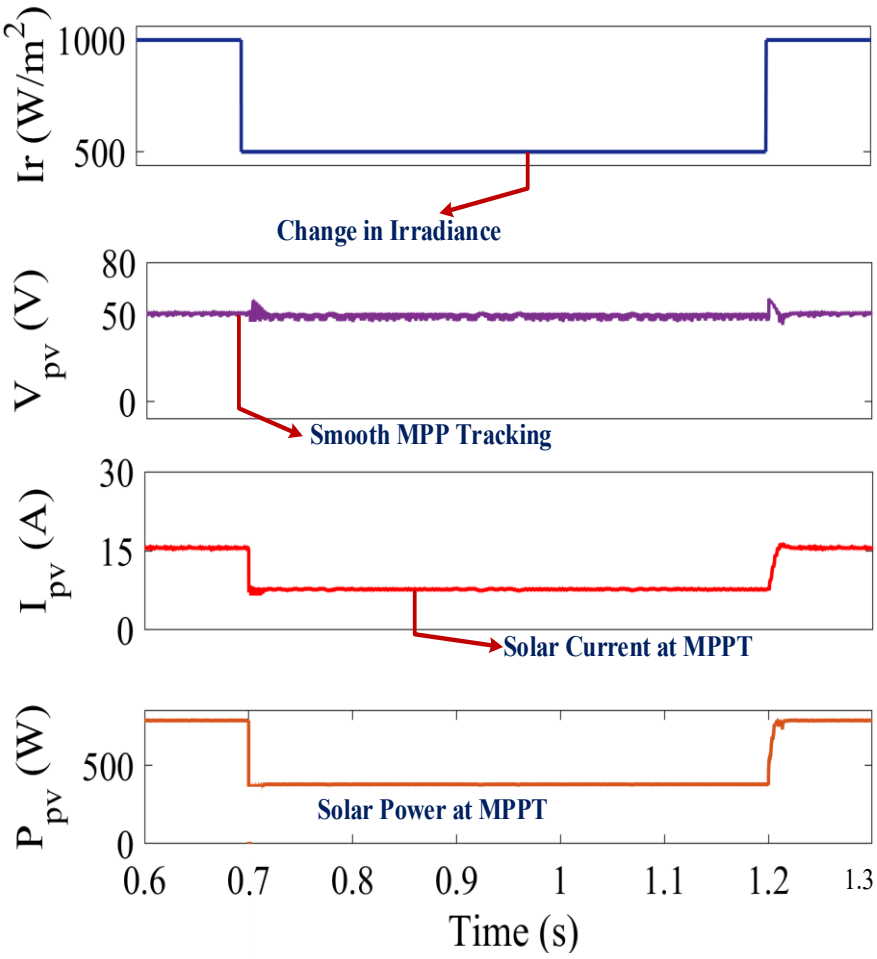

Figure 5.36. Simulated performance of solar PV array $(Irradiance, V_{pv}, I_{pv}, P_{pv})$.

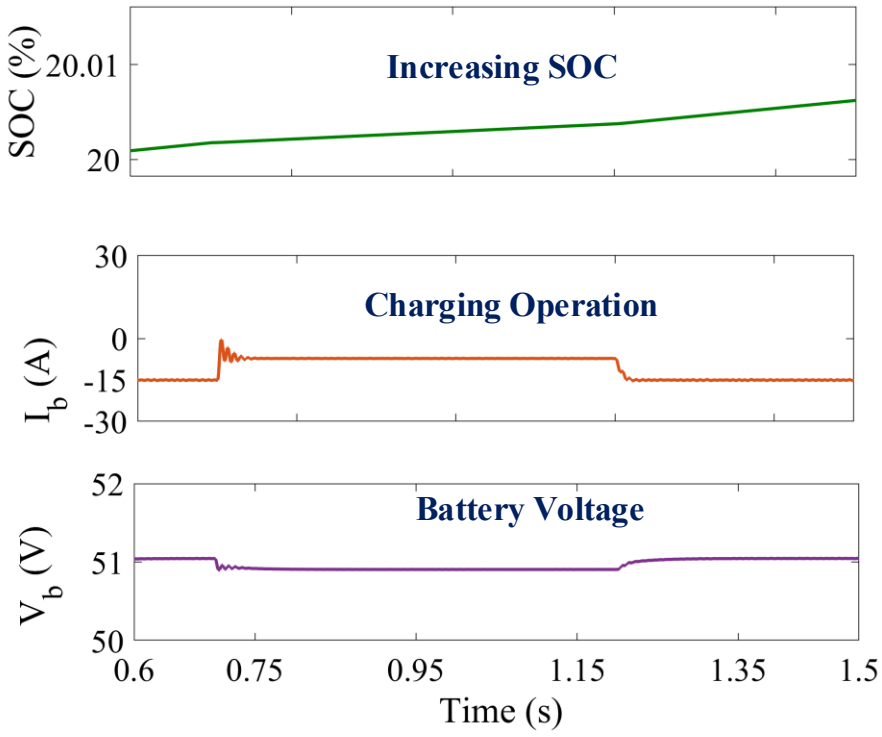

Figure 5.37. Simulated Performance of solar PV array-based charging (SOC, I_b, V_b).

20 The change in irradiance from 1000W/m^2 to 500W/m^2 and then to 1000W/m^2 which directly belongs to power produced by the array, (V_{pv}) is 54V, (I_{pv}) is 15A (charging), and (P_{pv}) is 800W is reffered in

Figure 5.36. the resulting investigations in Figure 5.37 reffers the state of charge (20%) of the battery during the change in irradiance, battery current (I_b) is -15A during 1000W/m^2, and -5A during 500W/m^2 and battery voltage (V_b) is 51.7V during 1000W/m^2, and 50.5V during 500W/m^2.

5.8.2.3 Brushless DC Motor Performance

The resulting investigation of the presented brushless DC is simulated, and the resulting waveforms is referred Figure 5.38 and Figure 5.39. This resulting waveform includes parameters like the power inverter three-phase voltages (V_{ab}, V_{bc} and V_{ac}), which are closed by 50V in Figure 5.38.

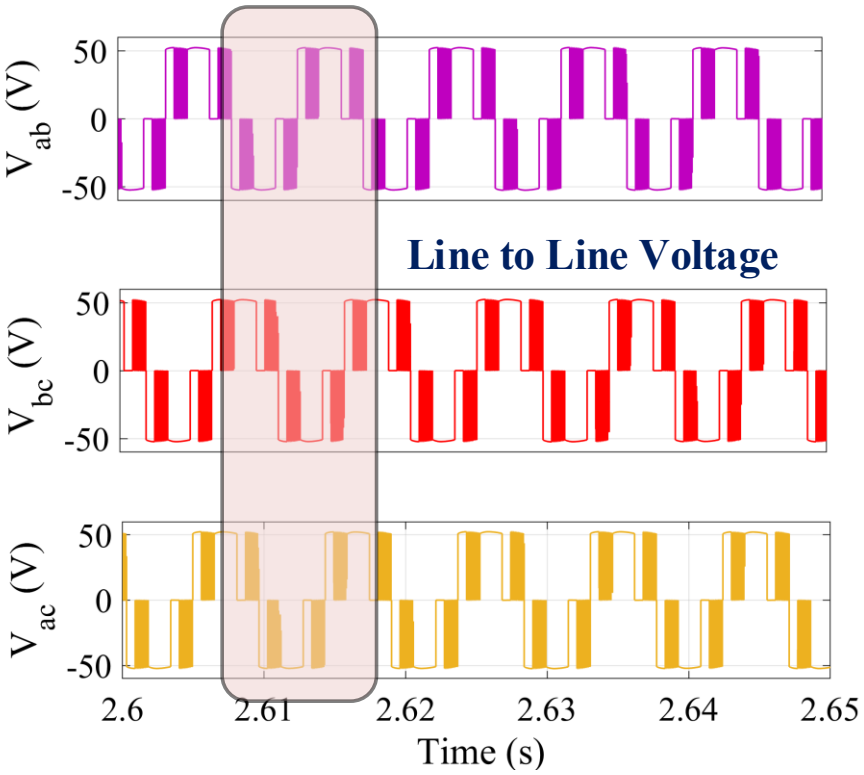

Figure 5.38. Simulated performance of line-line phase voltages (V_{ab}, I_{bc}, V_{ac}).

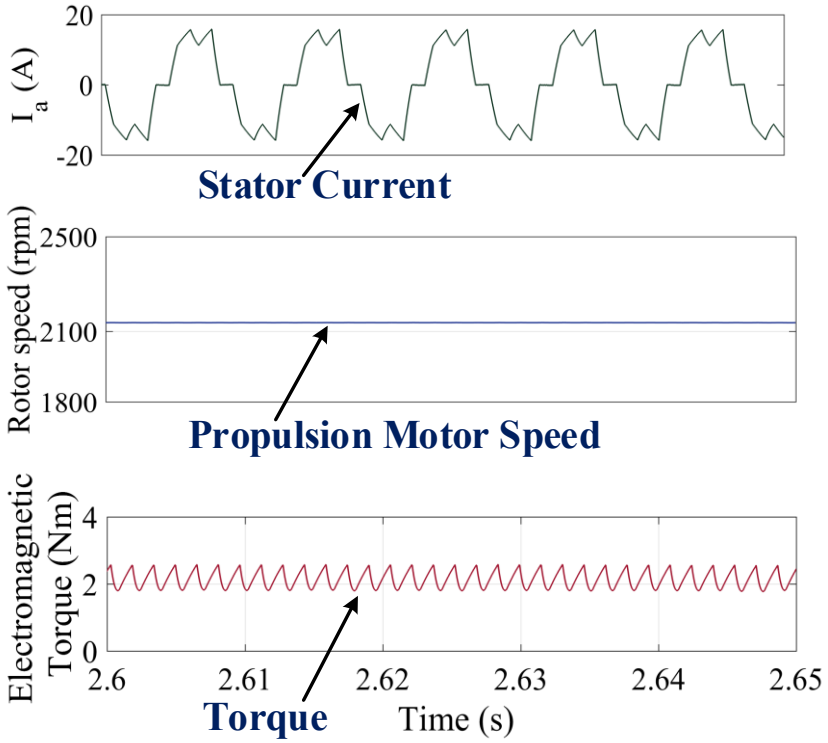

Figure 5.39. Simulated performance of BLDC motor in propulsion mode $(I_a, Rotor\ Speed, T_e)$.

According to Figure 5.39, the associated current (Ia) is closed by 20A, rotor speed closed by 2100 (in rpm), and torque varying from 2 N-m to 2.3 N-m. In this resulting waveform, current directs the current granted to the motor's stator and then this current direct the torque produced. Thus, the results justify that the BLDC functions in secure limits and that there are no overcurrent chances that can destroy the system.

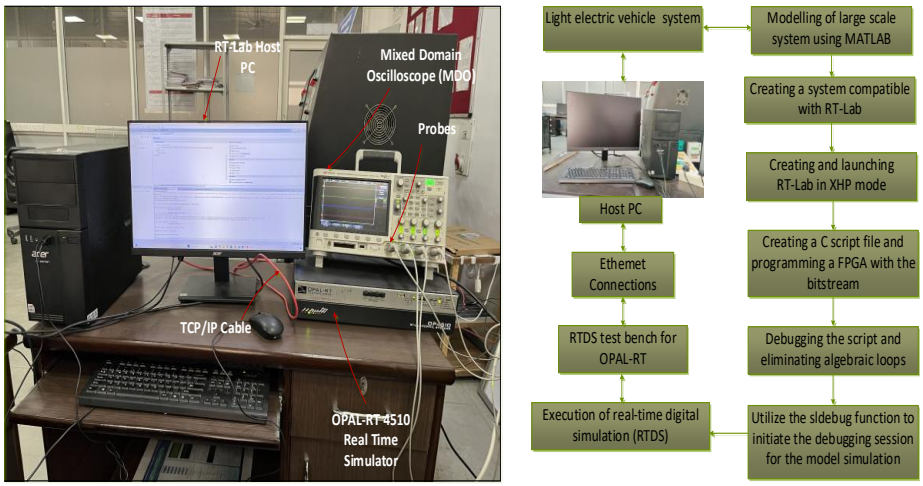

Figure 5.40. Real-time CHIL test setup.

5.9 Experimental Performance of Solar-Powered On-board LEV Utilizing Non-Isolated High-Gain Converter with G2V and V2G Capabilities

The designed model control is also validated through an OPAL-RT interface. Figure 5.40 shows a real-time CHIL (controller hardware in the Loop) test setup with test results in Figures 5.41. In this section, the system specifications are the same as those used in the simulation study. The test results are explained for the G2V/V2G mode of operations, PV-based charging, and BLDC motor performance.

5.9.1 Experimental Performance of Solar-Powered On-board LEV Using Coupled Inductor High-Gain Converter

In this section, the proposed coupled inductor high gain (SCBZ) converter is validated via an OPAL-RT interface to ensure optimal charging efficiency in both grid power supply and solar-powered conditions. Also, a hardware operation investigation of the BLDC motor is presented here.

5.9.1.1 Grid-Based Charging Performance

Figure 5.41 shows the result of the grid voltage V_g, grid current I_g, and DC link voltage V_{DC} at channels 1-3 of DSO during charging mode. Figure 5.41(b) presents the UPF operations, which show the waveforms of the grid voltage V_g and grid current I_g are in phase during G2V mode. Figure 5.42 shows the result of the grid voltage V_g, grid current I_g, DC link voltage V_{DC} and the battery current I_b during charging mode. Figure 5.43(a) shows the result of the grid voltage V_g, grid current I_g, and DC link voltage V_{DC} at channels 1-3 of DSO during discharging mode. Figure 5.43 (b) presents the UPF operations, which show the waveforms of grid voltage V_g and grid current I_g are out of phase during V2G

mode.

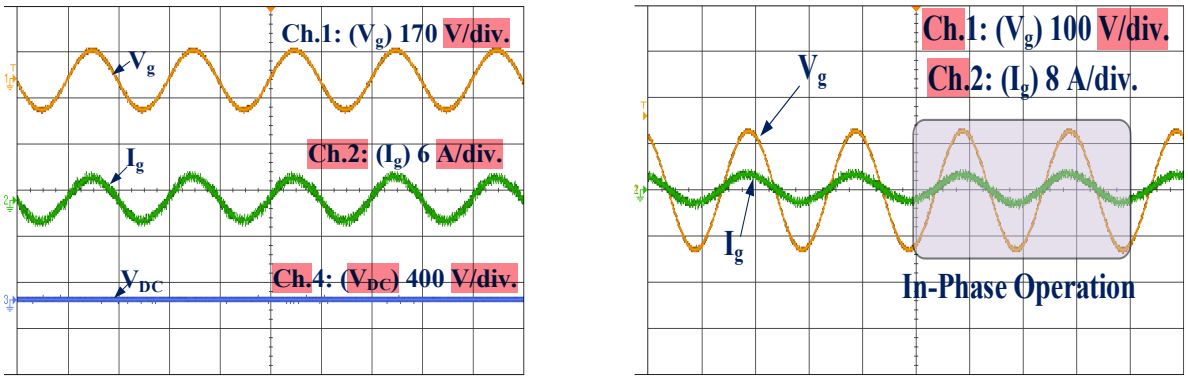

(a) (b)

Figure 5.41. Experimental performance of developed system during G2V, (a) (V_g, I_g, V_{DC}), (b) (V_g, I_g).

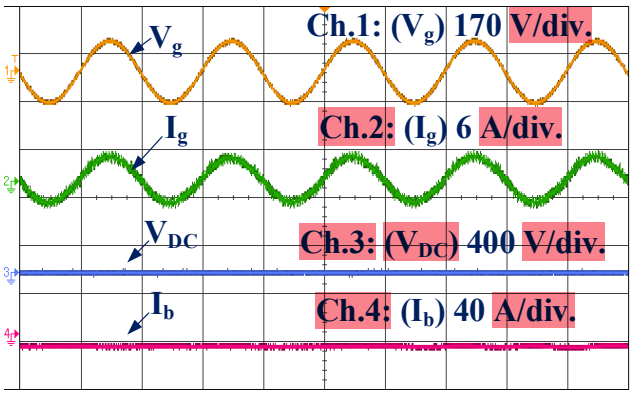

Figure 5.42. Experimental performance of battery charging operation (V_g, I_g, V_{DC}, I_b).

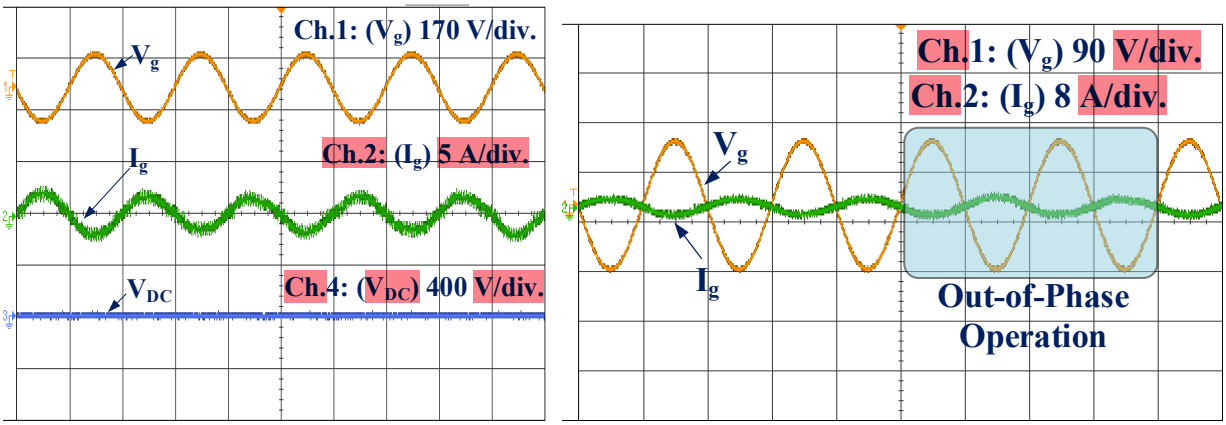

(a) (b)

Figure 5.43. Experimental performance of developed system during V2G, (a) (V_g, I_g, V_{DC}), (b) (V_g, I_g).

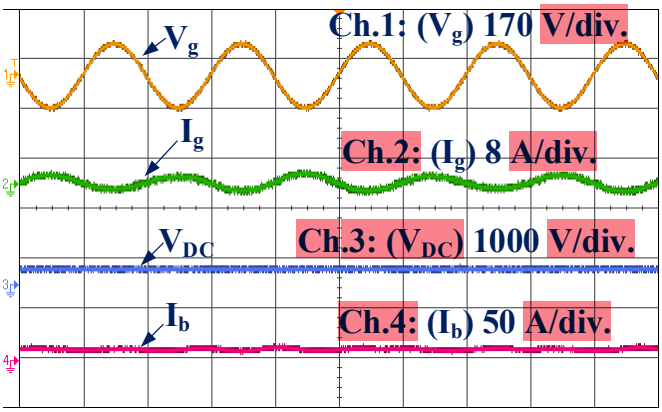

Figure 5.44. Experimental performance of battery discharging operation (V_g, I_g, V_{DC}, I_b).

Figure 5.44 shows the result of the grid voltage V_g, grid current I_g, DC link voltage V_{DC} and the battery current I_b during discharging mode. These results demonstrate the improved performance of the developed converter and control technique in maintaining UPF operation and low distortions in the grid current in the G2V and V2G modes of operations. This also ensures smooth charging/discharging of EV battery and regulation of DC link voltage in different operating modes.

5.9.1.2 Solar PV Based Charging Performance

Figure 5.45(a-b) illustrates the system's response to varying solar irradiance levels (i.e. 1000, 500, 200) and their impact on PV and battery parameters in a solar PV-based EV charging setup. As irradiance decreases in Figure 5.45(a), the PV current I_{pv} and battery current I_b reduce proportionally, reflecting the system's adaptation to lower solar input, while the PV voltage Vpv remains stable due to the effective operation of the Maximum Power Point Tracking (MPPT) mechanism. Similarly, the battery voltage V_b in Figure 5.45(b) stays within a safe range, highlighting the robustness of the controller. Notably, when irradiance levels return to higher values, the PV and battery currents adjust dynamically to optimize charging. These results confirm the system's reliability and efficiency under fluctuating environmental conditions, emphasizing the critical role of MPPT and power management strategies in maintaining consistent performance in PV-based EV charging systems.

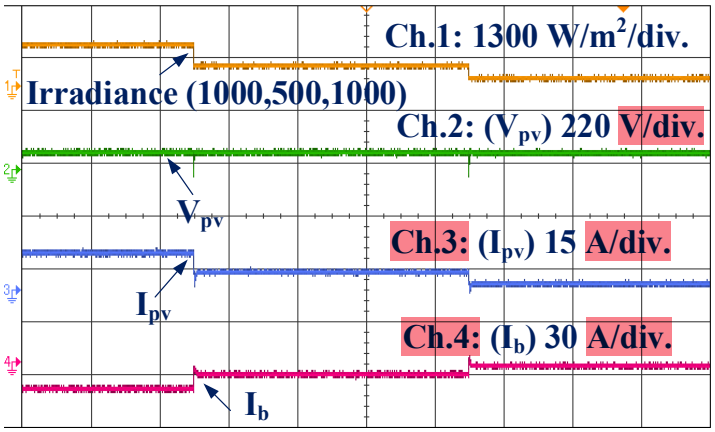

(a)

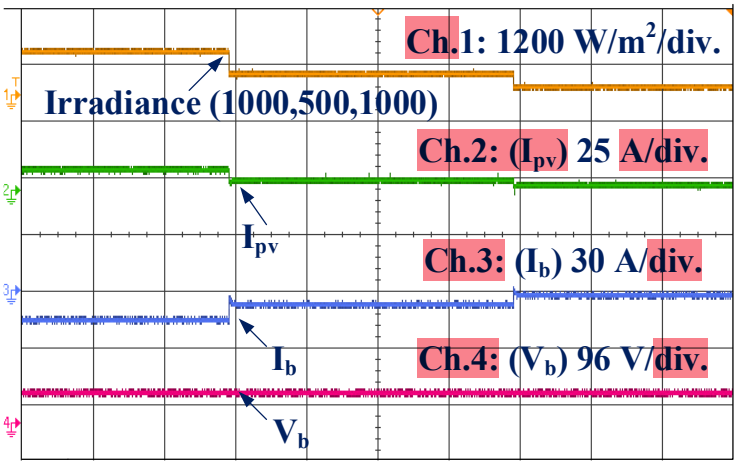

(b)

Figure 5.45. Experimental performance of Solar PV-based LEV battery charging, (a) $(Irradiance, V_{pv}, I_{pv}, I_b)$ (b)

$(Irradiance, I_{pv}, I_b, V_b)$.

5.9.1.3 Brushless DC Performance

Figures 5.46 and 5.47 provide insights into the dynamic behavior of a battery-powered motor drive system in an electric vehicle during various operating conditions. Figure 5.46 shows stable and balanced line-to-line voltages V_{ab}, V_{bc}, and V_{ca} throughout the operation, ensuring efficient motor performance, while the battery current reflects load variations. Overall, the system ensures smooth, efficient, and reliable operation, making it well-suited for electric vehicle applications. In Figure 5.47, the I_b battery

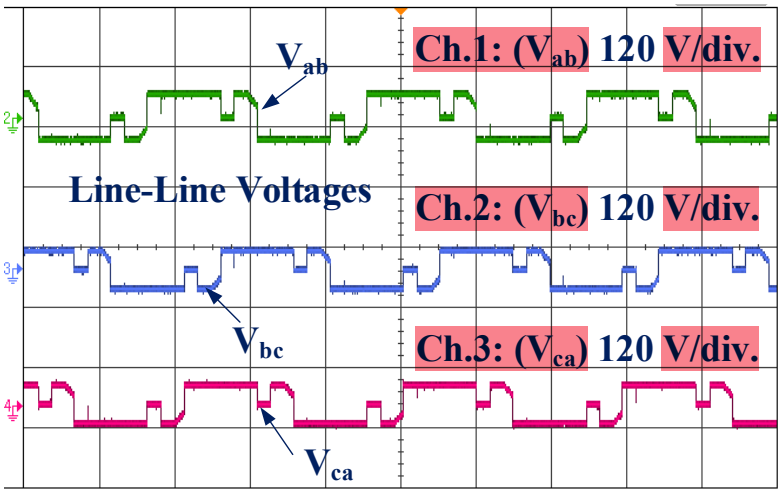

Figure 5.46. Experimental performance of all line-line phase voltages (V_{ab}, I_{bc}, V_{ac}).

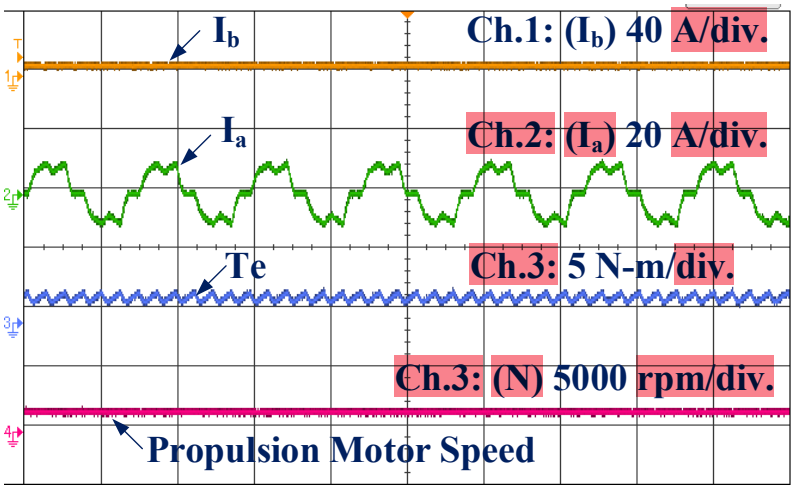

Figure 5.47. Experimental performance of BLDC motor in propulsion mode $(I_b, I_a, T_e, Rotor\ Speed)$.

current adjusts dynamically to meet the motor's energy demands, while the stator current I_a and electromagnetic torque T_e rise proportionally during acceleration, leading to a smooth increase in rotor speed.

5.9.2 Experimental Performance of Solar-Powered On-board LEV Using Switched Capacitor High-Gain Converter

The proposed switched capacitor high gain (SCBZ) converter is tested/validated via an OPAL-RT interface to ensure the optimal/good charging efficiency in both grid power supply and solar powered conditions in this section. Also, a hardware operation investigation of the BLDC motor is also resulted here.

5.9.2.1 Grid Based Charging Performance

The tested results at channels 1-4 of DSO in Figure 5.48(a) explaining the investigation of the UPF operations, grid voltage V_g, its current I_g, voltage V_{DC} and current I_b of the battery at the time of G2V in Figure 5.48(b). The tested result at channels 1-4 of digital storage oscilloscope in Figure 5.49(a) explaining opposite phase, grid voltage V_g, grid current I_g, DC link voltage V_{DC} and battery current I_b during V2G in Figure 5.49(b). These tests validate the enriched investigation of the proposed SCBZ converter and in keeping PFC operation of the grid current in both G2V and V2G.

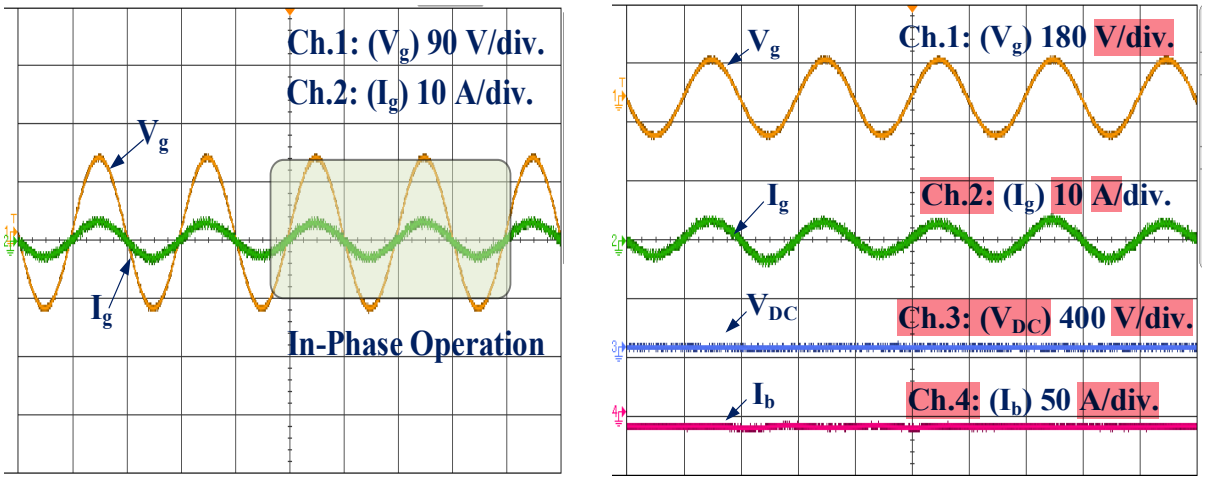

(a) (b)

Figure 5.48. Experimental performance of developed system during G2V, (a) (V_g, I_g) (b) (V_g, I_g, V_{DC}).

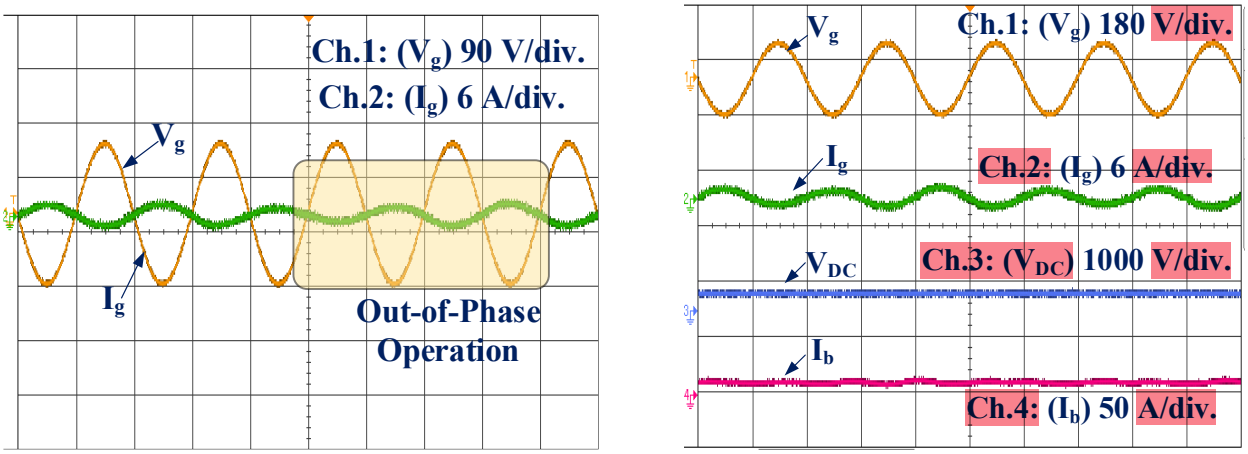

(a) (b)

Figure 5.49. Experimental performance of developed system during V2G, (a) (V_g, I_g) (b) (V_g, I_g, V_{DC}).

5.9.2.2 Solar PV-Based Charging Performance

Referring to Figure 5.50 (a-b), the on-board solar powered system with irradiance stages (i.e. 1000, 500, 200) and (i.e. 500, 1000) and their impact on system results is also explained. As irradiance decreases in Figure 5.50(a-b), the PV current I_{pv} and battery current I_b reduce proportionally, reflecting the system's adaptation to lower solar input, while the PV voltage *Vpv* remains stable due to the effective operation of the Maximum Power Point Tracking (MPPT) mechanism. Notably, when irradiance levels return to higher values, the PV and battery currents adjust dynamically to optimize charging. These results confirm the system's reliability and efficiency under fluctuating environmental conditions, emphasizing the

critical role of MPPT and power management strategies in maintaining consistent performance in PV-based EV charging systems.

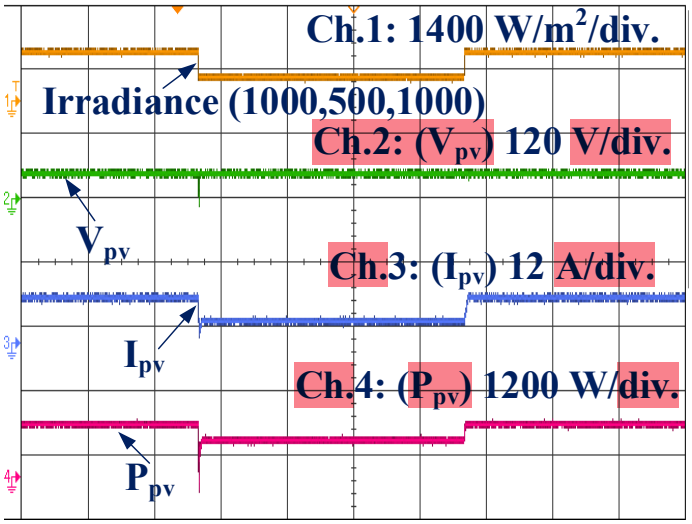

(a)

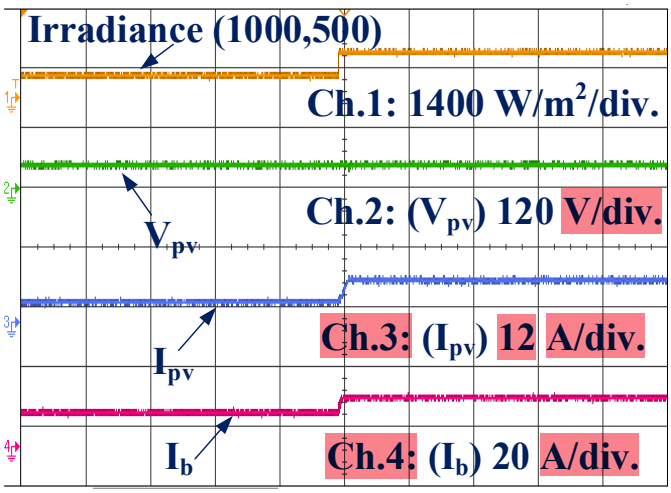

(b)

Figure 5.50. Experimental Performance of Solar PV based LEV battery charging, (a) $(Irradiance, V_{pv}, I_{pv}, P_{pv})$ (b) $(Irradiance, V_{pv}, I_{pv}, I_b)$.

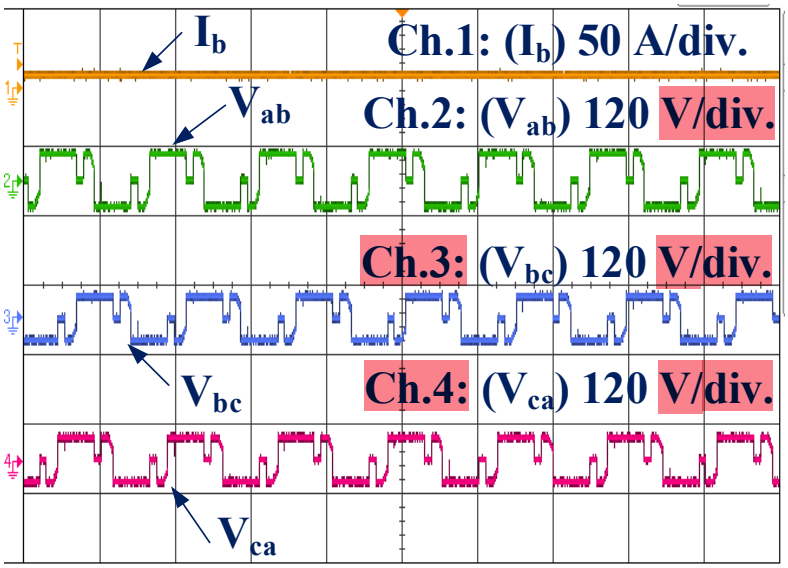

Figure 5.51. Experimental performance of all line-line phase voltages (V_{ab}, I_{bc}, V_{ac}).

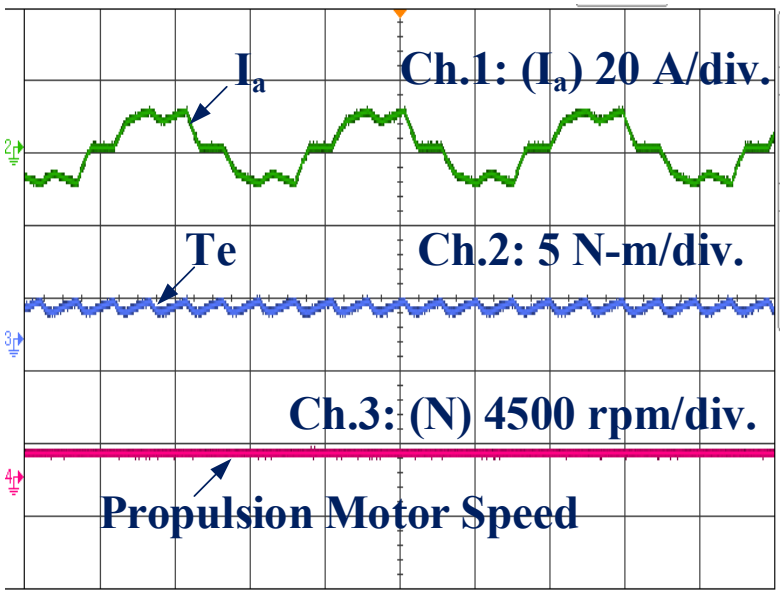

Figure 5.52. Experimental performance of BLDC motor in propulsion mode $(I_a, Rotor\ Speed, T_e)$.

5.9.2.3 Brushless DC Performance

Referring to Figures 5.51(a-b) it offers understanding of the changing strategy of a battery-operated drive system (V_{ab}, V_{bc}, V_{ca}, I_a, Te, and rotor speed) in an e-rickshaw during various operating conditions. Figure 5.51 shows the all line-line phase voltages. Overall, the system ensures smooth, efficient, and reliable operation, making it well-suited for electric vehicle applications. In Figure 5.52, the battery current adjusts dynamically to meet the motor's energy demands, while the stator current I_a and electromagnetic torque T_e rise proportionally during acceleration, leading to a smooth increase in rotor speed.

5.10 Losses and Efficiency Calculation

In developed system, power losses are inevitable and play a crucial role in determining the overall performance. These losses arise due to various factors such as switches operation, due to passive components, and power conversion. Efficiency calculation provides insight into how effectively the developed system works, helping to identify system configuration for better performance and improve efficiency.

5.10.1 Losses and Efficiency Estimation for Solar-Powered On-board LEV Using Coupled Inductor High-Gain Converter

The voltage & current stresses handled via various components of the developed bidirectional coupled inductor high-gain converter-based LEV charger are examined to ensure its safe, reliable, and efficient operation. The system performance is verified by performing power loss manipulations. The losses in diodes, capacitors, switches, and inductors are considered as power losses in converters. The mathematical formulations in (5.65)-(5.74) provide the calculation of power losses and efficiency of the proposed system, given as follows,

Switches $(Q_1 - Q_4)$ conduction losses (P_{closs}):

$$2\left(V_{CEO}.I_{Q1avg.} + r_{CE}.I_{Q1rms}^2\right) \quad (5.65)$$

Switches $(Q_1 - Q_4)$ switching losses (P_{swloss}):

$$2\left(V_{Q1max}.I_{Q1avg.}\left(t_r + t_f\right).f_s\right) \quad (5.66)$$

Switches (Q_5) switching losses (P_{swloss}):

$$\left(V_{Q1max}.I_{Q1avg.}\left(t_r + t_f\right).f_s\right) \quad (5.67)$$

Diode switching losses for $(Q_6 - Q_7)$ switches (P_{sdloss}):

$$2\left(V_{DQ5max}.I_{DQ5avg.}.\left(t_r + t_f\right).f_s\right) \quad (5.68)$$

Diode conduction losses for $(Q_6 - Q_7)$ switches (P_{cdloss}):

$$2\left(V_{F0}.+r_F.I_{DQ5rms}^2\right) \quad (5.69)$$

Input Inductor Losses $(P_{L_{sloss}})$:

$$I_{L_srms}^2 \cdot r_{L_s} \quad (5.70)$$

Output Inductors Losses $(P_{L_{oloss}})$:

$$2 \cdot I_{L_0rms}^2 \cdot r_{L_0} \quad (5.71)$$

Intermediate Capacitor Losses $(P_{C_{Iloss}})$:

$$2 \cdot I_{C_Irms}^2 \cdot ESR_{C_I} \quad (5.72)$$

The total power loss of the proposed converter is given in equation (5.73) and efficiency of the converter for the output power of 720W is calculated by using the Equation (5.74).

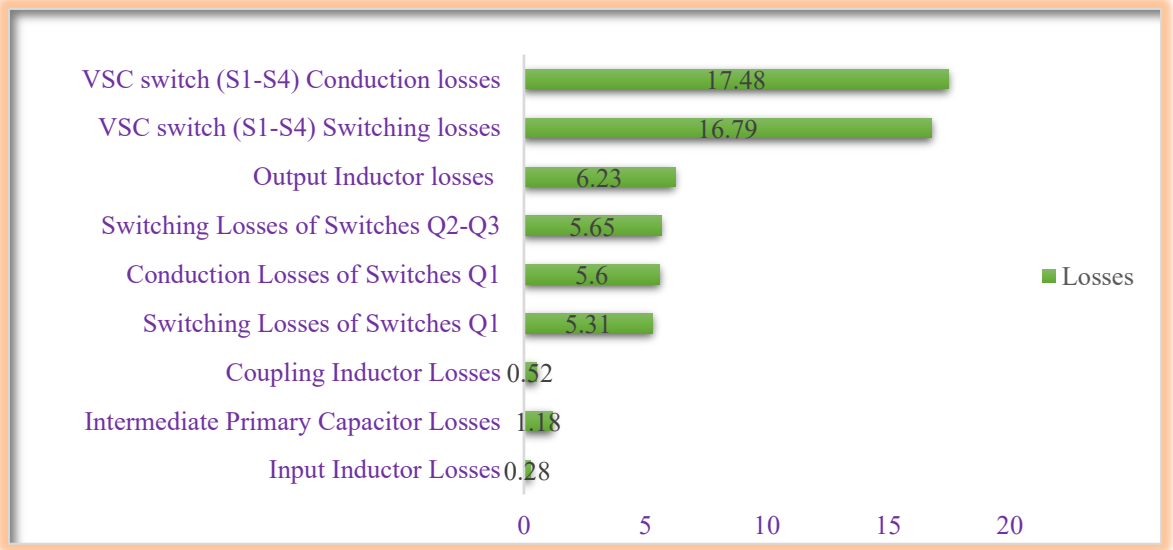

Figure 5.53. Graphical representation of power losses in coupled inductor high-gain converter.

$$P_{loss}^{Total} = P_{closs} + P_{swloss} + P_{sdloss} + P_{cdloss} + P_{L_{sloss}} + P_{L_{oloss}} + P_{C_{Iloss}} \quad (5.73)$$

$$\text{Efficiency } (\eta) = \frac{P_0}{P_0 + P_{loss}^{Total}} \quad (5.74)$$

Based on the proposed charger equations, Figure 5.53 depicts the charger's power losses and Figure 5.54 depicts efficiency for grid-to-vehicle mode and vehicle-to-grid mode, and it is found that the presented charger provides a well-regulated charging scenario for the charging and discharging. The efficiency of the presented charger is calculated as 92.3% during G2V and 88% during V2G.

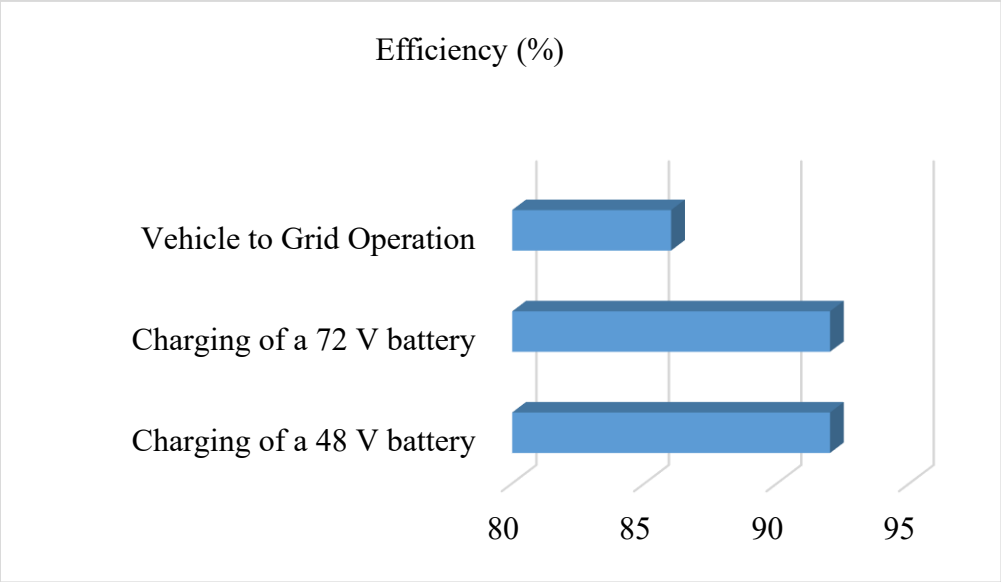

Figure 5.54. Graphical representation of efficiency of coupled inductor high-gain converter.

5.10.2 Losses and Efficiency Estimation for Solar Powered On-board LEV Using Switched Capacitor High-Gain Converter

The voltage & current stresses handled via various components of the developed bidirectional switched capacitor high-gain converter-based LEV charger are examined to ensure its safe, reliable, and efficient operation. The system performance is verified by performing power loss manipulations. Losses in diodes, capacitors, switches, and inductors are considered as power losses in converters in Figure 5.55. Mathematical formulations (5.75)-(5.80) explain the calculation of power losses and efficiency of the proposed system, given as follows,

Switches $(Q_1 - Q_4)$ conduction losses (P_{closs}):

$$2\left(V_{CEO}.I_{Q1avg.} + r_{CE}.I_{Q1rms}^2\right) \quad (5.75)$$

Switches $(Q_1 - Q_4)$ switching losses (P_{swloss}):

$$2\left(V_{Q1max}.I_{Q1avg.}\left(t_r + t_f\right).f_s\right) \quad (5.76)$$

Switches (Q_5) switching losses (P_{swloss}):

$$\left(V_{Q1max}.I_{Q1avg.}\left(t_r + t_f\right).f_s\right) \quad (5.77)$$

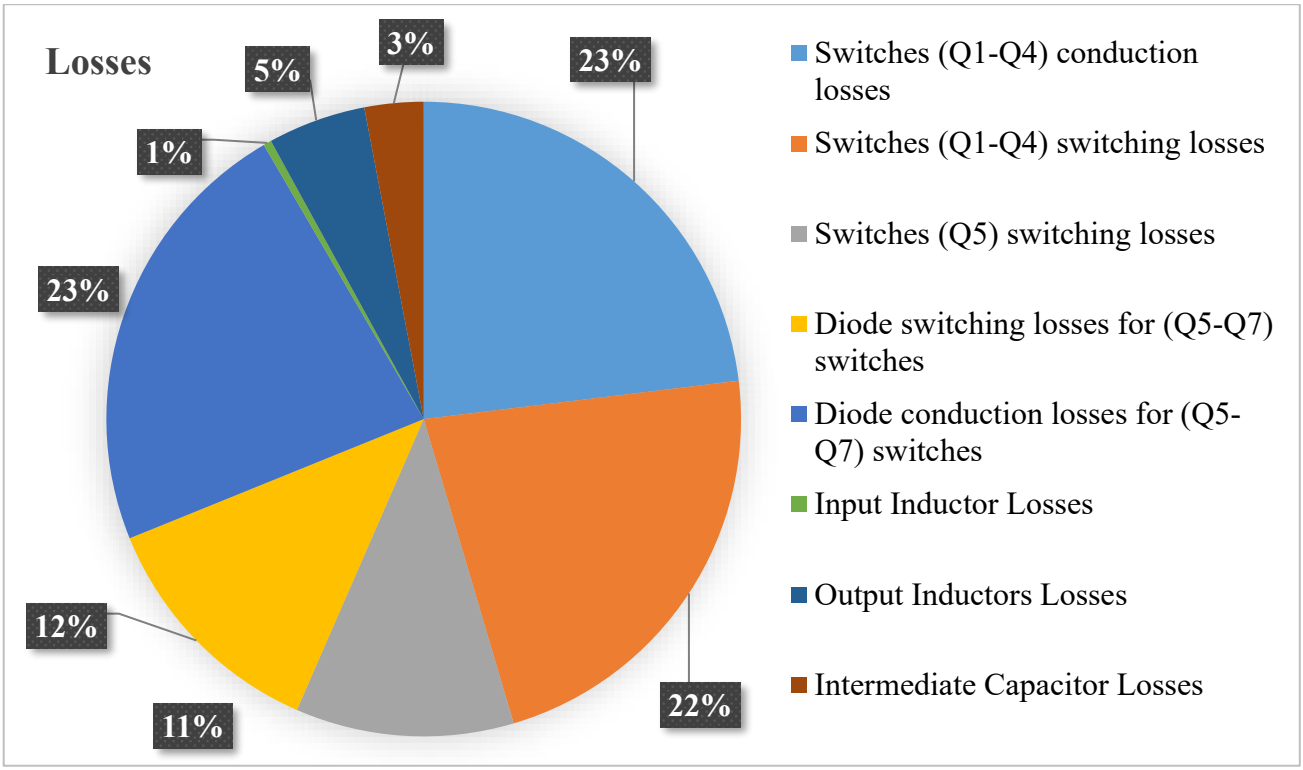

Figure 5.55. Graphical representation of power losses in switched capacitor high gain converter.

Diode switching losses for $(Q_6 - Q_7)$ switches (P_{sdloss}):

$$2\left(V_{DQ5max}.I_{DQ5avg}.\left(t_r + t_f\right).f_s\right) \tag{5.78}$$

Diode conduction losses for $(Q_6 - Q_7)$ switches (P_{cdloss}):

$$2\left(V_{F0}.+r_F.I_{DQ5rms}^2\right) \tag{5.79}$$

Input Inductor Losses $(P_{L_{sloss}})$:

$$I_{L_srms}^2 \cdot r_{L_s} \tag{5.80}$$

Output Inductors Losses $(P_{L_{oloss}})$:

$$2 \cdot I_{L_0rms}^2 \cdot r_{L_0} \tag{5.81}$$

Intermediate Capacitor Losses $(P_{C_{Iloss}})$:

$$2 \cdot I_{C_Irms}^2 \cdot ESR_{C_I} \tag{5.82}$$

Total power loss of the proposed converter is given in Equation (5.83) and efficiency of the converter for the output power of 720W is calculated by using the Equation (5.84).

$$P_{loss}^{Total} = P_{closs} + P_{swloss} + P_{sdloss} + P_{cdloss} + P_{L_{sloss}} + P_{L_{oloss}} + P_{C_{Iloss}} \tag{5.83}$$

$$\text{Efficiency } (\eta) = \frac{P_0}{P_0 + P_{loss}^{Total}} \tag{5.84}$$

Referring to the proposed SCBZ equations, Figure 5.56 defines the SCBZ charger's efficiency 93.65 %

in G2V mode and 88.95% in V2G.

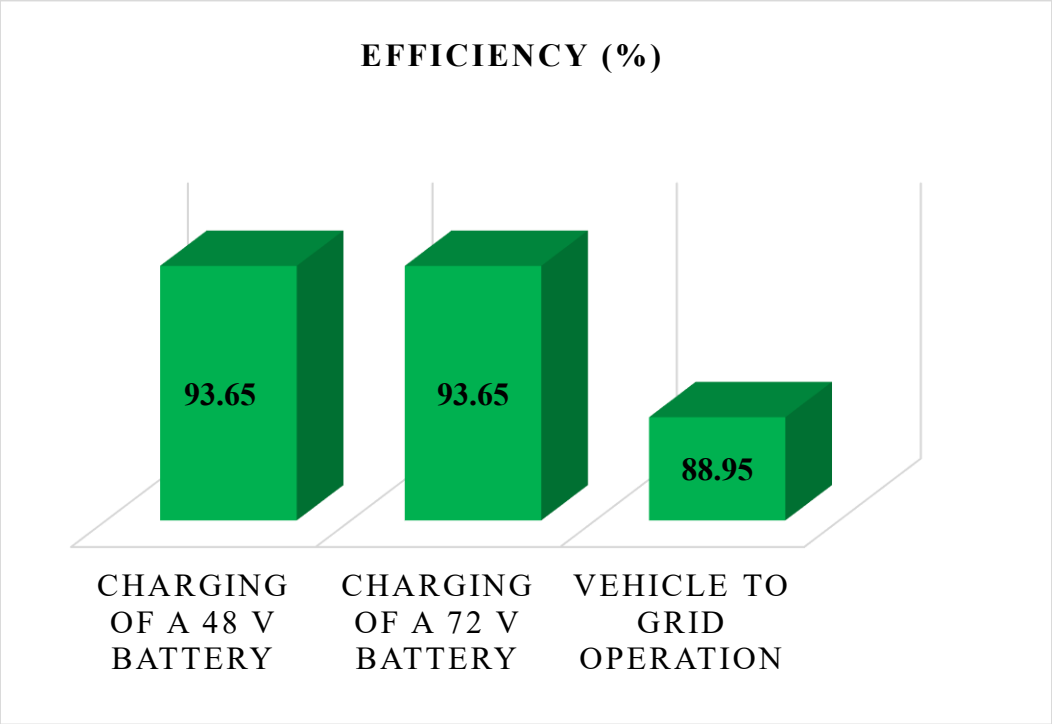

Figure 5.56. Graphical representation of efficiency of coupled inductor high gain converter.

5.11 Conclusion

The proposed solar-powered on-board charging system utilizing a coupled inductor and switched capacitor bidirectional high-gain converter demonstrates effective high-gain step-up and step-down operation. The CC/CV charging process has been successfully implemented, and the charger exhibits excellent steady-state performance in both grid-to-vehicle (G2V) and vehicle-to-grid (V2G) modes. Moreover, the unity power factor operation is also achieved in G2V and V2G modes. The control technique is well-suited for a 50 Ah battery, verified through MATLAB simulations and real-time OPAL-RT validation. This has been designed to operate in Grid-to-Vehicle (G2V) and Vehicle-to-Grid (V2G) modes with high gain functionality. An H-bridge active front-end converter (AFC) has been designed to convert AC-to-DC and maintain unity power factor (UPF) operation with bidirectional power flow. An improved mixed second-order–third-order generalized integrator (IMSTOGI) control algorithm has been developed to ensure robust operation of the AFC under grid disturbances and to achieve fast synchronization. Due to the AFC operation, the grid current THD has been achieved within the limit specified by international standards. The developed strategy utilizes hybrid sources such as the utility grid and solar PV system to enhance the reliability of the system. Additionally, in the absence of grid power, the on-board solar PV array successfully charges the battery under varying irradiance conditions, with waveforms confirming the effectiveness of the solar-based charging system. Finally, the control of the BLDC motor is validated through simulation and experimental waveforms, highlighting the system's overall improved performance. The developed system has soft-starting features of BLDC drive in propulsion mode without using any current and voltage sensors at the motor side. The developed systems

has been verified by simulation and real-time OPAL-RT testing. It offers several advantages over existing designs, including bidirectional capability, a reduced number of components, lower conduction losses, improved efficiency, and a shorter payback time.

CHAPTER-6

SOLAR POWERED ON-BOARD LEV UTILIZING ISOLATED HIGH-GAIN CONVERTER WITH G2V AND V2G CAPABILITIES

6.1 General

Fossil fuel-powered cars began to dampen the market due to factors like high prices, high pollution, and concerns about fossil fuel reliance, which directly accelerate the transportation industry towards electric vehicles (EVs) [1]. EVs have come a long way from their early days as niche inventions to becoming a critical part of the future of road vehicles. The advancements in performance of connected grid-side electrical equipment, as well as the battery life, mainly rely on the EV charging strategies.

These strategies must have one-stage charging, two-stage charging, and on/off-board charging. Furthermore, these strategies consist of non-isolated, isolated, bridgeless, and interleaved EV charging strategies. Additionally, the power factor (PFC) correction in compliance with charging standards is a key focus in optimizing the charging process [2]. Basically, the light electric vehicles (LEVs) use more on-board chargers than off-board chargers for vehicle charging. These on-board charging strategies have benefits such as lower initial costs, allowing EVs to charge from any standard electrical outlet or public charging station, space/weight saving portability (i.e., do not have any requirement to carry additional charging devices when traveling), improved charging control, and good safety [3].

The bidirectional strategy offers benefits like drawing power from the grid to charge the battery as well as sending power back from the battery to the grid or load. Bidirectional strategy also offers advanced energy management systems that guarantee efficient charging and discharging processes [4]. So, the strategic use of energy cycles can help to keep battery health over time.

Typically, isolated on-board battery chargers (OBCs) use a DC-to-DC converter with galvanic separation after an AC-to-DC converter. In the first stage, the solutions active front-end (AFC) converter, front-end AC-to-DC conversion is essential. Traditional front-end converters feature an AC-DC conversion, corrected power factor, and low THD. Essentialities like power factor correction (PFC), improved output voltage regulation, and a decrease in input current harmonics must be met by an AFC [5]. PFC-based AFC, an essential part of an EV charger, makes it easier to obtain an efficient regulated DC voltage.

Converter strategies are widely used in the DC-to-DC converters for on-board LEVs battery charging. These strategies convert DC-to-DC with a PI controller and then allow a suitable current for battery charging. However, this strategy introduces issues, including high CM noise, limited voltage step-down capability, poor current shaping, and worrisome amounts of losses. The advancements in performance of connected grid-side electrical equipment, as well as the battery life, mainly rely on the EV charging strategies [6].

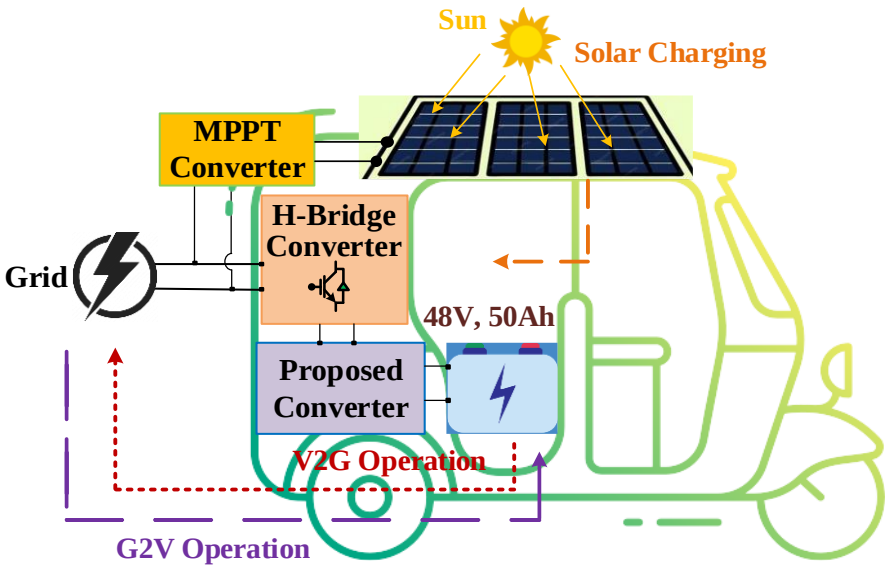

Figure 6.1. Schematic of the developed on-board grid-integrated solar-powered LEV utilizing an isolated integrated converter.

Isolated buck-boost strategies using zeta and SEPIC converters are not able to improve PF at the input of the battery charger, due to disadvantages such as discontinuous input and output current, accordingly. It directly hams the life of the LEV's battery, or makes the ripples from the input side to couple with the outputs [7]. So, the use of an isolated Cuk converter helps to be free from these disadvantages, as well as its inherent advantages, such as low ripples at the input and output [8]. Therefore, an isolated converter strategy with high-gain bidirectional Cuk converter with grid-to-vehicle (G2V) and vehicle-to-grid (V2G) capability, referred in this work. The charging of a 48V, 50Ah light EV battery is proposed in CC-CV (constant current and constant voltage) mode using a proportional-integral (PI controller). This strategy offers pros like a lower part count than other similar converter strategies, such as SEPIC, Zeta, Luo, and CSC [9].

An isolated integrated converter (IIC) with modified MPPT control-based solar array OBC for a brushless DC motor-driven light EVs is discussed in this work, as shown in Figure 6.1. IEEE/IEC criteria of maintaining THD are successfully met using the AFC converter with IMSTOGI control. The next control is the DC-to-DC CC/CV mode for IIC. It plays a role in

success, lessening the fluctuations in the charging/discharging operation. The buck converter with modified MPPT control charged the light EV's battery successfully, without using the grid. After the charging of the battery, the next operation is the run of the brushless DC motor via a voltage source converter (VSC) with a controller.

The main focus of the proposed work is on smart control to manage both bi-directional high-gain modes (i.e., G2V and V2G) as well as on-board solar-based charging during grid outage. Also, it focuses on reducing the number of overall drive train elements and efficiently work on the power management of all operational modes. The proposed strategy includes the following features and advantages,

- An isolated integrated converter (IIC) based high-gain strategy with bidirectional power flow features is designed for light EVs to incorporate G2V and V2G operations.
- The developed IIC converter with isolated bidirectional features has reduced the total number of components to improve efficiency, compact size, and increased reliability.
- The proposed IIC configuration also offers a high payback time, lowers stress on semiconductor devices, and passive components.
- The proposed charging strategy manages the battery charging process, as an onboard solar PV-powered array with improved MPPT control algorithms.
- The proposed charging strategy ensures less burden on the grid due to the availability of an alternate source, viz., solar PV.
- The proposed strategy also introduces a brushless DC drive system for propulsion and a regenerative mode of operation.

6.2 Configuration of Solar-Powered On-Board Light Electric Vehicle Using Integrated Isolated Converter

Figure 6.2 shows the schematic of an isolated integrated converter with dual power sources (i.e., single-phase grid and solar PV), employing a BLDC (brushless DC) motor drive. It consists of an AFC converter/reactifier, which provides 400 V regulated DC voltage as well as performs grid voltage and grid current power factor correction in both G2V and V2G operational modes. Further, the on-board solar panel of 800 W peak-power-capacity with a buck converter incorporates the modified drift-free P& O control strategy to optimize the solar PV panel performance. The PV panel gives an MPPT constant voltage during a change in irradiance conditions. A 750 W, 48V BLDC motor drive is used as a propulsion motor for the electric LEV. The bi-directional high-gain converter can meet G2V and V2G performance with

AFC and battery charging during grid outage with an on-board solar PV panel. The system can use both grid as well as solar energy to charge the LEV battery, and if necessary, it can operate in regenerative mode with two switches.

Figure 6.2. Circuit of Proposed Isolated Integrated Converter LEV Charging.

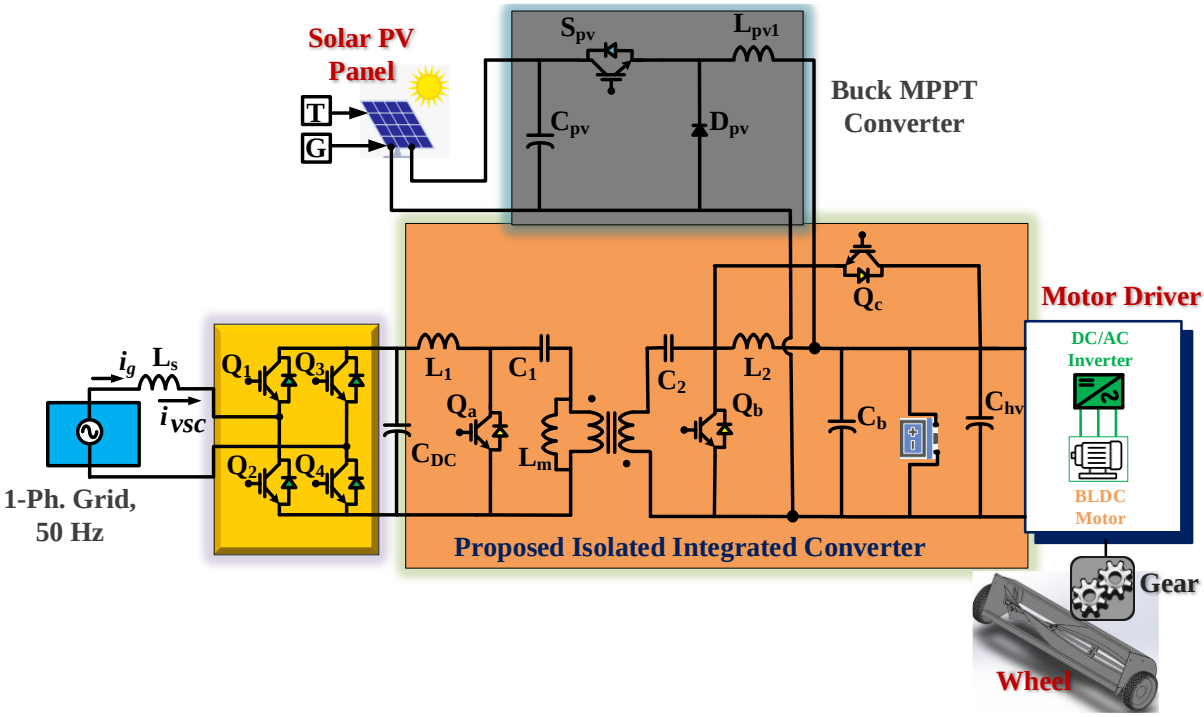

6.3 Modes of Operation of Solar-Powered On-Board Light Electric Vehicle Using Integrated Isolated Converter

13 The developed IIC perform both in grid-to-vehicle (G2V) and vehicle-to-grid (V2G) modes of operation as well as solar PV MPPT converters-based LEV charging as below,

6.3.1 Grid-to-Vehicle (Charging)

Mode I : In Figure 6.3(a-b), the circuit diagram of basic operations of G2V mode are shown. During this mode, switch $\boldsymbol{Q_a}$ is active, while others remain inactive. The input inductor $\boldsymbol{L_1}$starts storing energy, which results in a linear increase in current through it as shown by the dotted line in Figure 6.3(a). The discharging energy of the primary side capacitor $\boldsymbol{C_1}$ is converted into

122 the magnetizing inductance of the primary winding of the HFT. The voltage through the capacitor $\boldsymbol{C_1}$ start decaying as shown by the dotted line in Figure 6.3(a). Similarly, the capacitor

73 $\boldsymbol{C_2}$ connected at the secondary side of the HFT discharges to the inductor $\boldsymbol{L_2}$ as shown by the dotted line in Fig. 4 (a).

Mode II : During this mode, switch $\boldsymbol{Q_a}$ is set low, and diode $\boldsymbol{D_b}$ active. The discharging linearly as shown by the dotted line in Figure 6.3(b), and the capacitors $\boldsymbol{C_1}$ and $\boldsymbol{C_2}$ at the primary and

secondary sides primary and secondary side of HFT operate in charging mode. Concerently, the capacitor $\boldsymbol{C_{bat}}$ connected at LEV battery side, supplies power to the LEV battery. Form the circuit Figure 6.3(a-b) following equations (6.1)- (6.6) are observed,

$$\boldsymbol{v_{L1}} = \boldsymbol{L_1}\left(\frac{\boldsymbol{di_{L1}}}{\boldsymbol{dt}}\right) + \boldsymbol{G}\left(\frac{\boldsymbol{di_{L2}}}{\boldsymbol{dt}}\right) = \boldsymbol{v_{DC}} \tag{6.1}$$

$$\boldsymbol{G} = \boldsymbol{n}\sqrt{\boldsymbol{L_1}\boldsymbol{L_2}} \tag{6.2}$$

$$\boldsymbol{v_{Lm}} = \boldsymbol{L_m}\left(\frac{\boldsymbol{di_{Lm}}}{\boldsymbol{dt}}\right) = -\boldsymbol{v_{C1}} \tag{6.3}$$

$$\boldsymbol{i_{C1}} = \boldsymbol{C_1}\left(\frac{\boldsymbol{dv_{C1}}}{\boldsymbol{dt}}\right) = \boldsymbol{i_{Lm}} - \left(\frac{\boldsymbol{i_2}}{\boldsymbol{k}}\right) \tag{6.4}$$

$$\boldsymbol{i_{C2}} = \boldsymbol{C_2}\left(\frac{\boldsymbol{dv_{C2}}}{\boldsymbol{dt}}\right) = \boldsymbol{i_{L2}} \tag{6.5}$$

$$v_{L2} = L_2\left(\frac{di_{L2}}{dt}\right) + G\left(\frac{di_{L1}}{dt}\right) = \left(\left(\frac{v_{c1}}{k}\right) - v_{bat} - v_{C2}\right) \tag{6.6}$$

Here, k is the HFT turn ratio, v_{bat} is the battery side capacitor, v_{L1} is voltage of inductor at primary side, v_{L2} is voltage of inductor at secondary side, i_{C1} and i_{C2} is the current of capacitors, v_{Lm} is magnetizing inductance voltage, and G is the mutual inductor with n coupling coefficients.

6.3.2 Vehicle-to-Grid (Discharging)

Mode I : In Figure 6.4(a-b), the circuit diagram of basic operations of V2G mode are shown. During this mode, switch $\boldsymbol{Q_b}$ is active, while others remain inactive. The input inductor $\boldsymbol{L_2}$ starts storing energy, which results in a linear increase in current through it as shown by the dotted line in Figure 6.4 (a). The discharging energy of the secondary side capacitor $\boldsymbol{C_2}$ is converted into the magnetizing inductance of the secondary winding of the HFT. The voltage through capacitor $\boldsymbol{C_2}$ start decaying as shown by the dotted line in Figure 6.4(a). Similarly, the capacitor $\boldsymbol{C_1}$ connected at primary side of the HFT discharges to inductor $\boldsymbol{L_1}$ as shown by dotted line in Fig. 6.4(a).

Mode II : During this mode, switch $\boldsymbol{Q_b}$ is set low, and the diode $\boldsymbol{D_a}$ active. The input inductor $\boldsymbol{L_2}$ starts discharging linearly as shown by the dotted line in Figure 6.4(b), and the capacitor $\boldsymbol{C_2}$ and $\boldsymbol{C_1}$. The secondary and primary sides of HFT operate in charging mode but in reverse polarity. Consequently, the capacitor $\boldsymbol{C_{DC}}$ connected at the grid side, supplies power to the grid.

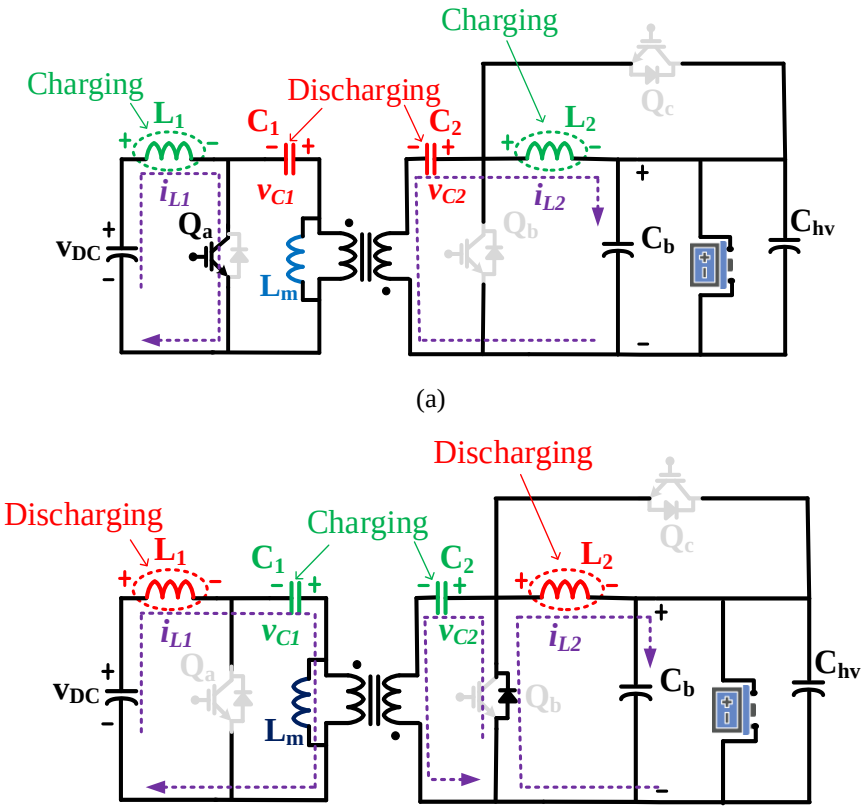

Figure 6.3. Modes of Proposed Isolated Integrated Converter: (a) When is Q_a on, (b) When is Q_a off.

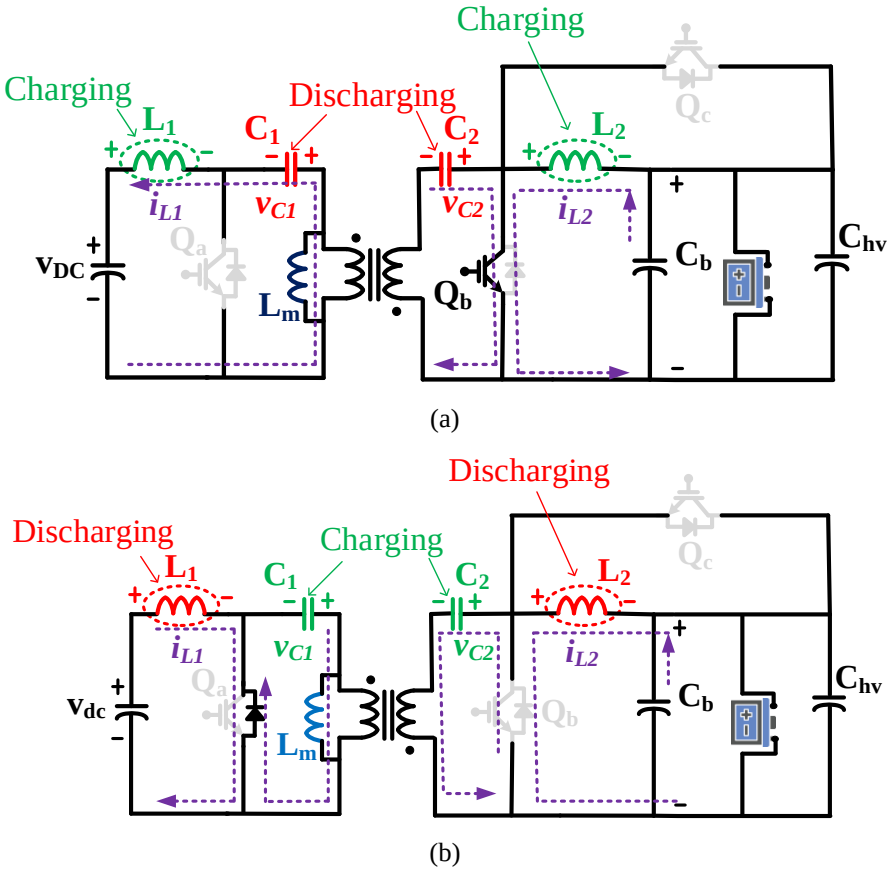

Figure 6.4. Modes of Proposed Isolated Integrated Converter: (a) When is Q_b on, (b) When is Q_b off.

From the circuit Figure 6.4(a-b), following equations of V2G mode are given below (6.7)-(6.8),

$$v_{L2} = L_2\left(\frac{di_{L2}}{dt}\right) + G\left(\frac{di_{L1}}{dt}\right) = -v_{bat} \tag{6.7}$$

$$v_{L1} = L_1\left(\frac{di_{L1}}{dt}\right) + G\left(\frac{di_{L2}}{dt}\right) = -(v_{C1} + v_{Lm} + v_{DC}) \tag{6.8}$$

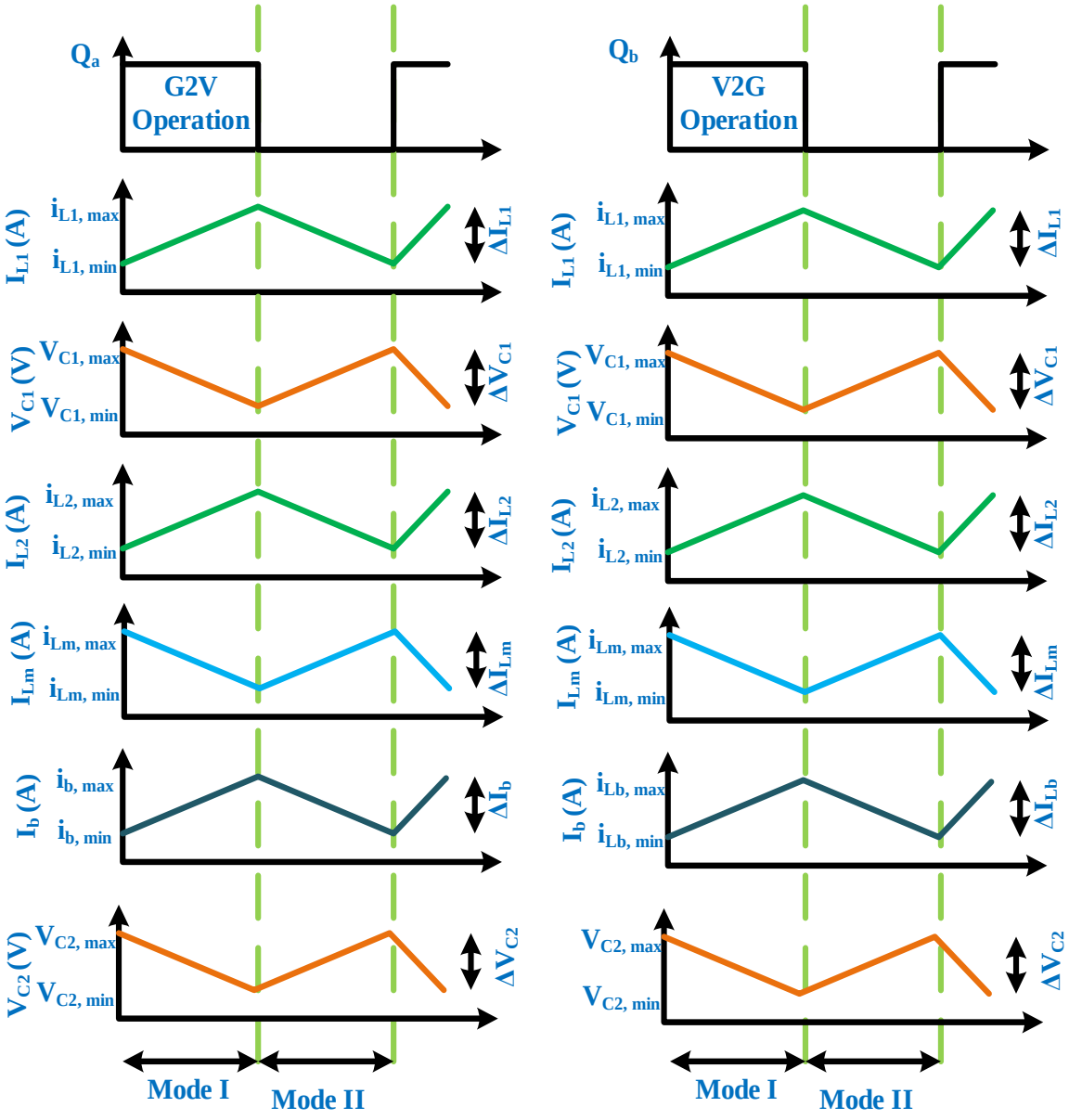

Figure 6.5. Electrical waveforms of the switching cycle for the isolated integrated converter, (a) G2V mode (Charging), and (b) V2G mode (Discharging).

6.3.3 Solar PV-based on-board charging

In this operational mode, the switch $\boldsymbol{Q_{pv}}$ remains active to facilitate the charging of the Light Electric Vehicle (LEV) battery packs during a power outage from the main grid. During such conditions, the photovoltaic (PV) array serves as the primary power source. The energy

harvested from the solar panels is routed through a buck-type Maximum Power Point Tracking (MPPT) converter, which ensures that the PV system operates at its optimal power point to maximize efficiency. As illustrated in Figure 6.6, this MPPT-controlled buck converter steps down the voltage from the solar panels to a suitable level required for charging the LEV battery packs. This arrangement not only ensures a reliable backup charging solution but also enhances the energy utilization from renewable sources during grid failure scenarios.

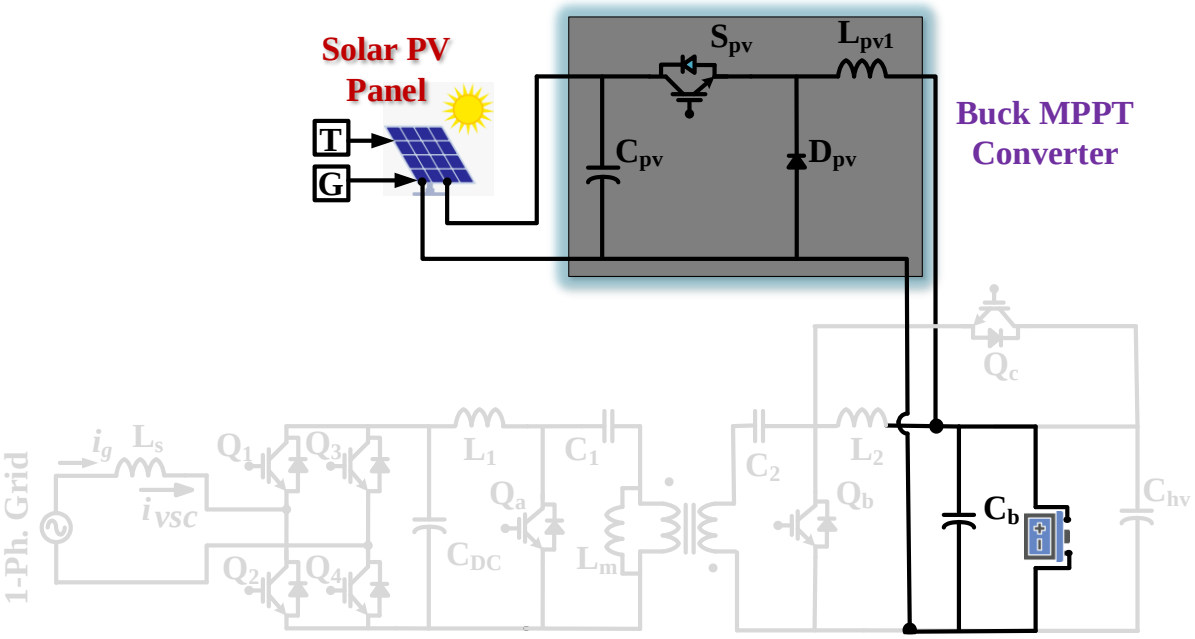

Figure 6.6. Schematic of on-board Solar PV-based Charging.

6.3.4 Regenerative mode

The LEV battery, which is charged through the grid and via an on-board solar PV panel, supplies power to the propulsion motor. In Figure 6.7(a-b), the circuit diagram shows two possible sub-modes. When the switch Q_b is active, the proposed high-gain converter basically acts as a boost converter. The input inductor L_2 starts storing energy, which results in a linear increase in current through it as shown by the blue dotted line in Figure 6.7(a). Further switch Q_b is set low, the output inductor L_2 starts releasing its stored energy to the DC-link capacitor C_{hv} via diode D_c as shown in Figure 6.7(a). The next sub-mode is activated during a grid outage or a disturbed weather condition. In this sub-mode switch Q_c is active while Q_b is inactive, the proposed high-gain converter is operating in regen mode. Although the regen mode is typically not used in the proposed system, it has been considered for potential future strategies. The output inductor L_2 is charged by regen via dc-link, and current flow through it as shown by blue dotted line in Figure 6.7(b). In this sub-mode the high-gain converter works as a buck converter and facilitates power from motor to the LEV battery.

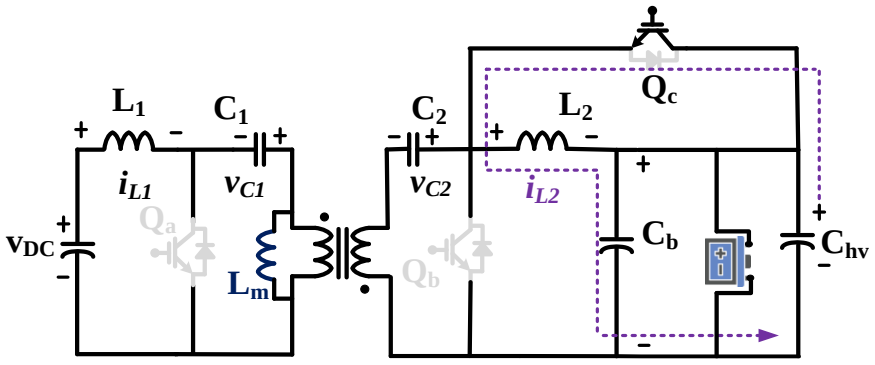

(a)

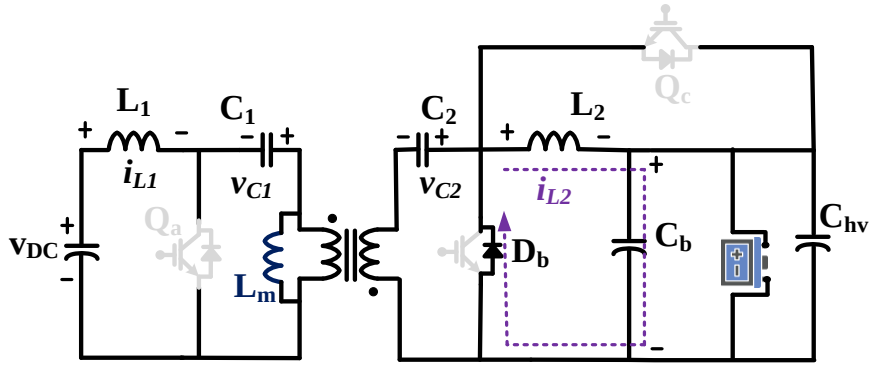

(b)

Figure 6.7. Converter operation in regen mode: (a) When is Q_c on, (b) When is Q_c off.

6.4 Designing of Solar Powered On-board LEV Utilizing Isolated Integrated High Gain Converter with G2V and V2G Capabilities

Designing the passive components for the AFC and the proposed bidirectional high-gain converter is a complex task, as some components operate in multiple modes. The switching frequency of 20 kHz is used for both G2V & V2G operations. Selecting the appropriate values of each component, the final design is proposed for 48V, 50 Ah battery in context, the following equations are calculated as (6.9)-(6.17),

6.4.1 Design of Active Front-End Converter

The inductor L_s and capaciotor C_{DC} used in AFC acts as a filter in grid current as well as DC voltage regulation is calculated as,

$$d_1(t) = \frac{2v_{bat}}{2v_{bat}+v_{DC}} = 0.80 \quad (6.9)$$

$$L_s = \frac{d_1(t)v_{DC}}{f_{sw}\Delta i_{Ls}} = 2.03\ mH \quad (6.10)$$

$$C_{DC} = \frac{P/v_{DC}}{2\omega\Delta v_{DC}} = 1244.01\ \mu F \quad (6.11)$$

Here $d_1(t)$ is the duty ratio, f_{sw} is the switching frequency of the converter, v_{DC} is the DC-link voltage of AFC, and v_{bat} is the voltage of the battery.

6.4.2 Design of Isolated Integrated DC-DC Converter

The inductor $\boldsymbol{L_1}$ and output inductor $\boldsymbol{L_2}$ used in an isolated bidirectional high-gain converter for LEV battery charging, discharging, propulsion, and regen mode is calculated as,

$$L_1 = \frac{d_1(t).v_{DC}}{(1+\alpha)f_{sw}\Delta i_{L1}} = 2.75\ mH \quad (6.12)$$

$$L_2 = \frac{d_1(t).v_{DC}}{(1+\beta)f_{sw}\Delta i_{L1}} = 2.75\ mH \quad (6.13)$$

where α and β are the coefficients respectively.

$$L_m = \frac{d_1(t).v_{DC}}{f_{sw}\Delta i_{Lm}} = 1.34\ mH \quad (6.14)$$

The energy transfer capacitors C_1 and C_2 are designed for allowable voltage ripple content, Δi_{C_1} and Δi_{C_2} as follows,

$$C_1 = \frac{P/v_{DC}(1-d_1(t))}{f_{sw}\Delta i_{C_1}} = 3.51\ \mu F \quad (6.15)$$

$$C_2 = \frac{P/v_{bat}.d_1(t)}{f_{sw}\Delta i_{C_2}} = 3.51\ \mu F \quad (6.16)$$

where P is the peak power, respectively.

$$C_{bat} = \frac{i_{bat}}{4\pi f_{sw}\Delta v_{bat}} = 1375.34\ \mu F \quad (6.17)$$

The selected value for L_s,$C_{DC,}$ L_1, L_2, C_1 , C_2, L_m and C_{bat} is shown in Table 6.1.

Table 6.1. Selected Parameters during G2V and V2G.

Parameter	Value
Grid voltage (V_g)	230 V_{rms}
Regulated (V_{DC})	400 V_{dc}
Frequency (f)	50 Hz
Battery Pack (V_b)	48V
SOC (G2V/V2G)	20%/85%
L_s/C_1 /L_1/C_2 /L_2/L_m	3mH/4mH/3mH/4mH/3mH/3mH
C_{dc}/C_o	1500 µF/1500 µF

Table 6.2. Selected Parameters during on-board Solar PV Charging.

Parameter	Value
Selected full power	800 W
Total Cell	36

Open circuit, $V_{o.c}$	21.3 V
Short circuit, $I_{s.c}$	6.6 A
Strings in series, N_s	3
Strings in parallel, N_p	3
MPP of voltage, V_{mpp}	13.55 V
MPP of current, I_{mpp}	16.83
Irradiance	1000

6.5 Control of Solar-Powered On-Board Light Electric Vehicle Using Integrated Isolated Converter

This section presents the effective implementation of appropriate controllers for the proposed system, along with the power management strategy for coordinating different sources under various operating modes. The detailed operation of the controller design is explained below,

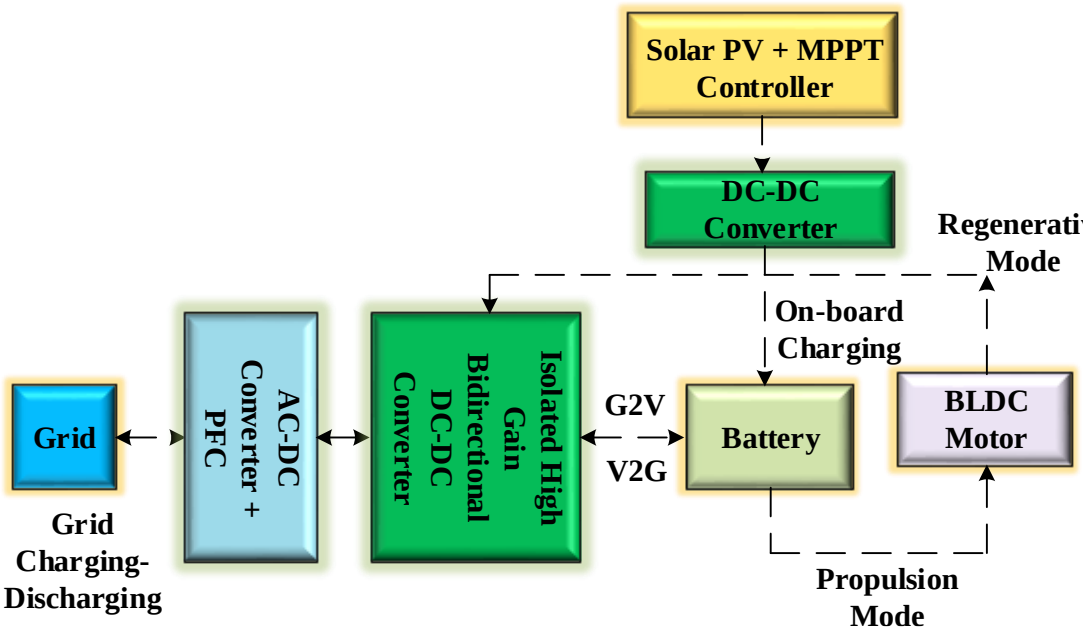

Figure 6.8. Power Management architecture for the proposed system.

6.5.1 *Power Management of Developed Integrated Isolated Converter*

The power management strategy presented in this paper aims to operate the grid, solar PV, and LEV battery pack within their optimal operating ranges as shown by Figure 6.8. During unfavorable weather conditions or when solar power is unavailable, the required power for charging the battery and powering the propulsion motors is supplied by the grid. In the event

of a grid outage, the solar PV system powers the battery. The core principle of the energy management strategy is to ensure the energy demand is met efficiently to enable reliable LEV charging and discharging. The LEV battery is charged either from the grid or the on-board solar PV system, after which it supplies power to the propulsion motors.

6.5.2 *Control of Active Front End Converter*

At the initial stage of the process, the AFC equipped with the IMSTOGI filter manages the grid current's power quality (PQ) in compliance with IEEE standard guidelines, as shown in Figure 6.9. The equations (6.18)-(6.22) are used to maintain the DC-link voltage at a defined reference value,

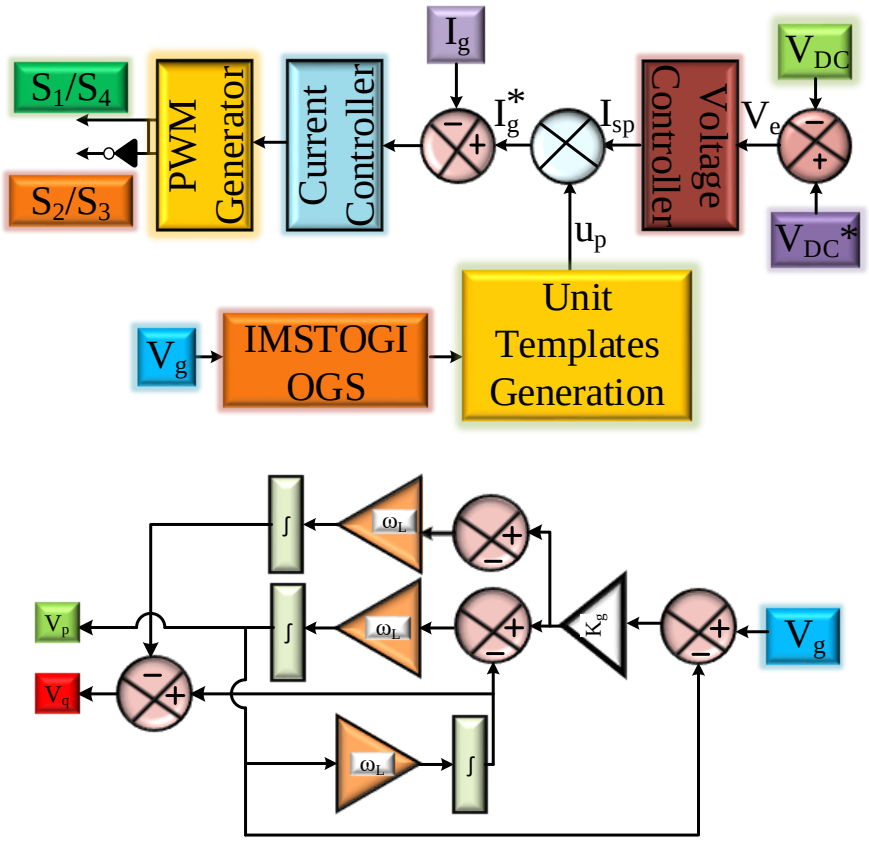

Figure 6.9. Control of AFC with IMSOTGI-based OSG method.

$$V_{err}(x) = V^{*}_{dc}(x) - V_{dc}(x) \quad (6.18)$$

$$I_{sp}(x) = I_{sp}(x-1) + k_{pc} * \{V_e(x) - V_e(x-1)\} + k_{ic} * V_e(x) \quad (6.19)$$

$$I_{sq} = (2 * Q_{ref}) / V_{time} \quad (6.20)$$

$$V_{time} = \sqrt{v_q^2 + v_p^2},\ u_p = v_p / V_{time},\ and\ u_q = v_q / V_{time} \quad (6.21)$$

$$i_{sp}(time) = I_{sq} * u_q,\ i_{sp}(time) = I_{sp} * u_p \quad (6.22)$$

From the estimation of the above equations, the IMSTOGI controller will be able to map the decided reference value of the DC-link throughout the process. This controller successfully

maintains UPF between grid voltage and current at both G2V and V2G modes.

6.5.3 *Control for IIC with CC/CV*

Notably, the IIC controller aims to keep the current coming for charging as per the applicable standard throughout the battery charging/discharging operation. CC/CV controller referred in Figure 6.10, then compute the voltage and current for the battery charging/discharging operation. Further, the PWM pulses successfully activate/deactivate switches. The equations (6.23)-(6.29) below confirm the satisfactory operation of the system.

$$i_s^*(time) = i_{sp}(time) + i_{sp}(time) \quad (6.23)$$

$$I_{er}(k) = I_{bat}^*(k) - I_{bat}(k) \quad (6.24)$$

$$d_c(n) = d_c(k\text{-}1) + g_{pc} * \{I_{er}(k) - I_{er}(k\text{-}1)\} + g_{ic} * I_{er}(k) \quad (6.25)$$

$$V_{er}(k) = V_{bat}^*(k) - V_{bat}(k) \quad (6.26)$$

$$d_v(k) = d_v(k\text{-}1) + q_{pc} * \{V_{er}(k) - V_{er}(k\text{-}1)\} + q_{ic} * V_{er}(k) \quad (6.27)$$

$$v_{Err,b}(x) = v_{ref}(x) - v_b(t_x - 1) \quad (6.28)$$

$$I_{Err,b}(x) = I_{ref}(x) - I_b(t_x - 1) \quad (6.29)$$

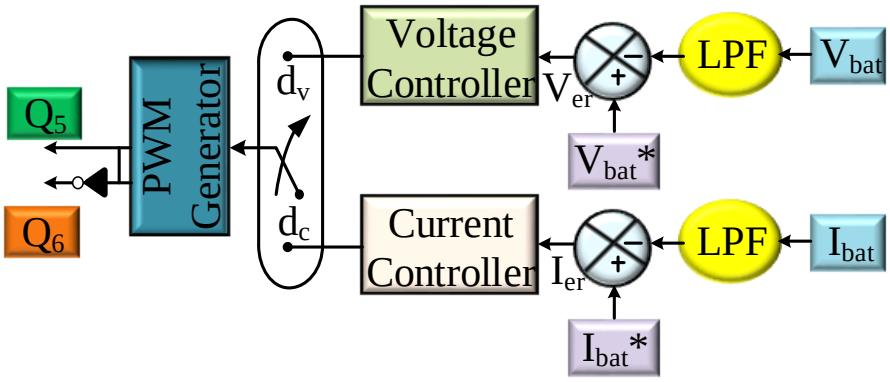

Figure 6.10. Control of an integrated isolated converter.

6.5.4 *MPPT Control for Solar PV Converter*

As the proposed system features a two-stage processing structure for on-board solar PV integration, a buck converter is used along with a modified, drift-free Perturb and Observe (P&O) MPPT algorithm to ensure efficient power delivery to the LEV battery under varying environmental conditions, as illustrated in Figure 6.11.

6.5.5 Control for Brushless DC Motor

Figure 6.12 illustrates the control of a brushless DC Motor for regulating speed and torque based on driver input, such as throttle position or vehicle load demand. The controller ensures efficient energy usage from the LEV battery while maintaining smooth and reliable motor operation. Here, the controller aims to maintain a stable HV-link voltage, which is crucial for

ensuring smooth vehicle operation.

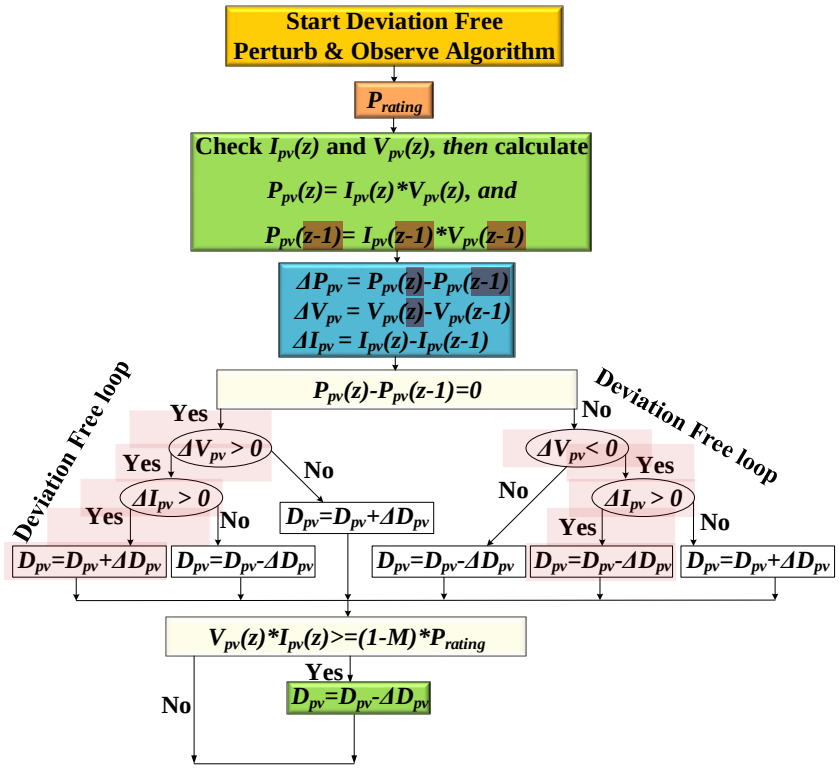

Figure 6.11. Flow chat of MPPT with modified P&O technique.

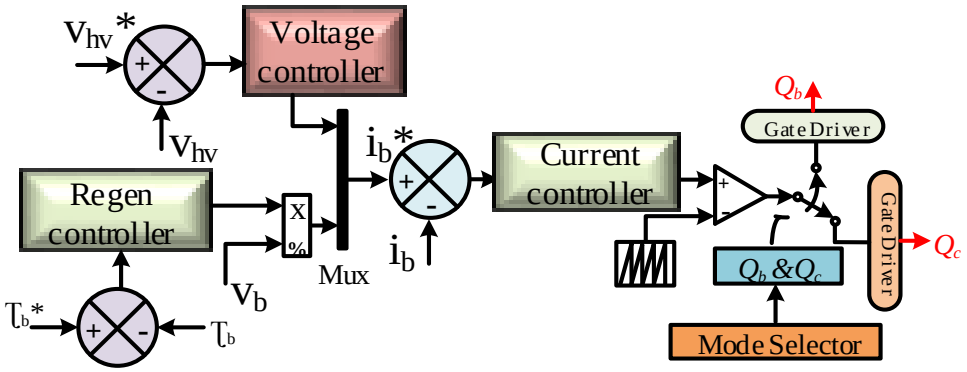

Figure 6.12. Control of the BLDC motor in propulsion and regenerative mode.

The resulting error is processed by the voltage control loop**,** which generates a reference signal for the battery discharge current. This reference current is then compared to the actual battery current, and the resulting error is passed through the current controller. Further, the coming signal from the driver gate is applied to the converter switch Q_b, thereby regulating power flow from the battery during propulsion. In regenerative braking mode, the controller operates differently. Here, the reference input is derived from the required braking torque. This torque is first converted into a corresponding charging power, which is then divided by the instantaneous battery voltage to compute the reference charging current. This current serves as the input for the current controller, ensuring accurate tracking and controlled battery charging

during braking. From Figure 6.12, the regenerative control strategy takes the braking torque command τb as the reference input to generate a corresponding reference charging current for the battery. Beyond this point, the control process closely resembles that of the propulsion mode, as shown in Figure 6.12. The regenerative controller itself consists of a basic PI controller, and the coming signal is used to drive the switch Q_c, enabling the converter to operate in buck-boost mode during energy recovery.

6.6 MATLAB-Based Modeling and Simulation of Solar-Powered On-Board Light Electric Vehicle Using Integrated Isolated Converter

The following models in Figure 6.13 shows the MATLAB based modeling and simulation of solar powered on-board charging system using integrated isolated converter. Model efficiently works on G2V and V2G modes, and on-board charge the LEV battery via solar PV MPPT converter. This charging strategies also run the BLDC motor drive system.

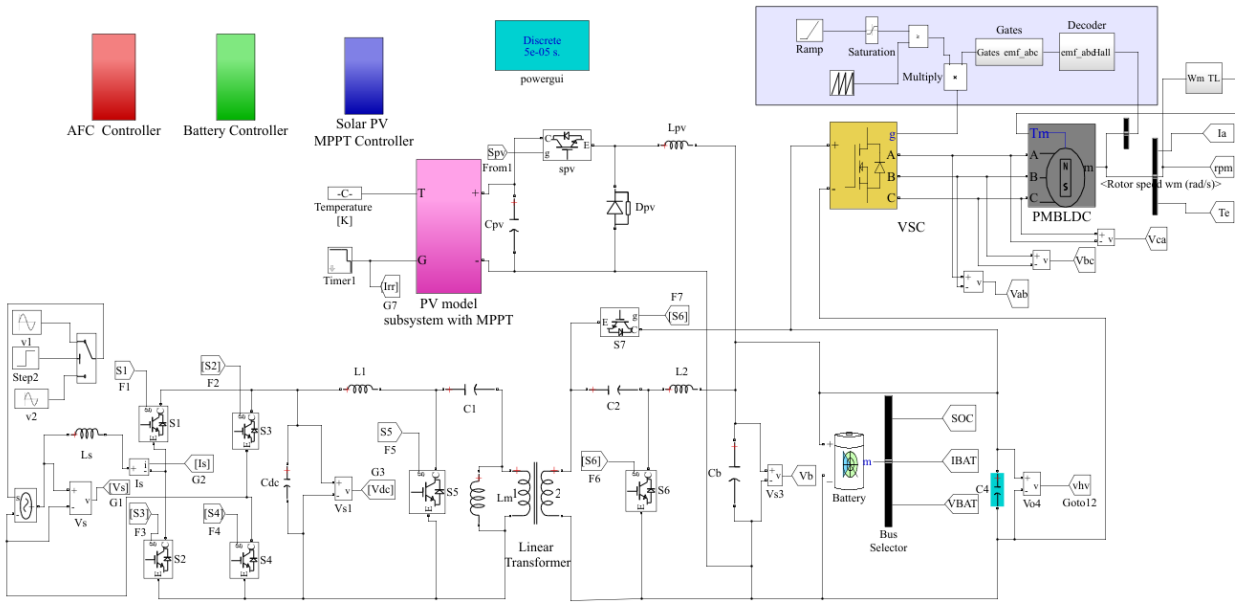

Figure 6.13. MATLAB-based modeling and simulation of solar-powered on-board charging system using an integrated isolated converter.

6.7 Results and Discussion

This section provides the performance of the developed system conducted for both simulation and in real-time to validate the effectiveness of the proposed system in all operational modes: G2V (charging), V2G (discharging), on-board solar PV-based charging, and propulsion mode as follows,

6.7.1 *Simulated Performance of Solar-Powered On-Board LEV Utilizing Isolated Integrated Converter*

In this section, the developed system is tested using the MATLAB/SIMULINK environment

to ensure optimal charging in both grid power supply and solar-powered conditions. The effectiveness of the developed charger is demonstrated via simulation results. Also, a simulation operation investigation of the BLDC motor is presented here. The operational performance of the developed system includes G2V (charging) and V2G (discharging) modes of operation, as depicted in Figures 6.14-6.29. The parameters like grid voltage (V_g) and grid current (I_g), power factor correction (PFC), distortion factor, state of charge (SOC), battery current (I_b), and battery voltage (V_b) are discussed by using the simulation results.

6.7.1.1 *Grid Based Charging Performance G2V or V2G under grid voltage sag condition*

In this operation, the performance of the IMSTOGI-based OSG control technique for both G2V and V2G is evaluated during grid voltage (V_g) sag up to 10% as depicted in Figure 6.14-6.15. As shown in Figure 6.14, a reduction in (V_g) during the sag condition is evaluated as an increase in (I_g) during G2V. As shown in Figure 6.15, an increase in (V_g) during the sag condition is evaluated as an increase in (I_g) in V2G mode. Moreover, IMSTOGI-based OSG control technique keeps regulated (V_{DC}) through both operations. Furthermore, the constant LEV battery charging in Figure 6.16 and discharging in Figure 6.17 shows the effectiveness of the developed system under sag condition. Figure 6.18 shows the low THD of (Ig) which is about 2.37% during sag at G2V. Similarly, 2.46 % of THD at V2G during sag condition in Figure 6.19.

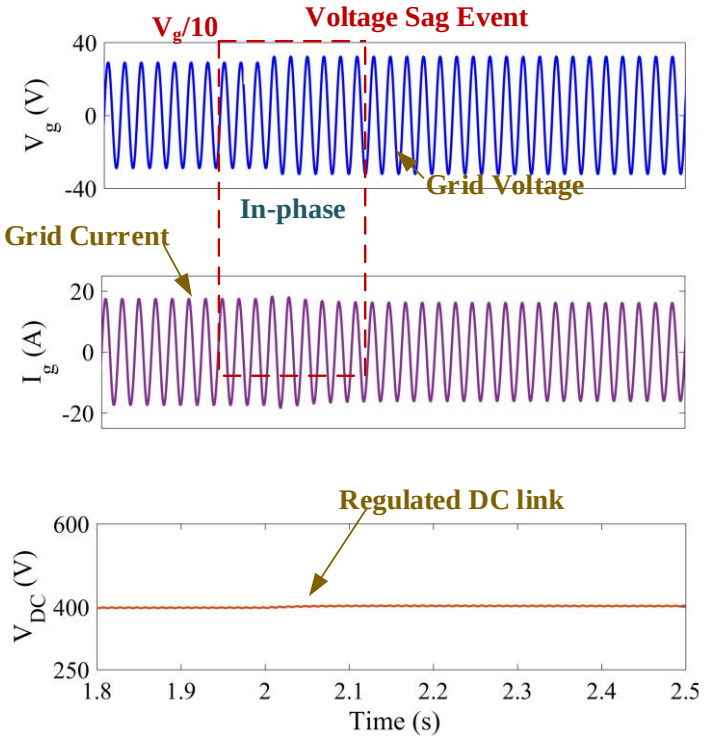

Figure 6.14. Simulated performance of G2V mode during voltage sag event (V_g, I_g, V_{DC}).

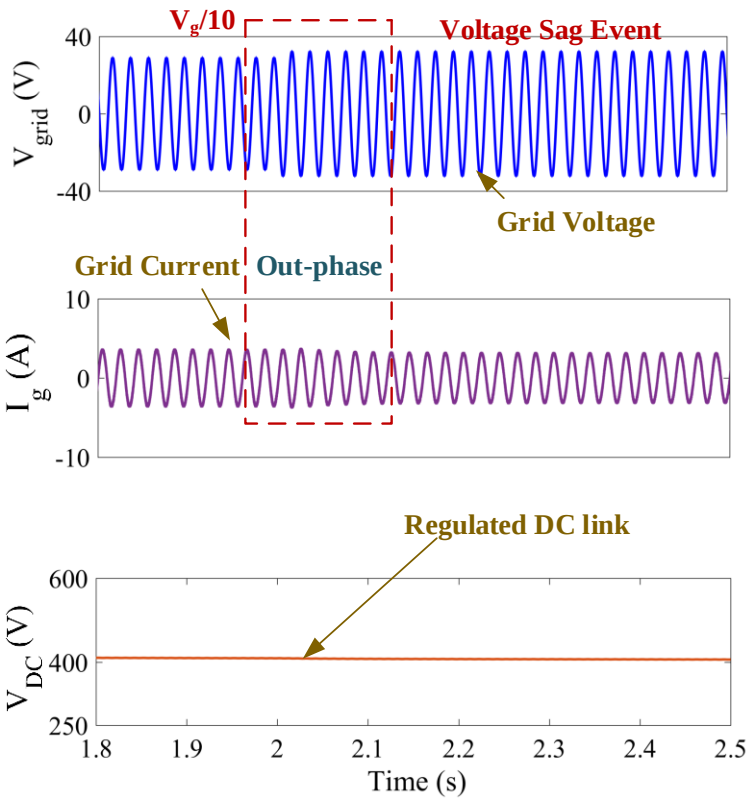

Figure 6.15. Simulated performance of V2G mode during voltage sag event (V_{grid}, I_g, V_{DC}).

24

6.7.1.2 *G2V or V2G under grid voltage swell condition*

In this operation, the performance of the IMSTOGI-based OSG control technique for both G2V and V2G is evaluated during grid voltage (V_g) sag and swell up to 10% as depicted in Figure 6.20 and Figure 6.21.

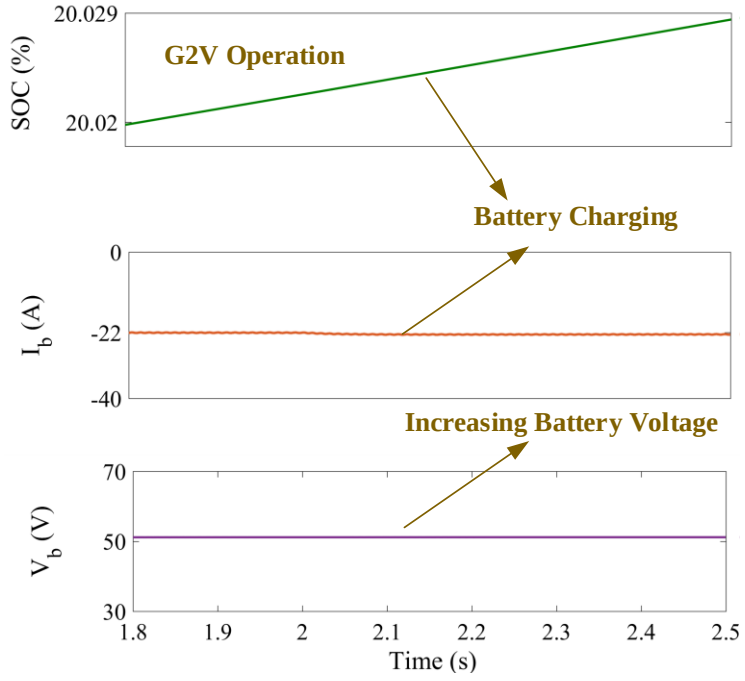

Figure 6.16. Simulated performance of LEV battery charging during a voltage sag event (SOC, I_b, V_b).

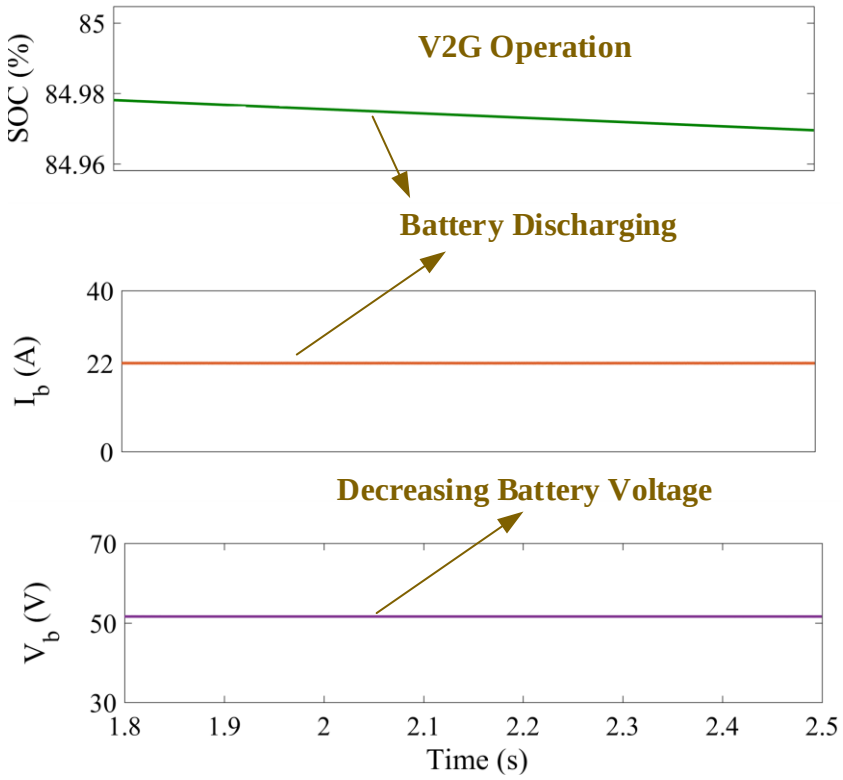

Figure 6.17. Simulated performance of LEV battery discharging during voltage sag event (SOC, I_g, V_b).

As shown in Figure 6.20, an increase in (V_g) during swell condition is evaluated as a decrease in (Ig) in G2V mode. As shown in Figure 6.21, an increase in (Vg) during swell conditions is evaluated as decrease in (Ig) in V2G mode.Moreover, IMSTOGI based OSG control technique keeps regulated (V_{DC}) through both operations.

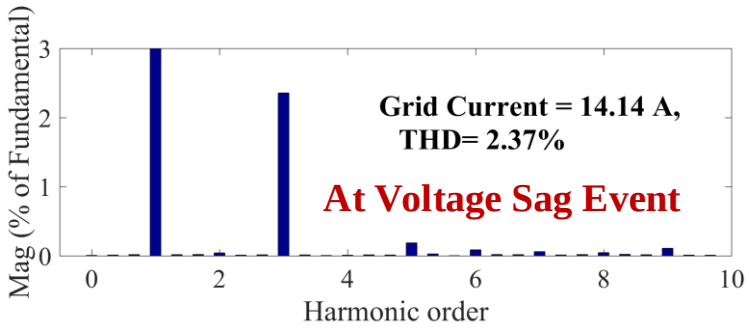

Figure 6.18. Simulated performance of G2V mode THD during voltage sag event.

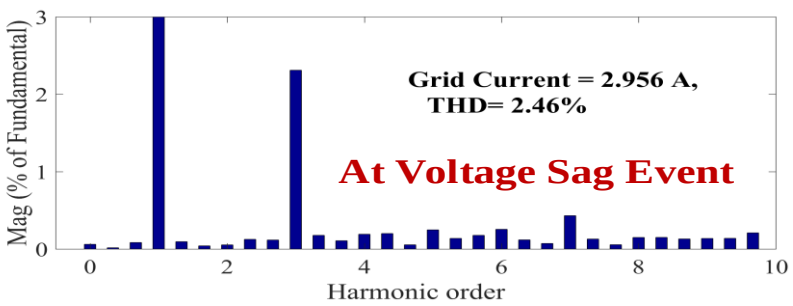

Figure 6.19. Simulated performance of V2G mode THD during voltage sag event.

78 Furthermore, the constant LEV battery charging in Figure 6.22 and discharging in Figure 6.23 shows the effectiveness of the developed system under swell condition. Figure 6.24 show the low THD of (Ig) which is about 1.58 % during swell at G2V. Similarly, 1.70 % of THD at V2G in Figure 6.25.

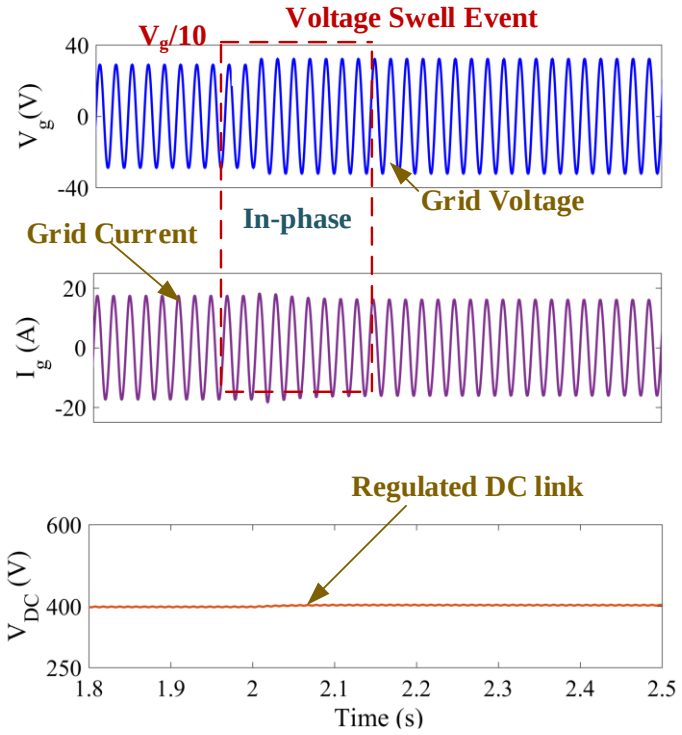

Figure 6.20. Simulated performance of G2V mode during voltage swell event (V_g, I_g, V_{DC}).

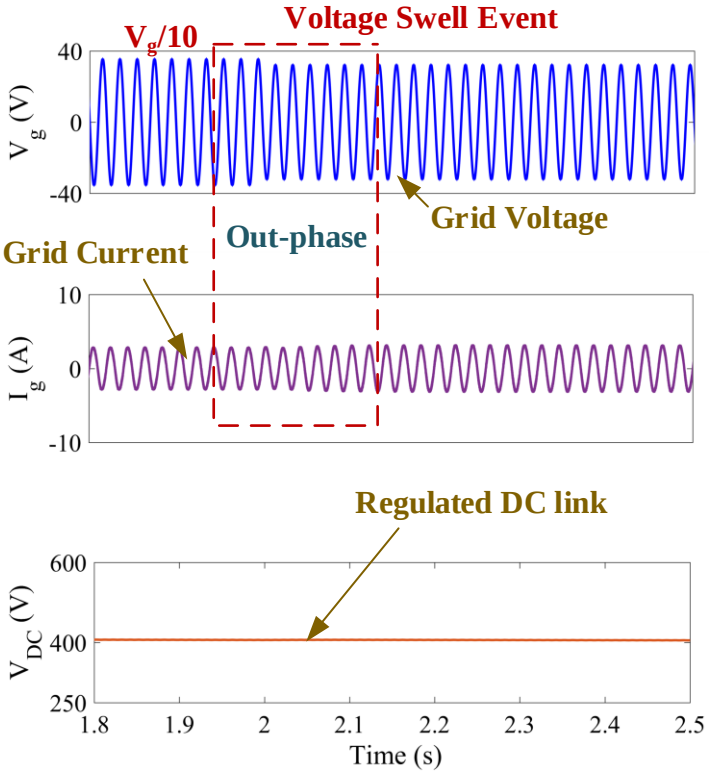

Figure 6.21. Simulated performance of V2G mode during voltage swell event (V_g, I_g, V_{DC}).

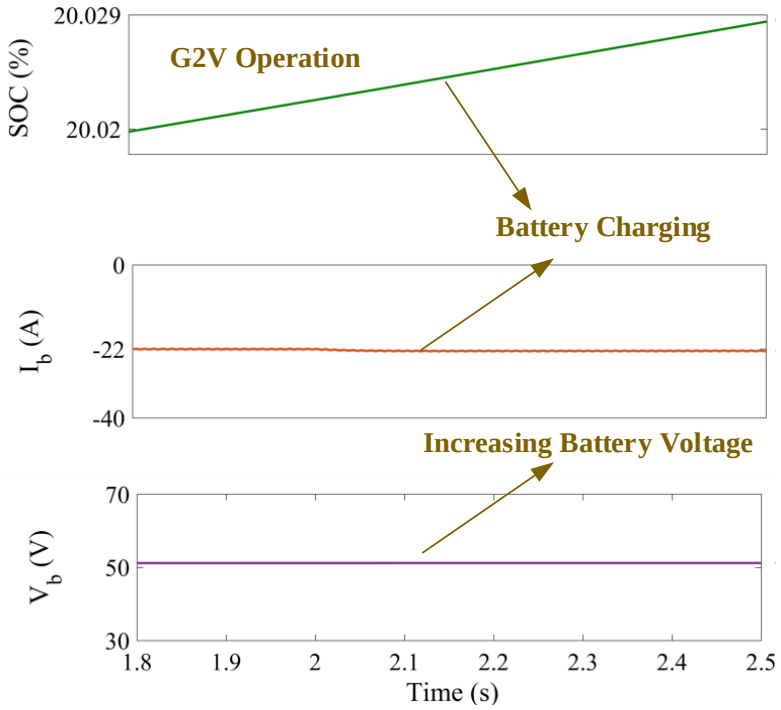

Figure 6.22. Simulated performance of LEV battery charging during voltage swell event $[SOC, I_b, V_b]$.

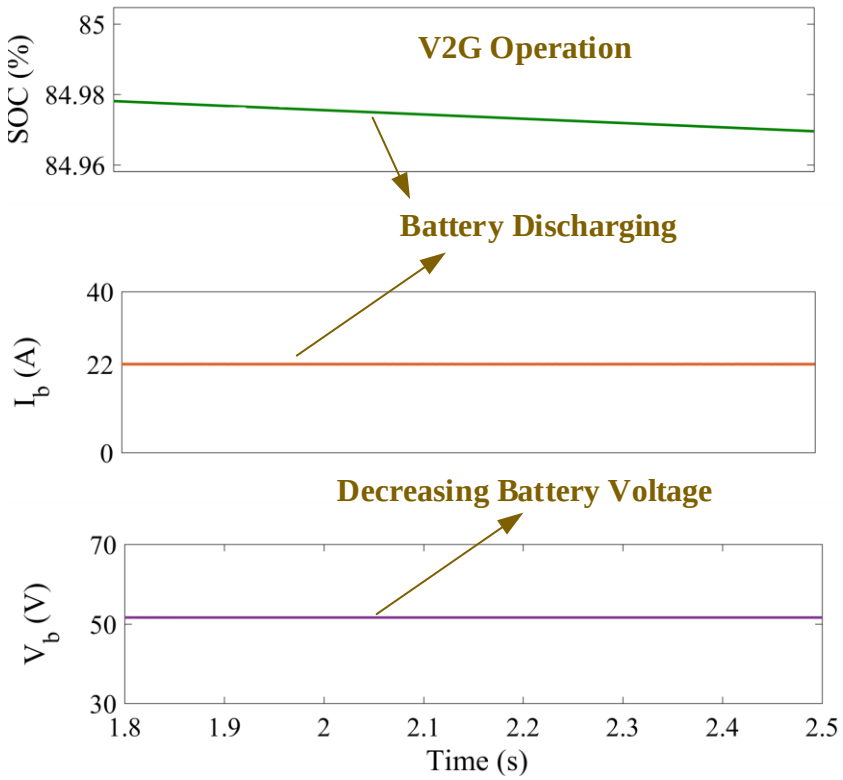

Figure 6.23. Simulated performance of LEV battery discharging during voltage swell event (SOC, I_b, V_b).

6.7.1.3 *Solar PV Based Charging Performance*

In this operation, the LEV battery system is connected directly to an solar powered source through MPPT converter. The on-board solar PV MPPT converter functions under solar

irradiation of (1000, 800, 1000) W/m². At this level of irradiation, the solar PV have maximum power output is 800 W. Figure 6.26 depicts change in irradiance implies no impact on PV voltage (V_{pv}), whereas PV current (I_{pv}), and battery current (I_b) show change.

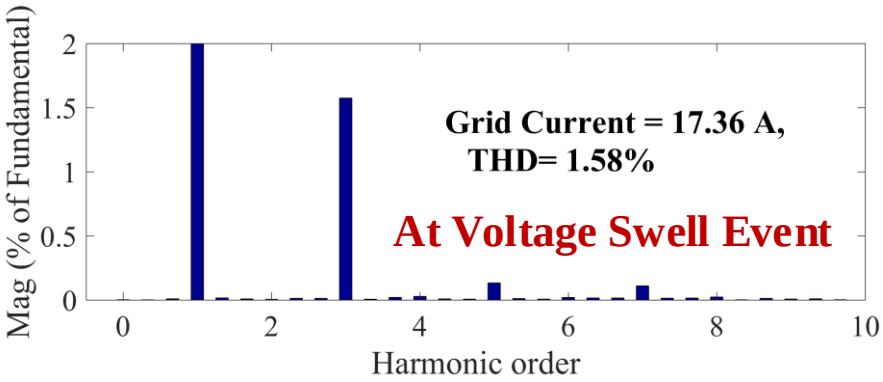

Figure 6.24. Simulated performance of G2V mode THD during voltage swell event.

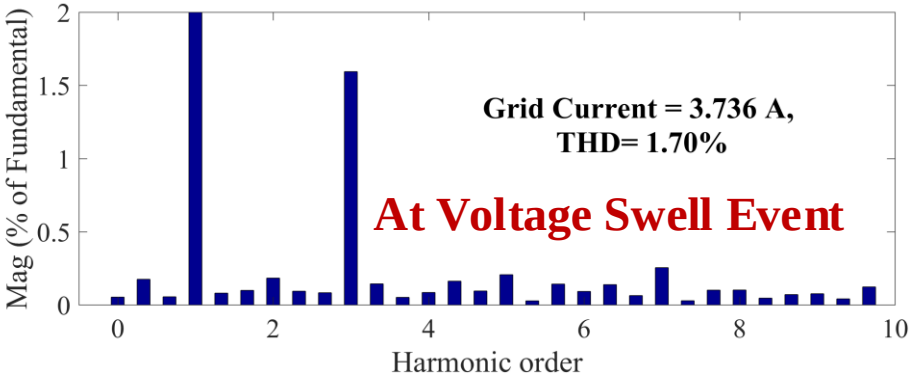

Figure 6.25. Simulated performance of V2G mode THD during voltage swell event.

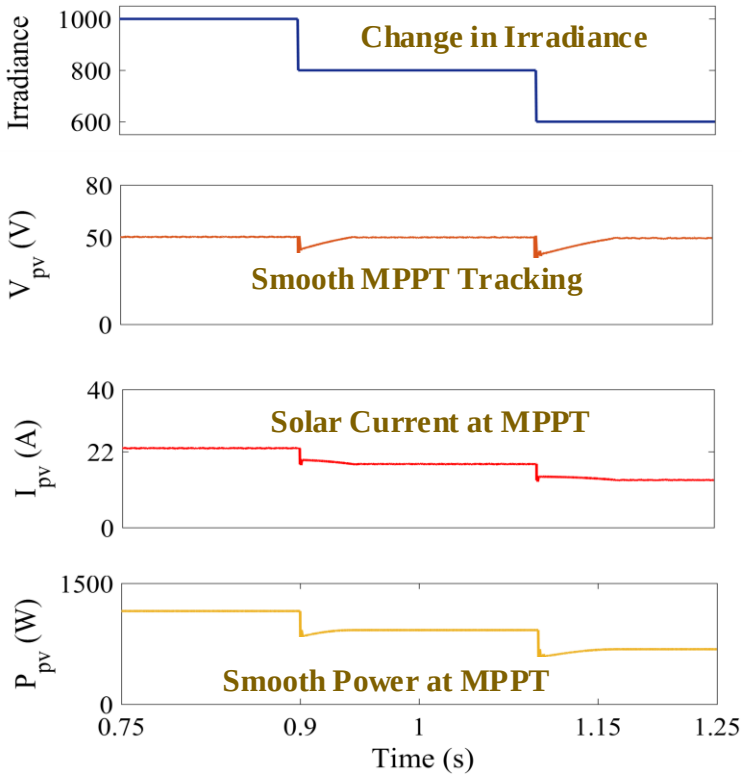

Figure 6.26. Simulated performance of solar PV array $(Irradiance, V_{pv}, I_{pv}, P_{pv})$.

Figure 6.27 also illustrated the PV power (P_{pv}), SOC(%), and battery voltage (V_{b}). It confirms the efficient energy conversion, stable LEV battery charging despite varying solar PV input.

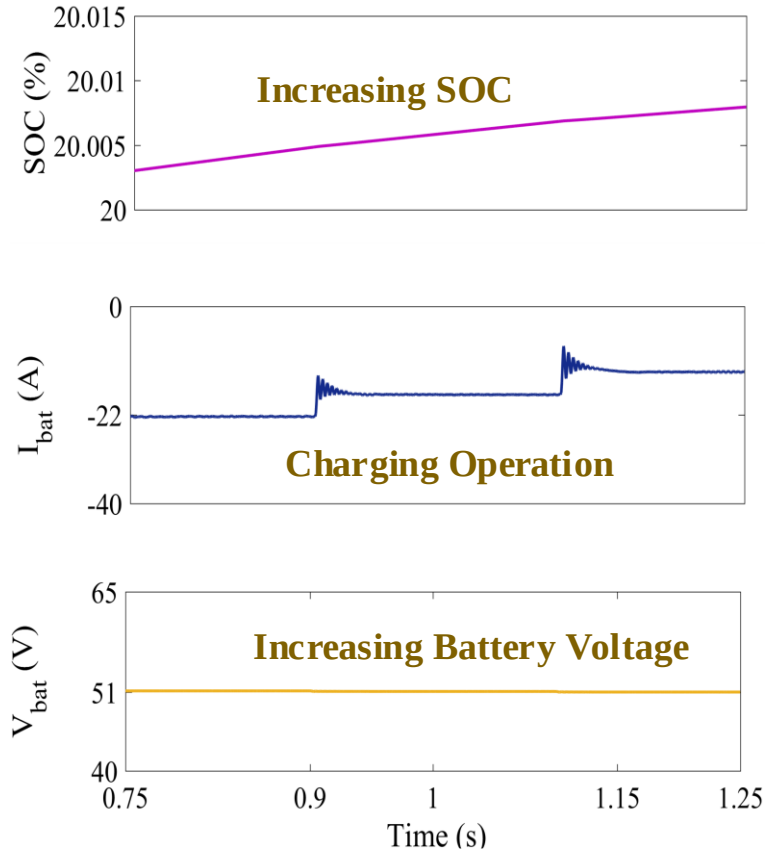

Figure 6.27. Simulated performance of solar PV array-based charging $(SOC\ , I_{bat}, V_{bat})$.

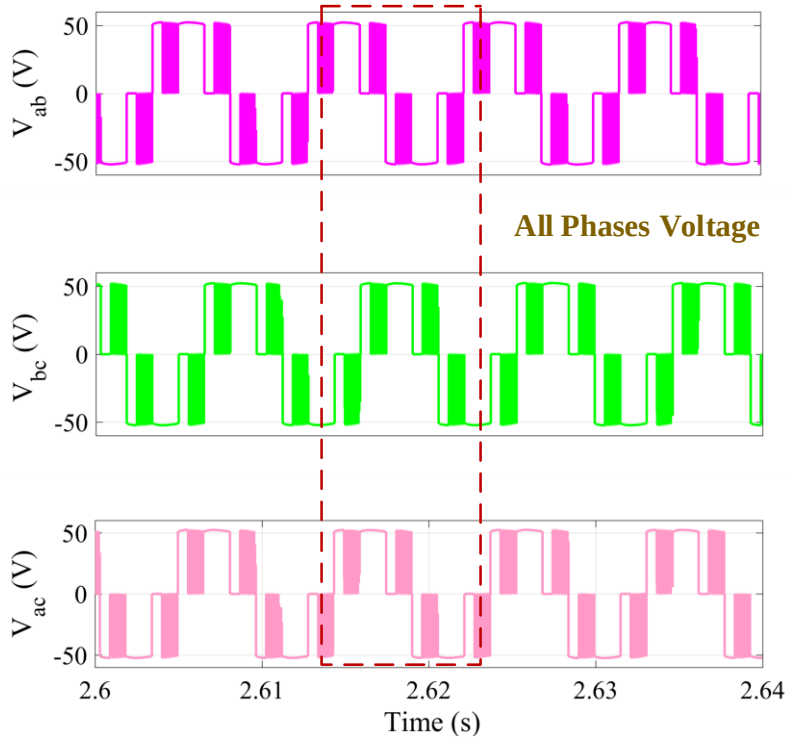

Figure 6.28. Simulated performance of BLDC motor three phase line-line voltages (V_{ab}, V_{bc}, V_{ac}).

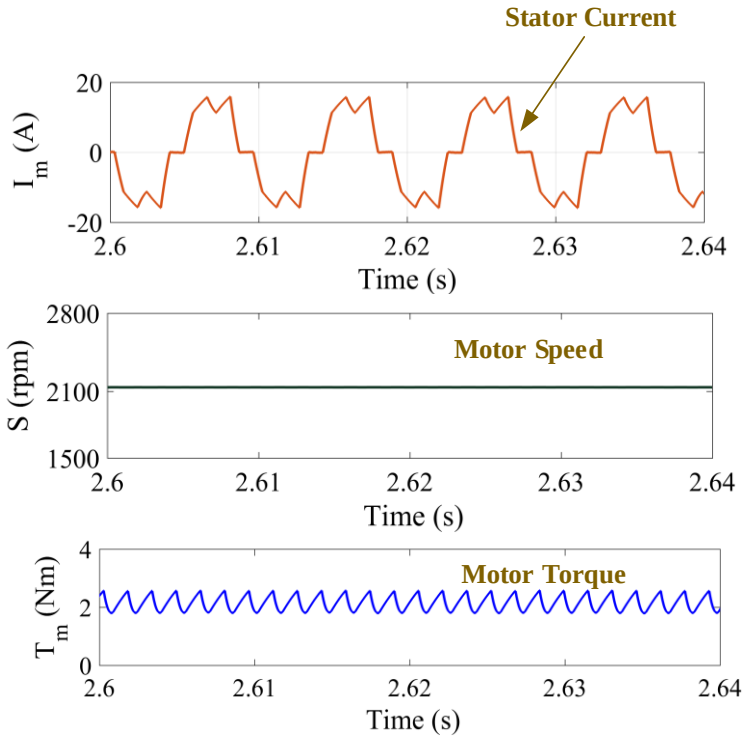

Figure 6.29. Simulated performance of BLDC motor during propulsion mode (I_m, S, T_m).

6.7.1.4 *Brushless DC Motor Performance*

In this operation, the LEV battery system provides power to the brushless DC motor to drive it in propulsion mode. Figure 6.28 depicts the effectiveness of motor parameters such as phase voltages (V_{ab}, V_{bc}, V_{ca}) of the inverter, stator current (I_m), propulsion speed (S) in rpm, and torque (T_m) in Figure 6.29. These waveforms illustrate that the BLDC motor operates efficiently under the given battery conditions, providing stable propulsion with reliable torque and speed characteristics.

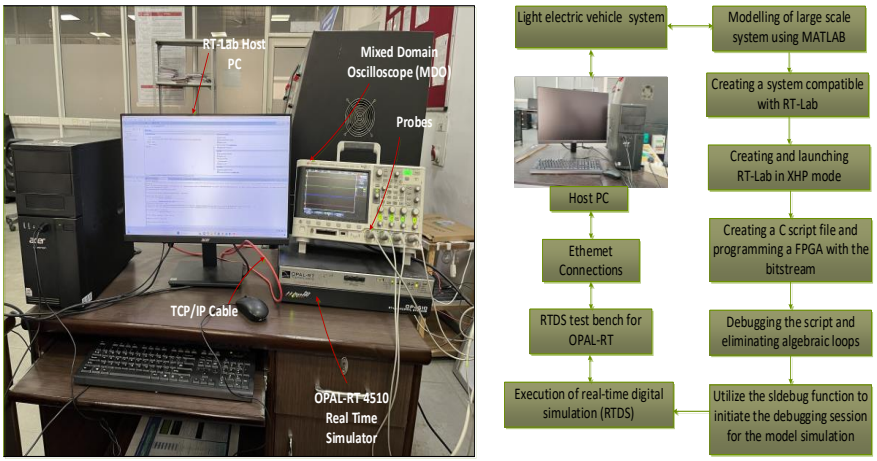

Figure 6.30. Real-time CHIL test setup.

6.7.2 *Experimental Performance of Solar-Powered On-Board LEV Utilizing Isolated*

Integrated Converter

24 The experimental analysis verifies the operation of the proposed concept under distinct operating conditions. The tested results of the CHIL (controller hardware in the Loop) setup is illustrated in Figure 6.30.

6.7.2.1 Grid-Based Charging Performance

Figure 6.31 depicts the experimental validation of G2V during 10% sag in grid voltage (Vg) and shows the efficient performance of LEV battery charging with no change in DC-link voltage and battery current. In Figure 6.32 the experimental validation of G2V during 10% swell shows the efficient LEV battery charging during G2V with no change in DC-link voltage and battery current. Similarly, Figures 6.33 and 6.34 depict the V2G key results during 10% (Vgrid) Sag and swell with no change in DC-link voltage and battery current during discharging. Despite these disturbances, the system maintains a stable DC-link voltage and exhibits no significant variation in the battery current, underscoring its robustness under such grid fluctuations.

98 14

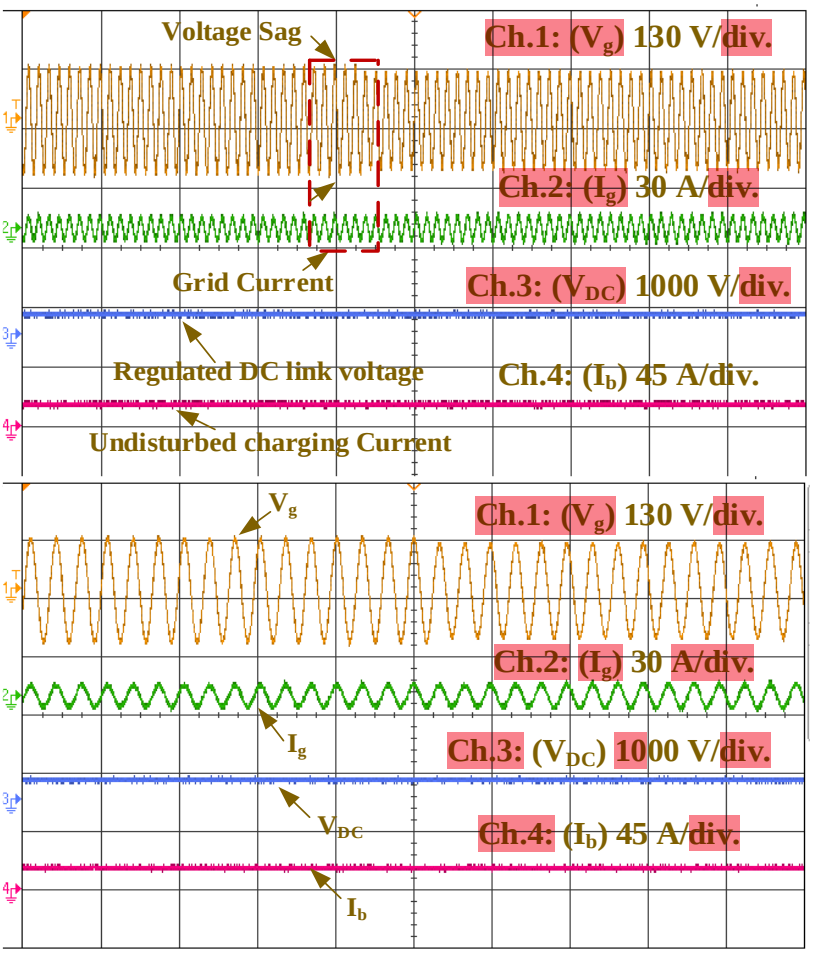

Figure 6.31. Experimental performance of G2V mode during voltage sag event (V_g, I_g, V_{DC}, I_b)

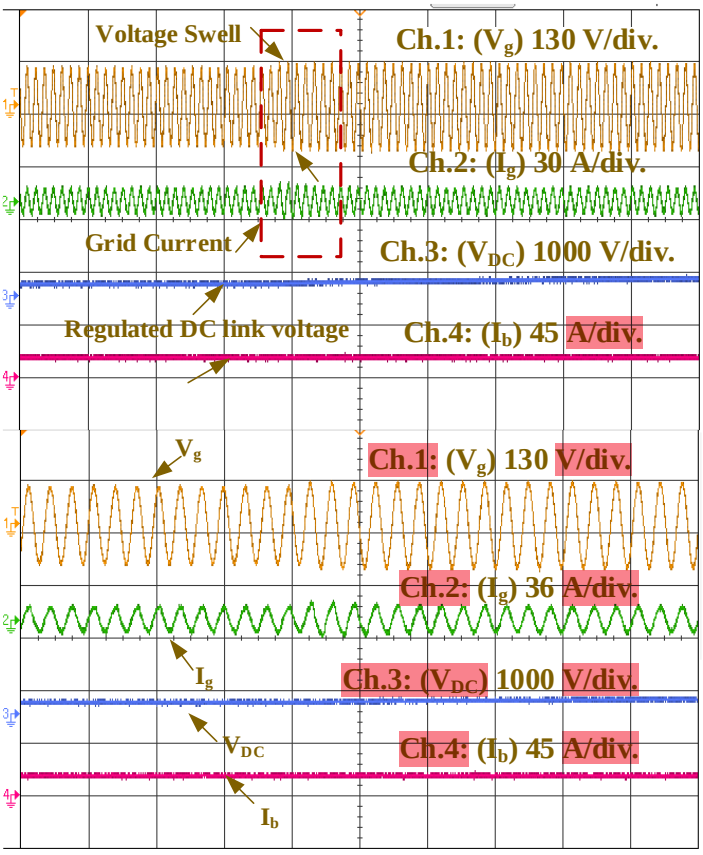

Figure 6.32. Experimental performance of G2V mode during voltage swell event (V_g, I_g, V_{DC}, I_b).

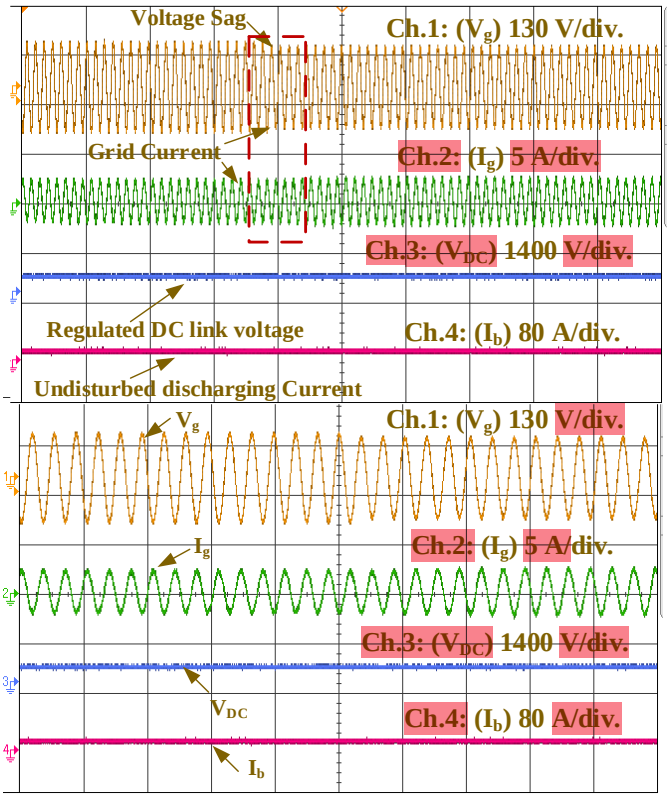

Figure 6.33. Experimental performance of V2G mode during voltage sag event (V_g, I_g, V_{DC}, I_b).

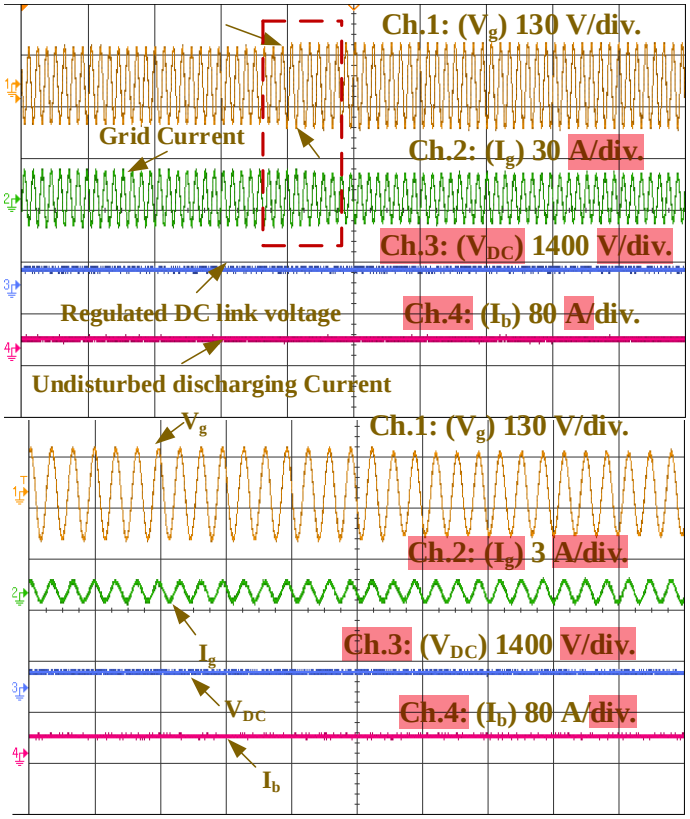

Figure 6.34. Experimental performance of V2G mode during voltage swell event (V_g, I_g, V_{DC}, I_b).

6.7.2.2 *Solar PV-Based Charging Performance*

Figure 6.35 (a-b) depicts the experimental behavior of on-board solar PV charging parameters, which is validated under different environmental conditions. The waveforms highlight key parameters such as change in irradiance, Smooth MPPT tracking, solar current at MPPT, and battery charging current, confirming the effective integration of PV sources into the LEV power architecture. The ability to harness solar energy enhances system sustainability and reduces dependency on the grid.

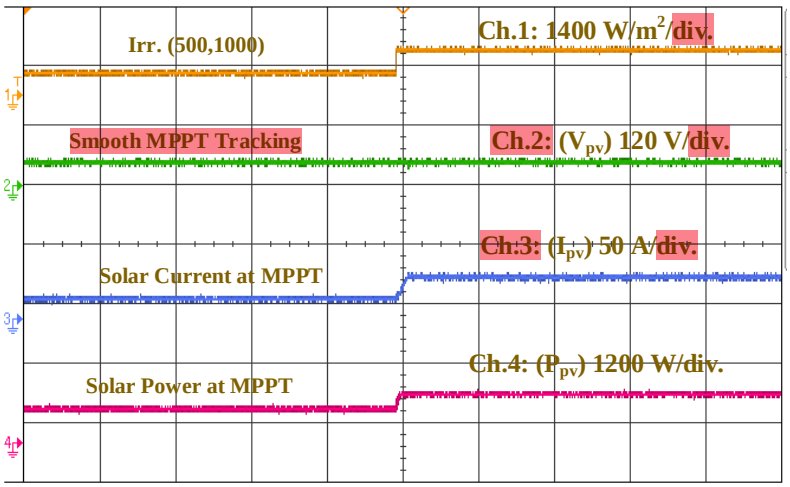

(a)

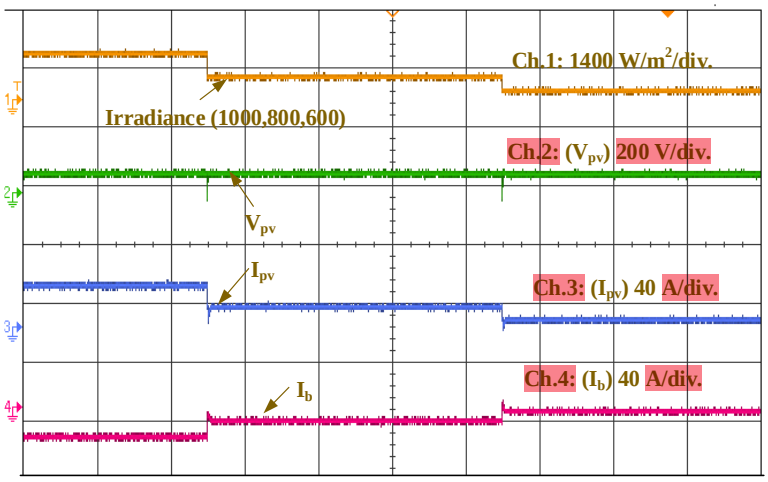

(b)

Figure 6.35. Experimental performance of on-board solar PV array-based LEV charging (a) $(Irradiance, V_{pv}, I_{pv}, P_{pv})$ (b) $(Irradiance, V_{pv}, I_{pv}, I_b)$.

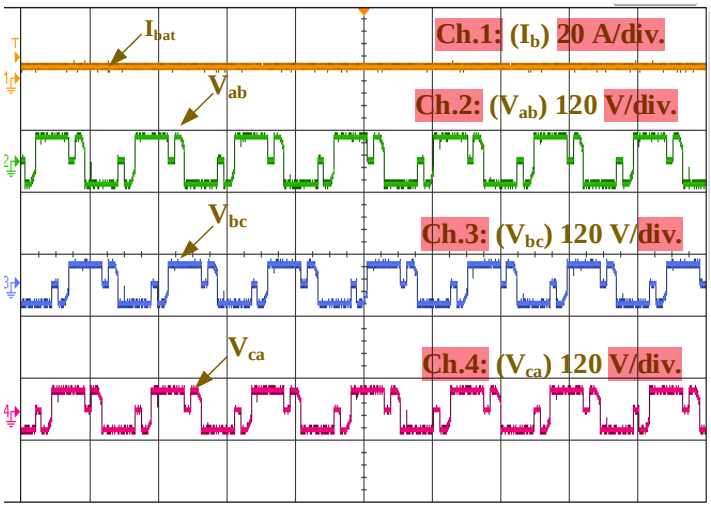

Figure 6.36. Experimental performance of the BLDC motor line-line voltages $(I_{bat}, V_{ab}, V_{bc}, V_{ca})$.

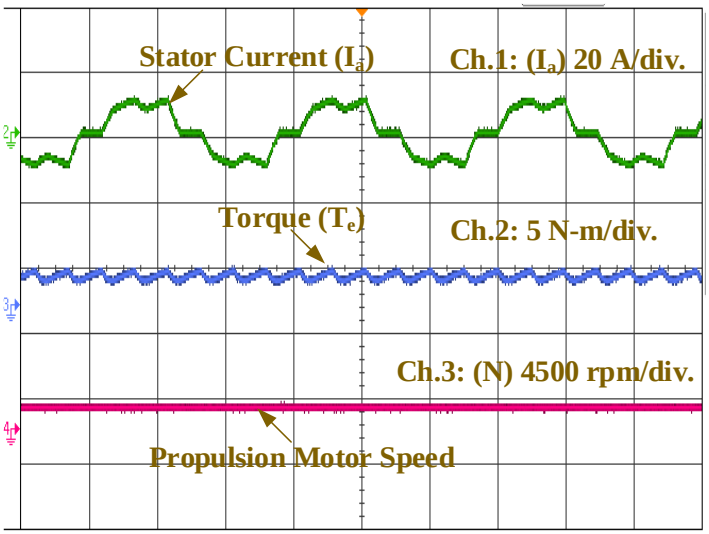

Figure 6.37. Experimental performance of the BLDC motor in propulsion mode $(I_a, T_e, Propulsion\ Motor\ Speed)$.

6.7.2.3 *Brushless DC Motor Performance*

Figure 6.36, brushless DC motor performance in propulsion mode is validated, like line-line voltages (V_{ab}, V_{bc}, and V_{ac}) of all three phases providing insight into the BLDC motor's voltage supply and switching characteristics, the stator current (I_a), motor torque, and rotor speed in propulsion mode are shown in Figure 6.37. This validation demonstrates the effectiveness of the BLDC motor control strategy in achieving smooth and stable operation.

6.8 Losses and Efficiency Calculation

This work mainly focuses on designing a bidirectional charger for LEV applications. The proposed bidirectional high-gain converter operates in both G2V and V2G modes efficiently and LEV batteries can be charged/discharged through it. But to prove the system performance, power loss calculations are necessary in Figure 6.38. The Table 6.3 explain the proposed system passive components power losses,

$$P_{loss}^{Total} = P_{closs} + P_{swloss} + P_{sdloss} + P_{cdloss} + P_{L_{sloss}} + P_{L_{0loss}} + P_{C_{Iloss}} \quad (6.30)$$

Table 6.3. Calculated losses of the system.

Losses Parameters	Equations	Losses in W
Switches $(Q_1 - Q_4)$ conduction losses (P_{closs})	$2\left(V_{CEO}.I_{Q1avg.} + r_{CE}.I_{Q1rms}^2\right)$	9.83 W
Switches $(Q_1 - Q_4)$ switching losses (P_{swloss})	$2\left(V_{Q1max}.I_{Q1avg.}\left(t_r + t_f\right).f_s\right)$	9. 46 W
Switches (Q_a) switching losses (P_{swloss})	$\left(V_{Q1max}.I_{Q1avg.}\left(t_r + t_f\right).f_s\right)$	3. 7 W
Diode switching losses for $(Q_a - Q_b)$ switches (P_{sdloss})	$2\left(V_{DQ5max}.I_{DQ5avg.}.\left(t_r + t_f\right).f_s\right)$	4.95 W
Diode conduction losses for $(Q_a - Q_b)$ switches (P_{cdloss})	$2\left(V_{F0}. + r_F.I_{DQ5rms}^2\right)$	7.65 W
Input Inductor Losses $(P_{L_{sloss}})$	$I_{L_s}^2 rms \cdot r_{L_s}$	0.21 W
Output Inductors Losses $(P_{L_{0loss}})$	$2 \cdot I_{L_0}^2 rms \cdot r_{L_0}$	2.56 W
Intermediate Capacitor Losses $(P_{C_{Iloss}})$	$2 \cdot I_{C_I}^2 rms \cdot ESR_{C_I}$	1.54 W

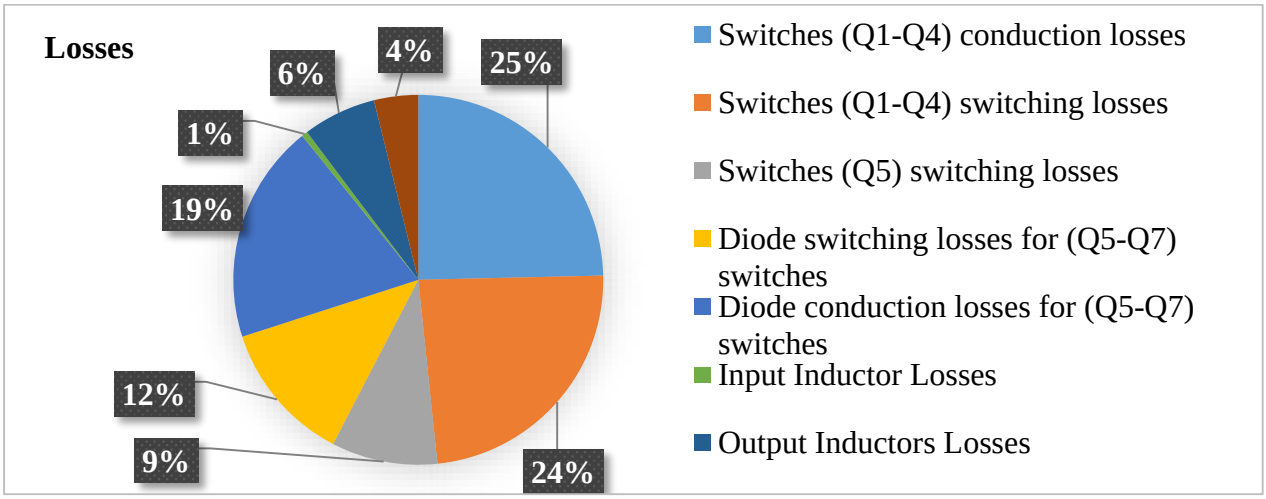

Figure 6.38. Power Management architecture for the proposed system.

$$\text{Efficiency } (\eta) = \frac{P_0}{P_0 + P_{loss}^{Total}} \tag{6.31}$$

6.9 Conclusion

In this work, an isolated integrated converter has been designed and developed for LEV battery charging using dual sources such as the grid and solar PV. The converter is developed to operate efficiently in G2V and V2G modes during grid supply. In a grid outage, the on-board solar PV efficiently charged the LEV battery through an MPPT converter under different environmental conditions. The proposed system, including all working operations and the power management scheme, is tested by real-time responses. The proposed isolated integrated converter has demonstrated its effectiveness and practicality, particularly in maintaining unity power factor (UPF) and constant current operation during grid voltage sag and swell events. To enhance robustness, an advanced mixed second-order–third-order generalized integrator (IMSTOGI) control algorithm is introduced to facilitate reliable operation of the Active Front-End Converter (AFC) under grid disturbances. The Active Front-End Converter (AFC) operation results in Total Harmonic Distortion (THD) of approximately 2.37% and 1.58% during voltage sag and swell events, respectively, under G2V mode. For V2G mode, the THD achieved is around 2.46% and 1.70% during similar voltage conditions, all well within the limits established by international standards. The system also features a soft-starting mechanism for the BLDC drive in propulsion mode, which operates without the need for current and voltage sensors on the motor side. Verification through simulation and real-time testing using an OPAL-RT prototype confirmed the system's performance. The developed

system offers several advantages, including bidirectional functionality, a reduced component count, lower conduction losses, enhanced efficiency, and a faster return on investment.

CHAPTER-7

SOLAR POWERED ON-BOARD LEV UTILIZING BRIDGELESS CONVERTER

7.1 General

The worldwide concern of global warming and fossil fuel, the transportation industry necessitated to presents an electric vehicle (EVs). In the last few years, the integration of these EVs sales to the transportation sector reached the highest level. While the benefits of EVs are clear, including reduced greenhouse gas emissions and lower operating costs, challenges such as infrastructure readiness and battery production sustainability remain significant hurdles to their widespread adoption. However, understanding of sustainable energy, betterment in battery technology and lowering in cost of EVs, the integration largely depends upon the efficient topologies and control techniques. For a good charging infrastructure-controlled charging technique demands low harmonics injected to the grid, improved power quality and a unity power factor (UPF) operation within guidelines. Furthermore, the main attention is to provide electrical power for the appropriate controlled battery charging speed Integrating solar, wind or other renewable sources can lower dependency on fossil fuels and decrease greenhouse gas emissions, supporting to a more sustainable transportation setup.

The charger required for EVs charging are; on-board and off-board charger. Moreover, the on-board charger is designed for vehicles having low charge capacities named as light electric vehicles. However, traditional LEV chargers have some significant drawbacks, such as high distortion of supply currents, low operating power factors, and reduced efficiency. These issues can place additional strain on the power supply system and hold the growth of LEVs. Talk about these problems, diverse solutions have been proposed, containing the use of passive filters on the supply side and active filtering strategies. Recently, power factor correction circuits (PFCC) have become more popular in chargers due to their advantages, such as lower cost, enhanced reliability, compact size, and improved efficiency.

Conversely, while conventional bridgeless converters have limitations, emerging designs, such as those utilizing soft-switching techniques or reduced component counts, show promise in overcoming these challenges, potentially leading to more efficient and cost-effective solutions for EV charging applications. Hard switching in conventional designs can lead to increased switching losses, reducing overall efficiency during the AC-DC conversion process.

Traditional bridgeless converters can still experience significant conduction losses, particularly at the input stage where diode bridges are typically employed. The limitations of conventional bridgeless converters for electric vehicle (EV) charging primarily stem from their design complexities and performance inefficiencies. The need for multiple sensors and control loops in some designs can complicate implementation and increase the potential for failure

Bridgeless converters are increasingly recognized for their efficiency in electric vehicle (EV) charging applications, primarily due to their ability to reduce conduction losses associated with traditional diode bridge rectifiers. These converters operate by utilizing fewer components, which enhances power factor correction (PFC) and overall performance. Bridgeless converters reduce conduction losses by minimizing the number of components involved in the rectification process, which enhances overall efficiency. This compactness not only lowers manufacturing costs but also simplifies the overall system architecture. These converters achieve a unity power factor operation, which is crucial for reducing input current harmonics and ensuring compliance with international standards. Many bridgeless designs operate in continuous conduction mode (CCM) or discontinuous conduction mode (DCM), allowing for soft switching, which further enhances efficiency by reducing switching losses.

The buck converter with modified MPPT control charged the light EVs battery successfully, without grid use. After the charging of battery, the next operation is run of brushless DC motor via a voltage source converter (VSC) with controller.

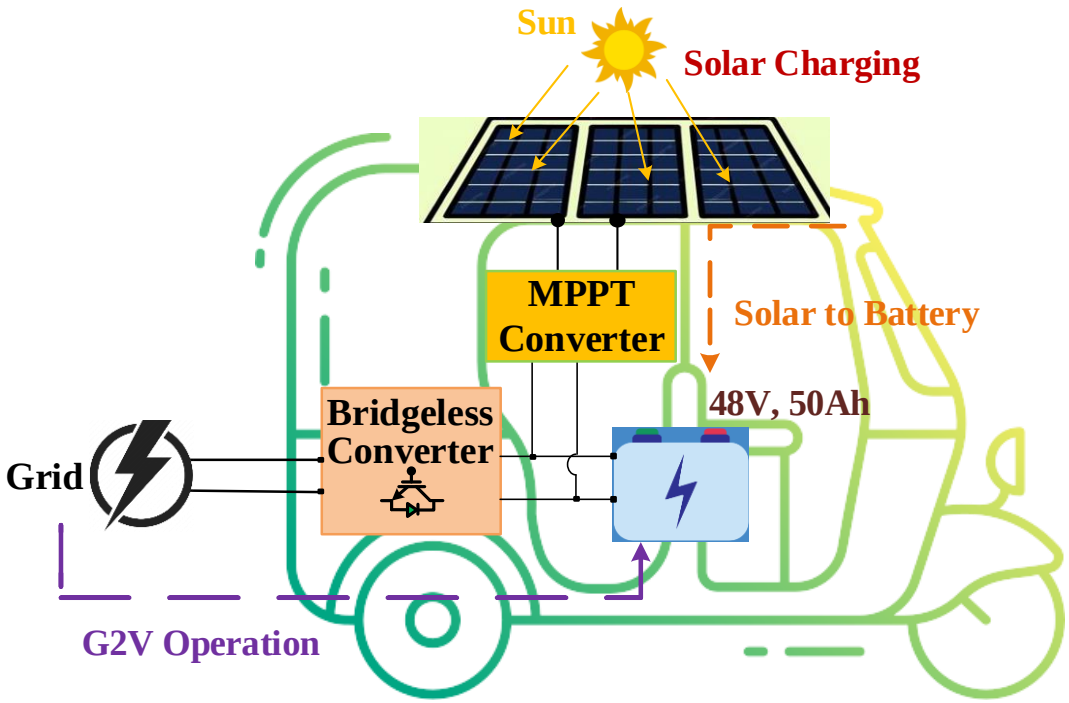

Figure 7.1. Schematic of the developed on-board grid-integrated solar-powered LEV utilizing a bridgeless converter.

The main focus of the proposed work is on smart control to manage charging from bridgeless converter as well as on-board solar-based charging during grid outage. Also, it focuses on reducing the number of overall drive train elements and efficiently work on the power management of all operational modes in Figure 7.1. The proposed strategy includes the following features and advantages,

- A bridgeless converter based charging strategy with on-board solar PV MPPT converter features is designed for light EVs to incorporate G2V and solar based charging operations.
- The developed bridgeless converter an achieve unity power factor operation, which is essential for reducing harmonic distortion and meeting regulatory standards.
- The developed bridgeless converter has reduced the total number of component count, to improve efficiency, compact size and increased reliability.
- The proposed bridgeless converter configuration also offers high payback time, lowers stress on semiconductor devices, and passive components.
- The proposed charging strategy manages the battery charging process, as an onboard solar PV-powered array with improved MPPT control algorithms.
- The proposed charging strategy ensures less burden on the grid due to the availability of an alternate source, viz., solar PV.
- The proposed strategy also introduces a brushless DC drive system for propulsion mode of operation.

7.2 Configuration of Solar Powered On-board Light Electric Vehicle Using Bridgeless Modified SEPIC Converter

Figure 7.2 shows the schematic of an bridgless converter with dual power sources (i.e. single phase grid and solar PV), employing a BLDC (burshless DC) motor drive. It employ modified bridgless SEPIC strategy which performe grid volatge and grid current power factor correction in both LEV battery charging mode. Moreover, an onboard photovoltaic module possessing a peak power capacity of 800 W, utilizes an enhanced drift-free Perturb and Observe (P&O) control methodology directly charge the LEV battery to maximize the efficacy of the solar photovoltaic system. A 750 W, 48V BLDC motor derive is used as a propulsion motor for the electric LEV. The develoled modified bridgless SEPIC strategy can meet charging performance with PFC and also use solar power to charge the LEV battery during grid outage. The developed modified bridgless SEPIC strategy undergoes grid based (G2V) and on-board

solar PV powered based charging mode of operations. Furthermore, it will drive the BLDC motor in propulsion mode.

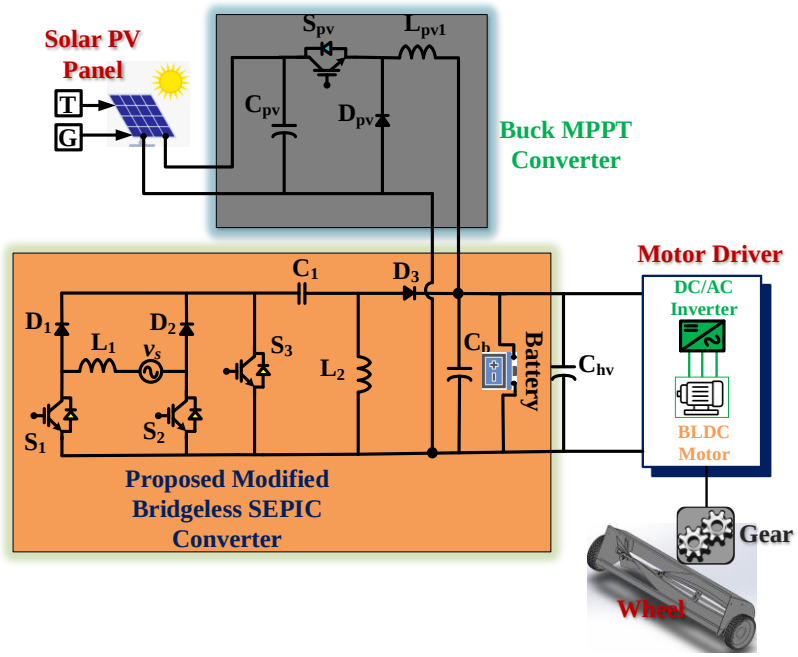

Figure 7.2. Circuit of Proposed Bridgeless AC-DC Converter LEV Charging.

7.3 Modes of Operations of Solar Powered On-board Light Electric Vehicle Using Bridgeless Modified SEPIC Converter

Mode I (Grid-to-Vehicle) : This mode depends upon the ON state of switches S_2, S_2 and S_3 as shown in Figure 7.3(a). Then inductor L_1 is charged through switch S_1 and S_2 as power is driven from grid as shown in Figure 7.3(a). While the inductor L_2 is charged through switch S_3, and capacitors C_1 and C_2 performs their discharging operation. The following equations related to this mode is as,

$$L_1 \frac{d_{L1}}{dt} = v_s \tag{7.1}$$

$$v_s = v_m \sin(\omega t) \tag{7.2}$$

$$I_{L1max} = \frac{v_s}{L1} K_i T \tag{7.3}$$

$$v_{L1} = -v_b \tag{7.4}$$

Where v_s is the grid voltage, v_m is the peak voltage, T is the time period, K_i is constant, I_{L1max} is the maximum current via inductor L_1 during period $K_i T$ and v_b is battery voltage.

Mode II (Grid-to-Vehicle) : In this mode switches S_1, S_2 and S_3 are inactive as shown in Figure 7.3(b). The store energy of inductor L_1 and L_2 is start decaying via diodes D_1 and D_3 to the capacitor C_b. When the current from inductor L_1 and L_2 is fully discharged then all diodes is immediately tuned off and capacitor C_b fed to LEV battery. Hence the battery charging is done

as shown in Figure 7.3(c). The following equations related to this mode is as,

$$L_1 \frac{d_{L1}}{dt} = -v_s \tag{7.5}$$

$$I_{L1max} = \frac{v_s}{L1} K_j T \tag{7.6}$$

$$\Delta I_{D2} = \frac{I_{L1max}}{2} K_j \tag{7.7}$$

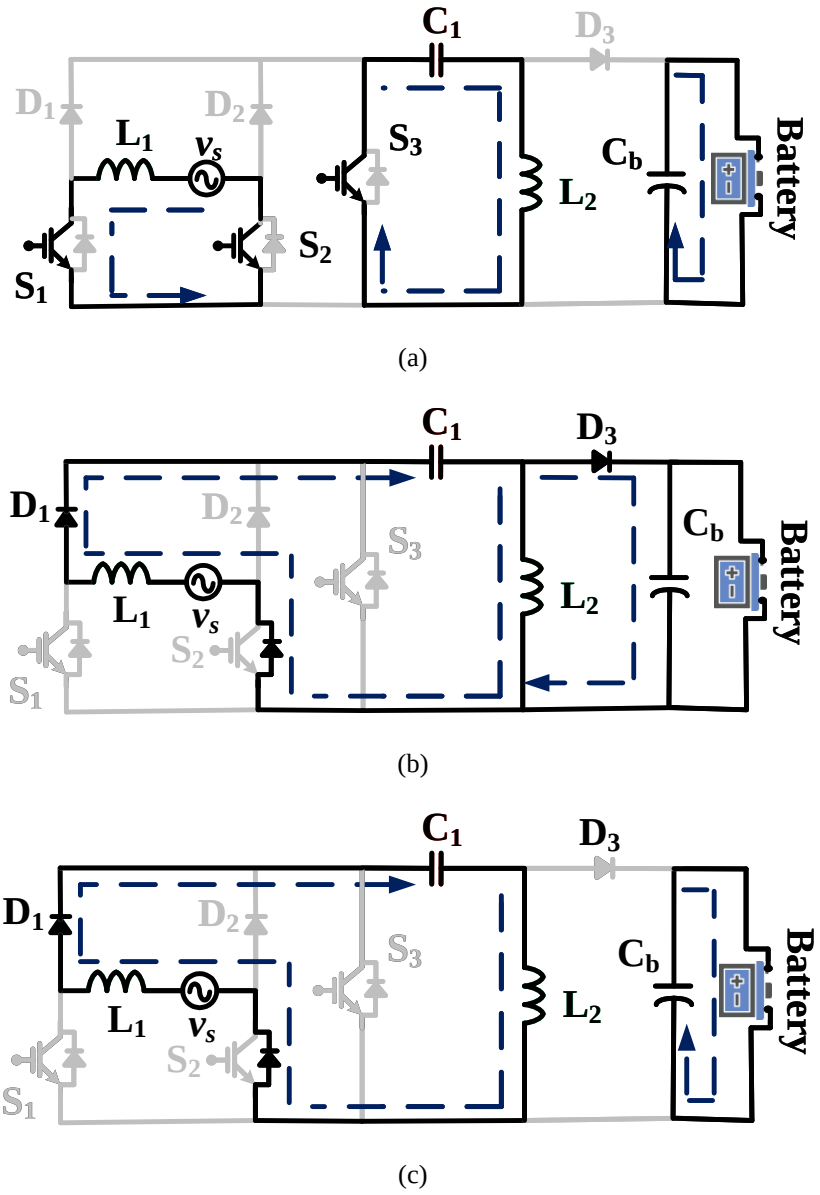

Figure 7.3. Circuit of charging modes of operations.

77

Where v_s is the grid voltage, v_m is the peak voltage, T is the time period, K_j is constant, inductor L_1 during period $K_j T$ is discharged to zero and ΔI_{D2} is the average current via diode $D2$.

Mode III (Solar PV based Charging): In this mode, the solar PV array directly charged the LEV battery during grid outage. The solar PV array directly gives power to dc link and the developed bridgeless converter act as MPPT converter for the solar PV array as shown in Figure 7.4.

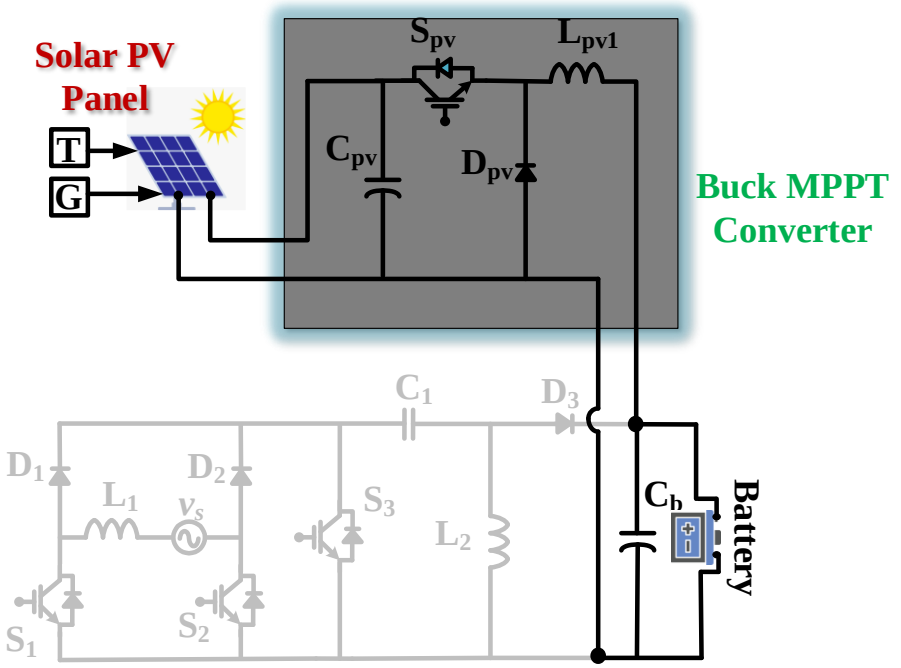

Figure 7.4. Solar based LEV Charging.

7.4 Designing of Solar Powered On-board LEV Using Bridgeless Modified SEPIC Converter

7.4.2 Design and Selection of Developed Bridgeless converter

In this developed bridgeless charging system, a single-phase supply (V_s) with a nominal voltage of 212 V, 50Hz is considered for the circuit design. The developed bridgeless charging system is designed for a 48V, 50Ah battery. The design of filter inductors and capacitors is crucial for optimizing performance in LEV charging applications. The focus on optimizing filter components is critical for performance, it is also essential to consider the trade-offs between size, cost, and efficiency. Balancing all the switches, diodes, and passive elements can lead to innovative designs that meet efficient charging demands. The following equations is related to designing of developed bridgeless charging system as,

$$f_{cut} = \frac{f_{sw}}{5} = \frac{1}{2\pi\sqrt{L_f C_f}} \tag{7.8}$$

$$i_{L_f} = C_f \frac{dv_{C_f}}{dt} + i_{L_1} \tag{7.9}$$

$$v_{c_f} = L \frac{di_{L_1}}{dt} \tag{7.10}$$

$$v_b = \frac{2D}{1+(1-D)^2} |v_s| \tag{7.11}$$

where f_{cut} is the cutting frequency, L_f is filter inductor, C_f is filter capacitor, and D is the duty ratio.

The values taken for simulation and hardware experimentation is shown in Table 7.1.

Table 7.1. Design parameter values for developed bridgeless converter

Parameter	Value
AC input voltage (V_g)	230 V
Line frequency (f)	50 Hz
Nominal Battery voltage (V_b)	48V
Initial SOC	20%
$L_1/L_2/C_1/C_b$	2mH/2mH/9.5µF /1500 µF
Nominal load power	750 W

7.4.2 *Design and Selection of Solar PV Array*

The solar PV array of 800 W (peak power) is designed for LEV battery charging. The value of 53.55 V is selected for the maximum power point (MPP) voltage V_{mpp} of the array with MPPT Buck converter. The other parameters of the PV array are given in Table II. Consequently, the rated current at this condition is stated as,

$$I_{pv} = \frac{P_{pv}}{v_{pv}} \tag{7.12}$$

The number of series-connected modules per string is as,

$$N_s = \frac{v_{pv}}{v_{mp}} \tag{7.13}$$

and the number of parallel-connected strings is as,

$$N_p = \frac{I_{pv}}{I_{mp}} \tag{7.14}$$

Table 7.2. Parameters of solar PV array

Parameter	Value
Peak Power (W)	800 W
Cell per module	36
Voltage at open circuit, $V_{o.c}$ (V)	21.3 V
Rated current at short circuit condition, $I_{s.c}$ (A)	6.3 A
Number of series strings, N_s	3
Number of parallel strings, N_p	3
MPP voltage rating, V_{mpp}	54.315 V
MPP current rating, I_{mpp}	10.83 A
L_{pv1}, C_{pv}, C_o	1mH/10µF/1500 µF

7.5 Control of Solar Powered On-board LEV Using Bridgeless Modified SEPIC Converter

7.5.1 *Control of Bridgeless Modified SEPIC Converter*

A single PI controller is commonly used to manage both power factor correction and output voltage regulation, ensuring stable operation during charging. The battery voltage is sensed via LEV battery and compared with reference battery voltage. After it, the output of PI controller is product with grid voltage template and the reference output is compared with grid current and then pluses entered to switches as shown in Figure 7.5.

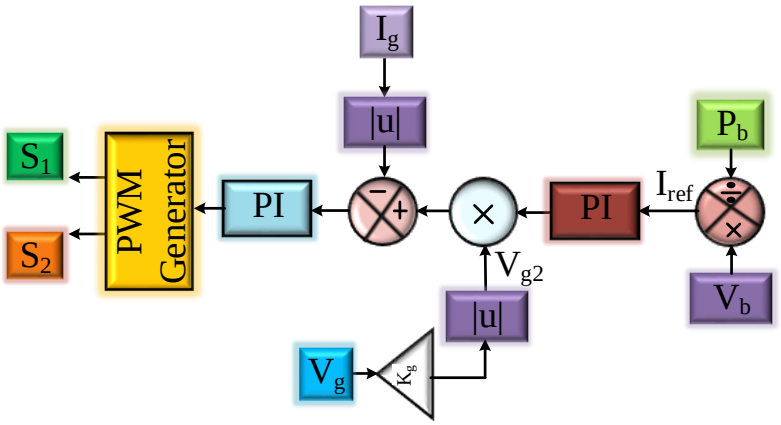

Figure 7.5. Control of bridgeless converter based LEV Charging.

7.5.2 *MPPT Control of Solar PV Array*

Even though the conventional P&O MPPT method is easy to implement and effective, it has serious deviation problems, particularly when there is variation in irradiance. It further results in additional power losses and tracking time lag. To attempt to solve this deviation problem, it

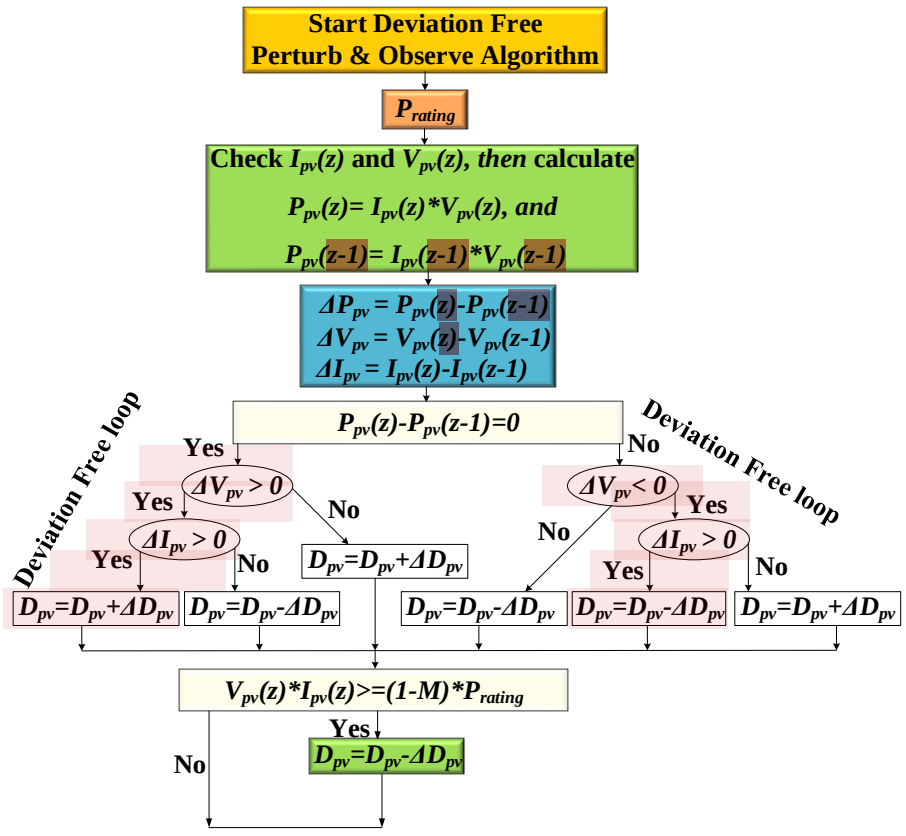

Figure 7.6. Flow chart of utilized modified P&O MPPT technique.

is crucial to take into account the current variation in both cases when there is a positive or negative change in the PV array voltage. Thus, by considering the magnitude of alteration in current (ΔI_{PV}) in addition to change in power (ΔP_{PV}) and change in voltage (ΔV_{PV}) in the decision process, the deviation-free MPPT to minimize the deviation difficulty that exists with the conventional P&O technique. This method lowered the MPPT tracking time in the region of 15% to 20% of the total tracking time. Figure 7.6 depicts a flow chart of the proposed deviation-free MPPT controller.

7.5.3 *Control of Brushless DC Motor Drive for Propulsion Mode*

The primary intent of the controller design for a BLDC motor is to maintain a stable DC-link voltage for smooth operation. Figure 7.7(a) depicts the block diagram of the BLDC motor, which includes a three-phase voltage source inverter (VSI), position sensor, torque command, current regulator, and commutation logic. The high-frequency PWM pulse 'S_b' is, as shown in Figure 7.7(b) is generated by propulsion mode control logic developed for the traction motor.

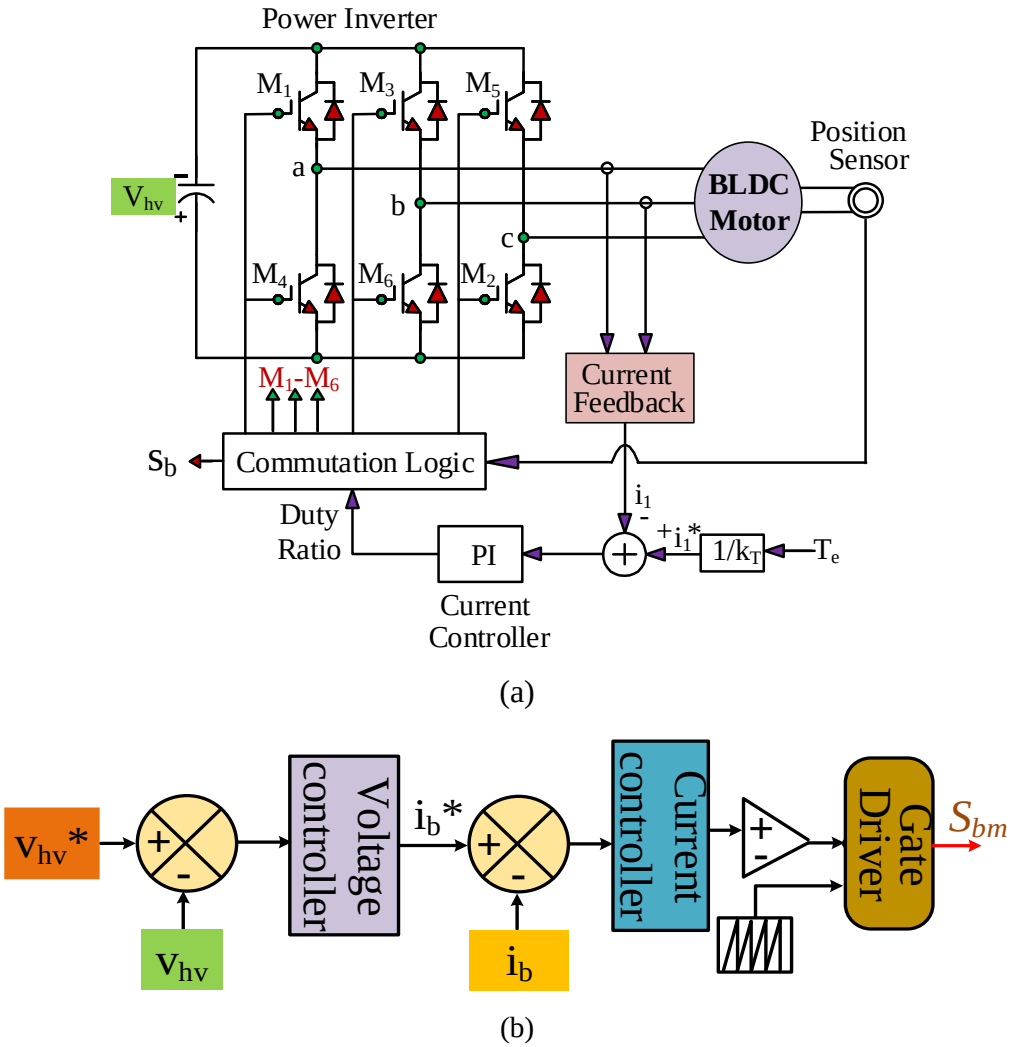

Figure 7.7. Block diagram (a) BLDC motor, (b) Controller.

As depicted in Figure 7.7(b) the input to the voltage control block receives the difference between the desired DC-link voltage, v_{hv}^*, and the assessed DC-link voltage, v_{hv}. Further, the output gives the reference value, which again acts as the battery current discharging value. After that, this coming value is again compared with the sensed i_b* (i.e. battery current), and the output error between the two is input to the current control block. The coming signal is then compared with the high-frequency carrier signal to generate the S_b (i.e. switching pulses).

7.6 MATLAB Based Modeling and Simulation of Solar Powered On-board Charging System Using Bridgeless Modified SEPIC Converter

The following models in Figure 7.8 shows the MATLAB based modeling and simulation of solar powered on-board charging system utilizing bridgeless modified SEPIC converter. Model efficiently works on G2V and V2G modes, and on-board charge the LEV battery via solar PV MPPT Buck converter. This charging strategies also run the BLDC motor drive system.

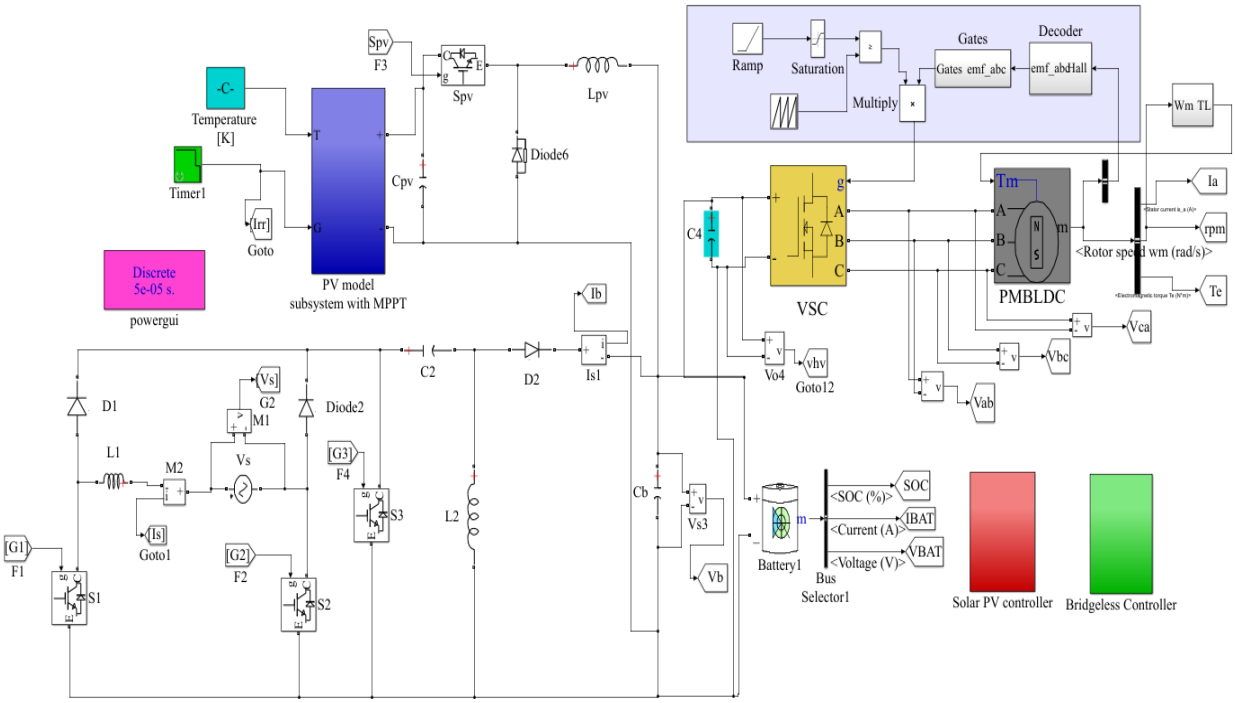

Figure 7.8. MATLAB based modeling and simulation of polar powered on-board charging system utilizing unidirectional non-isolated converter.

7.7 Results and Discussion

In order to ensure the adequate performance of the developed bidirectional high gain converter, the whole design and control of the charger are tested using MATLAB/SIMULINK environment and verified experimentally on OPAL-RT. The effectiveness of the developed system is investigated during the steady-state condition to validate the safe and reliable operations. Moreover, during the off condition of grid supply, battery charging through solar

PV array is shown through both simulation and real-time study. Also, a comprehensive operational analysis of the BLDC motor is carried out here.

7.7.1 *Simulated Performance of Solar Powered On-board LEV Utilizing Bridgeless Converter*

The developed system is tested using the MATLAB/SIMULINK environment, to ensure the optimal/good charging in both grid power supply and solar powered conditions in this section. The effectiveness/efficiency of the developed charger demonstrated via simulation results. Also, a simulation operation investigation of the BLDC motor is also resulted in this section.

7.7.1.1 Grid Based Charging Performance

Figure 7.9 illustrates the power factor correction (PFC) operation between grid voltage (V_g) of around 230V, and grid current (I_g) of 12.55A, and grid voltage at 230V. The in-phase operation between both sinusoidal shaped waveforms demonstrates that the developed system operates in high power factor (HPF). Figure 7.10 illustrates the voltages and current across the diodes. Figure 7.11 illustrates the voltage across the switches, and THD of 3.54 % is observed at grid current of 12.55A in Figure 7.12. It indicates that the converter have low harmonics in current and consumes very little reactive power from the grid, which helps reduce the electricity costs for LEV charging. The charging performance of LEV system such as battery SOC taken at 20%, battery voltage around 51V, and battery current of -12A is observed in Figure 7.13.

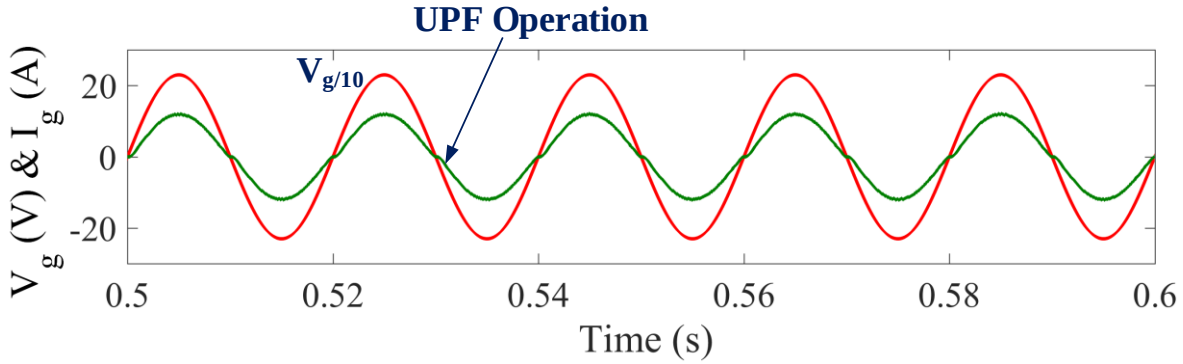

Figure 7.9. Simulated performance of PFC operation between grid voltage (V_g) and grid current (I_g) .

7.7.1.2 Solar PV Based Charging Performance

The simulated waveforms in Figure 7.14(a) illustrates the on-board solar PV charging operation during grid outage like change in irradiance, PV voltage (V_{pv}) AT MPPT, PV current (I_{pv}) at MPPT , PV power (P_{pv}) at MPPT, and in Figure 7.14(b) waveform of battery state of charge (SOC), battery charging current, and increasing battery voltage. It confirms the efficient energy conversion, stable LEV battery charging despite varying solar PV input. It confirms the efficient energy conversion, stable LEV battery charging despite varying solar PV input.

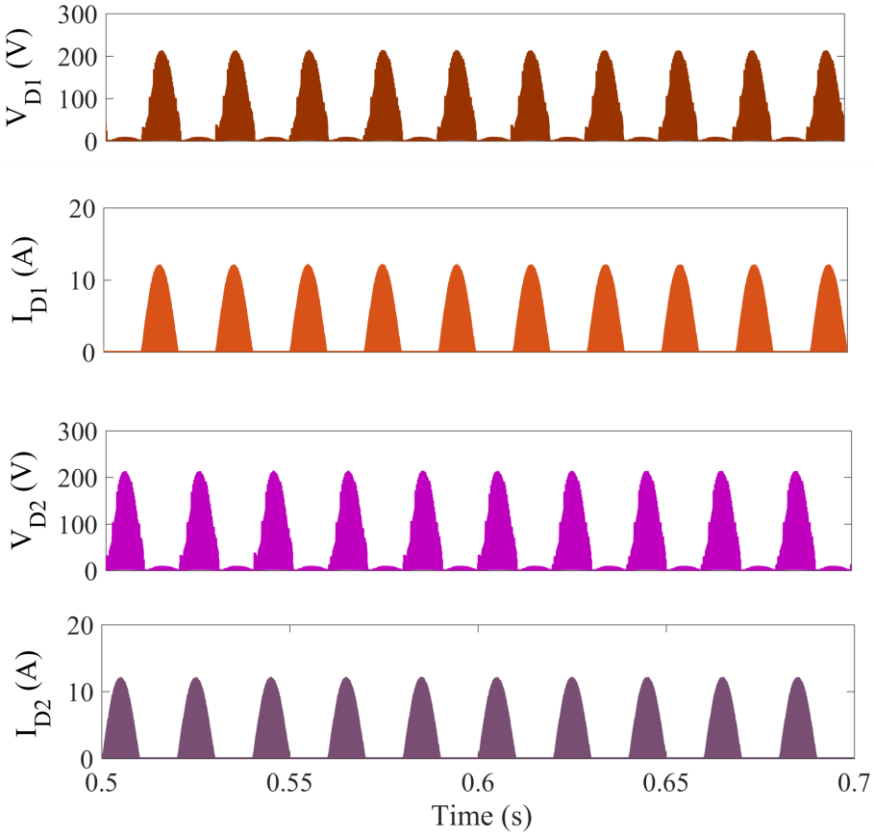

Figure 7.10. Simulated waveform of voltage and current across the diodes ($V_{D1}, I_{D1}, V_{D2}, I_{D2}$).

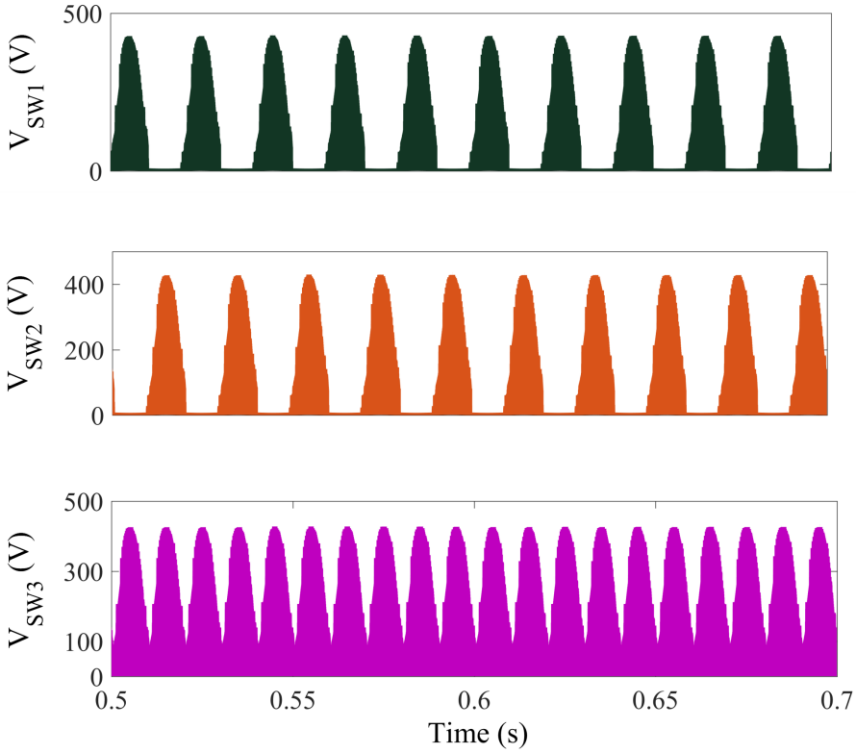

Figure 7.11. Simulated waveform of voltage across the switches ($V_{SW1}, V_{SW2}, V_{SW3}$).

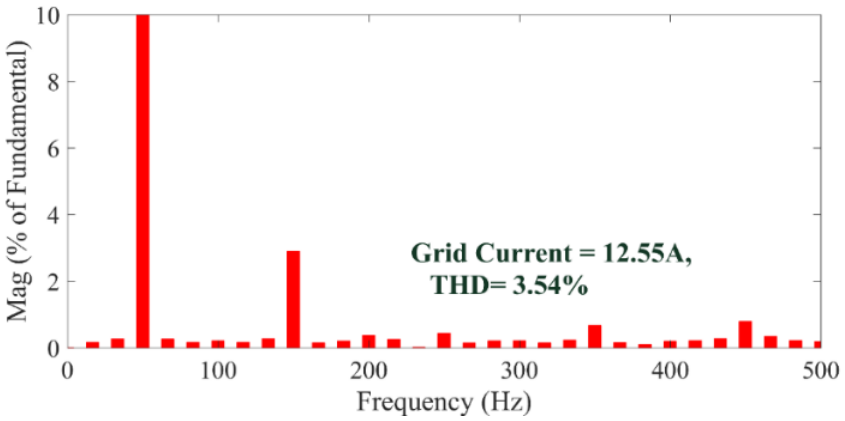

Figure 7.12. Simulated performance of THD of I_g during G2V.

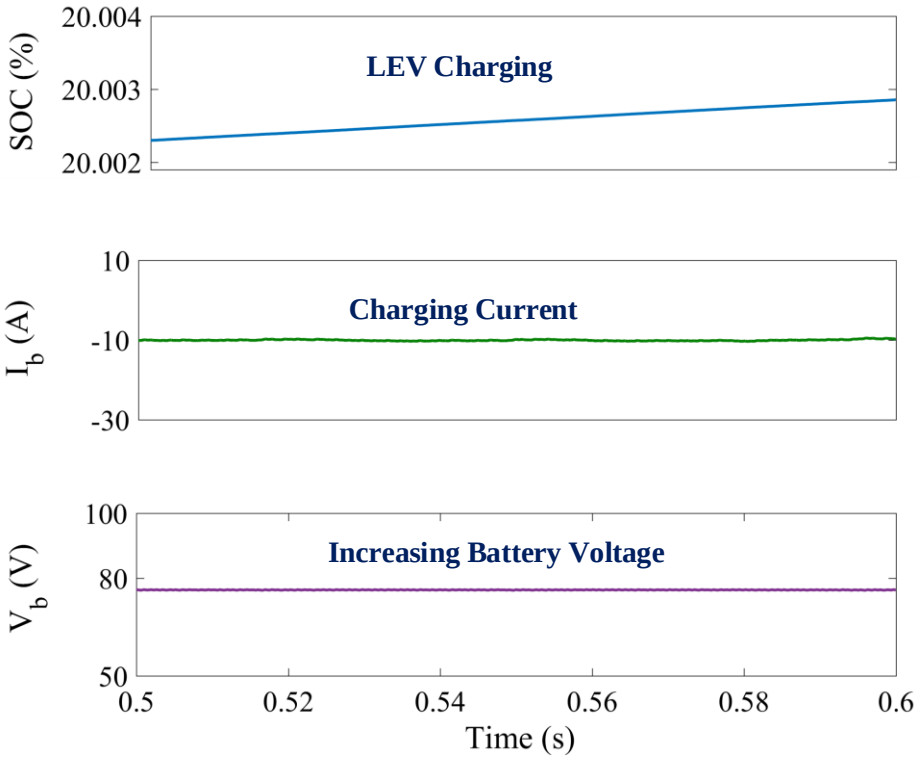

Figure 7.13. Simulated performance of LEV battery charging (SOC, I_b, V_b).

7.7.1.3 *Brushless DC Motor Performance*

The brushless DC motor performance in propulsion mode illustrates in Figure 7.15(a), like line-line voltages (V_{ab}, V_{bc}, and V_{ac}) of all three phases, which are around 50V, the stator current (I_a) is around 20 A, motor torque and rotor speed of 2100RPM shown in Figure7.15(b). These waveforms illustrate that the BLDC motor is operating efficiently under the given battery conditions, providing stable propulsion with reliable torque and speed characteristics.

7.7.2 Experimental Performance of Solar Powered On-board LEV Using Bridgeless Modified SEPIC Converter

The developed bridgeless converter is tested/validated via an OPAL-RT interface to ensure the optimal/good charging efficiency in both grid power supply and solar powered conditions in

this section. Also a hardware operation investigation of the BLDC motor is also resulted here.

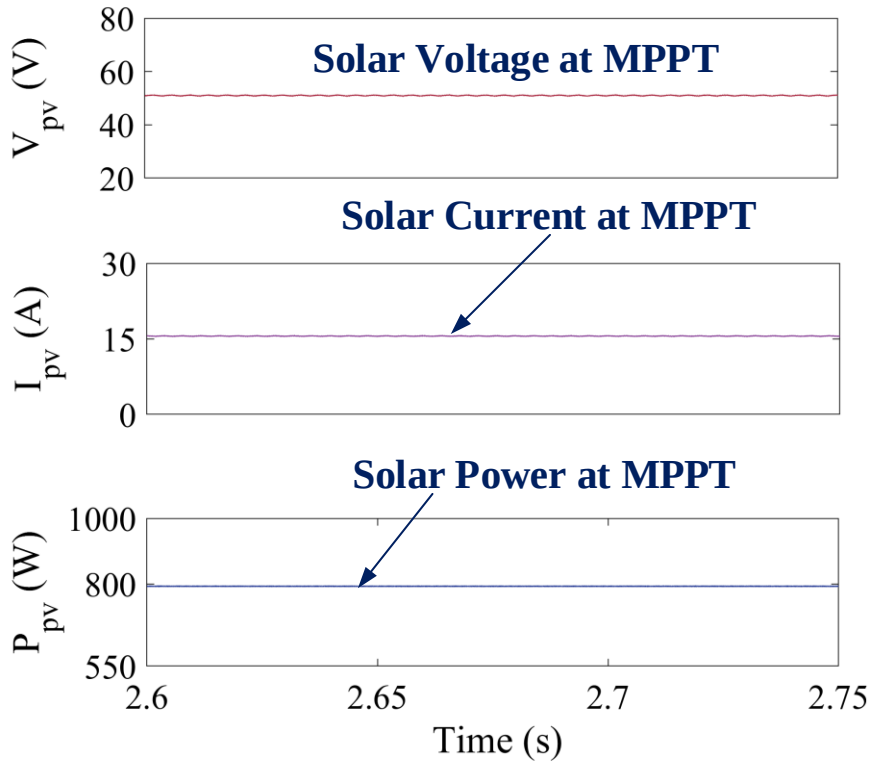

(a)

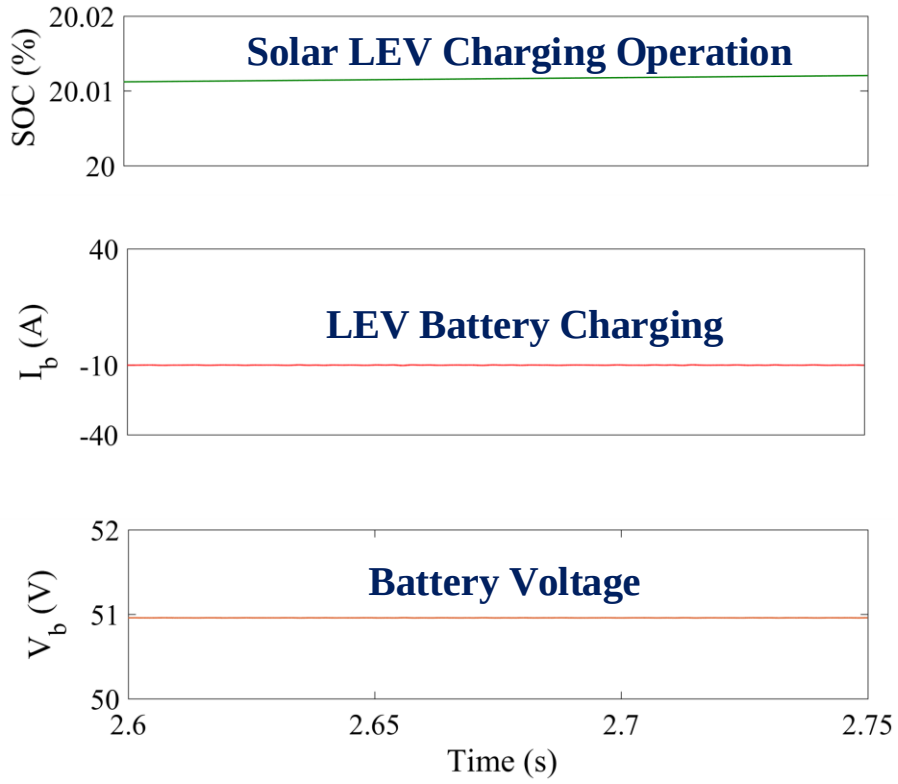

(b)

Figure 7.14. Simulated Waveform of on-board Solar PV array-based LEV charging (a) (V_{pv}, I_{pv}, P_{pv}), (b) $(SOC\%, I_b, V_b)$.

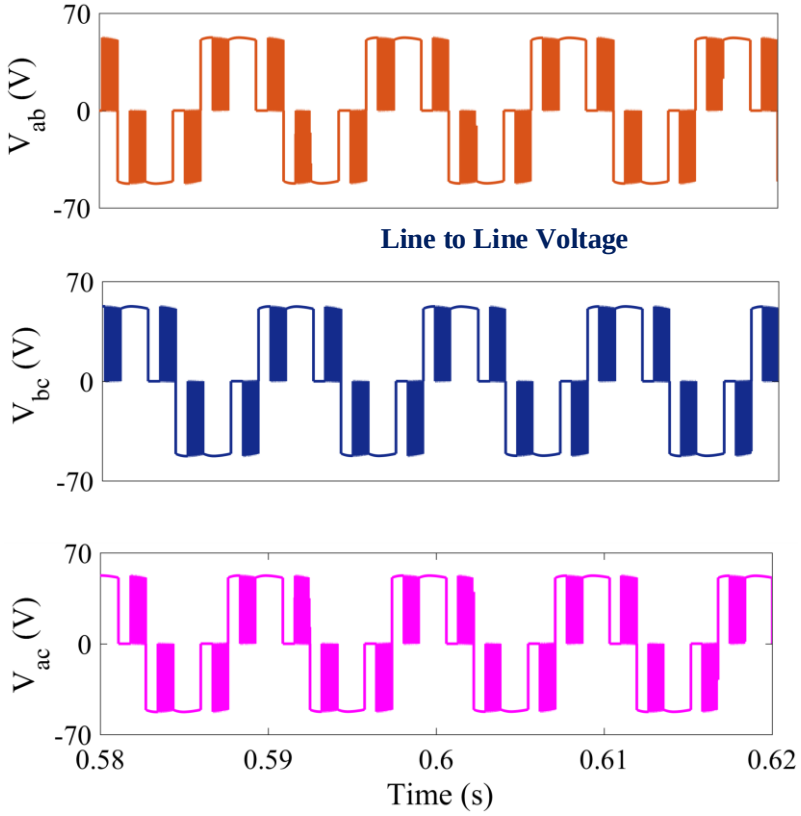

(a)

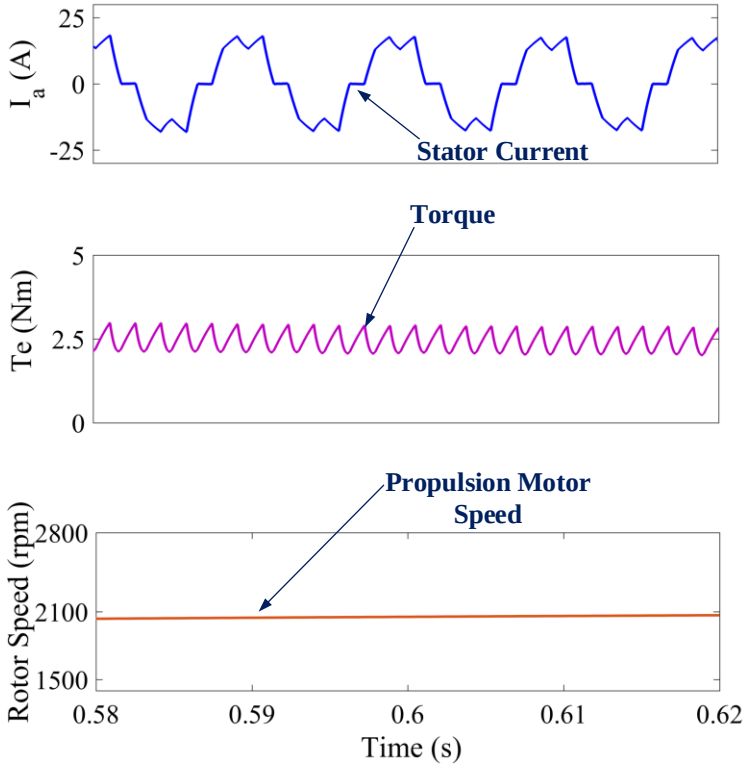

(b)

Figure 7.15. Simulated waveform of BLDC motor (a) (V_{ab}, V_{bc}, V_{ac}), (b) $(I_a, Te, Rotor\ Speed)$.

Referring to Figure 7.16 diagrammatic of CHIL (controller hardware in the Loop) test with algorithm is given. Various test results are performed in this setup as referred in Figure7.17-

7.21. This section explained the G2V operations, on-board solar PV-based charging, and BLDC motor operation.

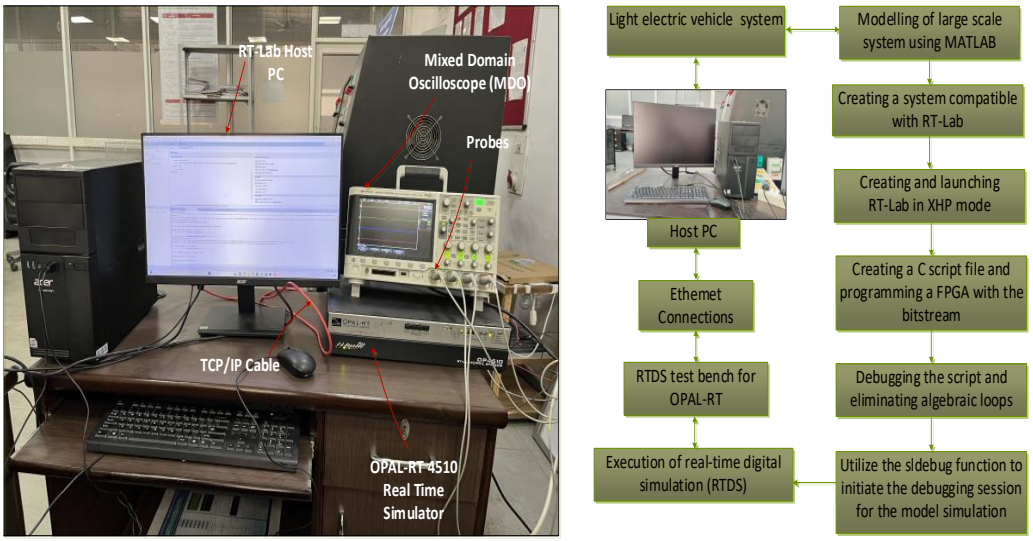

Figure 7.16. Real-time CHIL test setup.

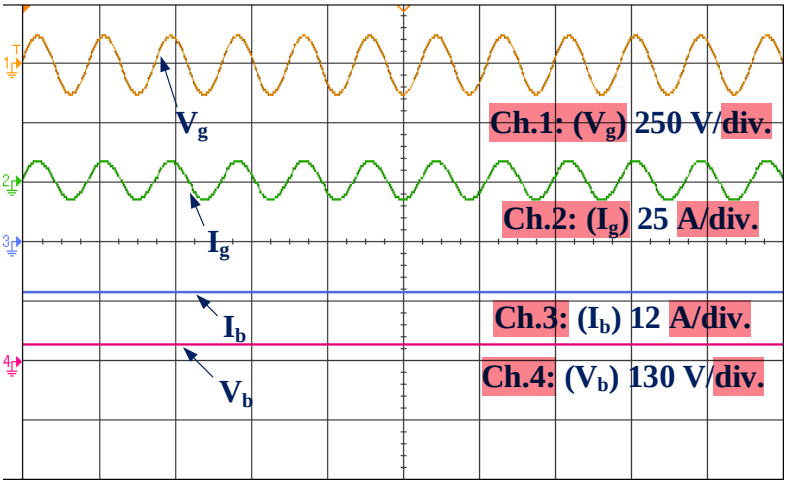

Figure 7.17. Experimental performance of LEV charging (V_g, I_g, I_b, V_b).

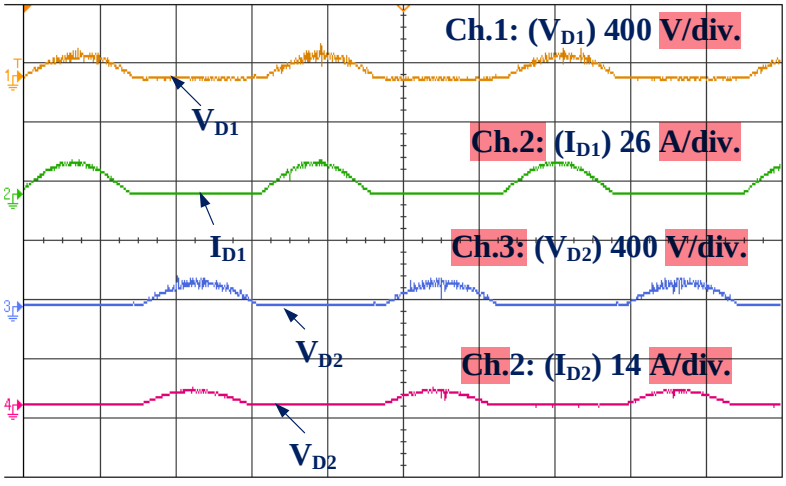

Figure 7.18. Experimental Performance across the diodes $(V_{D1}, I_{D1}, V_{D2}, V_{D2})$.

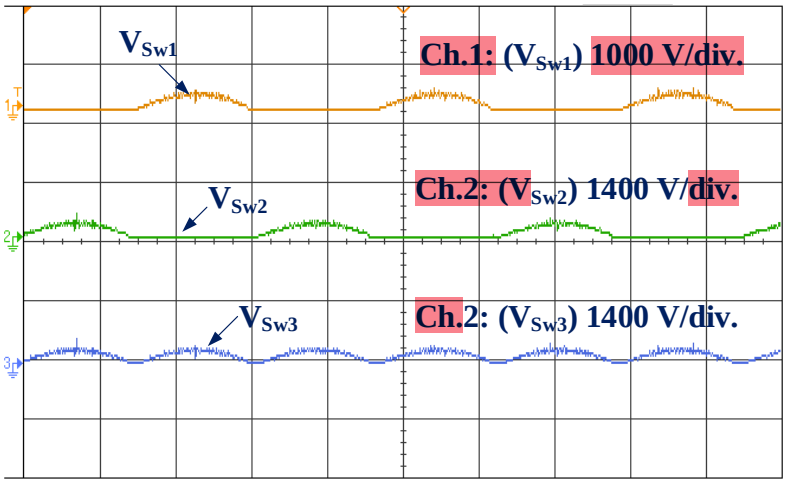

Figure 7.19. Experimental Performance across the switches $(V_{SW1}, V_{SW2}, V_{SW3})$.

7.7.2.1 *Grid Based Charging Performance*

Figure 7.17 illustrates the UPF operations between grid voltage V_g and grid current I_g during G2V mode. The LEV battery charging operation parameters like grid voltage V_g, grid current I_g, battery current I_b, and battery voltage V_b. Figure 7.18 illustrates the voltages and current across the diodes. Figure 7.19 illustrates the voltage across the switches.

7.7.2.1 *Solar PV Based Charging Performance*

In Figure 7.20 the performance of on-board solar PV based charging is validated, like change in irradiance, PV voltage (V_{pv}), battery current I_b, and battery voltage V_b.

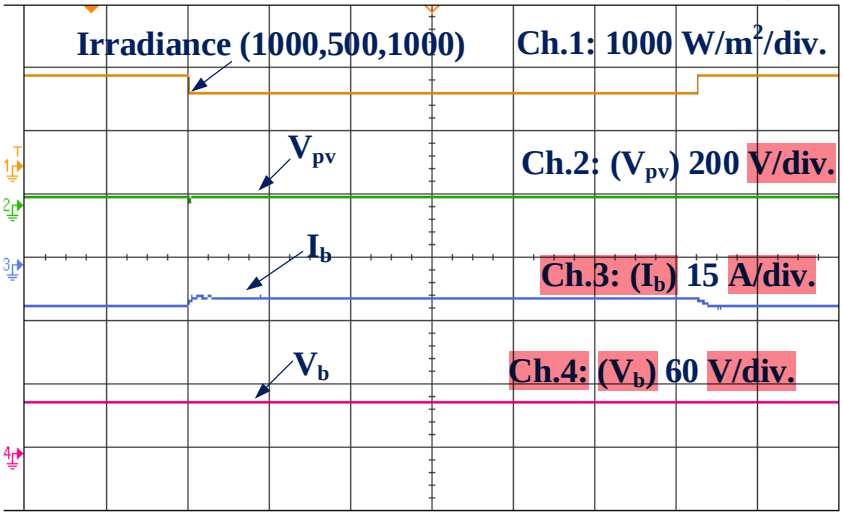

Figure 7.20. Experimental performance of on-board Solar PV array-based LEV charging $(Irradiance, V_{pv}, I_b, V_b)$.

7.7.2.2 *Brushless DC Motor Performance*

Figure 7.21(a), brushless DC motor performance in propulsion mode is validated, like line-line voltages (V_{ab}, V_{bc}, and V_{ac}) of all three phases, the stator current (I_a), motor torque and rotor speed in propulsion as shown in Figure 7.21(b). This validation demonstrates the effectiveness of the BLDC motor control strategy in achieving smooth and stable operation.

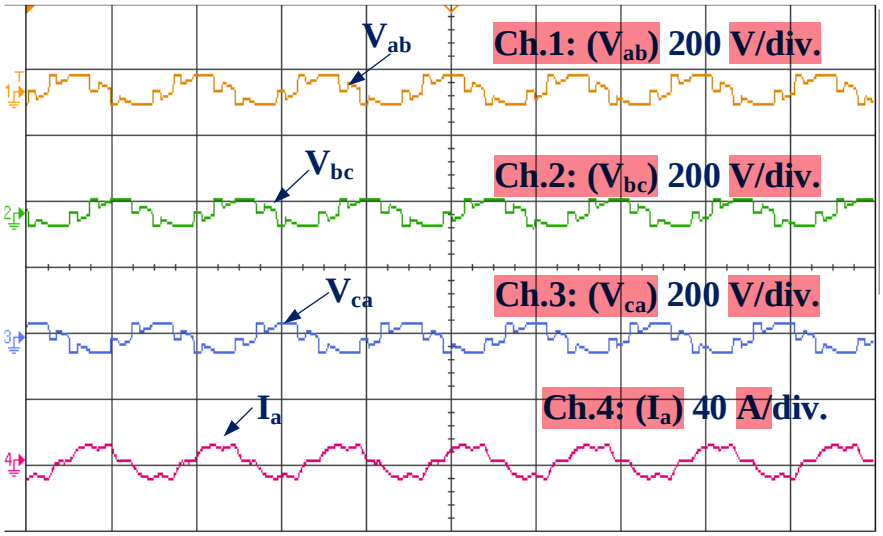

(a)

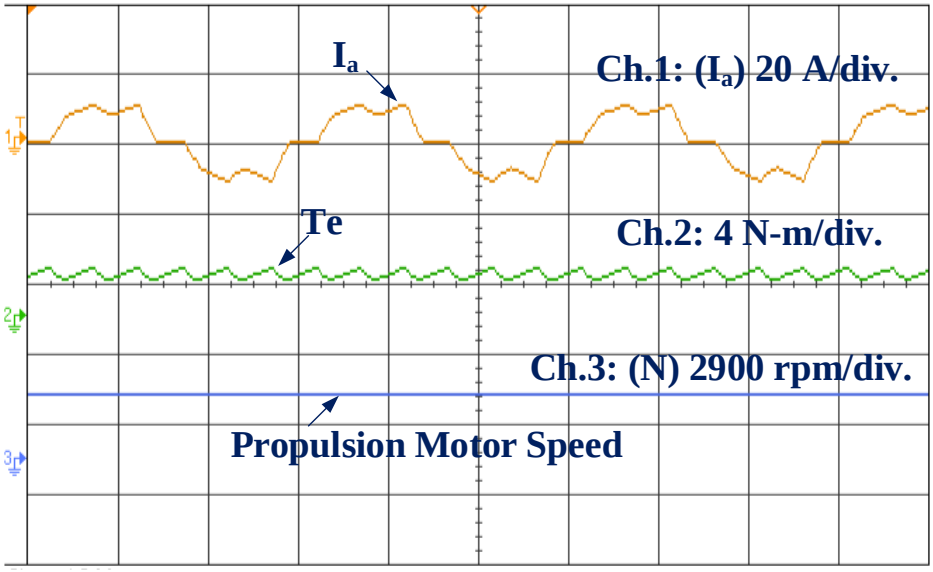

(b)

Figure 7.21. Experimental Performance of BLDC motor in propulsion mode (a) $(V_{ab}, V_{bc}, V_{ca}, I_a,)$, (b) $(I_a, Te, Propulsion\ Motor\ Speed)$

7.8 Losses and Efficiency Calculation

The voltage & current stresses handle via various components of the developed bridgeless LEV charger are examined to ensure its safe, reliable, and efficient operation. The system performance is verified by performing power loss manipulations. The losses in diodes, capacitors, switches, inductors are considered as power losses in converters as shown in Figure 22. The mathematical formulations (7.15)-(7.22) explain the calculation of power losses and efficiency of the proposed system given as follows,

Switches $(S_1 - S_2)$ conduction losses (P_{closs}):

$$2\left(V_{CEO}.I_{Q1avg.} + r_{CE}.I_{Q1rms}^2\right) \quad (7.15)$$

Switches $(S_1 - S_2)$ switching losses (P_{swloss}):

$$2\left(V_{Q1max}.I_{Q1avg.}\left(t_r + t_f\right).f_s\right) \quad (7.16)$$

Switches (S_3) switching losses (P_{swloss}):

$$\left(V_{Q1max}.I_{Q1avg.}\left(t_r + t_f\right).f_s\right) \quad (7.17)$$

Input Inductor Losses $(P_{L_{sloss}})$:

$$I_{L_s}^2 rms \cdot r_{L_s} \quad (7.18)$$

Output Inductors Losses $(P_{L_{oloss}})$:

$$2 \cdot I_{L_0}^2 rms \cdot r_{L_0} \quad (7.19)$$

Intermediate Capacitor Losses $(P_{C_{Iloss}})$:

$$2 \cdot I_{C_I}^2 rms \cdot ESR_{C_I} \quad (7.20)$$

The total power loss of the proposed converter is given in equation (7.21) and 97.67% efficiency of the converter for the output power of 720W is calculated by using the Equation (7.22).

$$P_{loss}^{Total} = P_{closs} + P_{swloss} + P_{sdloss} + P_{cdloss} + P_{L_{sloss}} + P_{L_{oloss}} + P_{C_{Iloss}} \quad (7.21)$$

$$\text{Efficiency } (\eta) = \frac{P_0}{P_0 + P_{loss}^{Total}} \quad (7.22)$$

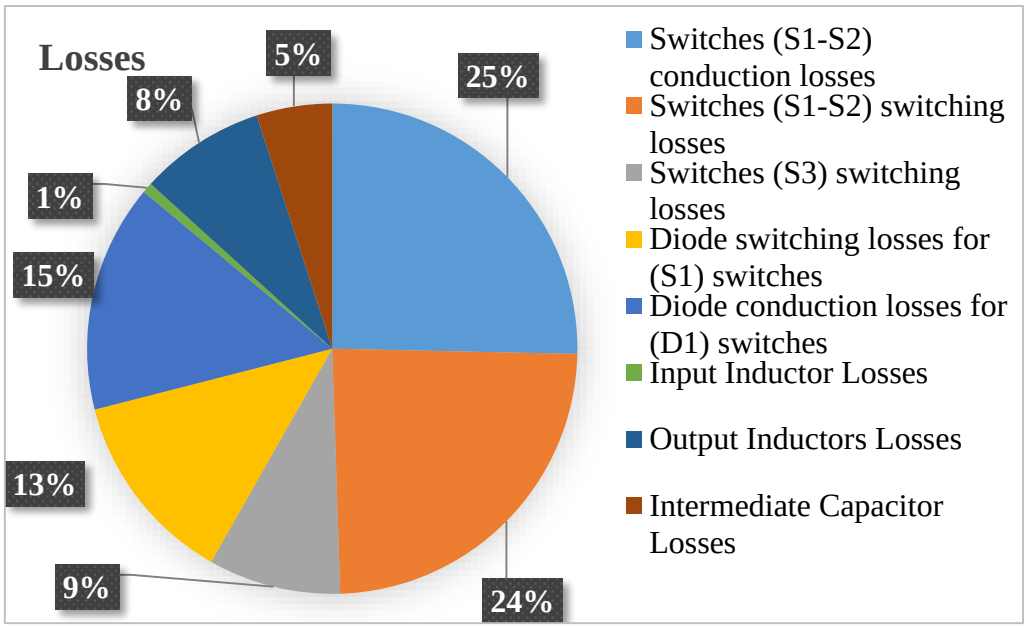

Figure 7.22. Graphical representation of power losses in the developed LEV charging system.

7.9 Conclusion

The proposed solar-powered on-board charging system utilizing a bridgeless Modified SEPIC converter demonstrates effective charging operation. The single-stage design of bridgeless converters reduces the size of passive components, making them more suitable for compact applications such as on-board LEV chargers. In the event of a grid outage, an integrated solar photovoltaic (PV) system efficiently charges the LEV battery using a Maximum Power Point Tracking (MPPT) converter, adapting to varying environmental conditions. Moreover, the unity power factor operation is also achieved in charging mode. The designed system offers soft-starting features of the BLDC drive in propulsion mode without using any current and voltage sensors on the motor side. The control technique is well-suited for a 48V, 50 Ah LEV battery, as verified through MATLAB simulations and real-time validation using Opal-RT.

CHAPTER-8

CONCLUSIONS AND FUTURE SCOPE

8.1 General

The main objective of this research work is to design and develop different converter strategies for light electric vehicle (LEV) charging with dual power sources such as single-phase grid and solar PV array. The developed charging strategies have been classified into three categories, viz., non-isolated, isolated, and bridgeless converters. The developed configurations with single-stage and two-stage operation, such as AC-to-DC and DC-to-DC, with improved control techniques efficiently charge the LEV battery. The active front-end converter (AFC) with PLL, IMSTOGI controller, performs power factor correction (PFC) and eliminates harmonics in grid current. Further, the high-gain DC-to-DC converters with CC-CV controller perform step-down (LEV charging) and step-up (LEV discharging) operations. Moreover, the on-board solar PV with MPPT converters successfully charges the LEV battery during the grid outage. The work has also presented a brushless DC (BLDC) motor operation in propulsion mode without using any current and voltage sensors on the motor side. The power management of the system has been controlled in such a manner to achieve grid-to-vehicle (G2V) and vehicle-to-grid (V2G) as well as solar PV-based LEV charging. The developed systems have fewer component counts, higher efficiency, and a high payback time.

8.2 Main Conclusions

The conclusions for each thesis chapter are summarized in the following bullet points.

- Initially, the classifications and configurations of various converter strategies integrated with dual energy sources for charging light electric vehicles (LEVs) have been discussed. The strategies have been classified as unidirectional and bidirectional DC-to-DC converters. These converters have been further divided into non-isolated, isolated, and bridgeless ones. Solar-powered on-board charging systems for Light Electric Vehicles (LEVs), integrating both unidirectional and bidirectional converter strategies, demonstrate effective and reliable performance across various operating conditions.
- Moreover, the proposed system has been developed using a Modified Single-Ended Primary-Inductor Converter (SEPIC) converter strategy to charge a Light Electric Vehicle (LEV). A diode bridge rectifier has been used to convert AC to DC from the

AC mains. An improved CC-CV control technique has been developed to ensure robust operation of the converter, maintaining unity power factor (UPF) operation. In the event of a grid outage, an integrated solar photovoltaic (PV) system efficiently charges the LEV battery using a Maximum Power Point Tracking (MPPT) converter, adapting to varying environmental conditions. The modified SEPIC converter manages LEV charging, emphasizing enhanced efficiency, low conduction losses, reduced component count, and high gain. The designed system offers soft-starting features of the BLDC drive in propulsion mode without using any current and voltage sensors on the motor side.

- Also, the proposed solar-powered on-board charging system has utilized a coupled inductor and switched capacitor bidirectional high-gain DC-to-DC converter with Grid-to-Vehicle (G2V) and Vehicle-to-Grid (V2G) operations. An on-board charger (OBC) design consists of an active front-end converter (AFC), firstly with a proposed coupled inductor bidirectional high-gain SEPIC converter, and secondly with a proposed switched capacitor bidirectional high-gain ZETA converter. The AFC has restricted the THD of supply current within the limits specified in international standards. In a grid outage, an integrated solar photovoltaic (PV) system efficiently charges the LEV battery using a Maximum Power Point Tracking (MPPT) converter, adapting to varying environmental conditions. In addition, the brushless DC (BLDC) motor has been used as a traction motor in this work due to its unique features such as high density, low cost, simple control, etc.
- Thereafter, this work has introduced the design and implementation of a high-efficiency bidirectional isolated integrated DC-to-DC converter intended for the optimal charging and discharging of Light Electric Vehicle (LEV) batteries, utilizing dual power sources. The proposed system supports both Grid-to-Vehicle (G2V) and Vehicle-to-Grid (V2G) operations, ensuring stable performance even during grid voltage disturbances, including sags, swells, and outages. To enhance robustness, an advanced mixed second-order–third-order generalized integrator (IMSTOGI) control algorithm has been introduced to facilitate reliable operation of the Active Front-End Converter (AFC) under grid disturbances. During normal grid conditions, the converter ensures unity power factor (UPF) and constant current performance. In the event of a grid outage, an integrated solar photovoltaic (PV) system efficiently charges the LEV battery using a Maximum Power Point Tracking (MPPT) converter, adapting to varying environmental

conditions. The functionality and power management strategy of the system are validated through real-time experiments, showcasing its effectiveness, reliability, and potential for seamless integration with smart grids and renewable energy sources.

- Subsequently, this work has introduced the design and implementation of a modified bridgeless SEPIC AC-to-DC converter topology with single-stage operations to facilitate LEV charging. The developed system utilizes two energy sources, solar PV and the single-phase grid. In a grid outage, an integrated solar photovoltaic (PV) system efficiently charges the LEV battery using a Maximum Power Point Tracking (MPPT) converter, adapting to varying environmental conditions. The developed bridgeless converter manages LEV charging, emphasizing enhanced efficiency, low conduction losses, reduced component count, and high gain. The designed system offers soft-starting features of the BLDC drive in propulsion mode without using any current and voltage sensors on the motor side.
- The performance of the 48V and 50Ah lithium-ion LEV battery system has been tested using MATLAB simulations and validated through a hardware prototype on OPAL-RT. The results have been observed and it demonstrate the effectiveness of the proposed converter strategies in this research work.

In summary, integrating these advanced converter strategies in LEV charging systems presents a balanced solution combining high efficiency, cost-effectiveness, and higher payback time. These have been tested successfully on a 48V, 50Ah battery platform, to validate the potential for widespread adoption of LEVs powered by dual sources, viz., the grid and solar-PV sources. Their low component count, efficient power conversion, PFC compliance, and flexible G2V and V2G operation collectively contribute to a future-ready, eco-friendly transportation ecosystem that supports the global transition toward renewable energy and smart grid technologies.

8.3 Suggestions for Further Work

Light electric vehicle (LEV) charging strategies have advanced significantly, but more study and implementation is needed in a converter and control strategies to improve the LEV charging system. The investigation and hardware implementation of more economical, compact, and efficient converter strategies is a crucial area for future research.

- In future work implementation of LEV charging systems capable of interfacing with smart grids and implementing demand response protocols, and remote monitoring for intelligent LEV charging management.

- Design and development of converter topologies that can seamlessly integrate grid power with fuel cell, solar PV and hydrogen energy for sustainable LEV charging solutions.
- Implementation of Advanced control strategies to optimize charger performance, ensure battery safety, and improve power quality.
- Design and development of converters integrated with communication protocols and smart grid interfaces.

REFERENCES

[1] C. Mi and M. A. Masrur, "Hybrid Electric Vehicles: Principles and Applications with Practical Perspectives," 2nd ed. Hoboken, NJ, USA: John Wiley & Sons, 2017.

[2] T. Muneer, M. L. Kolhe, and A. Doyle, "Electric Vehicles: Prospects and Challenges," Amsterdam, Netherlands: Elsevier, 2017.

[3] V. Gali, L. N. Canha, M. Resener, B. Ferraz, and M. V. G. Varaprasad, "Advanced Technologies in Electric Vehicles: Challenges and Future Research Developments," 1st ed. Amsterdam, The Netherlands: Elsevier (Academic Press), 2024.

[4] N. Patel, A. K. Bhoi, S. Padmanaban, and J. B. Holm-Nielsen, "Electric Vehicles: Modern Technologies and Trends,"1st ed. Singapore: Springer Nature Singapore, 2021.

[5] T. S. Babu, P. K. Balachandran, and N. Nwulu, "Renewable Energy for Plug-In Electric Vehicles: Challenges, Approaches, and Solutions for Grid Integration," Elsevier, 2024.

[6] K. T. Chau, "Electric Vehicle Machines and Drives: Design, Analysis and Application," Singapore: John Wiley & Sons, Ltd, 2015.

[7] A. Kumar, "Smart charging algorithms for electric vehicle integration with renewable energy sources," Ph.D. dissertation, *Dept. Elect. Eng.*, Massachusetts Institute of Technology, Cambridge, MA, USA, 2020.

[8] M. S. Chen, "Advanced converter topologies for high-efficiency electric vehicle battery chargers," Ph.D. dissertation, *Dept. Elect. Eng.*, University of Michigan, Ann Arbor, MI, USA, 2021.

[9] R. Kumar, "Modeling and control of BLDC motors for electric vehicle applications," M.S. thesis, *Dept. Elect. Eng.*, Indian Institute of Technology, Delhi, India, 2020.

[10] U. Sharma and B. Singh, "An Onboard Charger for Light Electric Vehicles," *9th IEEE Int. Conf. Power Electron. Drives Energy Syst. PEDES 2020*, vol. 2, pp. 1-6, 2020.

[11] M. Yilmaz and P. T. Krein, "Review of Battery Charger Topologies, Charging Power Levels, and Infrastructure for Plug-in Electric and Hybrid Electric Vehicles," *IEEE Trans. Power Electron.*, vol. 28, no. 5, pp. 2151-2169, 2013.

[12] X. Zhang and Z. Li, "Sliding-Mode Observer-Based Mechanical Parameter Estimation for Permanent Magnet Synchronous Motor," *IEEE Trans. Power Electron.*, vol. 31, no. 8, pp. 5732-5745, 2016.

[13] M. Kesler, M. C. Kisacikoglu, and L. M. Tolbert, "Vehicle-to-Grid Reactive Power Operation Using Plug-in Electric Vehicle Bidirectional Offboard Charger," *IEEE Trans.*

Ind. Electron., vol. 61, no. 12, pp. 6778-6784, 2014.

[14] S. M. Arif, T. T. Lie, B. C. Seet, S. Ayyadi, and K. Jensen, "Review of electric vehicle technologies, charging methods, standards and optimization techniques," *Electronics*, vol. 10, no. 16, pp. 1–21, 2021.

[15] M. Yilmaz and P. T. Krein, "Review of Battery Charger Topologies, Charging Power Levels, and Infrastructure for Plug-in Electric and Hybrid Vehicles," *IEEE Trans. Power Electron.*, vol. 28, no. 5, pp. 2151-2169, 2013.

[16] Narula and V. Verma, "Bi – directional Trans – Z Source Boost Converter for G2V/V2G Applications," *IEEE Transportation Electrification Conference (ITEC-India)*, pp. 1-6, 2017.

[17] M. Ahmadi, N. Mithulananthan and R. Sharma, "A Review on Topologies for Fast Charging Stations for Electric Vehicles," *IEEE International Conference on Power System Technology (POWERCON)*, pp. 1-6, 2016.

[18] J. C. Mukherjee and A. Gupta, "A Review of Charge Scheduling of Electric Vehicles in Smart Grid," *IEEE Syst. J.*, vol. 9, no. 4, pp. 1541-1553, 2015.

[19] K. M. Tan, V. K. Ramachandaramurthy and J. Y. Yong, "Bidirectional Battery Charger for Electric Vehicle," 2014 IEEE Innovative Smart Grid Technologies - Asia (ISGT ASIA), 2014, pp. 406-411.

[20] M. Fatnani, Di. Naware, and A. Mitra, "Design of Solar PV Based EV Charging Station with Optimized Battery Energy Storage System," *Proc. 2020 IEEE 1st Int. Conf. Smart Technol. Power, Energy Control. STPEC 2020*, 2020.

[21] B. Singh, A. Verma, A. Chandra, and K. Al-Haddad, "Implementation of Solar PV-Battery and Diesel Generator Based Electric Vehicle Charging Station," *IEEE Trans. Ind. Appl.*, vol. 56, no. 4, pp. 4007-4016, 2020.

[22] M. Fatnani, Di. Naware, and A. Mitra, "Design of Solar PV Based EV Charging Station with Optimized Battery Energy Storage System," *Proc. 2020 IEEE 1st Int. Conf. Smart Technol. Power, Energy Control. STPEC 2020*, 2020.

[23] T. Porselvi, J. Nisha., K. Thendral, and D. P. Vasantha, "Solar PV Fed Electric Vehicle Charging System with Hybrid Energy Storage System," 2019 International Conference on Computation of Power, Energy, Information and Communication (ICCPEIC), 2019, pp. 202-206.

[24] G. G. Rao and R. Gupta, "Standalone PV based Boost Derived Hybrid Converter for EV Charging Applications," *IECON Proc. (Industrial Electron. Conf.*, vol. 2021-October, 2021.

[25] N. Mohamed, F. Aymen, Z. M. Ali, A. F. Zobaa, and S. H. E. Abdel Aleem, "Efficient

Power Management Strategy of Electric Vehicles based Hybrid Renewable Energy," *Sustain.*, vol. 13, no. 13, 2021.

[26] M. Karki, D. R. Kunwar, B. Sharma, S. Paudel, and T. N. Ojha, "Power Flow Management among PV, BESS and Grid for EV Charging," *Tech. J.*, vol. 1, no. 1, pp. 102-112, 2019.

[27] F. Un-Noor, S. Padmanaban, L. Mihet-Popa, M. N. Mollah, and E. Hossain, "A Comprehensive Study of Key Electric Vehicle (EV) Components, Technologies, Challenges, Impacts, and Future Direction of Development," *Energies*, vol. 10, no. 8, 2017.

[28] Larminie James, Lowry John, Electric Vechile Technology Explained. Chichester, John Wiley and Sons Ltd, 2003.

[29] Z. Cao, A. Mahmoudi, S. Kahourzade, and W. L. Soong, "An Overview of Electric Motors for Electric Vehicles," *Proc. 2021 31st Australas. Univ. Power Eng. Conf. AUPEC 2021*, 2021.

[30] L. Shao, A. E. H. Karci, D. Tavernini, A. Sorniotti and M. Cheng, "Design Approaches and Control Strategies for Energy-Efficient Electric Machines for Electric Vehicles-A Review," *IEEE Access*, vol. 8, pp. 116900-116913, 2020.

[31] N. Hashemnia and B. Asaei, "Comparative study of using different electric motors in the electric vehicles," *International Conference on Electrical Machines*, pp. 1-5, 2008.

[32] Cao, W., Bukhari, A. A. S., & Aarniovuori, L, "Review of Electrical Motor Drives for Electric Vehicle Applications". *Mehran University Research Journal of Engineering & Technology*, vol. 38, no. 3, pp. 525-540, 2019.

[33] K. Rajashekara, "Present Status and Future Trends in Electric Vehicle Propulsion Technologies," *IEEE J. Emerg. Sel. Top. Power Electron.*, vol. 1, no. 1, pp. 3-10, 2013.

[34] M. Bazzi, A. P. Friedl, S. Choi, and P. T. Krein, "Comparison of Induction Motor Drives for Electric Vehicle Applications: Dynamic Performance and Parameter Sensitivity Analyses," *2009 IEEE Int. Electr. Mach. Drives Conf. IEMDC '09*, pp. 639-646, 2009.

[35] S. Gunther, S. Ulbrich, and W. Hofmann, "Driving Cycle-Based Design Optimization of Interior Permanent Magnet Synchronous Motor Drives for Electric Vehicle Application," *2014 Int. Symp. Power Electron. Electr. Drives, Autom. Motion, SPEEDAM 2014*, pp. 25-30, 2014.

[36] M. Ying and P. Zaiping, "A Novel Starting Method of Sensorless BLDC Motors for Electric Vehicles," *Proc. - Int. Conf. Electr. Control Eng. ICECE 2010*, pp. 3212-3215, 2010.

[37] Y. Anekunu, S. P. Chowdhury, and S. Chowdhury, "A Review of Research and Development on Switched Reluctance Motor for Electric Vehicles," *IEEE Power Energy Soc. Gen. Meet.*, 2013.

[38] S. S. Sayed and A. M. Massoud, "Review on State-of-the-Art Unidirectional Non-Isolated Power Factor Correction Converters for Short-/Long-Distance Electric Vehicles," *IEEE Access*, vol. 10, pp. 11308-11340, 2022.

[39] B. Saikumar and S. Balamurugan, "Dual-Input Single-Output Non-Isolated DC-DC Converter for GIHEVs," *3rd IEEE Int. Virtual Conf. Innov. Power Adv. Comput. Technol. i-PACT 2021*, pp. 1-5, 2021.

[40] K. Suresh *et al.*, "A Multifunctional Non-Isolated Dual Input-Dual Output Converter for Electric Vehicle Applications," *IEEE Access*, vol. 9, pp. 64445-64460, 2021.

[41] C. C. Lin, L. S. Yang, and G. W. Wu, "Study of a Non-Isolated Bidirectional DC-DC Converter," *IET Power Electron.*, vol. 6, no. 1, pp. 30-37, 2013.

[42] F. Akar, Y. Tavlasoglu, E. Ugur, B. Vural, and I. Aksoy, "A Bidirectional Nonisolated Multi-Input DC-DC Converter for Hybrid Energy Storage Systems in Electric Vehicles," *IEEE Trans. Veh. Technol.*, vol. 65, no. 10, pp. 7944-7955, 2016.

[43] M. Abbasi, E. Babaei, and B. Tousi, "New Family of Non-Isolated Step-up/down and Step-up Switched-Capacitor-Based DC-DC Converters," *IET Power Electron.*, vol. 12, no. 7, pp. 1706-1720, 2019.

[44] T. Buck, B. Dc, and D. C. Converter, "A Novel Structure for Single-Switch Nonisolated," *IEEE Trans. Power Electron.*, vol. 64, no. 1, pp. 198-205, 2017.

[45] F. L. Tofoli, D. de C. Pereira, W. J. de Paula, and D. de S. Oliveira Júnior, "Survey on Non-Isolated High-Voltage Step-up DC-DC Topologies Based on the Boost Converter," *IET Power Electron.*, vol. 8, no. 10, pp. 2044-2057, 2015.

[46] K. Varesi, S. Hossein Hosseini, M. Sabahi, E. Babaei, S. Saeidabadi and N. Vosoughi, "Design and Analysis of a Developed Multiport High Step-Up DC-DC Converter with Reduced Device Count and Normalized Peak Inverse Voltage on the Switches/Diodes," *IEEE Transactions on Power Electronics*, vol. 34, no. 6, pp. 5464-5475, 2019.

[47] X. F. Cheng, C. Liu, D. Wang, and Y. Zhang, "State-of-the-Art Review on Soft-Switching Technologies for Non-Isolated DC-DC Converters," *IEEE Access*, vol. 9, pp. 119235-119249, 2021.

[48] M. R. Mohammadi and H. Farzanehfard, "A New Family of Zero-Voltage-Transition Nonisolated Bidirectional Converters with Simple Auxiliary Circuit," *IEEE Trans. Ind.*

Electron., vol. 63, no. 3, pp. 1519-1527, 2016.

[49] Bhaskar, M. S., Ramachandaramurthy, V. K., Padmanaban, S., Blaabjerg, F., Ionel, D. M., Mitolo, M., & Almakhles, D. Survey of DC-DC Non-isolated Topologies for Unidirectional Power Flow in Fuel Cell Vehicles, *IEEE Access*, vol. 8, pp. 178130-178166, 2020.

[50] J. Anzola, I. Aizpuru, and A. Arruti, "Non-Isolated Partial Power Converter for Electric Vehicle Fast Charging Stations," *2020 IEEE 11th Int. Symp. Power Electron. Distrib. Gener. Syst. PEDG 2020*, pp. 18-22, 2020.

[51] S. W. Choi, S. T. Oh, M. W. Kim, I. O. Lee, and J. Y. Lee, "Interleaved Isolated Single-Phase PFC Converter Module for Three-Phase EV Charger," *IEEE Trans. Veh. Technol.*, vol. 69, no. 5, pp. 4957-4967, 2020.

[52] U. R. Prasanna, A. K. Singh, and K. Rajashekara, "Novel Bidirectional Single-phase Single-Stage Isolated AC-DC Converter with PFC for Charging of Electric Vehicles," *IEEE Trans. Transp. Electrif.*, vol. 3, no. 3, pp. 536-544, 2017.

[53] U. R. Prasanna, A. K. Rathore, and S. Member, "Novel Zero-Current-Switching Current-Fed Half-Bridge Isolated DC-DC Converter for Fuel Cell Vehicles," *IEEE Transactions on Industry Applications*, vol. 49, no. 4, pp. 1658-1668, 2013.

[54] P. Xuewei and A. K. Rathore, "Novel Bidirectional Snubberless Naturally Commutated Soft-Switching Current-Fed Full-Bridge Isolated DC-DC Converter for Fuel Cell Vehicles," *IEEE Trans. Ind. Electron.*, vol. 61, no. 5, pp. 2307-2315, 2014.

[55] W. S. Lee, J. H. Kim, J. Y. Lee, and I. O. Lee, "Design of an Isolated DC/DC Topology with High Efficiency of over 97% for EV Fast Chargers," *IEEE Trans. Veh. Technol.*, vol. 68, no. 12, pp. 11725-11737, 2019.

[56] P. He and A. Khaligh, "Comprehensive Analyses and Comparison of 1 kW Isolated DC-DC Converters for Bidirectional EV Charging Systems," *IEEE Trans. Transp. Electrif.*, vol. 3, no. 1, pp. 147-156, 2017.

[57] Y. Tang, J. Lu, B. Wu, S. Zou, W. Ding, and A. Khaligh, "An Integrated Dual-Output Isolated Converter for Plug-in Electric Vehicles," *IEEE Trans. Veh. Technol.*, vol. 67, no. 2, pp. 966-976, 2018.

[58] S. N. Vaishnav and H. Krishnaswami, "Single-Stage Isolated Bi-Directional Converter Topology Using High Frequency AC Link for Charging and V2G Applications of PHEV," *2011 IEEE Veh. Power Propuls. Conf. VPPC 2011*, pp. 9-12, 2011.

[59] B. Koushki, P. Jain, and A. Bakhshai, "Topology and Controller of an Isolated Bi-Directional AC-DC Converter for Electric Vehicle," *ECCE 2016 - IEEE Energy Convers.*

Congr. Expo. Proc., 2016.

[60] V. M. Thasni, P. C. Unnikrishnan, and R. Rajagopal, "Single Phase Isolated Converter for Light Electric Vehicle Charging with PFC and Battery Protection," *Proc. Int. Conf. Inven. Commun. Comput. Technol. ICICCT 2018*, vol 6, Icicct, pp. 1721-1726, 2018.

[61] M. Nassary, M. Orabi, M. Ghoneima, and M. K. El-Nemr, "Single-Phase Isolated Bidirectional AC-DC Battery Charger for Electric Vehicle-Review," *Proc. 2019 Int. Conf. Innov. Trends Comput. Eng. ITCE 2019*, vol 10, February, pp. 581-586, 2019.

[62] H. Nazi, E. Babaei, S. Tohidi and M. Liserre, "An Isolated SRC-Based Single Phase Single Stage Battery Charger for Electric Vehicles," *IEEE Trans. Transp. Electri.*, 2022.

[63] R. Kushwaha, B. Singh, and V. Khadkikar, "An Isolated Bridgeless Cuk-SEPIC Converter-Fed," *IEEE Trans. Power Electron*, vol. 58, no. 2, pp. 2512-2526, 2022.

[64] B. Singh and R. Kushwaha, "An EV Battery Charger with Power Factor Corrected Bridgeless Zeta Converter Topology," *India Int. Conf. Power Electron. IICPE*, vol. 12, no.2, pp. 1-6, 2016.

[65] J. Gupta and B. Singh, "Based High Power Factor Single Stage Charging Solution for Light Electric Vehicles,"*IEEE Trans. Ind. Appl.*, vol. 58, no. 1, pp. 732-741, 2022.

[66] Dixit, K. Pande, S. Gangavarapu, and A. K. Rathore, "DCM-Based Bridgeless PFC Converter for EV Charging Application," *J. Emerg. Sel. Top. Ind. Electron.*, vol. 1, no. 1, pp. 57-66, 2020.

[67] R. Kushwaha and B. Singh, "A Power Quality Improved EV Charger with Bridgeless Cuk Converter," *IEEE Trans. Ind. Appl.*, vol. 55, no. 5, pp. 5190-5203, 2019.

[68] B. Singh and R. Kushwaha, "A PFC Based EV Battery Charger Using a Bridgeless Isolated SEPIC Converter," *IEEE Trans. Ind. Appl.*, vol. 56, no. 1, pp. 477-487, 2020.

[69] H. Wang, S. Dusmez, and A. Khaligh, "Design and Analysis of a Full-Bridge LLC-Based PEV Charger Optimized for Wide Battery Voltage Range," *IEEE Trans. Veh. Technol.*, vol. 63, no. 4, pp. 1603-1613, 2014.

[70] F. Musavi, W. Eberle, and W. G. Dunford, "A High-Performance Single-Phase Bridgeless Electric Vehicle Battery Chargers," *IEEE Trans. Power Electron.,* vol. 47, no. 4, pp. 1833-1843, 2011.

[71] G. K. N. Kumar and A. K. Verma, "A Two-Stage Interleaved Bridgeless PFC based On-Board Charger for 48V EV Applications," *Proc. IEEE Energy Convers. Congr. Expo. (ECCE)*, pp. 1-4, 2021.

[72] J. Gupta, R. Kushwaha, and B. Singh, "Improved Power Quality Transformerless Single-Stage Bridgeless Converter Based Charger for Light Electric Vehicles," *IEEE Trans. Ind.*

Electron., vol. 36, no. 7, pp. 7716-7724, 2021.

[73] M. E. Kabir, S. Member, and C. Assi, "Optimal Scheduling of EV Charging at a Solar Power-Based Charging Station," *IEEE Trans. Smart Grid*, vol. 14, no. 3, pp. 4221-4231, 2020.

[74] Verma, B. Singh, A. Chandra, and K. Al Haddad, "An Implementation of Solar PV Array-Based Multifunctional EV Charger," *IEEE Trans. Ind. Appl.*,vol. 56, no. 4, pp. 4166-4178, 2020.

[75] S. M. Shariff, M. S. Alam, F. Ahmad, Y. Rafat, M. S. J. Asghar, and S. Khan, "System Design and Realization of a Solar-Powered Electric Vehicle Charging Station," *IEEE Syst. J.*, vol. 14, no. 2, pp. 2748-2758, 2020.

[76] M. Haritha, T. Thomas, and S. Induja, "A solar PV array based multipurpose EV charger," *Int. J. Adv. Eng. Res. Sci.*, vol. 8, no. 9, pp. 89–94, Sep. 2021.

[77] H. Wu, Y. Xing, Y. Xia, and K. Sun, "A Family of Non-Isolated Three-Port Converters for Stand-Alone Renewable Power System," *IECON Proc. (Industrial Electron. Conf.*, vol. 3, pp. 1030-1035, 2011.

[78] K. Singh, M. Badoni, and Y. N. Tatte, "A Multifunctional Solar PV and Grid Based On-Board Converter for Electric Vehicles," *IEEE Trans. Veh. Technol.*, vol. 69, no. 4, pp. 3717-3727, 2020.

[79] D. Venkatramanan and V. John, "Dynamic Modeling and Analysis of Buck Converter Based Solar PV Charge Controller for Improved MPPT Performance," *IEEE Trans. Ind. Appl.*, vol. 55, no. 6, pp. 6234-6246, 2019.

[80] P. Shukl and B. Singh, "Electric Vehicle Charging Station for Solar PV Based Grid-Interactive System," *ICPS 2021 - 9th IEEE Int. Conf. Power Syst. Dev. Towar. Incl. Growth Sustain. Resilient Grid*, 2021.

[81] Hassoune, M. Khafallah, A. Mesbahi, and T. Bouragba, "Smart Topology of EVs in a PV-Grid System Based Charging Station," *Proc. 2017 Int. Conf. Electr. Inf. Technol. ICEIT 2017*, vol. 2018-January, pp. 1-6, 2018.

[82] R. K. Lenka, A. K. Panda, R. Patel, and J. M. Guerrero, "PV Integrated Multifunctional Off-Board EV Charger with Improved Grid Power Quality," *IEEE Trans. Ind. Appl.*, 2022.

[83] Y. Hu, C. Gan, W. Cao, Y. Fang, S. J. Finney, and J. Wu, "Solar PV-Powered SRM Drive for EVs with Flexible Energy Control Functions," *IEEE Trans. Ind. Appl.*, vol. 52, no. 4, pp. 3357-3366, 2016.

[84] S. K. Ram, S. Devassy, B. K. Verma, S. Mishra, and S. A. Akbar, "Review on Renewable

Energy Based EV Charging System with Grid Support Functionality," *2021 7th Int. Conf. Adv. Comput. Commun. Syst. ICACCS 2021*, pp. 482-487, 2021.

[85] K. Singh, A. K. Mishra, K. K. Gupta, P. Bhatnagar, and T. Kim, "An Integrated Converter with Reduced Components for Electric Vehicles Utilizing Solar and Grid Power Sources," *IEEE Trans. Transp. Electrif.*, vol. 6, no. 2, pp. 439-452, 2020.

[86] S. S. G. Acharige, M. E. Haque, M. T. Arif, N. Hosseinzadeh, and S. Saha, "A Solar PV Based Smart EV Charging System with V2G Operation for Grid Support," *Proc. 2021 31st Australas. Univ. Power Eng. Conf. AUPEC 2021*, pp. 1-6, 2021.

[87] M. Premchand and S. K. Gudey, "Solar Based Electric Vehicle Charging Circuit in G2V and V2G Modes of Operation," *2020 IEEE Students' Conf. Eng. Syst. SCES 2020*, 2020.

[88] M. O. Badawy and Y. Sozer, "Power Flow Management of a Grid Tied PV-Battery System for Electric Vehicles Charging," *IEEE Trans. Ind. Appl.*, vol. 53, no. 2, pp. 1347-1357, 2017.

[89] H. Chen, F. Lu, and F. Guo, "Power Management System Design for Small Size Solar-Electric Vehicle," *Conf. Proc. - 2012 IEEE 7th Int. Power Electron. Motion Control Conf. - ECCE Asia, IPEMC 2012*, vol. 4, pp. 2658-2662, 2012.

[90] T. S. Biya and M. R. Sindhu, "Design and Power Management of Solar Powered Electric Vehicle Charging Station with Energy Storage System," *Proc. 3rd Int. Conf. Electron. Commun. Aerosp. Technol. ICECA 2019*, pp. 815-820, 2019.

[91] P. K. Ray, A. Bharatee, S. Panda and I. N. W. Satiawan, "Modeling and Power Management of Electric Vehicle Charging System," *International Conference on Smart-Green Technology in Electrical and Information Systems (ICSGTEIS)*, pp. 100-105, 2021.

[92] L. Rosario, P. C. K. Luk, J. T. Economou and B. A. White, "A Modular Power and Energy Management Structure for Dual-Energy Source Electric Vehicles," *IEEE Vehicle Power and Propulsion Conference*, pp. 1-6, 2006.

[93] Y. Gurkaynak and A. Khaligh, "Control and Power Management of a Grid-connected Residential Photovoltaic System with Plug-in Hybrid Electric Vehicle (PHEV) load," *Conf. Proc. - IEEE Appl. Power Electron. Conf. Expo. - APEC*, no. 1, pp. 2086-2091, 2009.

[94] C. Swetha, N. S. Jayalakshmi, K. M. Bhargavi and P. B. Nempu, "Control Strategies for Power Management of PV/Battery System with Electric Vehicle," *2019 IEEE International Conference on Distributed Computing, VLSI, Electrical Circuits and Robotics (DISCOVER)*, pp. 1-6, 2019.

[95] K. K. Nandini, N. S. Jayalakshmi, and V. K. Jadoun, "Energy Management System for

PV Integrated Utility Grid with Electric Vehicle as Storage System," *2022 2nd Int. Conf. Power Electron. IoT Appl. Renew. Energy its Control. PARC 2022*, pp. 1-6, 2022.

[96] Hassoune, M. Khafallah, A. Mesbahi, and T. Bouragba, "Power Management Strategies of Electric Vehicle Charging Station based Grid-tied PV-battery System," *Int. J. Renew. Energy Res.*, vol. 8, no. 2, pp. 851-860, 2018.

[97] M. Ali, R. Shivapurkar, and D. Soffker, "Development and Improvement of a Situation-based Power Management Method for Multi-Source Electric Vehicles," *2018 IEEE Veh. Power Propuls. Conf. VPPC 2018 - Proc.*, pp. 1-6, 2019.

[98] X. D. Xue, K. W. E. Cheng, and N. C. Cheung, "Selection of Electric Motor Drives for Electric Vehicles," *2008 Australas. Univ. Power Eng. Conf. AUPEC 2008*, pp. 1-6, 2008.

[99] Tashakori and M. Ektesabi, "Fault Diagnosis of In-Wheel BLDC Motor Drive for Electric Vehicle Application," *IEEE Intell. Veh. Symp. Proc.*, no. 4, pp. 925-930, 2013.

[100] Azam, A. F. N., Jidin, A., Ngatiman, N. A., Jopri, M. H., Manap, M., Herlino, A. L., & Alias, N. F. Current control of BLDC drives for EV application. "*IEEE 7th International Power Engineering and Optimization Conference"* pp. 411-416, 2013.

[101] R. Shanmugasundram, K. Muhammad Zakariah, and N. Yadaiah, "Implementation and Performance Analysis of Digital Controllers for Brushless DC Motor Drives," *IEEE/ASME Trans. Mechatronics*, vol. 19, no. 1, pp. 213-224, 2014.

[102] F. L. Luo and H. G. Yeo, "Advanced PM Brushless DC Motor Control & System for Electric Vehicles," *Conf. Rec. - IAS Annu. Meet. (IEEE Ind. Appl. Soc.*, vol. 2, no. 65, pp. 1336-1343, 2000.

[103] Alphonse, S. HosiminThilagar, and F. Bright Singh, "Design of Solar-Powered BLDC Motor-Driven Electric Vehicle," *Int. J. Renew. Energy Res.*, vol. 2, no. 3, pp. 456-462, 2012.

[104] D. Mohanraj *et al.*, "A Review of BLDC Motor: State of Art, Advanced Control Techniques, and Applications," *IEEE Access*, vol. 10, pp. 54833-54869, 2022.

[105] L. Chu, M. C. Tsai, and H. Y. Chen, "Torque Control of Brushless DC Motors Applied to Electric Vehicles," *IEMDC 2001 - IEEE Int. Electr. Mach. Drives Conf.*, pp. 82-87, 2001.

[106] K. Lee and M. Ehsani, "Advanced BLDC Motor Drive for Low Cost and High Performance Propulsion System in Electric and Hybrid Electric Vehicles," *IEMDC 2001 - IEEE Int. Electr. Mach. Drives Conf.*, pp. 246-251, 2001.

[107] O. C. Kivanc, O. Ustun, G. Tosun, and R. N. Tuncay, "On Regenerative Braking Capability of BLDC Motor," *IECON Proc. (Industrial Electron. Conf.*, pp. 1710-1715, 2016.

[108] M. A. Hassanin, F. E. Abdel-Kader, S. I. Amer, and A. E. Abu-Moubarka, “Operation of Brushless DC Motor to Drive the Electric Vehicle,” *2018 20th Int. Middle East Power Syst. Conf. MEPCON 2018 - Proc.*, pp. 500-503, 2019.

[109] X. Jiaqun and C. Haotian, "Regenerative brake of brushless DC motor for light electric vehicle," *2015 18th International Conference on Electrical Machines and Systems (ICEMS)*, pp. 1423-1428, 2015.

[110] A.K. Mishra and T. Kim, “A BLDC Motor-Driven Light Plug-in Electric Vehicle (LPEV) with Cost-Effective On-Board Single-Stage Battery Charging System,” *2021 IEEE Transp. Electrif. Conf. Expo, ITEC 2021*, no. 3, pp. 452-456, 2021.

[111] M. Rahul Charles and J. S. Savier, “Bidirectional DC-DC converter fed BLDC motor in Electric Vehicle,” *Proc. 2021 1st Int. Conf. Adv. Electr. Comput. Commun. Sustain. Technol. ICAECT 2021*, 2021.

[112] G. C. R. Sincero, J. Cros, and P. Viarouge, “Efficient Simulation Method for Comparison of Brush and Brushless DC Motors for Light Traction application,” *2009 13th Eur. Conf. Power Electron. Appl. EPE ’09*, 2009.

[113] S. Gao, X. Sang, Y. Wang, Y. Liu, Y. Guan, and D. Xu, "A DCM High-Frequency High-Step-Up SEPIC-Based Converter With Extended ZVS Range," *IEEE Journal of Emerging and Selected Topics in Power Electronics,* vol. 10, no. 6, pp. 7915-7924, Dec. 2022.

[114] U. Sharma and B. Singh, "A Non-isolated Onboard Charger for Electric Vehicle," 2021 *IEEE Transportation Electrification Conference & Expo (ITEC), Chicago, IL, USA,* pp. 446-451, 2021.

[115] Y. Liu, Y. Sun, M. Su, and F. Liu, "Control Method for the Sheppard–Taylor PFC Rectifier to Reduce Capacitance Requirements," *IEEE Trans. Power Electron.,* vol. 33, no. 3, pp. 2714-2722, Mar. 2018.

[116] M. A. Al-Saffar, E. H. Ismail, and A. J. Sabzali, "Integrated Buck–Boost–Quadratic Buck PFC Rectifier for Universal Input Applications," *IEEE Trans. Power Electron.,* vol. 24, no. 12, pp. 2886-2896, Dec. 2009.

List of Publications

Publication (SCI) from Research Work

- **Ajay Singh,** Manoj Badoni, and Anjanee Kumar Mishra, "Solar powered on-board charging system utilizing coupled inductor high gain converter with G2V and V2G operations," Electr. Power Syst. Res., vol. 244, no. February, p. 111553, 2025, **doi: 10.1016/j.epsr.2025.111553. (I.F.= 4.2)**
- **Ajay Singh,** Manoj Badoni, and Anjanee Kumar Mishra, "An Efficient On-Board Charging System for Light EVs Using High Gain SCBZ Converter with G2V and V2G Capabilities," IJCT., 2025, **doi:10.1002/cta.70017. (I.F.= 1.6)**
- **Ajay Singh,** Manoj Badoni, and Anjanee Kumar Mishra, "A Multifunctional High-Performance On-Board Charger for Sustainable Electric Mobility Enabling Vehicle-to-Grid Energy Exchange," IJCT., 2025. **(under Revision)**
- **Ajay Singh,** Manoj Badoni, and Anjanee Kumar Mishra, "Solar Powered On-board LEV Utilizing Unidirectional Non-Isolated Converter. **(Manuscript under communication)**
- **Ajay Singh,** Manoj Badoni, and Anjanee Kumar Mishra, "Solar Powered On-board LEV Utilizing Bridgeless Modified SEPIC Converter. **(Manuscript under communication)**

Publication (Conference) from Research Work

- **Ajay Singh,** Manoj Badoni and Anjanee Kumar Mishra, "Performance Analysis of Two-Stage Charging System for Light Electric Vehicles," 2023 IEEE 11th Region 10 Humanitarian Technology Conference (R10-HTC), Rajkot, India, 2023, pp. 548-551, doi: 10.1109/R10-HTC57504.2023.10461915.

Patent from Research Work

- Manoj Badoni, **Ajay Singh** and Anjanee Kumar Mishra, " A High-Performance Modified SEPIC Converter-Based On-board Charger (OBC) for Sustainable Light Electric Mobility,"ref. no. DoRDC/PT/177. **(Published)**

Other Publications

- Norm deep, Manoj Badoni, **Ajay Singh** and Sudhanshu Mittal, " A Multifunctional High-Performance Switched Capacitor Buck-Boost Converter for Sustainable Light

Electric Mobility," International Conference(ICE2CPT 2025) at NIT, Jamshedpur, Jharkhand.

Attend Conferences and Work Shops

1. 2023 IEEE 11th Region 10 Humanitarian Technology Conference (R10-HTC), Rajkot, India,
2. **Outstanding Student Volunteered** from IEEE Delhi Section, 2023.
3. **Certificate of Appreciation** from IEE-IAS PES SBC, TIET, Patiala.
4. IEEE Industry Application Society **(IAS)** Regional Leadership India, August 22-23, 2024.
5. **Certificate of Appreciation and Best Volunteer Award** from *Vidhya: STEM for Social Goodwill and Its Impact on Soceity, organized by the IEEE USA, 2025*, held at *Thapar University, Patiala 147004 (Punjab), 8th-13th February 2025.*
6. **Attended** "Guest Lectures, organized by the *Department Electrical and Instrumentation Engineering, TIET, Patiala.*